OXIDATIVE STRESS AND DNA DAMAGE IN WHITE MATTER LESIONS OF THE HUMAN AGEING BRAIN

by

Sufana A. Al-Mashhadi
(BSc, MSc)

Submitted for the degree of Doctor of Philosophy (PhD)

Sheffield Institute for Translational Neuroscience

University of Sheffield

November 2014

ABSTRACT

White matter lesions (WML), identified as hyperintensities on T_2-weighted magnetic resonance images (MRI) in the ageing brain, are associated with dementia and depression in the elderly. Ischaemia may contribute to their pathogenesis but the exact role of glial cell pathology remains unclear.

Recent studies have concluded that oxidative stress is present in high levels in the deep subcortical white matter lesions when compared to periventricular white matter lesions.

The current study investigates the hypothesis that oxidative DNA damage contributes to the pathogenesis of WML, specifically the deep subcortical WM (DSCL). Oxidative DNA damage was investigated in WML and control WM, both from cases with WML (referred to as lesional controls) and without WML derived from the MRC-Cognitive Function and Ageing Study. Lesions were previously identified using post mortem MRI. 8-hydroxy-2'-deoxyguanosine (8-OHdG) was detected by immunohistochemisty and nuclear expression quantified. Double staining was performed to colocalise 8-OHdG with markers for specific cell type (e.g. CD68 for microglia). Expression of Malonaldehyde (MDA) (marker of lipid peroxidation), gamma histone H2AX (ɣH2AX) and DNA dependent protein kinase (DNA-PK) (markers of DNA damage response) were quantified by Western Blotting. β-galactosidase and p16 were used to detect induction of cellar senescence as a downstream effect of persistent DNA damage response. QPCR array was carried out using whole tissue RNA extracts to measure differences in expression of key senescence and DNA damage response genes.

Both WML and lesional control WM showed significantly elevated level of DNA oxidation than control WM, whilst WML and lesional controls did not differ. Persistent DNA damage response was detected using MDA, ɣH2AX and DNA-PK antibodies which activated senescence pathways demonstrated in βgalactosidase activity as well as p16, p21

and p53 as other indicators of cellular senescence. Key genes involved in DNA damage and senescence pathways were highly expressed in CL tissue.

Oxidised DNA is up regulated in ageing WM in different levels and may contribute to pathogenesis of WML. The similarity in the level of oxidative DNA damage in lesional control WM and WML suggests that oxidative damage is widespread in WM in cases with lesions indicating that WML are associated with general WM damage. DNA damage potentially activates cellular senescence as well as cell cycle check proteins, particularly in astrocytes, in aged WM and WML.

ACKNOWLEDGMENTS

First of all, I would like to thank Allah, the most gracious, the most merciful, for giving me this chance to convert a dream into reality. My humble acknowledgment goes to my father, Anwar, and mother, Hind, for believing in me and soaking me with their unconditional support, courage and love which made me achieve a goal I considered impossible. Many thanks to my brother, Bander, and my sister, Rania, who provided me with the strength and advice especially when I needed them most. Thanks for making this journey easier and full of joyful memories.

Secondly, my endless appreciation goes to my supervisor, Prof. Stephen Wharton for his endless support, guidance and scientific input. The knowledge I gained from you during the course of this PhD made me develop scientifically, academically and personally. Being a student of yours, I have learnt to think clearly and precisely even during the most difficult times of stress. My special thanks goes to Dr. Julie Simpson for her tremendous technical and academic support. Your comforting words and big smile always cheered me up! Also, I would like to thank Prof. Paul Ince for his guidance and Dr. Paul Heath for helping with qPCR array analysis.

Thanks to Dr. Mahmoud Al-Yamany for his valuable and immeasurable support. I would like also to thank all my friends. I am truly blessed to have you in my life.

Last but not least, I would like to thank my best friend, my husband, Ala'a. Without your huge sacrifices I would never have been here writing this. You have stolen a dream from my eyes to create it into a thought, an effort and a reward. Rayan and Muhra, thank you for being grownups while you are still few years old. You were my comfort zone in the toughest moments and in your lovely eyes I felt the warmth even in the coldest nights. Our new edition, Abdul-Rahman, thank you for listening to me talking and moaning about my thesis writing and responding with the cutest smile having no clue what I am talking about!

This thesis is dedicated to my loving parents,
Hind and Anwar

PUBLICATIONS

Papers

Al-Mashhadi S, Simpson J, Heath P, Dickman M, Forster G, Matthews F, Brayne C, Ince P, Wharton S (2014) Oxidative Glial Cell Damage Associated with White Matter Lesions in the Ageing Human Brain. Brain Pathology

Garwood CJ, Simpson JE, **Al Mashhadi S**, Axe C, Wilson S, Heath PR, Shaw PJ, Matthews FE, Brayne C, Ince PG (2014) DNA damage response and senescence in endothelial cells of human cerebral cortex and relation to Alzheimer's neuropathology progression: a population-based study in the MRC-CFAS cohort. Neuropathology and applied neurobiology

Abstracts

Al Mashhadi S., Simpson JE., Heath P. Ince PG. Wharton SB. Oxidative stress and DNA damage in cerebral white matter lesions of the human ageing brain. Neuropathology & Applied Neurobiology. 2012. 38 Supplement 7: 26

Al Mashhadi S., Simpson JE., Heath P., Mark D. Ince PG. Wharton SB. Oxidative stress and DNA damage in cerebral white matter lesions of the human ageing brain. Neuropathology & Applied Neurobiology. 2013. 39 Supplement 192

Al Mashhadi S., Simpson JE., Heath P., Mark D. Ince PG. Wharton SB. Oxidative stress and DNA damage in white matter lesions of the human ageing brain. British Neurosci. Assoc. Abstr., Vol. 22: PXX, 2013. ISSN 1345-8301 2013

Table of Contents

LIST OF FIGURES

LIST OF TABLES

LIST OF ABBREVIATIONS

8-OHDG	8-hydroxy-2'-deoxyguanosine
aa	Amino acids
AD	Alzheimer Disease
AR	Attributable Risk
ARE	antioxidant response element
ATM	ataxia telangiectasia mutated
ATP	Alzheimer Type Pathology
BBB	Blood-Brain Barrier
CAA	Cerebral Amyloid Angiopathy
CC75C	Cambridge City over 75 Cohort Study
CFANS	Neuropathology Study
CL	Control lesional
CNL	Control non-lesional
CNS	Central Nervous System
Coll IV	Collagen IV
CSF	Cerebrospinal Fluid
DA	Deoxy-adenine
DAB	Diaminobenzidine Solution
DC	Deoxy-cytidine
DDR	DNA damage response
DG	Deoxy-guanosine
DLB	Dementia With Lewy Bodies
DNA-PK	DNA-protein kinase
DSB	DNA double strand breaks
DSCL	Deep Subcortical Lesions
DT	Deoxy-thymidine
DTI	Diffusion Tensor Imaging
DWM	Deep White Matter
FFPE	Formalin Fixed, Paraffin-Embedded Tissue
FMRI	Functional MRI
GAPDH	Glyceraldehyde 3-phosphate dehyrogenase
H&E	Heamatoxolyn and Eosin
H2AX	H2A histone family member X

HIF	Hypoxia-Inducible Factor HIF
HPLC MS	High Pressure Liquid Chromatography Mass Spectrometry
HR	homologous recombination
IGF	insulin like growth factor
IL- 1α	Interleukin 1 alpha
IL 6	Interleukin 6
IL 8	Interleukin 8
IR	Ionizing radiation
kDa	Kilo dalton
LFB	Luxol Fast Blue
MAP-2+13	Microtubule-Associated Protein-2 Expressing Exon 13
MCI	Mild cognitive impairment
MDA	malondialdehyde
MRC CFAS	Medical Research Council Cognitive Function and Ageing Study
MRI	Magnetic Resonance Imaging
mtDNA	Mitochondrial DNA
NAPDH	Reduced Nicotinamide adenine dinucleotide phosphate
nDNA	Nuclear DNA
NHEJ	nonhomologous end joining
nM	Nanomolar
OPC	Oligodendrocyte Progenitor (Precursor) Cells
OSP	Oligodendrocyte specific protein
PCR	Polymerase chain reaction
PD	Parkinson's disease
PDGFαR	Platelet-Derived Growth Factor A Receptor
PET	Positron Emission Tomography
PVL	Periventricular Lesions
PVWM	Periventicular White Matter
QPCR	Qualitative polymerase chain reaction
RNA	Ribonucleic acid
RNS	Reactive nitrogen species
ROS	Reactive oxygen species
RT	Room Temperature
SASP	Senescence associated secretory phenotype
SA-β-gal	Senescence associated beta galactosidase

SDFs	senescence associated DNA damage Foci
SDS-PAGE	Sodium dodecyl sulfate polyacrylamide gel
SOD1	Superoxide dismutase 1
SSB	Single-stranded break
SSBR	single-strand break repair
SVD	Small vessel disease
TBS	Tris Buffered Saline
TEMPO	Tetramethylpiperidine 1-oxyl
TGFβ1	transforming growth factor β1
TJ	Tight Junction
UV	ultraviolet
v/v	Volume to volume
w/v	Weight to volume
WM	White Matter
WML	White Matter Lesions
µl	Microliter
µM	Micromolar
µm	Micrometer

CHAPTER 1: INTRODUCTION

1.1 White matter lesions

White matter lesions (WML), a common feature of the ageing brain, are detected by Magnetic Resonance Imaging (MRI) as hyperintensities on T_2-weighted images and are classified as periventricular lesions (PVL) or deep subcortical lesions (DSCL) depending on their anatomical location (Fernando et al., 2004). Their frequency increases with normal ageing and they are associated with lower cognitive performance (Fernando et al., 2006). Although WMLs are associated with several neurocognitive disorders such as Alzheimer's Disease (AD) and other dementias, their pathological role and clinical significance are not fully understood (Fernando et al., 2006, Simpson et al., 2007b, Filley, 2010). Population based studies of the elderly have added crucial knowledge to the understanding of the common WML pathology and an important tool is to correlate post-mortem histological findings with the MRI scans taken during life (Fernando et al., 2004).

The Medical Research Council (MRC) Cognitive Function and Ageing Study (CFAS) (1998) is the only multi-centre longitudinal population based study in the UK of individuals aged 65 and over where its main objective is to assess the burden of frailty and dementia in the population in individuals identified from family practitioner registers. People were selected only on the basis of age and they were assessed using questionnaires and psychometric tests (www.cfas.ac.uk).

CFAS has been in existence since 1989 (2001) as CFAS and in 1993 CFAS Neuropathology Study (CFANS) was added to the study design mainly to investigate the relationship of pathologies to cognitive impairment and decline, (Fernando and Ince, 2004). Outcomes from such population studies have widely contributed in the formation of several theories explaining the origin of WML. The main theories are chronic cerebral hypoperfusion due to vascular degenerative changes of the small vessels, cerebrospinal fluid (CSF) accumulation and blood-brain barrier (BBB) dysfunction which is associated with altered vascular permeability (Fernando et al., 2006). Recent studies by the MRC CFANS

group have directly linked the existence of WML to hypoxia and cerebral small-vessel disease which highly contribute in decline in information processing speed, cognition and memory which are all typical scenarios seen in AD, Binswanger disease, dementia and dementia with Lewy bodies (DLB) (Fernando et al., 2004, Fernando et al., 2006, Simpson et al., 2007b).

1.2 Cognitive impairment in population based studies of the elderly

Despite the large number of clinic-based studies of dementia and AD in which data collection depends on incidence and prevalence of well-defined disease versus control groups, there has been no significant blind population-based study where the correlation between dementia and ageing was analysed until associations such as CFANS, Hisayama, Cambridge City over 75 Cohort Study (CC75C), Vantaa 85+, Honolulu-Asia Ageing Study's (HAAS), Cache County Study of Aging and Memory's (Cache County study) have been established over the last two decades. However, CFANS is the only one among those six population based neuropathology studies that looks at the general old age population (Zaccai et al., 2006, Inaba et al., 2011).

Psychological examination was the tool to assess the level of dementia during life in all six population studies which ranged from simple questionnaires about activities of daily living and interviews to sophisticated investigations such as Geriatric mental state AGECAT algorithm and Cambridge Cognition Examination that were all part of the assessment performed on the study population (Copeland et al., 1987, Blessed et al., 1991). Neuropathological approaches were applied to define the pathology. The general burden of pathology in the cohort was assessed using a modified CERAD (Consortium to Establish a Registry for Alzheimer's Disease) (Fillenbaum et al., 2008) assessment and Braak staging which is a classification system of AD stage of pathology according to accumulation of neurofibrillary tangles (Braak and Braak, 1991) for Alzheimer-type pathology, assessment

of other degenerative pathologies such as Lewy bodies and assessment of vascular pathology (Zaccai et al., 2006).

Although there are numerous differences in the study design between the six study-populations mentioned earlier, such as number of subjects, years of re-examination and number of brains collected, these studies have helped in the creation of new hypotheses about age-associated cognition impairment and related substrates that contribute to dementia (Zaccai et al., 2006).

Population based studies (CFANS, HAAS) have provided meaningful attributable risk (ARs) at death that correlates patho-biological factors with dementia in a well-separated fashion according to their percentage of prevalence (ARs is the difference in rate of condition between an exposed versus an unexposed population, whereas population prevalence is the total number of cases of the risk factor in the population at a given time) (Fernando et al., 2004, White et al., 2005, Matthews et al., 2009). Age (18%), brain atrophy (12%), hippocampal atrophy (10%), neocortical neuritic plaques (8%) and neurofibrillary tangles (11%), small vessel disease (12%), multiple vascular pathologies (9%) as well as lewy bodies (3%) and cerebral amyloid angiopathy (CAA) (7%) are all factors that contribute in AR for dementia at death in the CFANS recent study cohort (n=456) (Matthews et al., 2009).

1.2.1 Cognitive function and ageing neuropathology study (CFANS)

CFANS is a multi-centre population based study where respondents were identified from local Health Care Registers at six different UK sites (Gwynedd, Ely, Newcastle upon Tyne, Oxford, Nottingham and Liverpool) (Fernando and Ince, 2004). Using ethically approved methods, permission and 'declaration of intent' of participation in CFAS as well for brain donation was obtained from the respondents. Post mortem brain collection was performed after a member of the family or care-giver of the respondent informs the concerned member of CFAS of the occurrence of death.

The data from the first 209 subjects who were part of CFANS brain donation program revealed several key points in regards to the pathology of cognitive impairment in a population setting. Firstly, a high prevalence of neuropathological markers in the brain (e.g. WML, mild to severe infarctions, vascular pathology) are usually associated with demented individuals but were also seen in non-demented post-mortem brains of non-demented respondents (2001, Matthews et al., 2009). Moreover, vascular pathology and angiopathy were highly correlated to dementia and would definitely increase the frequency of its expression during life (Fernando et al., 2006).

Secondly, CFAS has revealed the limitations of well-selected diseased-control approaches to studying cognitive impairment in the elderly as it demonstrated the common co-existence of pathologies, particularly AD and vascular, that in a population setting can contribute to dementia. WML may be considered as one aspect of vascular pathology and may also contribute to dementia, either in isolation or more commonly in conjunction with other pathologies (Fernando and Ince, 2004, Simpson et al., 2007b).

Finally, an important finding of CFANS study group (2001) was the degree of overlap of Alzheimer Type Pathology (ATP) (based on CERAD and Braak assessments of plaques and tangles) between non-demented and demented individuals (based on geriatric mental state AGECAT algorithm) in this old age group regardless of their degree of vascular pathology. Moreover, the study done by Savva G. et al (2009) shows that the overlap in burdens of pathology between demented and non-demented individuals increases with age. This result emphasizes the difficulty of establishing a threshold for a diagnosis of AD in this age group where some respondents remain intellectually intact although having plaques and ATP, while others experienced declined cognition despite their minimal pathological involvement.

1.3 White Matter

WM, which comprises a large proportion of the human brain (Filley, 2010), is composed mainly of the axons of neurons whose cell bodies lie in the gray matter, and their myelin sheaths. Myelin (which is 70% lipid and 30% protein) is produced by oligodendrocytes and covers the entire axon except for intervals which are called nodes of Ranvier (Filley, 2010). Myelin is an essential component for the conduction and acceleration of signal transfer along axons (Turken et al., 2008). Despite the effort of researchers in previous years, the role of WM in human brain function is not as well established as that for gray matter. It is worth mentioning that the lion's share of credit goes to the inspiration that was brought to neurologists in 1965 where a landmark paper by (Geschwind, 1965) (Disconnexion Syndromes in Animals and Man) was published to look into the higher role that WM has on human behaviour. Since then, dramatic progress has occurred in WM investigation revealing its importance in cognition and emotional behaviour (Filley, 2010).

The study of WM entered a new era in the 1980s with the advent of magnetic resonance imaging (MRI). Instead of relying mainly on autopsies, in vivo imaging was routinely done by physicians in the clinic which allowed them to demonstrate WM and its abnormalities in parallel with other tests as a diagnostic tool for the assessment of cognitive impairment and senescence (Filley, 2010). Functional MRI (fMRI) and positron emission tomography (PET) scanning were added recently and they are also valuable tools for investigating WM and localising cognition and emotion (Bandettini, 2009). However, it is worth mentioning that fMRI and PET are capable of demonstrating mainly cortical regions, whereas deep WM accessibility to imaging remains very limited (Filley, 2010). Using the principle of isotropy (i.e. random diffusion of water along an abnormal area) and anisotropy (i.e. the non-random diffusion of water along a normal pathway), diffusion tensor imaging (DTI) has recently been added as the most important imaging tool to show connectivity

between brain regions, demonstrating normal WM and abnormal conduction of cross signal interactions of areas with WML (Mori et al., 2009).

1.3.1 WML and MRI

Although MRI is excellent in detecting severe areas with myelin attenuation associated with large lesions (>10 mm), it is not sensitive to the smaller ones (Bronge et al., 2002). This potential limitation could have a serious effect on cognitive impairment studies where the number and the size of an individual's lesions are both important in the analysis and interpretation of the results. Also, unless the WML were severe, they cannot be detected by naked eye examination. CFAS has addressed this issue by doing MRI on post mortem coronal brain slices where this pathological approach was unique to CFANS where MRI was used to guide sampling for pathological (Fernando et al., 2004, Fernando et al., 2006) (Figure.1.2). Three anatomical levels of the brains' hemispheres were looked at the levels of anterior, medial and posterior (Newcastle coronal brain map reference levels 10/12, 19/20, 24/25 which represents WM taken from the coronal levels 4 – 6 parietal, 0-1 and 6 temporal WM respectively) (Perry and Oakley, 1993, Scheltens et al., 1993). WML were divided into deep subcortical lesions (DSCL) and periventricular lesions (PVL) depending on their anatomical site (Figure 1.1), and were evaluated using a modified principle of Scheltens's semi-quantitative scale (Table 1.1) (Scheltens et al., 1993, Fernando et al., 2004).

Table 1.1: Modified Schelten's rating scale for periventricular and deep subcortical white matter lesions (Scheltens et al., 1993)

Periventricular lesions (PVL)		***Deep subcortical lesions (DSCL)***	
0	Absent	0	No abnormality
1	≤5 mm	1	<4 mm; n<6
2	>5 mm– <10 mm	2	<4 mm; n≥6
3	≥10 mm	3	4-10 mm; n<6
		4	4-10 mm; n≥6
		5	>10 mm
		6	Confluent lesion

In Fernando et al's (2004) study, the WML identified using MRI scans were histopathologically examined for myelin attenuation and for vascular endothelial and microglial (Fig.1.3). This study has offered a sensitive correlation of WM change detected by post-mortem MRI to its histology. Since then, several studies on behalf of the MRC CFANS group have relied on this technique in tissue sampling resulting in significantly broader understanding of the pathological basis of WML (Simpson et al., 2009, Simpson et al., 2010b, Simpson et al., 2010d).

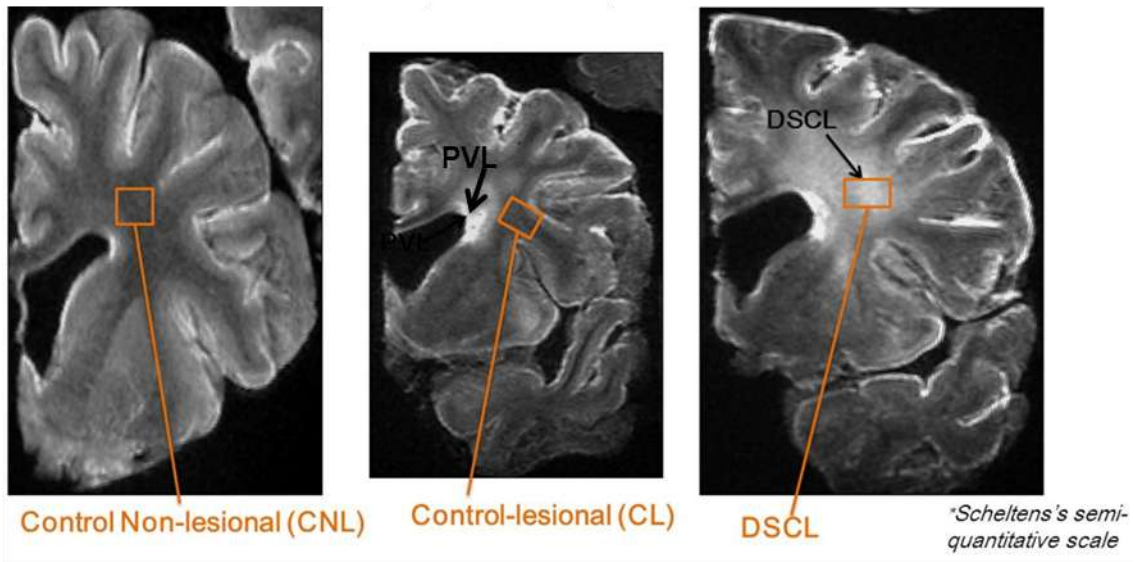

Figure 1.1: WML identification and anatomical classification using MRI scans. Left: MRI scan of a control coronal brain slice free of lesion. Middle: Coronal brain slice showing a periventricular WML shown as hyperintensity in MRI signal. The orange frame shows an area that is free of lesion in a lesional brain. Right: A coronal brain slice showing hyperintensity MRI scan demonstrating a deep subcortical white matter lesion

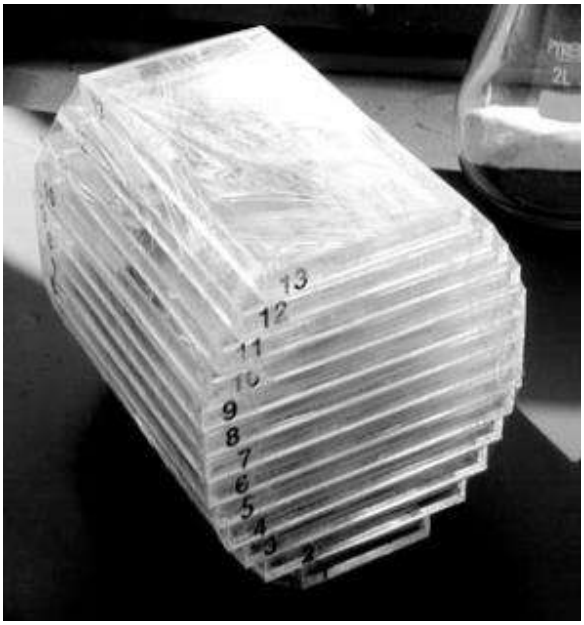

Figure 1.2: Post-mortem MRI. Fixed post-mortem coronal brain slices were sealed in polythene bags and placed in 'self-locking' stack to fit into the MRI scanner (Fernando et al., 2004)

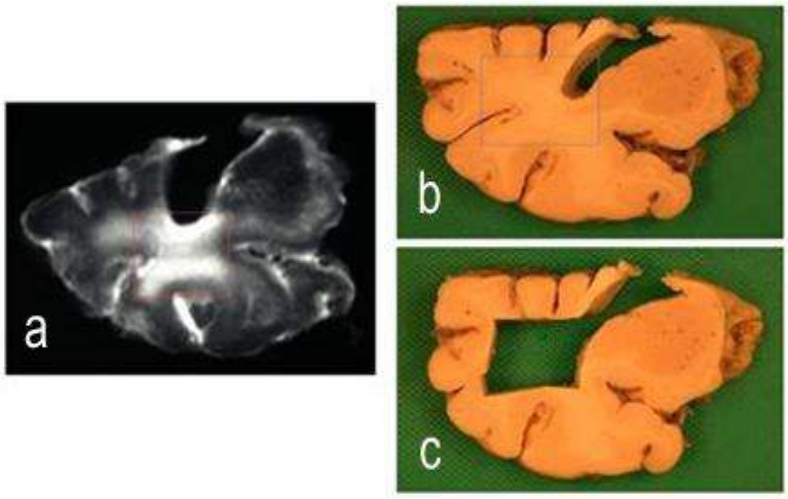

Figure 1.3: WML sampling. (a) Allocation of WML in the assistance of post-mortem MRI scan. (b,c) Retrieving WML to create a tissue block for further studies

1.3.2 Histology of WML

The main histopathological feature of WML is myelin attenuation. However, WML might differ in PVL versus DSCL in terms of demyelination, axonal loss and increased interstitial fluid which could be related to altered vascular supply to periventicular white matter (PVWM) (located adjacent to the ventricles) compared to deep white matter (DWM) (located in the centrum semi-ovale) (Fernando et al., 2006, Wharton et al., 2011).

Histological sections of DSCL show reduced Luxol Fast Blue (LFB) staining (myelin stain) compared to normal WM, reflecting a loss of myelin (Fernando et al., 2004). PVL are closely located to the ventricles and demonstrate in addition loss of ependymal lining and subependymal gliosis (Leaper et al., 2001). Degenerated myelin extends beyond this area and deep into the WM and it has been concluded that PVL have a higher frequency than DSCL in brain ageing (Fernando et al., 2004).

1.4 WML: Aetiological factors and mechanism of pathology

1.4.1 Aetiological factors

The causes of WML and their relationship to broader context of WM ageing, remain incompletely understood. Studies strongly support the association of WML with vascular risk factors such as stroke, hypertension and cardiac disease, suggesting a role for hypoperfusion (2001, Matthews et al., 2009). However, other factors such as autoimmune inflammatory responses and blood brain barrier disruption with interstitial fluid accumulation in the brain may also play a role (Roman et al., 2002, White et al., 2005).

1.4.2 Mechanism of pathology

Several mechanisms have been proposed to contribute to the underlying pathophysiological changes that lead to WML. These include hypoxia (hypoperfusion), BBB disruption that might contribute to failed drainage of interstitial fluid, resulting in fluid

accumulation in the white matter (Carare et al., 2014); microglial activation and ischaemia (2001, Fernando et al., 2006, Simpson et al., 2007b). These mechanisms are not mutually exclusive, and may operate together.

I. Hypoxia

Cortical arteries nourish deep white matter (DWM) of the centrum semi-ovale through their long branched capillaries. This anatomical system would potentially jeopardize the oxygenated blood supply and drainage in the presence of small vessel disease (including arteriolosclerosis and/or CAA) and lead to hypoperfusion (Fernando et al., 2006). Periventicular white matter (PVWM) is more subject to interstitial fluid accumulation compared to DWM which could be related to the loss of ventricular ependyma associated with the proximity of ventricles in this anatomical site (Fernando et al., 2006). However, the alteration in the thickness of arterioles and in blood supply and drainage in SVD associated with enlarged periventricular spaces and their relation to the formation of WML is not fully understood (Fernando et al., 2006).

The expression of the molecular marker hypoxia-inducible factor HIF1α in brains which had the shortest intervals between death, collection, fixation and process along with MMP7 and Ngb (molecules up regulated in hypoperfusion) that were all shown to be upregulated in the WML in studies reported by CFANS group, strongly suggest the pathological role played by hypoxia in WML formation (Fernando et al., 2006, Matthews et al., 2009).

Simpson et al. (2009) have also concluded in a CFAS study that DSCL show a significant increase in hypoxia related proteins as well as hypoxia-regulated transcription factors which strengthens the idea of cerebral hypoperfusion being one of the causes of WML.

II. BBB disruption

BBB is strictly required to control the brain microenvironment and its dysfunction, resulting from leaky blood vessels, is associated with a number of neurodegenerative pathologies including multiple sclerosis (MS) and AD (Starr et al., 2009, Simpson et al., 2010d). Malfunctioning of the BBB is closely related to loss of tight junction (TJ) complexes composed of claudin-5 (Cln-5), zona occludin-1 (ZO-1) and occludin (transmembrane proteins and accessory proteins) that are considered the structural components of BBB which bind brain capillary endothelial cells (Simpson et al., 2010d). The contribution of increased permeability in BBB dysfunction to WML formation was described previously in several studies (Farrall and Wardlaw, 2009, Popescu et al., 2009) and is associated with the presence of fibrinogen-immunoreactive clasmatodendritic astrocytes, which are astrocytes with swollen cell body and shorter cellular processes that showed reactivity to plasma proteins suggesting a leaky BBB (Fernando et al., 2006). Although the cause of WML is not fully explained, serum plasma extravasation due to BBB dysfunction could contribute to the pathogenesis of WML (Qiao et al., 2001). Qiao study has concluded that the different hypoxic-ischemic changes in MRI hyperintensity in older mice brain are associated with differences in alterations in water content plus extravasation of protein, consistent with age-dependent differences in hypoxic-ischemic alterations in vascular permeability (Qiao et al., 2001). A recent study by the CFANS group has used the extravasation of albumin as a marker for the existing BBB dysfunction in WML in the brain ageing, and concluded that albumin extravasation was widespread in the ageing brain and enhanced in WML, suggesting dysfunction of the BBB may contribute to the pathogenesis of WML. This was not accompanied by significant changes in the endothelial expression of TJ proteins suggesting a variation in other expressed junction adhesion molecules and proteins that were not looked at in that paper (Simpson et al., 2010d).

III. Glial cell pathology

Although much of dementia research has been done on neurons and on the nature of protein deposits in the grey matter of the demented elderly, cellular activity has been recently considered as a characteristic change indicating an on-going pathology in WML in brain ageing (Simpson et al., 2007a, Wharton et al., 2011). These cells include macro- and micro-glia, oligodendrocytes and their precursor cells (Simpson et al., 2009).

Microglia as such, are highly ramified cells and counted as the immune resident cells of the CNS. However, their activated role is sophisticated where it can be toxic and be involved in several pathological mechanisms of neurodegenerative diseases and immune responses in the CNS (Wojtera et al., 2005). For instance, it has been shown that chronic hypoxia will contribute to the formation of WML and activate microglia in the rat's brain following ischaemia (Farkas et al., 2004, Curtis et al., 2006).

Although the role of microglia in WML is not fully established, recent literature supports the idea that activated microglia play an important role in the pathology of WML where microglia have been widely looked at histologically using immunohistochemistry in both PVL and DSCL versus controls (Fernando et al., 2006, Simpson et al., 2007b). PVL significantly show a higher level of major histo-compatibility complex (MHC II) activated microglia expressing B7-2 and CD40 than control WM with a higher proliferation activity in PVL versus DSCL (Simpson et al., 2007b). DSCL showed a significant increase in the population of amoeboid microglia demonstrated by CD68 (a microglia marker) reactivity compared to PVL (Simpson et al., 2007b). However, a significant increase in the expression of MHC II associated with activated microglia was observed in PVL but not in DSCL suggesting a different pathological process of ramified microglia in those two distinguished anatomical sites (Simpson et al., 2007b).

Astrocytes are essential in the survival of neurons in the central nervous system (CNS). They offer support by maintaining local homeostasis and by participating in the

tripartite synapse (Volterra et al, 2005). Damage to astrocytes would alter their normal functioning where they could show evidence of hypertrophic and degenerative change that might contribute to the pathology seen in brain ageing (Rodriguez et al, 2009).

In a recent study done by Simpson et al (2010a), reactive astrocytes reveals population variation in markers of DNA damage and oxidative stress in Alzheimer-type pathology in selected CFANS samples. These markers were seen even in those with low Braak stage suggesting an early astrocyte reactivity that is not exclusively associated with well-established AD pathology (Simpson et al, 2010a; Wharton et al, 2011). The role of reactive astroglia which is thought to respond to different forms of insult by gliosis in the ageing brain that could in turn contribute to the pathology of WML creates an important hypothesis that is still to be tested.

NG2-expressing cells are mitotically active population that act as oligodendrocyte progenitor (precursor) cells (OPC) in the adult spinal cord and cerebral cortex (Horner et al., 2000, Tang et al., 2000). Moreover, NG2+ cells are thought to maintain local homeostasis and take a part in glutamate signalling (Bergles et al., 2000).

Several markers for OPC and oligodendrocytes have been used to study the pathology in an unselected cohort of the elderly from CFAS. These included microtubule-associated protein-2 expressing exon 13 (MAP-2 +13) which is an intracellular protein that reflects the processes of myelinating oligodendrocytes, and Platelet-derived growth factor α receptor (PDGFαR) which is expressed by OPC as and could be expressed by reactive astrocytes (Shafit-Zagardo et al., 1999, Simpson et al., 2007a). High levels of PDGFαR reactivity has been seen in PVL suggesting a potential remyelination process. However, extension of such a research would determine the effectiveness of the suggested remyelination activity in WML, specifically in PVL (Simpson et al., 2007a).

It is clear now that several mechanisms of pathology might contribute in the formation of DSCL and PVL. Although there are several characteristic histological features

of lesions in both anatomical sites such as myelin attenuation and microglial cell activation when compared to corresponding non-lesional control WM, the detailed pathological investigation shows differences between the two areas. This suggests a complex of on-going pathogenesis that extends far behind the hypothesis of gliosis as such. The novel conclusion represented in Simpson et al's (2007a) paper that a possible remyelination process which might be on-going solely in PVL clearly suggests that cerebral WML in different anatomical sites of the brain show different biological reactivity and pathological profiles (Figure 1.4).

1.4.3 Field-effect of activated microglia in normal appearing WM

The fact that DSCL and PVL show clear histological and pathological changes compared to normal WM from non-lesional (WM[C]) brains gives arise to an important question to be addressed in the field of WML research of the elderly: Is normal appearing WM (WM[L]) located around lesional areas actually normal?? The study by Simpson et al (2007b) has concluded that in (WM[L]), an immunorectivity identified by MHCII increase is observed. A further study by the same group which used whole-genome RNA microarray technology in comparing gene expression in DSCL with (WM[L]) and (WM[C]) revealed an altered regulation of 419 genes in (WM[L]) whereas DSCL show 502 differently regulated genes in comparison to WM[C]. The known coding for those genes is mainly associated with immune function, ion transport, proteolysis and the cell cycle in which they were all upregulated in the normal appearing WM when compared to actual lesions. However, other genes are associated with cell structure and metabolism. Although non-lesional deep white matter sampled from lesional brain appeared free of lesions on MRI, it contains significantly increased level of activated microglia (expressed using MHCII) when compared to control WM (Simpson et al., 2007b). The significance of this field-effect changes in WM[L] is unknown and until further investigated, the role of this reactive change in central WM remains unclear whether it is a protective response or a foundation ground for a progression towards WML formation (Simpson et al., 2007b).

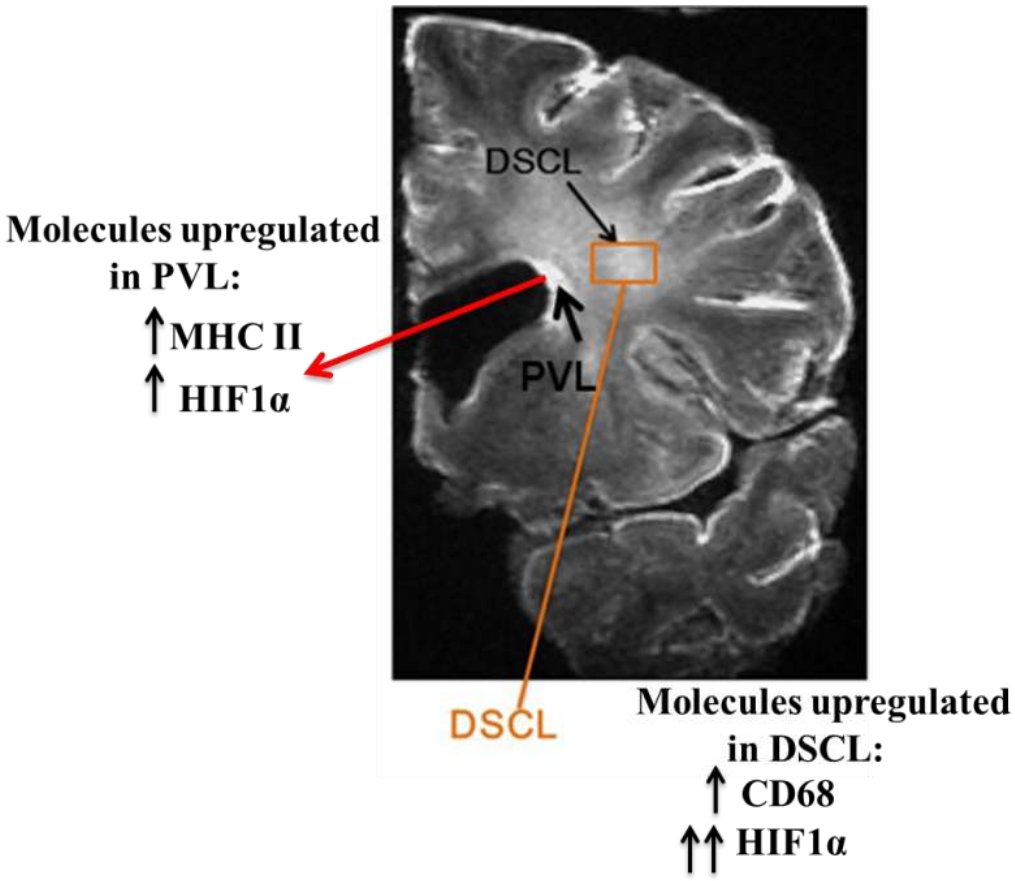

Figure 1.4: Variation in expression of different molecular markers between PVL and DSCL. Recent CFAS studies have shown that although PVL and DSCL are types of WML which are revealed as hyperintensities on T2 wheighted scale MRI scan, they reveal changes in the expression of molecular markers that reflect hypoxia and inflammation. Microglial activation was revealed by MHC II reactivity and was significantly higher in PVLs compared to DSCL in elderly brains. However, CD68 was significantly higher in DSCL. Although the hypoxia marker HIF1α (gets activated in the presence of ischamia) was expressed both in PVL and DSCL, its expression was significantly higher in DSCL. These important findings suggest a different pathological process in those two distinguished anatomical sites

1.5 Oxidative stress and DNA damage in ageing

Cellular damage is a feature of brain ageing and a contributor to cognitive impairment (Davydov et al., 2003, Lovell and Markesbery, 2007). DNA damage due to oxidative stress is hypothesised to have a main role in several neurodegenerative diseases and is a major cause of premature cell death and senescence (Keller et al, 2005; (Simpson et al., 2010b). To date, most studies have investigated DNA damage in cortical neurons in a well-defined AD population against healthy controls, and do not take into account the effect of oxidative stress on glial cells (Wang et al, 2006; Shackelford, 2006). A recent CFAS study demonstrated a large variation in the DNA damage response and oxidative stress in astrocytes and neurones in the temporal cortex of the ageing brain which suggests altered astroglial function may impact neuronal support and contribute to neuronal dysfunction and cognitive impairment (Simpson et al., 2010a).

Current markers of oxidative damage include oxidized LDL and malondialdehye (MDA) (Halliwell et al, 1997). Recent research has expanded the understanding of oxidative insult of DNA by reactive oxygen species (ROS) which could lead to DNA double strand breaks and the initiation of about 20 oxidised base products in which 8-hydroxyguanine (8-OHdG) is the most prominent (Cooke et al, 2001). Guanine among other three DNA bases has the lowest oxidation potential and therefore is the most vulnerable oxidative stress (Figure 1.5).

Oxidative stress is an indicator of on-going pathology that involves activation of microglia andastrocytes i(Simpson et al, 2010). The inability of a cell to repair the damage to its DNA could lead to cell death through the activation of different apoptotic pathways (involving p53 molecules, caspase-3), or could lead to its permanent damage and eventually to senescence (expression of β-galactosidase molecules) (Andreassi et al, 2008; Psychol Med, 2008; Simpson et al, 2010).

While there is growing evidence of the role of direct DNA oxidative damage in the ageing brain and its contribution to cognitive decline, there are limited studies on DNA repair mechanism(s) in glial cells and only few studies have investigated γH2AX for instance, which is an important marker of DNA damage response, in response to DNA double strand breaks (DDSB) due to ROS accumulation (Mah et al, 2010). H2AX is a protein that is part of the histone family where by it gets phosphorylated in the presence of DNA double strand break to become γH2AX. γH2AX acts as an anchor connecting the two sites of DNA break and attracts other DNA damage response molecules to the site of damage, including DNA-protein Kinase (DNA-PK). The study done by Simpson et al (2010) has extended the analysis of DNA damage response to oxidative insult in brain ageing and correlated gliosis and the astrocytic response to Alzheimer type pathology in the temporal cortex. The study showed there was no increase in the astrocyte DNA damage response associated with increasing Braak stage suggesting that the DNA damage response may be independent of AD pathology and may be an early event. Other studies such as Nunomura's (2001) also suggest that oxidative nucleic acid damage is an early feature of AD progression (Nunomura et al., 2001)

To date, only a single paper known to be in the current literature investigating the role of DDR in WML in the presence of oxidative stress and how it might contribute in cell senescence and apoptosis (Al-Mashhadi et al., 2014).

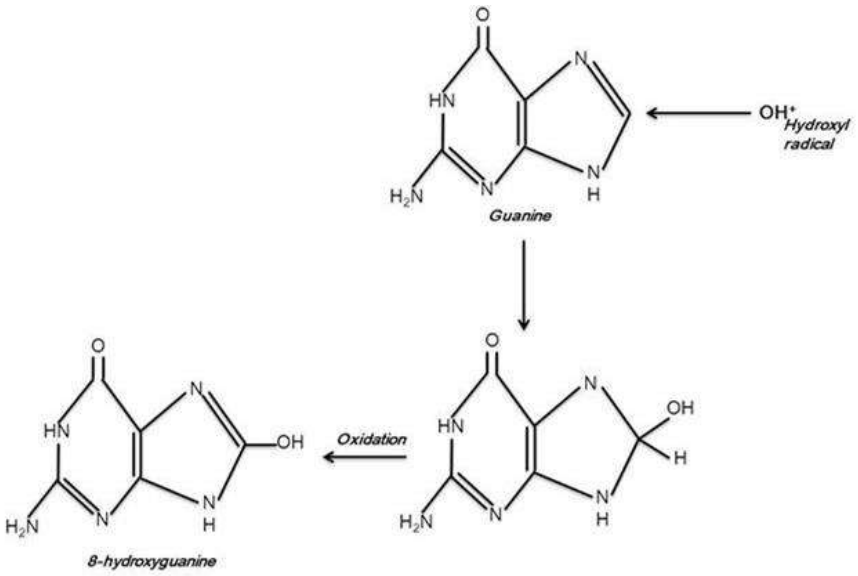

Figure 1.5: Oxidation of Guanine to form 8-OHdG. Hydroxyl radical attack of guanine to form 8-hydroxyguanine

1.5.1 Oxidative stress

Under normal physiological states, reactive oxygen species (ROS) create an essential part of redox signalling cascade that is important to maintain cellular haemostasis and gene expression. However, an imbalance between production and detoxification of ROS will result in oxidative stress (Figure 1.6). Redox homeostasis is maintained through antioxidant defence mechanisms, which target and remove ROS, thereby preventing free radical facilitated damage (Inoue et al., 2003, Praticò, 2008). ROS is the product of vital aerobic metabolic cellular processes that involves leakage of electrons from the mitochondrial respiratory chain (Lenaz et al., 1998) . A large number of ROS and reactive nitrogen species (RNA) are known to exist in biological systems, in which the species most studied and known to be related to disease include superoxide, hydrogen peroxide, and the hydroxyl radical (Miwa et al., 2008).

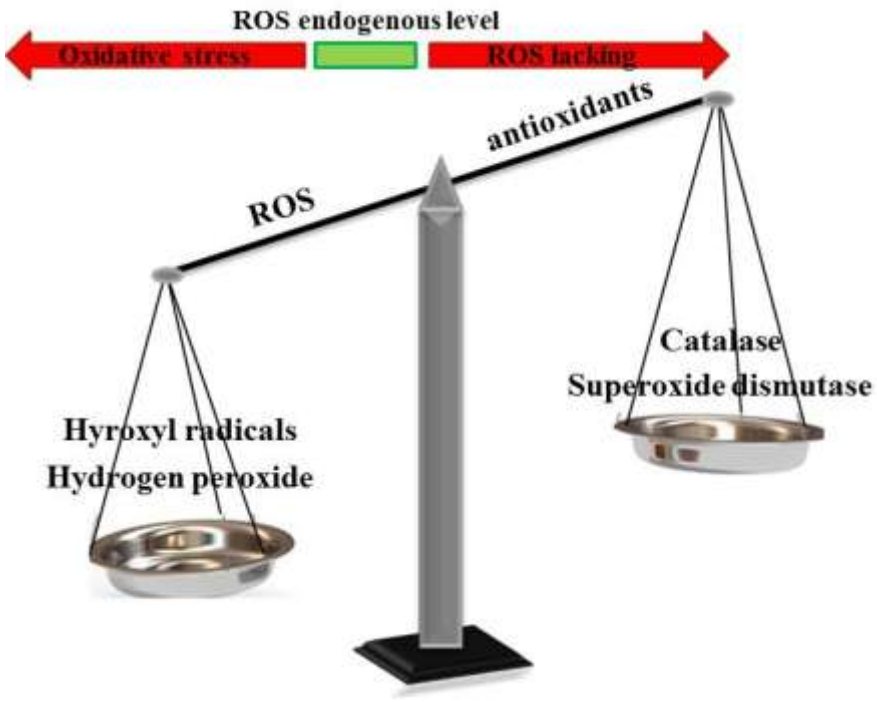

Figure 1.6: The formation of oxidative stress by ROS. An increased level of endogenous ROS production that associated with insufficient anti-oxidant defence mechanism will create oxidative stress and would potentially expose the cell, its component and the surrounding environment to oxidative damage

It has long been recognised that excessive ROS cause damage to macromolecules including lipids, protein and DNA (Blumberg, 2004), where lipids are one of the most sensitive targets for oxidative stress due to the high content of unsaturated fatty acids that are easily peroxidised . Once lipid peroxidation is initiated, a series of reactions will occur and end products accumulate such as malondialdehyde (MDA) (Kregel and Zhang, 2007). DNA bases are also very vulnerable to ROS oxidation where the predominant detectable marker of oxidative stress *in vivo* is 8-hydroxy-2-deoxyguanosine (8-OHdG). Almost all amino acids in a protein can be oxidised by ROS. A variety of amino acids oxidised products that have been studied in relation to different pathologies include carbonyl derivatives (Andersen, 2004). Since it is very difficult to estimate the amount of ROS in a biological system, quantification of lipid, protein and nucleic acid oxidised products is the current preferred method of studying oxidative damage (Radak et al., 2011).

Mounting evidence suggests that oxidative stress is a major contributor to age-related decline of physiological functions, and the contribution of increased ROS production to ageing and age related disease has long been studied in variety of models ranging from *C. elegans* to humans (Sohal and Weindruch, 1996, Beckman and Ames, 1998, Navarro et al., 2002, Bokov et al., 2004, Navarro and Boveris, 2004). During ageing the susceptibility of neurons to ROS oxidative damage increases such that changes to cellular macromolecules accumulate (Radak et al., 2011). Moreover, increased ROS production may cause changes in signal transduction associated with altered gene expression, which are all a typical characters of disease states.

Oxidative alteration to biomolecules depends upon several factors such as the location of produced ROS, the availability of metal ions and the susceptibility of the molecule to be oxidised. These changes contribute to protein expression/function modification and disrupted cellular metabolic pathways, which all together jeopardise the defence mechanism of a cell and its ability to repair the oxidative damage (Uttara et al., 2009). A reduction in cellular defence/repair mechanism in the presence of oxidative stress is associated with ageing and neurodegeneration (Nakabeppu et al., 2004), and subsequent exposure of these cells to environmental insult prevents their ability to cope up with additional stress.

1.5.2 Free Radical Theory

Free radicals are molecules containing unpaired, highly reactive electrons, and are proposed as fundamental agents in the process of aging. In the 1950s, Harman proposed "the free radical theory" in which he hypothesised that accumulation of free radicals that are produced by cellular metabolism in an aerobic condition could damage cellular macromolecules and could be a major life span determinant (Harman, 1955). This postulation has received much attention in the last 50 years especially as it has beendiscovered that ROS contribute to the accumulation of oxidative damage to cellular

components (Kregel and Zhang, 2007). The free radical/oxidative stress theory is now considered as a prime candidate for causing ageing. It proposes that the cumulative stress to cellular components by ROS causes a decline in neuronal function and the surrounding glia (Andersen, 2004).

Oxidative damage is detected by the accumulation of injury markers in biological tissues such as lipid peroxidation, protein oxidation and nucleic acid damage where ROS can alter cellular function by disrupting signalling cascades through activation/inhibition of key enzymes such as protein kinases and phosphatases (Trachootham et al., 2008). The CNS is principally susceptible to oxidative stress by ROS due to (i) the high content of unsaturated fatty acids which are easily oxidised, (ii) the high oxygen consumption and (iii) the low capacity of anti-oxidant mechanisms. In order to understand the effect of oxidative damage on tissue ageing, markers of oxidative stress have been widely studied in different models of ageing, coupled with the study of tissue response to such an insult including gene-expression changes. Several threads of evidence indicate that oxidative stress is can be considered life span determinant including: (1) expression of anti-oxidant enzymes in a mouse model significantly increased its longevity, (2) oxidative stress markers significantly increase with ageing and (3) introduction to change in life style paired with high consumption of anti-oxidants can significantly decrease ROS production and increase life span (Parkes et al., 1998, Wickens, 2001, Johnson et al., 2013). However, other studies concluded conflicting results making it difficult to understand the direct effect of oxidative stress on life span (Griswold et al., 1993). Having said that, the majority of evidence suggests that the ability of cells to cope with oxidative damage decreases with age (Kregel and Zhang, 2007).

1.5.3 Oxidative stress and gene expression changes

In order for a cell to maximise its survival in the presence of an insult, a manipulation in gene expression might occur where gene expression changes are considered an important indicator of oxidative stress. An immediate response to oxidation occurs in the

nucleus as well as post-transcriptional modification of certain genes to ensure an efficient change in signalling pathways that are essential for repair or for cell survival. Gene expression is tightly regulated and in the presence of stress, kinetics are rapidly changed to ensure a slow consistent adaptation (de Nadal et al., 2011). ROS when present in high concentrations are known to function as damaging products to cells, however, more recently it has been concluded that low levels of these pro-oxidants have the ability to control transcription factor activators (Finkel, 2001, Martindale and Holbrook, 2002). The intra-cellular redox status is thought to have the capability to modulate a large number of molecules such as kinases (Lo et al., 1996, Pombo et al., 1996), phosphatases (Keyse and Emslie, 1992), and transcriptional factors (Sun and Oberley, 1996, Finkel and Holbrook, 2000, Esposito et al., 2001, Zhang et al., 2002) through a wide range of signal transduction pathways. Rac, which is the small GTP-binding protein, is a transcription factor that is known to activate ROS-generating enzymes such as NADPH oxidase to produce ROS as a modulator of downstream molecules (Wang et al., 2004). NADPH has a wide-range of functions involving antioxidant response. The antioxidant response element (ARE) acts to mediate the transcriptional induction of genes during oxidative stress and is found in the promoter of genes encoding detoxifying enzymes and antioxidants (Reddy, 2008). Activation of gene transcription through ARE is mainly controlled by nuclear factor erythroid 2-related factor 2 (Nrf2) (Nguyen et al., 2009) which is a key transcription factor modulated by oxidative stress. It acts as a regulator for several important detoxifying enzymes such as superoxide dismutase, glutathione peroxidases and peroxiredoxins (Itoh et al., 2003, de Vries et al., 2008). Studies on post-translational modification of Nrf2 showed an ARE-induction by cysteine modification or serine phosphorylation. These types of studies provide evidence for the role of Nrf2-mediated regulation on gene expression which could act as a protector against oxidative stress (Venugopal and Jaiswal 1996). Studies have also concluded that regulation of Nrf2 can protect cells from free radical damage, inhibit premature apoptosis and support long cellular life span (Jaiswal, 2004, Copple et al., 2008).

ROS regulation to transcriptional factors can be by direct modification of critical amino acids residues mainly through formation of disulphide bonds at DNA-binding sites or indirectly through phosphorylation/dephosphorylation that occur in response to change in redox-modulated signalling pathways. These pathways were found to be implicated in ageing and age related pathology, and include the p53 pathway which controls cell apoptosis, cell cycle arrest and cellular senescence (Harris and Levine, 2005). The p53 tumour suppressor activates downstream gene expression responses depending on the level and type of stress faced by a cell through two major signalling pathways: the intrinsic and extrinsic pathway, in either caspase-dependent or caspase-independent manners (Cho and Choi, 2002). The intrinsic pathway mainly acts on post-translational modifications to activate apoptogenic factors, such as cytochrome *c* and apoptosis-inducing factor that are released from the mitochondria to the cytoplasm of the cell. This in turn activates a cascade of downstream signals, including caspases that control cellular apoptotic response. On the other hand, the induction of apoptosis by extrinsic pathways involves the attachment of ligands to cell membrane receptors and attraction of cytosolic adaptor proteins, which will consequently activate a chain of initiator and effector caspases (Kregel and Zhang, 2007). ROS and ROS-modulated molecules are implicated in both the intrinsic and extrinsic pathways and thus, act as an activator for cell cycle arrest or premature cellular death (Matsuzawa and Ichijo, 2005).

1.5.4 Oxidative stress to nucleic acids

The remarkable process of ageing is a very interesting area of research, however understanding the mechanism underneath it still remains a mystery. Ageing and age related pathologies such as AD and PD were found to be associated with an increased level of DNA oxidative damage in the brain (Shan et al., 2007). The CNS is the most vulnerable system in the human body to oxidative damage due to its high content of unsaturated fatty acids, high Oxygen consumption and low anti-oxidant potential as a defence mechanism (Nunomura et al., 2006). The accumulation of oxidised end product of cellular macromolecules including

DNA bases in ageing pathologies identifies the significance of understanding the effect of oxidative stress on neurons and on glial cells (Ding et al., 2004).

Among the four DNA bases, guanine is the base that is most susceptible to oxidative damage due its low reduction potential and high affinity to oxidation. Guanine is altered mainly by the hydroxyl radical where it is exposed to base attack by singlet oxygen or electron transfer response which modifies the base at C8 (Burrows and Muller, 1998, Candeias and Steenken, 2000). Although studies have identified more than twenty base modification products, the product 8-hydroxyguanine (8-oxoG) is the most abundant and well recognised in ageing studies as a marker of oxidative stress (Boiteux et al., 2002, Nishimura, 2002, Cooke et al., 2003). The current study utilises 8-OHdG in its pathological investigation hence the focus of this review will be on 8-OHdG as a product of oxidation.

Studies have shown that 8-OHdG levels in DNA is increased in association with ischemia/reperfusion, ageing and neurodegenerative diseases (Radak and Boldogh, 2010). When 8-oxoG is not repaired, it will bind to adenine (A) instead of cytosine (C) changing G:C toT:A (Nishimura, 2002) resulting in base mispairing which in turn will lead to faulty protein production (Shibutani et al., 1991).

Oxidative damage to DNA may alter gene expression and could lead to a variety of disrupted cascades of important cellular pathways such as metabolic processes, result in translational errors and gene expression changes that will in turn produce misfolded protein. The collection of such alteration in regular cellular process will contribute to cellular loss of function and lead to cellular degeneration. Current research has focused more on establishing mechanisms to avoid the damage, or repair it when it occurs which will facilitate new potential approaches for therapies and defines new therapeutic targets in age-associated diseases.

1.5.5 Oxidative DNA damage prevention and repair

The phenomenon that maintains genomic integrity must protect DNA from environmental damage, which include the exposure to ionizing radiation (IR) and ultraviolet (UV) light; and damage that might be induced spontaneously during DNA metabolism. Damage to DNA can occur as a result of a variety of causes including DNA base modification by alkylation, DNA base oxidation and DNA breaks that can be generated by ROS (Lindahl and Barnes, 2000, Hoeijmakers, 2009). Exposure to some certain chemicals, such as chemotherapeutic agents, can cause DNA single strand breaks (SSB) and DNA double strand breaks (DSB) (Ciccia and Elledge, 2010). SSBs are repaired by single-strand break repair (SSBR), whereas DSBs are repaired by homologous recombination (HR) (which utelises sister chromatids as a template for repair by joining the two broken ends of the DNA and precisely restoring the genomic sequence); or nonhomologous end joining (NHEJ) (which promotes less accurate DNA relegation) (West, 2003, Caldecott, 2008).

The repair of damaged DNA requires the recruitment and activation of a plethora of enzymes including nucleases, recombinases, phosphatases and kinases. These healing tools must be tightly controlled in order to avoid further damage that could happen from accessing damaged DNA at the wrong site or at the wrong time. Thus, to facilitate sufficient DNA repair, DNA repair enzymes must be utilised at the right place at the right time (Ciccia and Elledge, 2010).

DNA damage response (DDR) is a signalling pathway that is conducted in the presence of DNA damage or replication stress, and sets a response to save the cell from threat (Harper and Elledge, 2007, Jackson and Bartek, 2009). The DDR is mainly facilitated by proteins of the ataxia telangiectasia mutated (ATM) family and the DNA-protein Kinase family (DNA-PK) in which they both get activated by DSBs (Meek et al., 2008). Recruitment of catalytic DNA-PK can trigger the onset of DNA repair or apoptosis by activation of p53 pathway via phosphorylation of the amino terminal site (Soubeyrand et al.,

2004). Activated DNA-PK will in turn attracts the H2A molecule which is part of histone family X (H2AX), where it gets phosphorylated on serine 139 and acts as an anchor between the two sites of a broken DNA in response to DSB. Phosphorylation of H2AX will form γ-H2AX which a well-recognised marker used in variety of studies as an indicator of DNA damage response (Rogakou et al., 1998, Stiff et al., 2004).

1.5.6 Oxidative stress and cellular response

In the presence of oxidative stress, ROS and ROS-affected macromolecules can alter a variety of cellular functions that is accompanied with damage to cellular components. This will trigger cellular repair mechanisms to become activated. As described above, damage to DNA would activate DDR to reverse the effect of oxidative damage. However, prolonged exposure to cellular insult is obviously associated persistent DDR that can lead to two possible scenarios, one is that the DNA gets repaired, or two, the DDR fail to repair the damaged DNA, which will potentially activates senescence or apoptotic pathways (Figure 1.7) (Kregel and Zhang, 2007, Haigis and Yankner, 2010).

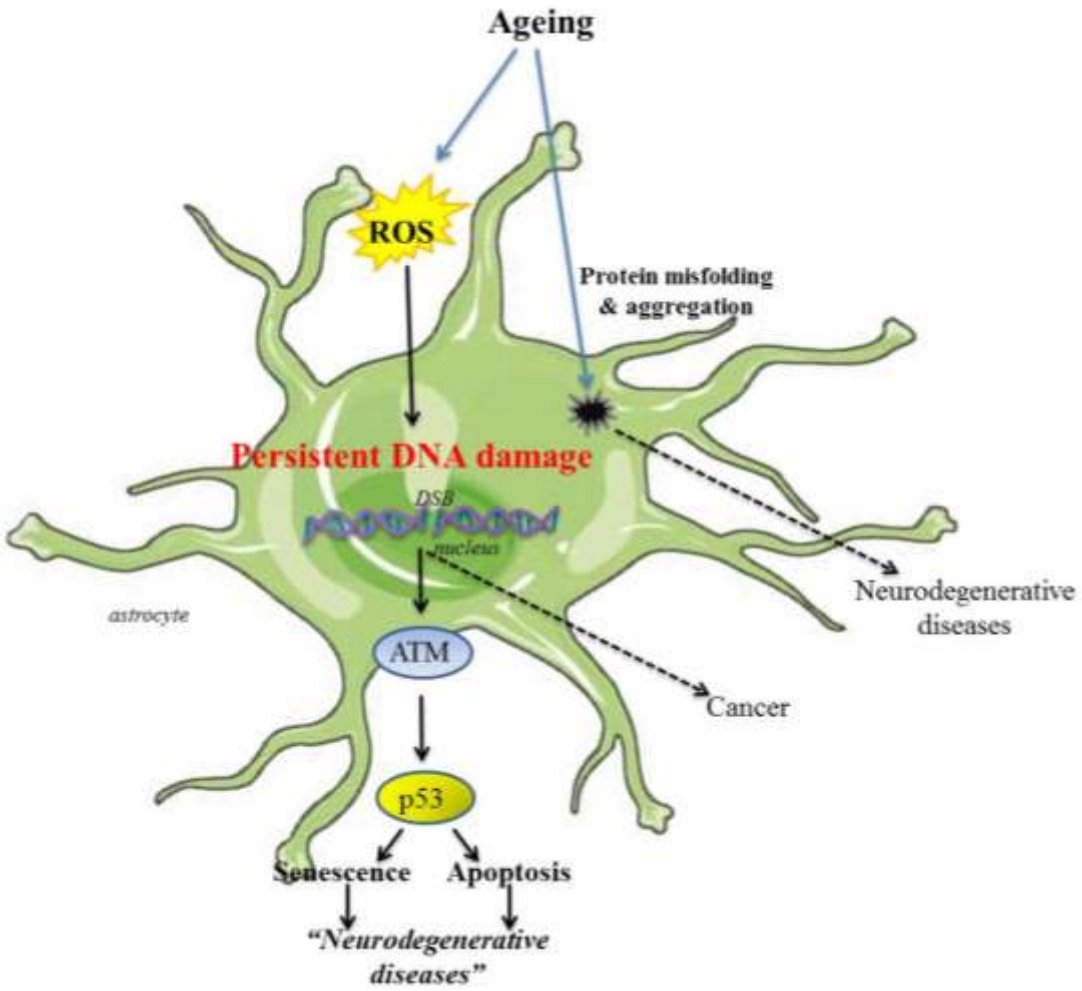

Figure 1.7: Age related stress response. Ageing is associated with an increased level of ROS which create a threat of oxidative stress that will affect major cellular components including DNA of a glial cell. Oxidative damage to DNA will activate DDR through multiple pathways but mainly ATM-ATR pathway to fix DSB. Unrepaired DNA will potentially expose the cell to a prolonged DDR which is associated with persistent DNA damage. As a consequence, cell cycle check proteins will be activated (including p53) which will drive the cell to senescence or apoptosis which are known to be implicated in neurodegenerative disease

1.6 Cellular Senescence

Cellular senescence is a process in which cells stop dividing and undergo an alternative phenomenon where cell's functions are changed (Campisi, 2013, Tchkonia et al., 2013). Hayflick and Moorhead first introduced cellular senescence as the inability of cells to further divide after a certain number of passages (cell division) in a cell culture model where they described this phenomenon to be irreversible and it was later named as 'replicative senescence' (Hayflick and Moorhead, 1961, van Deursen, 2014). Since this time, studies have suggested multiple explanations for potential triggers of cell senescence including the presence of damage in one or more of the cellular components such as telomere dysfunction which leads to chromosomal instability. This important observation supports the original hypothesis that senescence protects organs and tissue from unrestricted growth of damaged cells (Hayflick and Moorhead, 1961, Bodnar et al., 1998). Subsequent studies have emphasised the important role of replicative senescence in cancer cells where senescence act as a safeguard against tumour growth (Serrano et al., 1997). However, mounting evidence indicates cellular senescence extends beyond tumour suppression and suggests it is implicated in wound healing, tissue repair and ageing (Baker et al., 2008, Baker et al., 2011, van Deursen, 2014). The multifunction nature of senescent cells raises the question whether different senescence mechanisms are responsible for these different biological roles. In the following sections the causes and types of senescence will be discussed, however, the main focus will be on the role of senescence in ageing and how it contributes to age related pathologies.

1.6.1 Causes of senescence

To date, very little is known about the causes and effector pathways that might initiate senescence where these studies mostly rely on cell cultures of *in vitro* models. In addition to telomere dysfunction, a variety of other stresses have been found to induce *in vitro* growth arrest including DSBs and ROS (Von Zglinicki, 2002) (Figure 1.8). Similar to

telomere damage, DSBs and ROS activate DDR in which ATM prevents cell-cycle progression by maintaining the cell cycle check protein p53 which will in turn activate the cyclin-dependant kinase inhibitor p21 (van Deursen, 2014). However, senescence can be initiated in response to other causes that are DDR-independent such as E2F3 activation which is another cell cycle check protein that involves stimulation of p16 (Denchi et al., 2005).

Although the relative association of p53/p21 and p16 in initiating growth arrest can vary depending on the source, both pathways might engage during cellular senescence. For instance, DDR will activate senescence through the p53/p21 pathway, however if the DNA lesion persists, p16 is activated via ROS production (Passos et al., 2010, Freund et al., 2011).

While the current research focusses on *in vitro* models to understand the senescence phenomenon, a limited number of studies have been conducted using animal models. A study performed by Baker et.al (2013) group using a progeroid mouse model showed elevated levels of p53, p21 and p16 that were

associated with overall mouse developmental decline (Baker et al., 2008, Baker et al., 2013). *In vitro* studies using genetic knock-out mice of the p16 cell cycle check protein showed that p16 is associated with senescence and ageing (Baker et al., 2008).

One of the main limitations of using a cellular model to study senescence is the number of stresses that the cells are exposed to. Traditionally, a single stimulus is introduced to *in vitro* models which does not completely mimic biological systems where senescence is triggered through multiple stimuli such as genotoxic and mitotic stresses; where it is widely agreed that senescence in higher vertebrates is a multi-factorial process (Siegel and Amon, 2012, López-Otín et al., 2013).

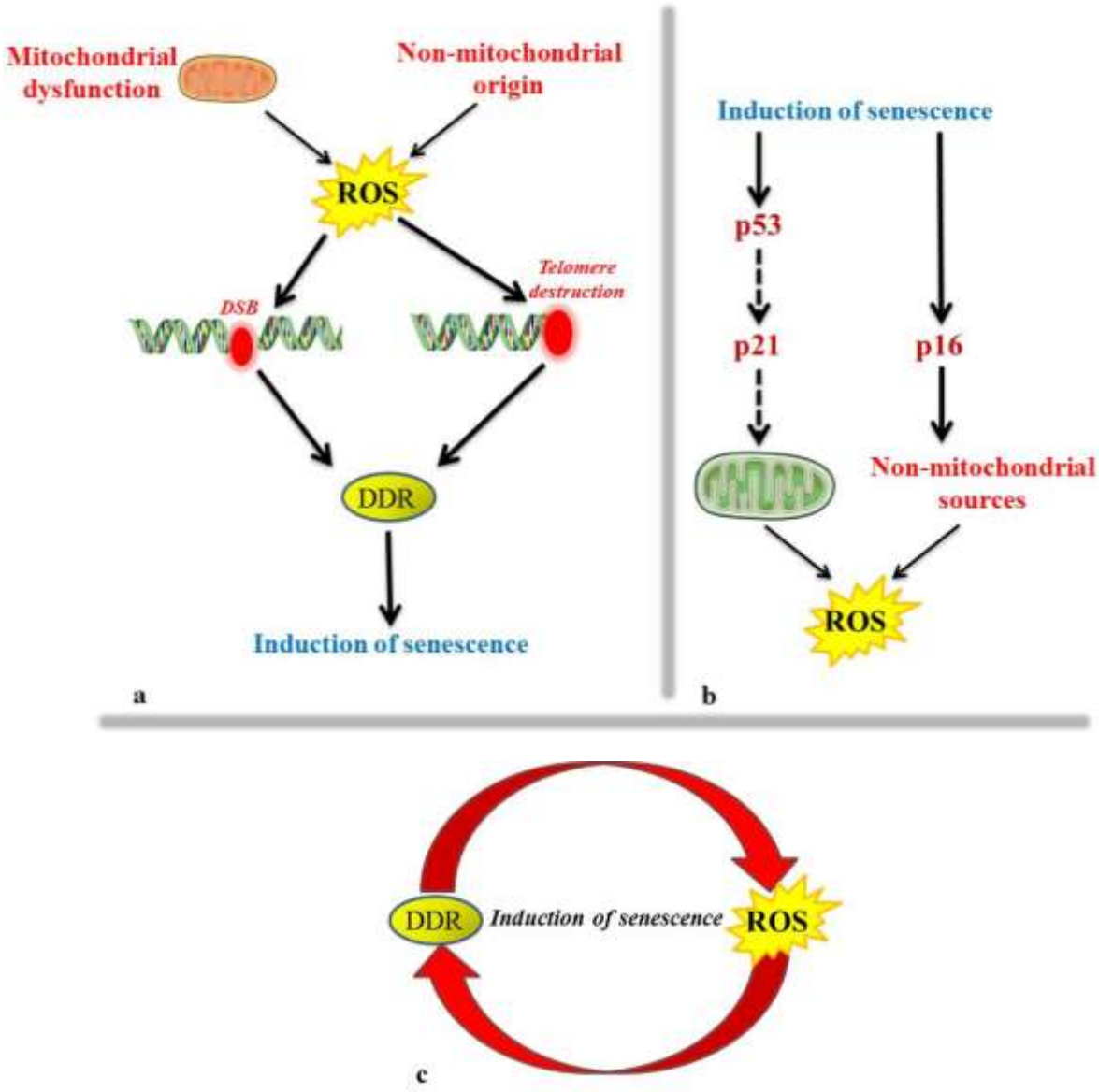

Figure 1.8: The implication of ROS on senescence induction. (a) Oxidative stress that is associated with increased ROS production can arise from dysfunctional mitochondria as well as other non-mitochondrial sources. This leads to genomic DNA damage as well as telomere shortening, both of which activate DDR pathways. Persistent DDR stimulates cell cycle check proteins that are known to be associated with senescence induction. (b) Cell cycle arrest is tightly regulated by activation of p53 pathway in which prolonged p53 elevation activates p21. Another major pathway involved in senescence induction and which is DDR-independent, is the p16 pathway. However, overlap between the two pathways will likely occur downstream to maintain senescence growth arrest. ROS mediated senescence induction increases ROS production from mitochondrial and non-mitochondrial sources. (c) Generation of excessive ROS and DDR activation will create a feed-back loop into those two elements where increased ROS production will potentially activate DDR by which unrepaired genome will compromise cell ability to proliferate and drive the cell into senescence

1.6.2 Senescence associated secretory phenotype (SASP)

Until recently, it was thought that senescence is the fixed endpoint of cell proliferation where the senescent cell loses its function. However, a growing number of papers suggest that senescent cells are active, dynamic and functionally altered cells (Purvis et al., 2012). Induction of senescence has been shown to be tightly associated with oxidative stress, genomic and proteomic change in biological systems. Among the set of genes that are transcriptionally altered in senescence are genes encoding for proteases, cytokines, chemokines and growth factors, which all have proinflammatory properties and ultimately can cause changes to tissue structure and function. The increased secretion of some or all of the above mentioned proteins by a senescent cell is referred to as the senescence-associated secretory phenotype (SASP) (Campisi, 2005, Coppé et al., 2008, Rodier et al., 2009). The SASP has been demonstrated in many cell types including fibroblasts, endothelial cells and astrocytes (Salminen et al., 2011).

To date, not much is known about the mechanism underlying SASP activation, however, it is thought that the SASP is triggered by ROS mediated DDR which feeds into a positive loop (Figure 1.6,c). Interestingly, not all types of cellular senescence are associated with SASP, for example independent DDR mediated growth arrest which involves the activation of p16 does not produce SASP, suggesting the presence of DDR-independent kinetics (Kaplon et al., 2013). Also, SASP secreted factors vary from one cell type to another depending on the stimulus. This flexibility within the SASP likely reflects both the diversity between biological cells, the specific cell types, and the specific stressor (van Deursen, 2014). Having said that, cytokines and chemokines are SASP factors that are highly conserved between cells of different types and stimulus, indicating the involvement of immune system and establishment of a proinflammatory response as an important characteristic of SASP-associated cellular senescence (Coppé et al., 2008). However, accumulation of senescent cells is not always associated with the involvement with the

immune system (Benz et al., 1991). Most experimental observations regarding the SASP and its characteristics were obtained from tissue culture models and to date, very little is known about the role of the SASP in higher biological systems. Thus, to understand the SASP phenomenon in these systems, *in vivo* studies should be conducted to determine the role of SASP in different pathologies.

1.6.4 Senescence in ageing and age-associated diseases

The lack of specific markers for cellular senescence has greatly hindered the efforts characterising the senescent cells that develop *in vivo* in different biological tissues and organs. The most reliable growth-arrest detection methods that are currently used to define the characteristic changes associated with senescence are elevated expression and activation of p53, p16, p21; detection of senescence-associated β-galactosidase activity and DSBs foci that are associated with phosphorylated γ-H2AX (van Deursen, 2014). The use of such markers reveals the accumulation of senescent cells in rodents and humans with age (Herbig et al., 2006, Jeyapalan et al., 2007). Additionally, studies have shown the presence of senescent cells at sites of injuries that are related to certain pathologies, such as AD (Naylor et al., 2012, Campisi, 2013), which provide evidence that senescence is associated with ageing and age related pathologies.

Several mechanisms have been proposed regarding the accumulation of senescent cells and cellular dysfunction in chronic age-associated diseases. One of these mechanisms is the involvement of the SASP in which chemokine and protease secretion is increased which disrupts tissue homeostasis and subsequently causes the destruction of the extracellular matrix. It is thought that the SASP will also affect adjacent cells by inducing paracrine senescence in healthy neighbouring cells through the secretion of growth factors and chemokines (Nelson et al., 2012, Acosta et al., 2013).

In recent studies of ageing, astrocyte pathology has been shown to associate with tissue pathology and have been shown to be highly susceptible to injury in the presence of

chronic stress during the ageing process (Salminen et al., 2011). However, the effect of stressed astrocytes in promoting the SASP is yet to be defined. Studies have shown the increased expression of TNF-α, IL-1β and IL-6by astrocytes, but not neurons or microglia, in the cortex of a rat model with ageing (Campuzano et al., 2009). *In vitro* studies have shown astrocytes can initiate different senescence pathways in response to different types of stressors, where induction of oxidative stress and exhausted passaging increase the expression of p16 and β-galactosidase activity (Bitto et al., 2010). These studies indicate that astrocytes can adopt a SASP phenotype and highlight the need for further research to understand the astroglial effect on ageing and age related pathologies.

1.7 Hypothesis to this study

This study will test the hypothesis that DNA damage dysregulation contributes to the pathogenesis of WML by altering the transcriptome, leading loss of glial cell function, and through activation of cell-injury/apoptotic mechanisms leading to senescence and cell death (Figure 1.9).

1.8 Aims of the study

The study will determine:

1. The population-variation and nature of DNA damage in glial cells in white matter and in WML

2. Whether increased DNA damage/ damage responses occur in WML

3. Whether this is associated with the induction of senescence and cell death pathways

4. Whether there is a field effect of wide-spread DNA damage in WM in lesional brains

The project is based on human autopsy brain tissue, derived from the MRC CFAS where a population based study is used to examine neuropathological basis of dementia.

Expression of DNA damage/response apoptosis and senescence related molecules will be determined by immunohistochemistry of control, lesional (DSCL) and non-lesional WM cases. One of the main points of investigation in this project is to study the early forms of pathology associated with oxidative stress in the areas that are free of lesions in a lesional brain; and for this, DSCL were selected over PVL since the area of deep WM is anatomically. PVL are associated with a small area with a restricted anatomical location adjacent to the ventricles, making it very difficult to find NAWM that is also surrounding the ventricle.

Evidence of DNA damage will be assessed and correlated to histological findings using molecular methods including qPCR arrays and Western blotting.

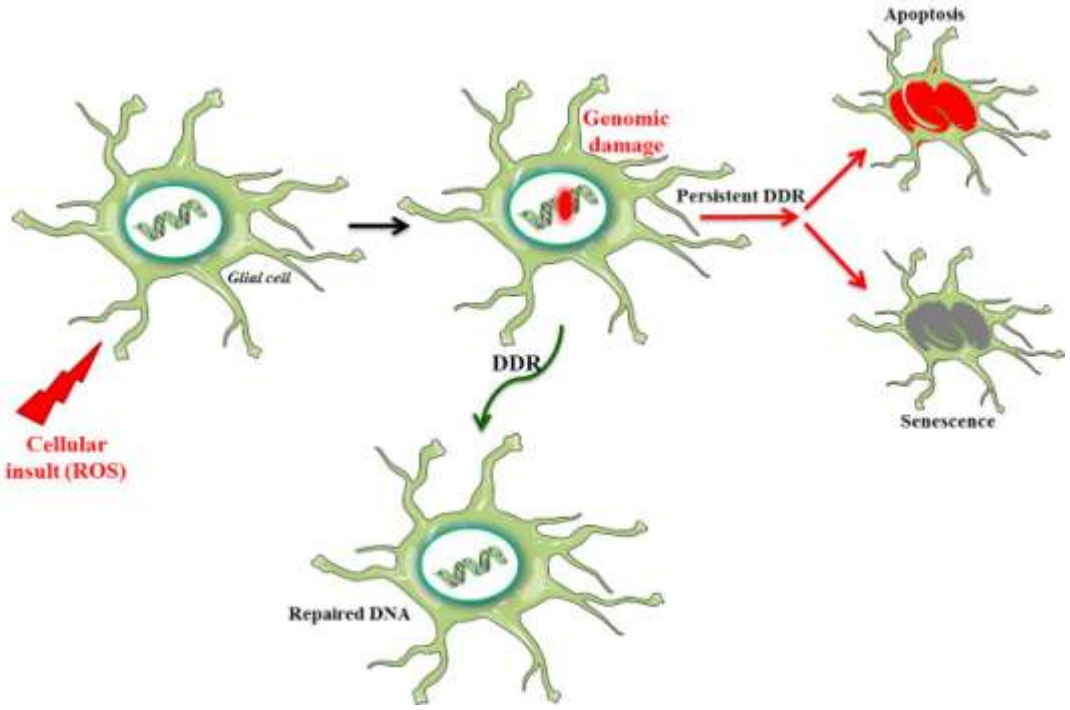

Figure 1.9: Hypothesis of the current project. Oxidative stress is a major cellular insult that can cause genomic damage (DSBs). As a consequence, DDR is activated to repair the damaged DNA. However, if the damage to DNA persists, loss of vital cell functions might occur and the glial cell will be potentially driven to apoptosis and/or senescence

CHAPTER 2: MATERIALS AND METHODS

2.1 Materials

2.1.1 Commonly used chemicals

All commonly used chemicals were purchased from Sigma-Aldrich (Poole, UK) or Thermo Fisher Scientific Inc. (Loughborough, UK), Analytical grade solvents including ethanol, methanol, formaldehyde and xylene were purchased from Fisher Scientific (UK). Pipette tips were purchased from Fisher Scientific (UK). Nuclease free water was purchased from Ambion, USA.

For histochemistry Haematoxylin and Eosin stains were purchased from Leica (UK) and luxol fast blue (LFB) from Sigma (UK). For immunohistochemiatry Vectastain Elite ABC kits for mouse IgG and rabbit IgG, peroxidase substrate kit and alkaline phosphatase substrate kit were purchased from Vector Laboratories (UK).
Slides, coverslips and mounting media (DPX) were supplied by Leica (UK).
Image capture of stained sections was performed using both BX61 upright microscope supplied by Olympus (UK) and Nikon Eclipse (80i) microscope (UK).
The Olympus Cell^R image analysis system was used to quantitatively assess immunoreactivity when applicable.

β-galactosidase histochemical staining kit was purchased from Sigma (UK).

2.1.2 Western blotting

For Western blotting (WB), Tissue was homogenised manually using tissue homogeniser (Anachem, UK). Cell lysis was performed using a sonicator. Bradford assay was performed to determine protein concentration, with reagents and protein standards purchased from Thermo Scientific (UK). Sodium dodecyl sulfate polyacrylamide gel (SDS-PAGE) was prepared using SDS from Melford Laboratories (UK), ammonium persulphate (APS) from Sigma (UK), 30% acrylamide from National Diagnostics (UK) and

Tetramethylethylenediamine (TEMED) from Melford Laboratories (UK). Filter papers purchased from Whatman Laboratories (UK). Polyvinyl difluoride (PVDF) Immobilin transfer membrane was purchased from Millipore (US). Anti-mouse and anti-rabbit secondary antibodies were from DakoCytomation (Denmark). Protein molecular weight marker was Precision plus protein dual colour standards (Bio-Rad, UK). An enhanced chemiluminescence (ECL) kit for chemiluminescence based-immunodetection of horseradish peroxidase (HRP) was purchased from Biological Industries (UK). G:box was used for membrane development, (Syngene,UK).

2.1.3 RNA extraction

For RNA extraction the Direct-zol RNA MiniPrep kit supplied by Zymo research (UK) or Tri-zol reagent supplied by Ambion (UK) was used. Isolated RNA quality was checked using Nano chips from Agilent RNA 6000 Nano kit (UK). RNA concentration was measured on the Nanodrop Spectrophotometer (ND1000) supplied by Labtech International (UK).

2.1.4 qPCR array

An initial screen was performed using randomly selected samples from CNL, CL and DSCL RNA extract on a commercially available 96 well RT-qPCR array plate. The plate was probed with 81 genes that are known to be implicated in DNA damage response and in senescence/cell cycle check. The result showed an alteration in a number of genes in between the three groups of WM, and for this, a selection of genes was made to customise 96 well qPCR array plate which contained only the genes of our interest, along with the housekeeping and quality control genes (Qiagen-UK) (Table 2.1).

cDNA was synthesised using RT first strand kit supplied by Qiagen (UK). Thermo-cycler was supplied by Quanta Biotech (UK). SYBR Green master mix, PCR plates and sealing caps were purchased from Qiagen (UK).

Table 2.1: Selected genes for qPCR study

Symbol	*Description*
ALDH1A3	Aldehyde dehydrogenase 1 family, member A3
AKT1	V-akt murine thymoma viral oncogene homolog 1
ATM	Ataxia telangiectasia mutated
CDKN1A	Cyclin-dependent kinase inhibitor 1A (p21, Cip1)
CDKN1B	Cyclin-dependent kinase inhibitor 1B (p27, Kip1)
CDKN2A	Cyclin-dependent kinase inhibitor 2A (melanoma, p16, inhibits CDK4)
CHEK2	CHK2 checkpoint homolog (S. pombe)
GSK3B	Glycogen synthase kinase 3 beta
IGF1	Insulin-like growth factor 1 (somatomedin C)
IGFBP3	Insulin-like growth factor binding protein 3
MAP2K6	Mitogen-activated protein kinase kinase 6
PIK3CA	Phosphoinositide-3-kinase, catalytic, alpha polypeptide
SERPINE1	Serpin peptidase inhibitor, clade E (nexin, plasminogen activator inhibitor type1), member 1
TGFB1	Transforming growth factor, beta 1
TP53	Tumor protein p53
H2AFX	H2A histone family, member X
OGG1	8-oxoguanine DNA glycosylase
PCNA	Proliferating cell nuclear antigen

2.1.5 DNA extraction

DNA extraction from whole tissue human brain samples was performed as part of sample preparation for Mass spectrometry experiments using QIAmp DNA mini kit (Qiagen, UK).

2.1.6 DNA hydrolysis

For DNA hydrolysis, DNA degradase plus kit, purchased from Zymo research (UK) was used. DNA degradase plus contains endogenous Alkaline phosphatase which hydrolyse genomic DNA into individuals nucleoside component (lacking the negatively charged phosphate). This makes the degraded DNA ideal for whole genome DNA analysis by LC/MS.

2.1.7 Mass spectrometry

For Mass spectrometry, ESI-Mass spectrometry was performed using an ultrahigh resolution time-of-flight (UHR-TOF) mass spectrometer (maXis, Bruker Daltonics) and an ion trap mass spectrometer (HCT Ultra PTM Discovery System, Bruker Daltonics) coupled with an online capillary liquid chro-matography system (U3000 Dionex, UK) which was set to perform data acquisition in the negative mode with a selected mass range of 110−500 m/z. The ionisation voltage of -3500 V was set to maintain capillary current between 30−50 nA. The temperature of nitrogen was set to 120°C at a flow rate of 4.0 L/h and N2 nebuliser gas pressure at 0.4 bar.

2.1.8 Solutions

Washing reagents:

50mM Phosphate buffered saline (PBS)

3.2mM Na_2HPO_4

0.5mM KH_2PO_4

1.3mM KCl

135mM Nacl, pH 7.4

PBS-Tween (PBST)

0.05% (v/v) Tween-20 (Sigma, UK) in 50mM PBS

50mM Tris-buffered saline (TBS)

50mM Tris

150mM NaCl, pH 7.6

TSB-Tween (TBST)

0.1% (v/v) Triton X-100 in 50mM TBS

Western Blotting (SDS-PAGE) solutions:

10% Sodium Dodecyl Sulphate (SDS)

10% (w/v) SDS in deionized water

Running buffer (10x)

144g Glycine

30.2g Tris

10g SDS in 1L of water

Transfer buffer (10x)

144g Glycine

30.2g Tris in 1L of water

Resolving buffer (4x)

1.5M Tris-HCL

0.4% (w/v) SDS

8% Resolving gel, pH 8.8

8% (w/v) acrylamide

25% (v/v) resolving buffer

0.01% (w/v) ammonium persulphate (APS)

0.1% (v/v) N,N,N',N' tetramethylethylenediamine (TEMED)

12% Resolving gel, pH 8.8

12% (w/v) acrylamide

25% (v/v) resolving buffer

0.01% (w/v) ammonium persulphate (APS)

0.1% (v/v) TEMED

Stacking buffer (4x)

0.5M Tris-HCL, 0.4% (w/v) SDS

4% stacking gel, pH6.8

4% (w/v) acrylamide

25% (v/v) stacking buffer

0.075% (w/v) APS

0.1% (v/v) TEMED

10% Ammonium Persulphate (APS)

0.9g APS in 9ml deionized water

Laemlli sample buffer (2x)

1.5M Tris-HCL

4% (w/v) SDS

100mM dithiothreitol (DTT)

20% (w/v) Glycerol,

0.02% (w/v) Bromophenol blue (Fisher Scientific)

Blocking buffer

5% (w/v) powdered milk in PBS-Tween (0.05%)

Immunohistochemistry solutions:

Trisodium Citrate buffer (TSC)

3g of $Na_3C_6H_5O_7$, made up to 1L with deionized water, pH6.5

Ethylenediaminetetraacetic acid (EDTA) (x1)

10mM Tris-base

1.26 mM EDTA

0.1% Tween-20 (pH 8)

Blocking solution

1.5% (v/v) normal goat serum or 15% (v/v) normal horse serum (Vector Laboratories UK, antibody dependent) in 50mM TBST

Peroxidase blocking solution

1% (v/v) Hydrogen peroxide (H_2O_2) in 50mM Methanol

IHC antibody incubation solution

The required calculated concentration of the Ab diluted in 1.5% blocking solution

Avidin-biotin peroxidase complex

1.5% blocking solution

0.5% secondary

DAB solution

2 drops of solution A

2 drops of solution B, in 5mL of water

Histochemical staining for β-galactosidase

β-galactosidase staining mixture:

1mL of 10x staining buffer (pH6)

125µL of reagent B (400 mM Potassium Ferricyanide)

125µL of reagent C (400 mM Potassium Ferrocyanide)

250µL of preheated X-gal solution (40 mg/ml)

8.5mL of deionized water

Nuclear fast red counter stain:

0.1% nuclear fast red, 5% aluminium sulphate in deionized water

Whole tissue protein extraction:

Homogenisation buffer

10mM Tris HCL pH7.4

0.8M NaCl

1mM EDTA

10% sucrose $C_{12}H_{22}O_{11}$

0.1 mM phenylmethanesulfonylfluoride (PMSF) $C_7H_7FO_2S$

0.44ml of 10ml mini protease inhibitor cocktail tablet (Roche Diagnostics) to inhibit the action of serine, cysteine and metallo-proteases

DNA hydrolysis

DNA hydrolysis (Standard Reaction Setup, total volume of 25µl)

2 µl DNA at 500 ng/µl

2.5 µl 10X DNA Degradase™ Reaction Buffer

1 µl DNA Degradase Plus™ (5 units/µl)

19.5 µl ddH2O

Gel Electrophoresis

Tris Acetate-EDTA buffer (TAE)

40 mM Tris-acetate

0.01% glacial acetic acid

1mM EDTA (pH 8.0)

Mass spectrometry (MS) solutions

Buffer A:

0.4 M of 1,1,1,3,3,3,-hexafluoro-2-propanol (Aldrich, UK)

Triethylamine (Fisher Scientific, UK) to pH7.6

0.1mMtriethylammonium acetate.

Buffer B:

0.4 M of 1,1,1,3,3,3-hexafluoro-2-propanol

triethylamine to pH 7.6 containing 50% methanol

0.1 mM triethylammoniumacetate (Fluka, UK)

2.1.9 Antibodies

Table 2.2: Antibodies used in IHC study and their conditions

Antibody	*Species*	*Dilution and conditions*	*Antigen retrieval*	*Supplier*
8-OHdG	Mouse monoclonal	1/400 1 hour RT	Pressure cooker Access Revelation (x10, PH 6.5)	Abcam, UK
ɣH_2AX	Rabbit monoclonal	1/1000 1 hour RT	Pressure cooker EDTA pH8	R&D systems, UK
DNA-PK	Mouse monoclonal	1/400 1 hour RT	Pressure cooker EDTA pH8	Calbiochem, UK
GFAP	Rabbit polyclonal	1/1000 1 hour RT	Pressure cooker TSC pH6	Dako, UK
OSP	Rabbit polyclonal	1/250 1 hour RT	Pressure cooker TSC pH6	Abcam, UK
CD68	Mouse monoclonal	1/100 1 hour RT	10 min in microwave TSC pH6.3	Dako, UK
Collagen IV	Mouse monoclonal	1/500 O/N at 4ºC	10 min in microwave TSC pH6.3	Sigma, UK
p16	Mouse monoclonal	1/100 1 hour RT	Pressure cooker EDTA pH8	Bio-genex, USA
p53	Mouse monoclonal	1/50 O/N at 4ºC	Pressure cooker EDTA pH8	Santa-cruz, USA
p21	Mouse monoclonal	1/50 O/N at 4ºC	Pressure cooker TSC pH6	Abcam, UK

8-OHdG: 8-hydroxy-deoxy-guanosisne; **ɣ H_2AX:** Gamma Histone2AX; **DNA-PK:** DNA-protein Kinase; **GFAP:** Glial fibrillary acidic protein; **OSP:** Oligodendrocyte specific protein

Table 2.3: Primary Ab used in Western Blotting study

Antibody	*Species*	*Dilution*	*Source*
γH_2AX	Rabbit monoclonal	1/1000	R&D systems, UK
DNA-PK	Mouse monoclonal	1/1000	Abcam, UK
MDA	Rabbit polyclonal	1/1000	Cell biolabs, Cambridge, UK
β -actin	Mouse monoclonal	1/1000	Abcam, UK

Table 2.4: Secondary Ab used in Western Blotting study

Antibody	*Species*	*Dilution*	*Source*
Goat anti-mouse HRP	Mouse polyclonal	1/5000	Dako
Goat anti-rabbit HRP	Rabbit polyclonal	1/5000	Dako

2.1.10 Human central nervous system tissue

Post mortem human brain tissue was obtained from participants who were part of the MRC CFAS brain donation programme. Participants based around six centres were selected based on their age (65 and over) and not their medical history where they have undergone a baseline assessment and screening upon enrolment in CFAS. CFAS interview included a variety of questions such as level of education and occupation, questions on residence, social status and cognitive measurements (Mini mental state examination with augmentation). At death, a revision of dementia status was determined using information gathered from the respondents and their care-givers during the last years of life (Wharton et al., 2011; Fernando et al., 2006). Donated brains were retrieved after obtaining the permission from the care givers/ family of the respondents. Ethical approval has been given to the collection and use of post mortem CNS tissue at all six CFAS UK sites (a copy of the form is available in the appendix).

In the current study, brain tissue retrieved from Nottingham and Oxford (formalin fixed cohort) (Table 2.5) and from Cambridge centre (frozen cohort) (Table 2.6) were used to carry out the designed experiments (Table 2.7 and Table 2.8).

Table 2.5: Formalin fixed tissue demographic data

Case	*Centre*	*Sex*	*Age*
DSCL			
NP 75/98	Nottingham	M	86
RI 1050/96	Oxford	M	73
NP 115/96	Nottingham	M	89
NP 362/00	Nottingham	F	97
RI 1053/00	Oxford	M	82
RI 1079/00	Oxford	M	78
RI 1107/94	Oxford	M	83
RI 1150/95	Oxford	F	89
NP118/99	Nottingham	F	94
RI 1183/99	Oxford	F	88
NP137/01	Nottingham	F	82
NP138/01	Nottingham	F	92
NP162/01	Nottingham	F	90
NP242/96	Nottingham	F	85
NP46/99	Nottingham	F	75
Control(non lesional)			
RI 1106/98	Oxford	M	93
RI 1175/94	Oxford	M	68
NP 224/95	Nottingham	F	72
NP 253/97	Nottingham	M	86
NP 296/98	Nottingham	F	91
NP62/03	Nottingham	M	88
NP45/98	Nottingham	F	89
NP60/96	Nottingham	F	100
RI 1303/95	Oxford	M	74
NP104/96	Nottingham	M	84
NP274/95	Nottingham	F	72
NP279/95	Nottingham	F	73
NP561/00	Nottingham	F	87
NP728/99	Nottingham	F	80
Control(lesional)			
RI 03/03	Oxford	F	90
RI 1161/93	Oxford	M	71
RI 1194/99	Oxford	M	87
RI 1257/96	Oxford	M	85
RI 1268/97	Oxford	F	87
RI 1315/96	Oxford	M	85
RI 50/01	Oxford	F	90
RI 55/02	Oxford	F	86
RI 1192/93	Oxford	M	74
NP119/01	Nottingham	F	84

Table 2.6: Frozen tissue demographic data

Case	*Centre*	*Sex*	*Age*
DSCL			
RH36	Cambridge	F	92
RH43	Cambridge	F	87
RH54	Cambridge	M	89
RH55	Cambridge	F	101
RH57	Cambridge	F	86
RH67	Cambridge	F	78
RH69	Cambridge	F	95
RH75	Cambridge	F	74
RH91	Cambridge	M	89
RH96	Cambridge	F	87
Control (non lesional)			
RH22	Cambridge	F	89
RH33	Cambridge	M	87
RH44	Cambridge	M	95
RH52	Cambridge	F	89
RH59	Cambridge	M	87
RH06	Cambridge	M	88
RH63	Cambridge	M	75
RH66	Cambridge	M	81
Control (lesional)			
RH64	Cambridge	F	84
RH81	Cambridge	F	93

Table 2.7: Formalin fixed paraffin embedded tissue cohort and type of experiment

- **DSCL cohort:**

	Experiment		
DSCL Sample no.	***IHC (8-OHdG)***	***IHC (GFAP)***	***IHC (P16)***
75/98	✔	✔	✔
1050/96 M1	✔	✔	✔
115/96 A1	✔	✔	✔
362/00 A2	✔	✔	✔
1053/00 A2	✔	✔	✔
1079/00 A1	✔	✔	✔
1107/94 M2	✔	✔	✔
1150/95 M1	✔	✔	✔
118/99 A	✔	✔	✔
1183/99 M1	✔	✔	✔
137/01 M1	✔	✔	✔
138/01 M1	✔	✔	✔
162/01 A2	✔	✔	✔
242/96 A1	✔	✔	✔
46/99 P1	✔	✔	✔

- **CL cohort:**

	Experiment		
CL Sample no.	***IHC (8-OHdG)***	***IHC (GFAP)***	***IHC (P16)***
03/03 M1	✔	✔	✔
1050/96 A2	✔	✔	✔
1161/93 M1	✔	✔	✔
1194/99 M1	✔	✔	✔
1257/96 M1	✔	✔	✔
1268/97 M1	✔	✔	✔
1315/96 M2	✔	✔	✔
50/01 M1	✔	✔	✔
55/02 A2	✔	✔	✔
46/99 M1	✔	✔	✔
1192/93 A1	✔	✔	✔
1183/99 A1	✔	✔	✔
119/01 M1	✔	✔	✔

- **CNL cohort:**

	Experiment		
CNL Sample no.	***IHC (8-OHdG)***	***IHC (GFAP)***	***IHC (P16)***
1106/98 A1	✔	✔	✔
1175/94 A1	✔	✔	✔
224/95 M	✔	✔	✔
253/97 A	✔	✔	✔
296/89 P1	✔	✔	✔
62/03 A	✔	✔	✔
45/98 M1	✔	✔	✔
60/96 M1	✔	✔	✔
1303/95 A1	✔	✔	✔
1106/98 M1	✔	✔	✔
104/96 A	✔	✔	✔
274/95 A1	✔	✔	✔
279/95 M1	✔	✔	✔
561/00 M1	✔	✔	✔
728/99 P1	✔	✔	✔

Table 2.8: Cambridge frozen tissue cohort and type of experiment

- **DSCL cohort:**

	Experiment				
DSCL Sample no.	***RT-qPCR (whole tissue RNA extract)***	***WB (MDA)***	***WB (γH2AX)***	***WB (DNA-PK)***	***DNA isolation for MS***
RH36 H4	✔		✔	✔	✔
RH43 H5	✔	✔	✔	✔	✔
RH54 H5	✔		✔	✔	✔
RH55		✔			✔
RH57 H3					✔
RH67		✔			✔
RH69 H3		✔	✔	✔	✔
RH75 H9	✔	✔	✔	✔	✔
RH91 H5					✔
RH96 H3		✔	✔	✔	✔
RH81 B			✔	✔	✔

- **CL cohort:**

	Experiment				
CL Sample no.	***RT-qPCR (whole tissue RNA extract)***	***WB (MDA)***	***WB (γH2AX)***	***WB (DNA-PK)***	***DNA isolation for MS***
RH43 H3	✔		✔	✔	✔
RH54 H3		✔			✔
RH64 H3		✔			✔
RH69 H5		✔	✔	✔	✔
RH75 H4	✔	✔	✔	✔	✔
RH81 H3		✔	✔	✔	✔
RH96 H4			✔	✔	✔
RH36 H4B	✔		✔	✔	✔

- **CNL cohort:**

	Experiment				
CNL Sample no.	***RT-qPCR (whole tissue RNA extract)***	***WB (MDA)***	***WB (γH2AX)***	***WB (DNA-PK)***	***DNA isolation for MS***
RH22 H3	✔	✔	✔	✔	✔
RH33	✔	✔	✔	✔	✔
RH44 H5		✔			✔
RH52			✔	✔	✔
RH59 H4B		✔	✔	✔	✔
RH6	✔	✔	✔	✔	✔
RH63 H5		✔	✔	✔	✔
RH66		✔	✔	✔	✔

2.2 Methods

2.2.1 Brain retrieval and storage

Core information regarding the age, gender, pH, PMD of the WM blocks obtained from the Newcastle and Cambridge CFAS cohort, is shown in tables 2.5 and 2.6. Upon donation, one cerebral hemisphere was cut following a standard protocol (Fernando et al., 2004), snap frozen and coronal brain slices stored at -80ºC. The contralateral hemisphere was fixed in 10% buffered formalin for a minimum of four weeks, and 1cm coronal slices were taken for MRI analysis (Newcastle coronal brain map reference levels 10/12 (anterior), 19/20 (middle), and 24/25 (poseterior) (Fernando et al., 2006).

2.2.2 WML identification

2.2.2.1 MRI procedures

MRI analysis of WM pathology was previously completed to identify and categorise deep WML (Fernando et al., 2004). Full details of the study approach and tissue/data collection are described in chapter 1. The technique involved multiple formalin-fixed brain slices that were placed sealed in polythene bags and put in a custom built Perspex slice stack for magnetic resonance imaging. For additional stability and cleanliness, the slice stack was wrapped in cling-film (Figure 1.1from chapter 1)**.** Using pulse sequences previously optimized for studying post-mortem WML, MRI scans were performed on a 1.0-T machine (Siemens, Munich, Germany) with the following settings: T2-weighted spin echo (2500/98 ms; repetition time/echo time (TR/TE) excitations, proton density (2500/25 ms) and T1-weighted inversion recovery image (TR 6838 ms, inversion time (TI) of 600 ms with a TE of 60 ms) (Fernando et al., 2006). Lesions were rated by 2 independent radiologists blind to any clinical or neuropathological information. WML were agreed to be present if hyperintensities were detected on T_2 weighted images as well as on the proton density images. A modified Schelten's semi-quantitative scale was used to rate the hyperintensities

present in the deep subcortical WM (DSCL) and periventricular WM (PVL) which provides more detailed insight with good inter- and intra-observer reliability (Scheltens et al., 1992). Research in the current study focussed on DSCL and non-lesional WM from both lesional and non-lesional brains, as approximately 95% of ageing brains contained PVL and hence few cases (<5%) had no periventricular pathology. WM MRI scans were rated blind to any clinical condition and were based solely on the presence/absence of radiologically detected WML. Three groups of WM were identified (Figure 2.1):

1. Control WM sampled from control, non-lesional brains (hereafter referred to as 'Control Non-Lesional' (CNL))
2. normal appearing white matter from cases with MRI-detectable lesions (hereafter referred to as 'Control Lesional' (CL))
3. DSCL, which are the actual deep WML

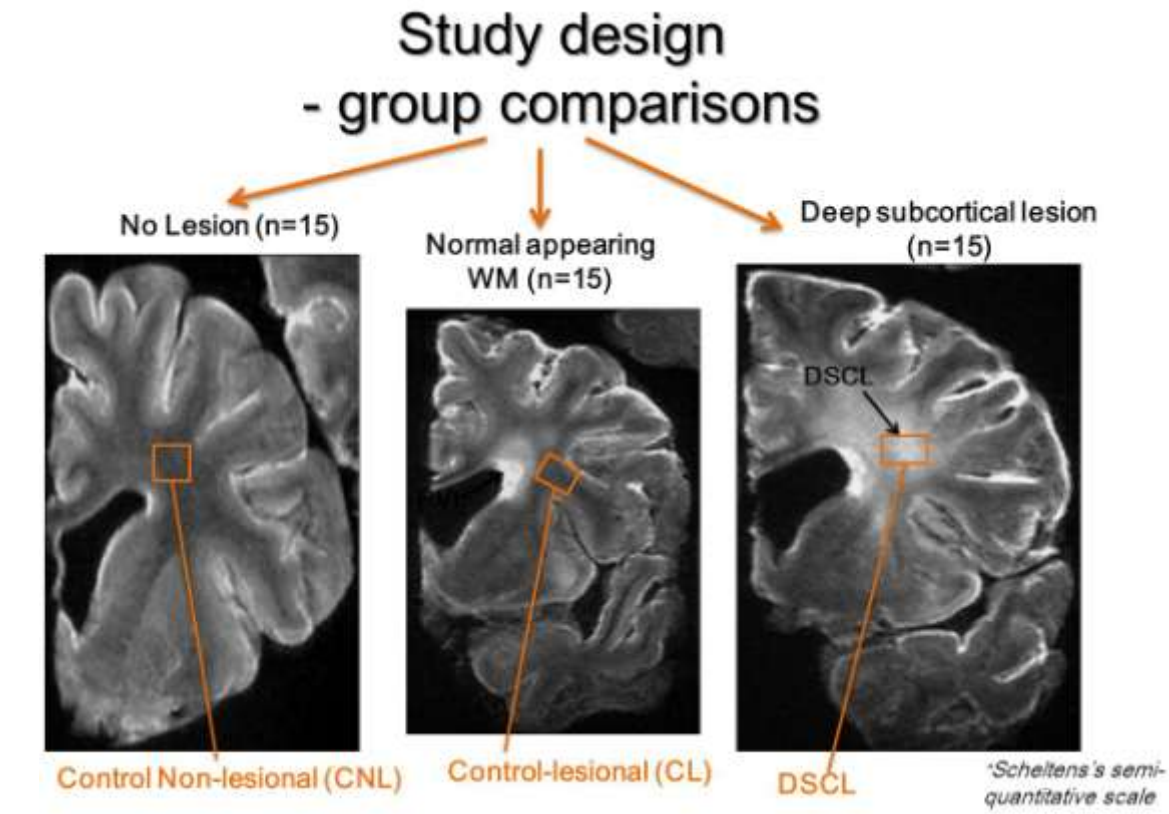

Figure 2.1: Categorising WM in the assistance of *post-mortem* MRI scans. WM was categorised into three groups: 1. control non-lesional (control brains free of lesions). 2. Control brains (areas free of lesions from a lesional brain). 3. Deep sub-cortical lesions (actual WML retrieved from the deep WM)

2.2.2.2 Histology and immunohistochemistry

Tissue sampling of the WM from formalin fixed coronal brain slices was guided by the MRI scans to create paraffin blocks (Figure 1.2 from chapter 1). For frozen tissue sectioning, MRI scans of the formalin fixed contralateral brain hemispheres were used as a guide to map NAWM and DSCL since WML are thought to be distributed symmetrically between the two brain hemispheres (Fernando et al., 2004). Histological interrogation of WM was essential to confirm the lesion/non-lesional white matter had been sampled and to ensure accurate categorisation of WM. Previous studies in CFAS (Simpson et al, 2007; Fernando et al, 2004) have demonstrated DSCL show severe myelin attenuation and the presence of large numbers of amoeboid microglia when compared to both CL and CNL, which have better preserved myelin and microglia with a resting, ramified morphology.

All formalin fixed paraffin-embedded (FFPE) and frozen tissue were initially stained with Haematoxylin and Eosin, CD68 (which was the microglial marker of choice and was previously used by the study group) and LFB to confirm the MRI categorisation of WM. H&E stain revealed the morphology of glial cells and the histological anatomy of the section. CD68 (microglial marker) was used to identify areas of increased microglial phagocytic reactivity (amoeboid microglia) (DSCL) and to distinguish them from WM containing ramified microglia (CL and CNL).

MRI hyperintensities representing a lesion was visualised histologically as severe loss of myelin by LFB staining when compared to the intact myelin seen in CNL sections. Together, those three parameters (H&E and LFB staining, IHC with CD68) enabled us to map DSCL, CL areas and match them to corresponding MRI scans while proofing the absence of any lesions in healthy control brains.

2.2.3 Immunohistochemistry

2.2.3.1 Tissue preparation

6µm sections from FFPE were collected onto positively charged slides and dried overnight in an oven at 37ºC. Prior to staining, FFPE sections were dewaxed by placing them in two changes of xylene for 5min each, followed by tissue rehydration to water through immersion in a graded series of alcohol (100% EtOH for 5min, 100% EtOH for 5min, 95% EtOH for 5min, 70% EtOH for 5min) followed by a 5min incubation in d.H_2O. Endogenous peroxidase activity was supressed by placing the sections in 3% H_2O_2/methanol for 20min at room temperature (RT). Sections were rinsed in d.H_2O prior to immunostaining. Antigen retrieval was an essential step for the preparation of FFPE tissue for staining. It is performed after placing the tissue in 3% H_2O_2. This treatment of tissue will detach clusters of polymers that have formed from formalin particles on the tissue's antigen binding sites. The longer the tissue is embedded in formalin, the more complex the clusters become. Inadequate Ag retrieval will remain some clusters that will shield the Ag binding site and prevent the Ab of the stain of our interest from attaching to it. Several approaches of Ag retrieval were available in the lab and part of Ab optimisation, the best one is chosen to be used for FFPE tissue treatment. One of the methods of Ag retrieval is to put the tissue in 0.01M Tri-sodium citrate (pH 6.5) in the microwave for 10min. Another approach is to place the tissue in pressure cooker in 0.01M Tri-sodium citrate (pH6) for 1min incubation where the tissue is let to cool down for approximately an hour after that before the rest of staining steps are completed.

Since frozen sections were not placed in formalin, no Ag retrieval was required. Sections (5µm) were collected onto charged slides, warmed to room temperature (RT) for 5min, fixed in ice-cold acetone at 4^{O}C for 10 minutes and air dried for 5min prior to immunostaining.

2.2.3.2 Antibody optimization

All antibodies used in this study were optimised prior to staining of the cohort. Recommended conditions from the manufacturer and previous CFAS studies were used as a guide in the addition to a range of antibody concentrations with a comprehensive variety of antigen retrieval conditions. Two independent observers (S.M and S.W) assessed the staining and identified optimal antibody conditions (Table 2.2) which resulted in specific antibody staining with minimal non-specific background staining.

2.2.3.3 IHC for formalin fixed, paraffin-embedded tissue (FFPE)

IHC was performed using a standard avidin-biotinylated enzyme complex (ABC) method (Vector Laboratories, Peterborough, UK) (Table 2.2). Following antigen retrieval (Table 2.2), non-specific binding was minimised by incubating sections in 1.5% species specific relevant normal serum for 30min at RT. Then, sections were incubated with the desired primary antibody at its optimum dilution (Table 2.2). Parallel incubations of an isotype control with a concentration equal to the highest antibody IgG concentration were carried out to confirm the specificity of the staining pattern. Tissue incubation in the absence of the primary antibody was also used as negative control. *Post-mortem* cortical tissue of a previously confirmed Alzheimer disease case was used as a positive control. All three controls were included in each and every immuno run.

Following the blocking step, excess blocking solution was removed by tapping the slide and the section was then incubated with the optimal concentration of primary antibody for 1h at RT. Sections were then washed in TBS buffer and incubated at RT for 30min in 0.5% of the relevant biotinylated secondary antibody. After another thorough wash with TBS for 5min at RT, sections were incubated in avidin–biotin complex solution (Vector Laboratories, made at least 30min before use) for 30min at RT, followed by a TBS wash and addition of the peroxidase enzyme substrate 3–3 diaminobenzidine solution (DAB). The

reaction was stopped by washing the sections with deionized water; typically after 5min. Sections were counterstained in haematoxylin, dehydrated through a graded series of EtOH (70%, 95%, 100%) and cleared in xylene, before being mounted with DPX.

2.2.3.4 IHC for frozen tissue

Despite for a comprehensive range of antigen retrieval methods (including microwave, pressure cooker and enzyme digest retrieval techniques), the commercially available antibodies used to detect DNA damage response did not work consistently on the CFAS FFPE cohort; therefore, frozen sections from the contralateral hemisphere were used.

Following fixation in ice-cold acetone (4ºC) for 10min, frozen sections were blocked in 1.5% relevant normal serum at RT for 30min, incubated with the primary antibody for 60min at RT (γH2AX 1:1000 for 60min at RT) followed by a thorough wash with TBS. As for the FFPE protocol outlined above, the horseradish peroxidase conjugated avidin–biotin complex method was used (Vectastain Elite kit, Vector Laboratories, UK). Where the antibody had bound to the section was visualised by incubating the sections with 3–3 diaminobenzidine solution (DAB) as the chromagen (Vector Laboratories) for 5min. The reaction was stopped by a thorough wash of sections with distilled water. Sections were then counterstained with haematoxylin, dehydrated, cleared in xylene and mounted in DPX, as outlined above. Relevant positive, negative and isotype controls were included with every run.

2.2.3.5 Haematoxylin and Eosin stain

Although MRI is a reliable tool to detect severe myelin loss, it has potential limitations in detecting mild myelin attenuation and cannot detect cellular changes with respect to WM pathology (Fernando et al., 2004). Therefore, basic histological techniques were employed to assess WM and WML pathology and confirm the relevant WM had been

sampled correctly. Heamatoxolyn and Eosin (H&E) stain was performed to investigate the basic pathology of the WM.

Sections were de-waxed in two changes of xylene for five minutes at RT, followed by rehydration through a graded series of alcohol (100% EtOH for 5min, 100% EtOH for 5min, 95% EtOH for 5min, 70% EtOH for 5min) followed by a 5min incubation in d.H_2O. Sections were placed in Haematoxylin for 2 min, rinsed in water, blued in Scott's tap water for 2 min, rinsed in water, stained with Eosin for 5min, rinsed in water, dehydrated through a graded series of alcohol before cleared xylene and mounted in DPX.

2.2.3.6 Luxol fast blue

Luxol Fast Blue (LFB) stain was performed to confirm myelin loss in radiologically-identified lesions where severe myelin attenuation was predicted.

Sections were dewaxed in two changes of xylene for five minutes and rehydrated through a graded series of alcohols (100% EtOH for 5min, 100% EtOH for 5min, 95% EtOH for 5min, 70% EtOH for 5min) followed by a 5min incubation in d.H_2O. Sections were then placed in pre-warmed LFB at 60^{o}C for two hours. This was followed by dipping sections in % 95 alcohols for 15 seconds before rinsing in deionized water. For differentiation, sections were then placed in freshly prepared lithium carbonate for 30 seconds followed by dehydration through a graded series of alcohol before being cleared in xylene and mounted in DPX.

2.2.3.7 Double-label immunohistochemistry

Double-staining experiments to co-localise DNA damage (8-OHdG) with cellular phenotype: GFAP [glial fibrillary acidic protein, astrocytes], CD68 (microglia), OSP [oligodendrocyte specific protein, oligodendrocytes], CollIV (collagen IV, vessels) were carried out on selected representative FFPE cases from the three groups.

Staining with the first primary antibody (8-OHdG) was performed using the IHC FFPE protocol as outlined above. Following visualisation of oxidative damage using DAB chromogen, sections were placed in TBS buffer and then incubated with 1.5% relevant normal sera for 1 hour at RT before they were incubated with avidin-biotin blocking kit (Vector Laboratories) sequentially at RT for 15min in avidin solution and then biotin solution, according to the manufacturer's instructions. Sections were then incubated with the second primary antibody of interest (GFAP, CD68, OSP, collagen IV) at 4°C over night (Table 2.2). Sections were washed thoroughly with TBS buffer and incubated with the relevant biotinylated secondary antibody, followed by streptavidin-TRITC (1:100 in TBS) for an hour at RT in the dark. Sections were rinsed in TBS, air dried in the dark and mounted with Vectamount containing DAPI (Vector Laboratories). Sections were stored in the dark at 4°C and visualised in bright field to view oxidative damage (8-OHdG) and a fluorescent field to co-localise the damage with specific cellular phenotypes. Image capture was performed using Cell^R (Olympus Biosystems, Watford, UK) and Leica DMI4000B, UK. Co-localisation of staining was analysed using Corel Paint Shop Pro X (Corel, Maidenhead, UK).

2.2.3.8 Histochemical staining for β-galactosidase

β-galactosidase (β-gal) is hydrolase enzyme that catalyzes the hydrolysis of β-galactosides into monosaccharides (Cristofalo, 2005). The presence or absence of an active β-galactosidase can be detected by X-gal (an organic compound consisting of galactose linked to a substituted indole) which produces a characteristic blue dye when cleaved by β-galactosidase.

Prior to use, all components of the β-galactosidase histochemical staining kit were thawed on ice and the X-gal solution heated to 37ºC for one hour (for activation). The frozen sections were warmed to RT for 5 minutes , fixed in ready-made fixation solution for 6 minutes at RT followed by three rinses in 1x PBS. Freshly prepared staining mixture was

then added, the sections were covered with parafilm and the sections were incubated overnight at 37°C. Sections were rinsed in TBS, counter stained with nuclear fast red for 30 seconds followed by a rinse in deionized water before they were dehydrated, cleared and mounted in DPX.

Senescence associated β-gal (SA- β-gal) activity was microscopically detected by the presence of a blue, insoluble precipitate within the cell.

To determine if SA-β-gal activity was associated with astrocytes, GFAP stained sections (using a standard ABC method) were double labelled with β-gal. Similarly, to determine the associations of SA-β-gal activity with cell cycle check point, p16 immunolabelled frozen sections (using ABC kit) were double labelled with β-gal.

To determine if SA-β-gal activity was associated with other types of glia, the SA-β-gal stained sections were stained with oligodendrocyte marker (OSP) and with microglial marker (CD68) using the Alkaline Phosphatase kit and the signal was visualized with Vector Red (Vector Laboratories) as substrate.

2.2.3.9 Quantification of 8OHdG immunostaining

Regions ofWM (DSCL, CL and CNL) were identified using LFB and CD68 reactivity as a guide, and mapped onto consecutive 8-OHdG immunostained slides. Within these regions of interest, images of 5 random fields were captured at x20 magnification using Nikon Eclipse (80i) microscope. Images were then transferred to power point programme where a grid had been overlaid on each image (Figure 2.2) and they were then assessed by two independent observers (Sufana Al-Mashhadi and Julie Simpson). The total number of 8-OHdG positive nuclei (reflecting DNA oxidation) was counted proportionally to the number of total number of nuclei present in the field. Cytoplasmic staining was not taken into account.

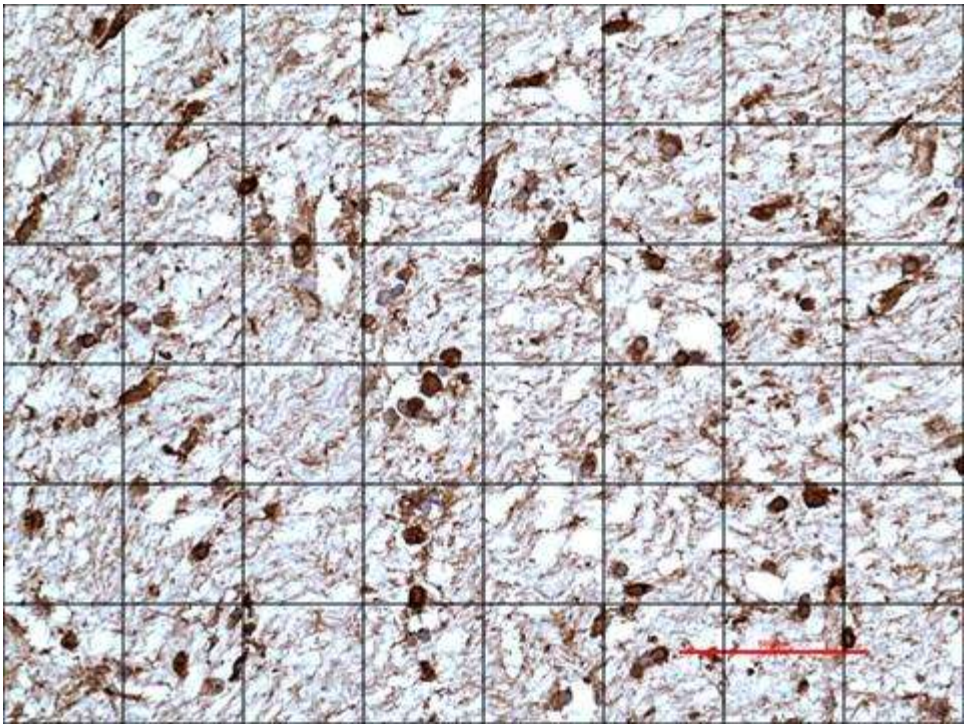

Figure 2.2: 8-OHdG scoring. A method has been developed to score the 8-OHdG staining which involved laying a grid using the power-point programme which facilitated the precise cell count. Scale bar=100μm

2.2.3.10 Image analysis of GFAP and p16

The Olympus CellA^R analysis system was used to calculate the percentage area immunoreactivity of GFAP and p16 in all three groups of WM. Again, CD68 and LFB were used to the white matter regions of interest on GFAP andp16 immunostained slides. Images of 5 random fields in the shape of a cross were captured at x40 magnification using BX61 upright light microscope. Images were then transferred to CellR image analyser soft-ware where the percentage area of immunoreactivity was calculated for each image.

2.2.3.11 Statistical analysis of immunohistochemical staining

Statistical analyses were performed using PASW Statistics 10 software. 8-OHdG, GFAP and p16 data did not show equality of variances between three groups and were not normally distributed; therefore, non-parametric statistical methods were applied. The level of oxidative DNA damage, gliosis and cell cycle check point activation between groups were compared using Kruskal–Wallis Test. In the case of a significant result, post hoc pairwise comparisons were performed using the Mann Whitney *U*-test with correction for multiple testing using the Bonferroni method.

The percentage area of both GFAP andp16 immunoreactivity were scored individually but the statistical analysis was done using the average % reactivity from each frame (5 fields). GFAP and p16 data correlation were calculated as a nonparametric measure of statistical dependence between two continuous variables using Spearman's rank correlation coefficient (rho).

2.2.3.12 Semi-quantitative scoring of β-gal staining

Semi-quantitative scoring was performed by capturing a low magnification image (20x) of areas of interest (images of four fields/case were scored) that were determined by mapping CD68 and LFB throughout the cohort and creating the below criteria for scoring:

Less than 2 isolated positive cells visible in a randomly selected field were scored (+), 2–5 positive cells (++) and more than 6 isolated positive cells (+++).

2.2.4 Molecular studies of oxidative stress

2.2.4.1 Brain homogenate preparation

Brain tissue from the frozen hemispheres was sampled from DSCL, CL and CNL WM. Approximately 50µg brain tissue was collected in a 1.5mL sterile eppendorf followed by addition of 300µL of homogenisation buffer. The tissue was homogenised and sonicated for 30 seconds. Samples were kept on ice during sonication. Samples were then microfuged at 14,000 rpm for 30 mins at 4ºC. The supernatant was collected and stored at -80ºC until required, while the pellet, which contained insoluble protein, was discarded.

2.2.4.2 Protein determination (Bradford assay)

A standard curve was created using known concentrations (250, 500, 750 and 1500 µg/mL) of Bovine serum albumin (BSA). For each case (standard and unknowns) two measurements were taken to increase reliability. 2µL of each sample homogenate or standard was transferred to a 96 well-plate, in duplicate. 50µL of 'Coomassie Plus- The better Bradford reagent' was added to each well. This reagent undergoes a colour change (from brown to blue) on binding to protein where this shift in wavelength can be read using spectrophotometer indicating the concentration of protein present in the sample. A darker blue colour indicates a higher amount of protein present in the sample.

After the removal of any bubbles that were present in the wells, absorbance readings were recorded at 595nm using a plate reader. The read-out was transferred into a spreadsheet where the mean of the two readings for each sample was calculated. Absorbance readings of standards were used to create the standard curve. Mean values of the samples (wavelength in nm) were compared to the standard curve to determine protein concentration in µg/µL. Prior

to blotting, protein samples were diluted in an appropriate volume of homogenate buffer to ensure equal protein concentrations for loading.

2.2.4.2 SDS PAGE preparation

The percentage resolving gel required depends on the protein size of interest. The larger the molecular weight of the protein, the lower percentage of resolving gel required and vice versa. Protein molecules travel through the gel when connected to the current, so if the percentage resolving gel is high (i.e. 12%-15%), the movement of large proteins is more restricted than. lower percentage gels (i.e. 8%-4%) which allow proteins with a higher molecular weight to travel. Polyacrylamide gels were prepared as detailed in table 2.9 with numbers adjusted according to number of gels prepared. A 4% stacking gel was prepared and used with all resolving gels (Table 2.10).

Table 2.9: 5mls resolving gel preparation

Solutions	***8% (mls)***	***10% (mls)***	***12% (mls)***	***15% (mls)***
Purified water	2.3	2.0	1.7	1.2
30% acrylamide	1.3	1.7	2.0	2.5
1.5M Tris(pH8.8)	1.3	1.3	1.3	1.3
10% SDS	0.05	0.05	0.05	0.05
10% APS	0.05	0.05	0.05	0.05
TEMED	0.003	0.002	0.002	0.002

Table 2.10: 2mls stacking gel preparation

Solutions	***4% (mls)***
Purified water	1.35
30% acrylamide	0.67
1.5M Tris(pH6.8)	0.5
10% SDS	0.04
10% APS	0.04
TEMED	0.004

Samples of protein extracts were mixed with x2 Laemmli sample buffer. After vortexing , samples were heated at 95ºC for five mins on a heat block to allow complete denaturation of proteins, briefly microfuged and left for few mins to cool down to RT.

During this time, the gel recipe was prepared (Table 2.8) and mixture was loaded into a glass cassette to a level of approximately 3cm below the top of the glass plate to allow the loading gel to be added. The cassette was assembled according to the manufacturer's instructions (Bio-Rad, Hemel Hempstead, UK). 1mL of 100% isopropanol was carefully added on top of the resolving gel to ensure removal of air bubbles and to even the edge of gel surface. Prior to adding the stacking mixture, isopropanol was removed from the top of the gel by flushing with distilled water. Excess water was removed gently by using a small piece of filter paper. A suitable comb was inserted into the stacking gel swiftly before the gel set to create the loading wells.

40µg of each sample was then loaded carefully into each well with loading the appropriate molecular size standard. Gels were then electrophoresed at 50V for 30 mins (until samples entered the resolving gel) and the current increased to ~90-120V (depending on the size of protein of interest). Current was disconnected as soon as the edge of the dye frontreached the bottom of the gel.

2.2.4.3 Immunoblotting

The next step was to transfer the proteins from the acrylamide gel onto a PVDF membrane suitable for immunoblotting. The PVDF membrane was cut to an appropriate size and activated by immersion in methanol for 15 seconds before being rinsed in transfer buffer. To carry out the process of transfer, eight fitted pieces of filter papers, four sponges and a PVDF membrane were soaked briefly in transfer buffer, and then sandwiched with the gel between the covers of transferring cassette (Bio-Rad, Hemel Hempstead, UK). Proteins were transferred onto PVDF at 250mA for 60 minutes where the sandwich is kept surrounded by ice to ensure the solutions are kept chilled.

Non-specific binding of the primary antibodies was prevented by incubating the membranes in blocking solution for 60 mins at RT, and membranes were incubated overnight at 4°C with primary antibodies diluted in blocking solution placed on a tube roller (Table 2.3)

Membranes were washed 3 times for ten mins each in PBST before they were incubated with secondary antibody diluted in 5% skimmed milk powder in PBS-T (Table 2.4). Membranes were incubated for 1 hour at RT followed by a 3 ten mins washes in PBST at RT.

Proteins were detected using ECL chemiluminescence (Amersham Ltd., Amersham, UK). Equal volumes of EZ-ECL Reagent A and EZ-ECL Reagent B (developing reagent) were mixed thoroughly for one min prior to addition to the membrane. The acridan-based substrate present in reagent B interacts with the HRP of the secondary Ab and generates a detectable chemoluminescence.

2.2.4.4 Development of membrane and densitometric analysis

Membranes were developed and scanned using the G:BOX (Syngene, UK). The software scanned the membrane and automatically calculated the time required for membrane development according to the intensity of the bands. Images were captured using the Intelli Chemi setting in the GeneSnap software. Intelli Chemi works through patented technology to detect chemiluminecence and automatically capture a sub-saturated image of the membrane. To enable detection of saturation and presentation of the raw data of the image, a histogram was automatically generated.

Densitometric analysis was carried out in GeneTools (Syngene). Developed bands were manually framed in equal size rectangular boxes that were manually designed to fit the largest band. Background was corrected by the software automatically. Raw data of the pixel intensity and the intensity of the bands in proportion to a defined control was

calculated and the intensity of developed bands of interest was normalized to the loading control.

2.2.5 RT qPCR array

2.2.5.1 RNA extraction

Whole brain tissue RNA extraction was performed on the WM frozen cohort (Table 2.8). 50µg of tissue was placed in a sterile 1.5mL eppendorf and homogenized in 500µL of Tri-reagent (Ambion, UK). The homogenate was then centrifuged at 12000g for 1 min at RT. This was followed by the addition of 500µL of absolute ethanol (volume equal to Tri-reagent added previously) and mixed thoroughly by vortexing. The mixture was then loaded into zymo-spin IIC column in collection tubes and centrifuged at 12000g for 1 min at RT. The flow through was discarded. 400µL of direct-zoe RNA prewash reagent was then added to the column and centrifuged at 12000g for 1 min at RT. The flow through was discarded. The RNA pre-washing step was repeated twice. After that, 700µL of RNA washing buffer was added and the tube was centrifuged at 12000g for 1 min at RT. The flow through was discarded. The column was then transferred into a sterile collection tube and 25µL of RNase free water was added and centrifuged for 1 min at maximum speed at RT. The flow through was the purified RNA which was collected and checked after that for its quality and concentration.

2.2.5.2 Determination of RNA concentration

The RNA concentration was determined using the Nano-drop Spectrophotometer (Labtech International). To do this, 1µL of RNase free water was pipetted onto the spectrophotometer pedestal to act as a blank. This was removed and replaced by 1µL of the

RNA sample. The sample is analysed use fiber optic technology and the software automatically calculates the RNA concentration.

2.2.5.3 Quality assessment of RNA

Following determination of RNA concentration, the quality of the RNA was checked on the Agilent 2100 Bioanalyser using an RNA 6000 Nano kit. This kit is capable of analysing 5-500ng/µl RNA concentration sample by calculating the 28s/18s ribosomal ratio. A qualitative assessment of RNA integrity is then provided.

2.2.5.4 cDNA synthesis

cDNA was synthesized from the extracted RNA samples using the RT^2 first strand kit. The kit includes a proprietary buffer that eliminates any residual genomic DNA contamination in RNA samples, before amplification, that would otherwise produce erroneous results. The quality of reverse-transcription controls (RTC) on the PCR array can only be checked with the built-in external RNA control of the RT^2 first strand kit. These controls are not evaluated when used with other cDNA synthesis kits. This makes it essential and critical to use the RT^2 first strand kit to ensure a high quality RT qPCR array experiment.

Genomic DNA elimination mix was prepared for each RNA sample according to table 2.10. The prepared mix containing the RNA extract was then incubated for 5 mins at 42ºC followed by incubation on ice for at least 1 min. After that, the reverse-transcription mix was prepared (Table 2.11) where the volumes were adjusted according to the number of reactions, and 10µL was added to 10µL of genomic DNA elimination mix. Samples were then incubated at 42ºC for exactly 15 mins. The reaction was stopped by incubating at 95ºC for 5 mins. Then, 91µL of RNase free water was added to each reaction tube and samples were then stored at -20^{o} C until required for use in the RT-qPCR array.

Table 2.11: Genomic DNA elimination mix preparation

Component	***Amount***
RNA	25ng-5µg
Buffer GE	2µL
RNase free water	variable
Total volume	**10µL**

Table 2.12: reverse-transcription mix preparation

Component	***Volume for 1 reaction***
5x buffer BC3	4µL
Control P2	1µL
RE3 reverse transcriptase mix	2µL
RNase free water	3µL
Total volume	**10µL**

2.2.5.5 RT2 SYBR-Green master mix

To ensure accuracy and precision in PCR arrays, it is essential to use the RT^2 first strand kit in combination with RT^2 SYBR Green mastermix. This will ensure a maximum level of sensitive with nanogram to microgram amounts of total RNA.

The PCR component mix was prepared in a sterile loading reservoir (Table 2.12)**.** The components of the mix were adjusted to fit the customized 96-well plate which was designed to fit 4 samples in each array run.

Table 2.13: PCR component mix preparation

Array format	***4 columns of 96-well plate (A,B,C,D)***
2x RT^2 SYBR Green mastermix	337.5µL
cDNA synthesis reaction	25.5µL
RNase-free water	312µL
Total volume	**675µL**

2.2.5.6 RT2 profiler PCR array

Initially, RNA isolated from 3 brains (CNL, CL, DSCL) were run on a readymade qPCR array plate that contained 81 selected genes known to be affected or involved in DDR and senescence/apoptotic pathways. From there, I have analysed the qPCR data and chose the key genes that showed to be altered in the primary screen. 96 well RT-qPCR arrays were customised with 18 primers of 18 key genes involved in DNA-damage response and senescence pathways (Figure 2.3).

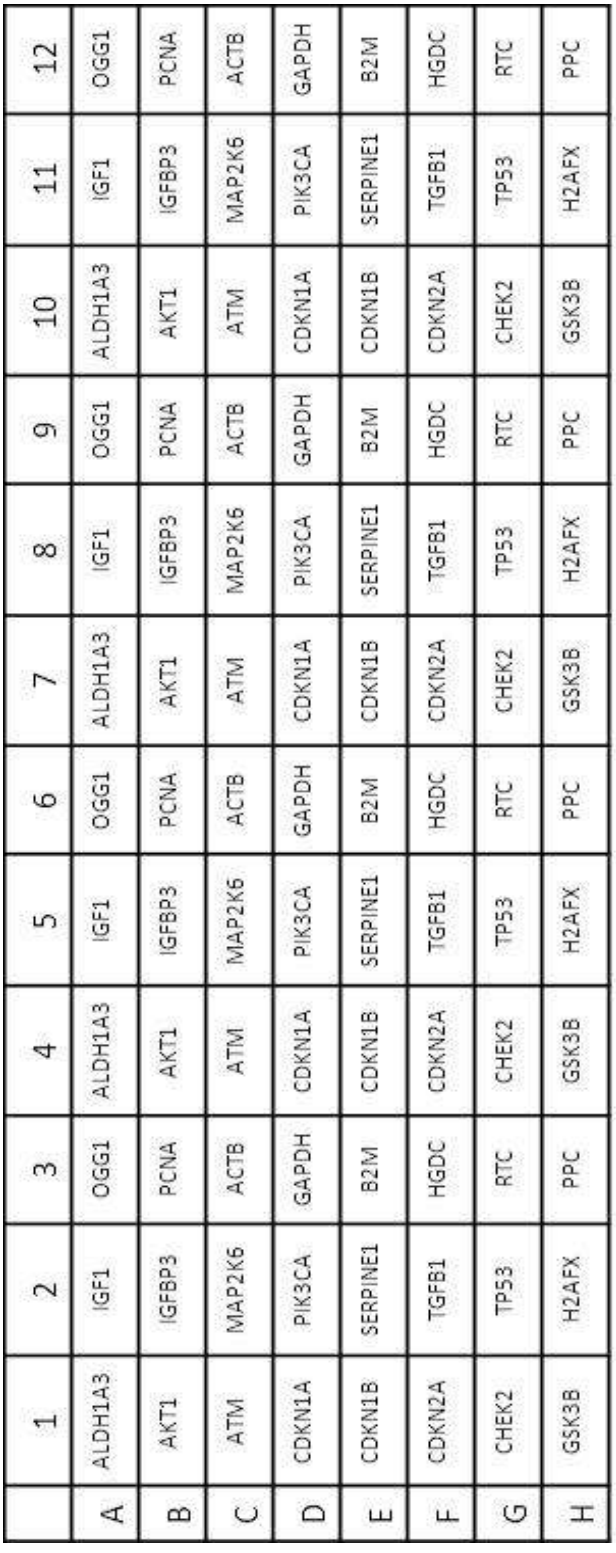

	1	2	3	4	5	6	7	8	9	10	11	12
A	ALDH1A3	IGF1	OGG1	ALDH1A3	IGF1	OGG1	ALDH1A3	IGF1	OGG1	ALDH1A3	IGF1	OGG1
B	AKT1	IGFBP3	PCNA	AKT1	IGFBP3	PCNA	AKT1	IGFBP3	PCNA	AKT1	IGFBP3	PCNA
C	ATM	MAP2K6	ACTB	ATM	MAP2K6	ACTB	ATM	MAP2K6	ACTB	ATM	MAP2K6	ACTB
D	CDKN1A	PIK3CA	GAPDH	CDKN1A	PIK3CA	GAPDH	CDKN1A	PIK3CA	GAPDH	CDKN1A	PIK3CA	GAPDH
E	CDKN1B	SERPINE1	B2M	CDKN1B	SERPINE1	B2M	CDKN1B	SERPINE1	B2M	CDKN1B	SERPINE1	B2M
F	CDKN2A	TGFB1	HGDC	CDKN2A	TGFB1	HGDC	CDKN2A	TGFB1	HGDC	CDKN2A	TGFB1	HGDC
G	CHEK2	TP53	RTC	CHEK2	TP53	RTC	CHEK2	TP53	RTC	CHEK2	TP53	RTC
H	GSK3B	H2AFX	PPC	GSK3B	H2AFX	PPC	GSK3B	H2AFX	PPC	GSK3B	H2AFX	PPC

Figure2.3: Array layout. A customised qPCR array plate has been designed probed with 18 key genes that are involved in DDR and senescence/apoptotic pathways. The array also included 3 housekeeping genes and quality control probes

Following the preparation of PCR components mix, the PCR array plates were warmed for 1 min at RT and 25µL of PCR mix was added to each well using an 8-channel pipette. Wells were then tightly sealed using optical thin wall 8-cap strips. The plate was then centrifuged at 1000g for 1 min at RT to remove bubbles and placed in the Real Time PCR cycler.

2.2.5.7 Assessing the quality of SYBR Green-based qPCR reaction

3 housekeeping genes were included in the arrays to enable normalization of the data. The plate was also designed with a genomic DNA control (GDC) which detects non-transcribed genomic DNA contamination with a high level of sensitivity. The reverse-transcription control (RTC) tests the efficiency of the reverse-transcription reaction. The positive PCR control (PPC) tests the polymerase chain reaction itself.

The combination of these sensitive assays with normalization of the data with housekeeping genes yields high quality and tightly monitored PCR array results. For this reason, each sample was run only once and the obtained data was considered highly reliable for analysis.

2.2.5.8 qPCR array data analysis

After the end of each qPCR run, raw qPCR data was exported into an excel spread sheet, and thedata categorized into three groups: DSCL, CNL and CL. Data analysis was done using the relative quantification comparative delta threshold cycle (ΔC_T) method (Schmittgen and Livak, 2008), where C_T stands for the cycle number at which the fluorescence passes the detection threshold. The first step of the analysis was to consider any individual C_T value which was less than 35 as a negative call, except for the genomic DNA control well (GDC) where C_T value should be greater than 35 thereby indicating that the level of genomic DNA contamination is too low to affect gene expression profiling results.

For each WM group (DSCL, CNL, CL), the average ΔC_T for each gene was calculated using the C_T value for the gene of interest (GOI) and the average of the housekeeping genes (HKG) used for normalization using the formula below:

$$\Delta C_T = C_T^{AVG\ GOI} - C_T^{AVG\ HKG}$$

After that, ΔΔCT was calculated using the following formula

$$\Delta\Delta C_T = \Delta C_T^{AVG\ GOI} - \Delta C_T^{AVG\ HKG}$$

The relative expression of the gene of interest to the endogenous control in each sample was then calculated using the following formula:

$$Relative\ expression = 2^{-\Delta\Delta CT}$$

2.2.6 Mass spectrometry

2.2.6.1 Whole tissue DNA extraction

Total genomic DNA extraction was performed on CFAS frozen cohort (Table 2.8) using the QIAamp DNA mini kit. As per the manufacturer's instructions, 25mg of WM was collected into a sterile eppendorf containing 80µL PBS. Tissue was then homogenized in 100µL of buffer ATL. After that, 20µL of Proteinase K was added, mixed thoroughly and sample incubated at 56ºC for 1-2 hours with occasional vortexing until the tissue completely lysed. Tubes were then centrifuged briefly and 200µL of buffer AL was added to the sample, mixed by pulse-vortexing for 15 seconds, and incubated at 70°C for 10 mins. 200µL of absolute ethanol was added to the sample and mixed by pulse vortexing for 15 seconds. After that, the mixture (including the precipitate) was carefully transferred to the QIAamp Mini spin column (in a 2mL collection tube) and centrifuged at 8000 rpm for 1 min. The QIAamp Mini spin column was placed in a sterile 2mL collection tube and the filtrate was discarded. 500µL of buffer AW1 was then added to the sample, centrifuged and the column was then transferred to a sterile collection tube and the filtrate discarded. 500µL of buffer AW2 was added to the column, and centrifuged at full speed for 3 mins. Columns were placed in a sterile 2mL collection tube and centrifuged at full speed for 1 min. The QIAamp mini spin columns were placed in sterile1.5mL microcentrifuge tubes. 200µL of RNase free water was added and let to stand in RT for 5 mins. Samples were then centrifuged at 8000 rpm for 1 min and the flow through collected and stored at-20^{o}C until required.

2.2.6.2 DNA hydrolysis

For enzyme hydrolysis, DNA concentrations were determined by the nano-drop spectrophotometer (Labtech) with the ND-1000 v3.2.1 software, and concentrations were adjusted to approximately 1µg/µL. DNA hydrolysis was done in a simple single step protocol which efficiently degrades DNA to its individual nucleoside

components using the DNA degradase plus (which has Alkaline Phosphatase). The nucleosides product which lacks the negatively charged phosphate makes the digested DNA ideal for DNA analysis using the LC/MS (Figure 2.4). Typically, 5 µg of genomic DNA is incubated with 1µl (5 U) of DNA Degradase Plus™ in 25µl reaction volume and incubated at 37°C for 1 hour in the presence of 3µl of TEMPO (1.5M) to eliminate any possibility of artificial oxidation formation. Foraccurate quantitation of 8-oxo-dG, 500 fmol of [$^{15}N_5$]8OHdG was added.

2.2.6.3 Gel electrophoresis

In order to ensure the adequate hydrolysis of DNA by the degradase enzyme, a simple agarose gel was prepared loaded with digested vs non-digested DNA. The agarose gel was prepared by dissolving 500mg agarose in 50mL Tris Acetate-EDTA (TAE) buffer, heated in a microwave to homogenise the mixture. After that, 1µL of Ethidium Bromide (EtBr) was added. The hot gel mixture was then poured into a sealed gel cast (Bio-Rad) with a comb and left for 30 min to solidify. The gel was then placed in the electrophoresis apparatus filled with TAE buffer.

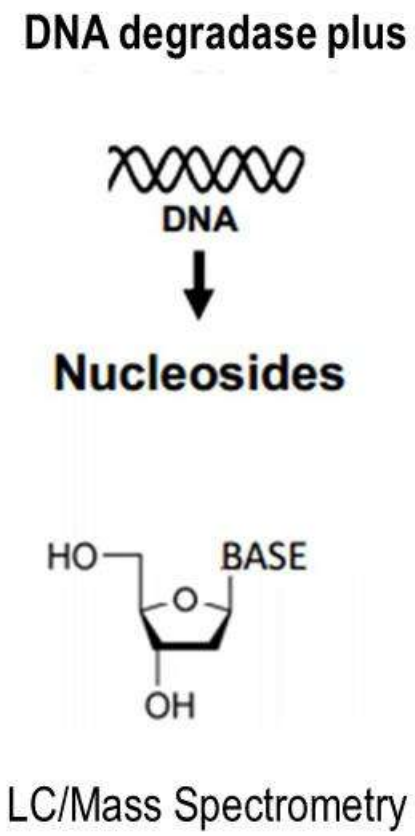

Figure 2.4: DNA hydrolysis by DNA degradase enzyme. In the presence of Alkaline Phosphatase, DNA is hydrolysed by degradase enzyme to its individual nucleosides which makes the product ideal for LC/MS analysis

CHAPTER 3: OXIDATIVE STRESS AND DNA DAMAGE RESPONSE IN WM AND WML OF THE HUMAN AGEING BRAIN

3.1 Introduction

The pathogenesis of WML in the brains of the elderly is not completely understood. However, theories of their origin have been proposed: chronic cerebral hypoperfusion established from the presence of small vessel disease, BBB dysfunction, CSF accumulation and glial cell activation are all thought to play a major role in WML formation and the pathology of the surrounding WM (Fernando and Ince, 2004, Simpson et al., 2007a, Simpson et al., 2010d).

Cellular damage is a known feature of brain ageing and a contributor to cognitive impairment (Davydov et al., 2003, Lovell and Markesbery, 2007). DNA damage due to oxidative stress is hypothesised to have a main role in several neurodegenerative diseases and is a major cause of pre-mature cellular death and senescence (Keller et al., 2005, Simpson et al., 2010d). Wang group have conducted a study in 2005 using post-mortem brain tissue from previously defined MCI and AD subjects to detect and quantify direct DNA damage in the cortex. The study used Mass spectrometry technique to quantify Guanine base modification as a result of oxidative DNA damage and concluded that DNA oxidative damage is upregulated in MCI brains when compared to controls and may be one of the earliest events which contribute to cognitive impairment and decline (Nunomura et al., 2001, Wang et al., 2005).

During oxidative phosphorylation, some of the oxygen consumed by the cell is transformed into ROS which can attack DNA bases and cause nucleic acid damage (Wang et al., 2005). DNA oxidative damage is seen in the form of single strand breaks (SSBs), double strand breaks (DSBs), base modifications and DNA-protein cross links. DNA double strand breaks can initiate about 20 oxidised base products in which 8-hydroxyguanine (8-OHdG) is the most prominent (Fiala et al., 1989, Cooke et al., 2001). Guanine among other three DNA bases has the lowest oxidation potential and therefore is most vulnerable to be oxidised (Singh et al., 2009) (Figure 1.4 from chapter 1).

As a consequence of DNA oxidative damage, changes in protein expression can occur and could be fatal to glial cells or cause altered function, such as an upregulation in p16 and p53, which are the two main cell cycle check proteins that get activated in the presence of persistence DNA damage response to either activate apoptosis or senescence (Wang et al., 2005). ROS may also react with proteins and cause changes in critical cellular metabolic pathways which cause changes in neuronal function (Poon et al., 2004). Lipid peroxidation can also occur from oxidative stress and cause structural membrane damage which has been shown to be toxic to neurons grown in culture media (Lovell et al., 2000, 2001).

The products of oxidative stress, including mitochondrial and nuclear DNA damage, trigger the cellular mechanisms for DNA damage removal. DNA repair mechanisms are a complex system, whilst failure in maintaining genome integrity is implicated in ageing and disease (Hoeijmakers, 2009). The DNA damage response is associated with activation of several proteins that are involved mainly in DNA double strand break repair, such as DNA-PK and H2AX (Stiff et al., 2004). DNA-PK activates p53 through phosphorylation of the amino terminal site and either triggers the onset of DNA repair or drives the cell to apoptosis (Soubeyrand et al., 2004, Ho and Li, 2010). Phosphorylation of H2AX, a member of the histone family of proteins, in response to DSB formation results in the formation of γ-H2AX which acts as an anchor between the two strands of DNA at the sight of a break and initiates DNA repair to maintain genomic stability (Stiff et al., 2004, Stucki and Jackson, 2006).

Recent studies have shown that DNA damage and an associated DNA damage response occur in different types of cells in the ageing brain including neurons, astrocytes and microglia (Simpson et al., 2010a, Bradley-Whitman et al., 2014). This ROS mediated cellular activity is considered as a characteristic change in the brain of the elderly (Simpson et al., 2007a). To date, studies have focused on studying oxidative cellular damage in early stages of AD, MCI and in well-defined AD patients but only very limited number of studies have looked into early changes in human brain during the earliest pathological phase of

disease progression. Accumulating evidence from studies based on the CFAS cohort suggest higher levels of oxidative stress and a DDR occur in subjects at low Braak and Braak neurofibrillary tangle stages (Simpson et al., 2010c). However, the role of oxidative stress and DNA damage in the pathogenesis of WML remains unknown.

Studies of the pathology and pathogenesis of WML are hampered by the difficulty in recognising these lesions in the autopsy brain. The CFAS approach has been to use post-mortem MRI of brain slices to guide sampling of WML (Fernando et al., 2004). This allows sampling of lesions, and of control white matter from cases with deep subcortical lesions and from cases without lesions. These studies have defined the glial pathology of WML and have shown up-regulation of microglial activity (Simpson et al., 2007b). Recent CFAS studies showed that the presence of hypoxia markers in WM areas free of lesions from lesional brains (Simpson et al., 2010d). A study done by the same group also demonstrated that apparently normal white matter from cases with lesions also shows microglial up-regulation and altered cellular pathways, similar to those of the lesions (Simpson et al., 2007b, Simpson et al., 2009). This "field effect" suggests that WML (in a deep subcortical location) are associated with more widespread white matter abnormality which indicates an early change that could contribute towards an established form of the disease (Simpson et al.). These interesting findings established an important question about WML formation in ageing brain: Is oxidative stress only present in a well-defined WML, or is it present at a very early stage where it might impair glial cell function and contribute to WML formation?

The hypothesis of the current study is that glial cells in WM and WML are exposed to oxidative stress which will affect macrocellular components including lipids, proteins and DNA through oxidation by which these end products might contribute to glial cell dysfunction and/or WML formation. The main aim is to assess the level of oxidation in glial cells in WM and WML in a selected CFAS cohort using 8-OHdG as a marker of oxidative damage; and γH2AX and DNA-PK as markers of DDR. Detection of oxidation endpoint

products including damaged DNA, oxidised protein and peroxidised lipids will define the presence and type of oxidative damage in three groups of WM (CNL, CL, DSCL).

3.2 Results

3.2.1 Histological characterisation of WM and WML

Following the categorisation of WM into three groups (DSCL, CL, CNL) using MRI post-mortem brain scans as a guide (Figure 1.2 from chapter 1), tissue blocks were taken from the formalin fixed material and from the contralateral frozen brain hemispheres. Histological characterisation of the tissue was carried out using haematoxylin and eosin (H&E), luxol fast blue (LFB) and cluster of differentiation 68 (CD68).

3.2.1.1 H&E characterisation of DSCL, CL and CNL WM

The histomorphology of three groups of WM was determined using H&E stained tissue sections. Haematoxylin stains basophilic structures blue, and eosin stains eosinophilic structures red.

Overall tissue morphology of DSCL was distinguished from CNL and CL in which the first showed dense astrogliosisa associated with increased intra-space between glial cells and a severe loss of the surrounding myelin tissue. Glial cells were mainly round and small resembling oligodendrocytes while astrocytes had larger oval shape nuclei (Figure 3.1).

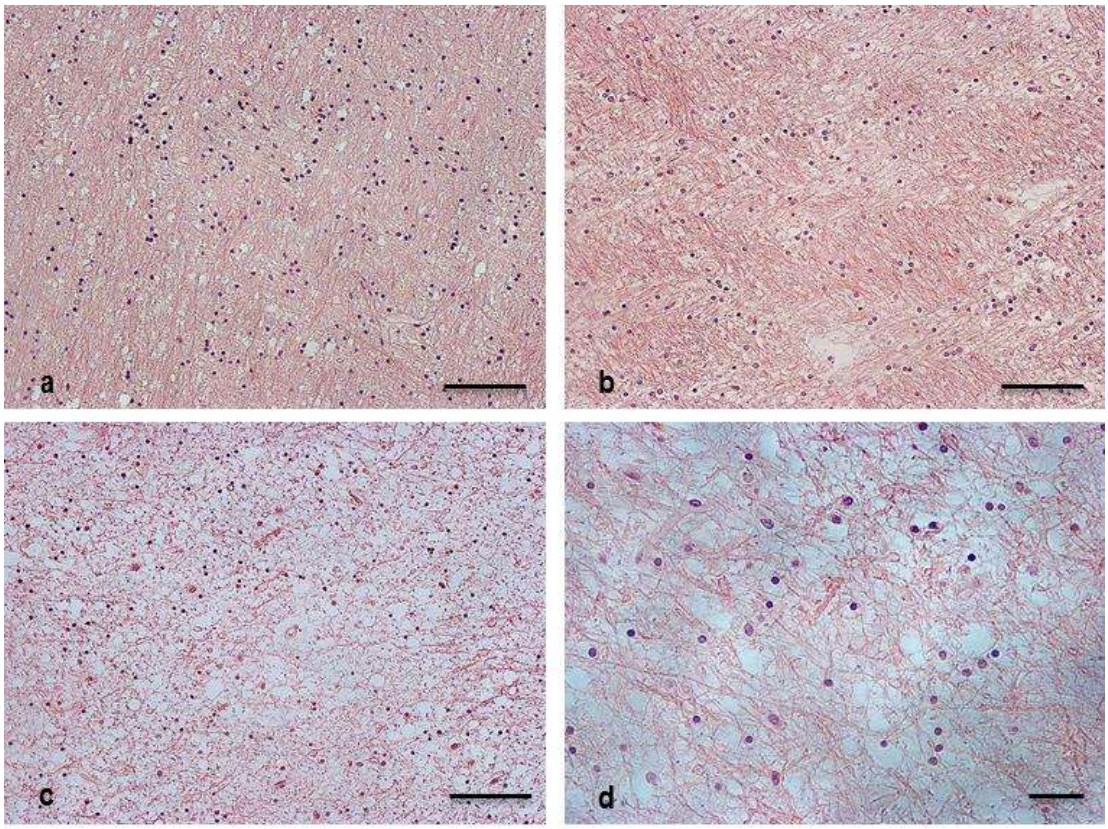

Figure 3.1: H&E staining of three groups of WM. (a, b) H&E immunostaining of a CNL and CL brains respectively, showing round small shaped cells resembling astrocytes in the presence of intact interspaces (rarefaction) which is thought to be reserved myelin. (c) H&E immunostaining of a DSCL brain showing large interspaces between glial cells which reflect the loss of myelin associated with a lesion. Scale bar=100µm. (d) Higher magnification of DSCL brain. Scale bar=50µm

3.2.1.2 Histological examination of myelin attenuation

In order to confirm the excessive loss of myelin that was reflected in the form of hyperintensities using the MRI scans, tissue sections were stained with luxol fast blue (LFB) which stains myelin. DSCL displayed little or no LFB reactivity indicating severe myelin attenuation. In contrast both CNL and CL WM had a regular distribution of LFB staining indicating intact myelin (Figure 3.2).

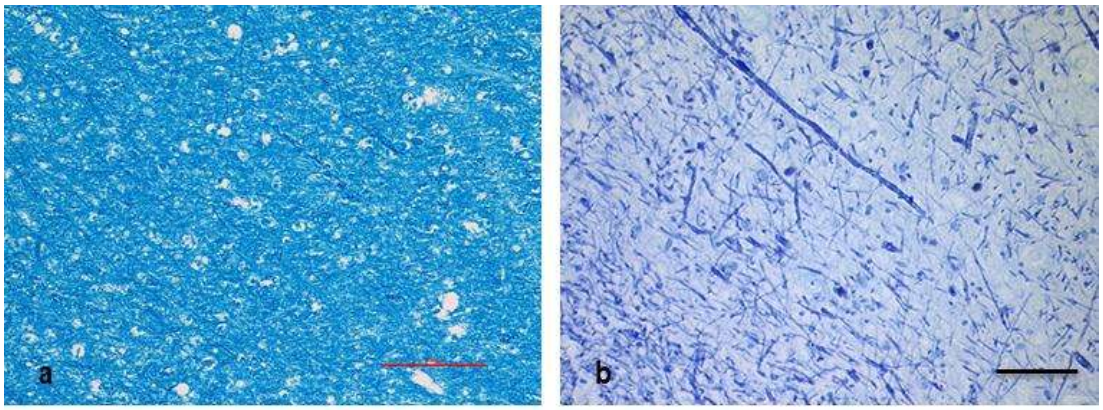

Figure 3.2: LFB staining of CNL and DSCL brains. (a) LFB staining of CNL brain showed intense blue colour reflecting the preservation of myelin when compared to (b) which showed severe loss of myelin associated with a DSCL. Scale bar=100µm

3.2.1.3 Microglial morphology as a landmark of WML

IHC with CD68 antibody was performed on both FFPE and frozen CFAS tissue sections to confirm the lesion which was detected by MRI analysis had been successfully sampled. DSCL predominantly contained large numbers of microglia with an amoeboid phagocytic morphology compared to the smaller ramified bipolar morphology of microglia detected throughout the CNL (Figure 3.3).CL Sections stained for CD68 showed a mix of amoeboid as well as resting microglial morphology.

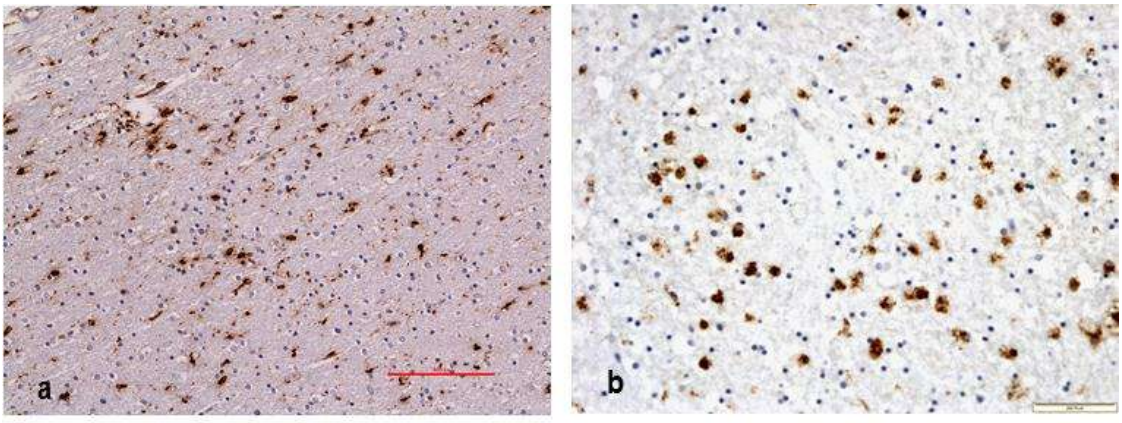

Figure 3.3: CD68 staining of CNL and DSCL brains. The microglial (or possibly a mix of microglia with perivascular macrophages) morphology demonstrated by CD68 was used as indiacator of the presence of a lesion. (a) CNL brain stained with CD68 showed ramified (resting) by-polar microglia. (b) DSCL brain stained with CD68 showed large swollen ameboid microglia. Scale bar=100µm

3.2.2 8-OHdG reactivity displays direct DNA damage in WM and WML

Nucleic acid oxidation of glial cells in the three groups of WM was investigated histologically using 8-OHdG as a marker of direct DNA damage. 8-OHdG reactivity was detected in the nuclei and cytoplasm of glial cells morphologically resembling astrocytes, microglia and oligodendrocytes in a consistent manner between the groups: (i) CNL brains showed reactivity to 8-OHdG intracellularly as well as in the extra cellular matrix but it was not as intense as the staining observed in (ii) CL and (iii) DSCL brains where by those two lateral showed high reactivity to 8-OHdG (Figure 3.4). None the less, 4 out of 15 CNL brains showed intense 8-OHdG which mimics the staining intensity in CL and DSCL brains. Different types of cells were reactive to 8-OHdG where by morphologically resembling astrocytes, oligodendrocytes and microglia. However, reactive cells thought to be microglia from their morphology were in their resting ramified state in CNL brains, while clear swelling of what is thought to be amoeboid microglia was associated with DSCLbrains. CL showed a mixture of both reactive cells, amoeboid and ramified.

Although there was wide spread oxidative damage in all three groups of WM, DSCL in specific showed occasional staining to be associated with star shaped cells resembling astrocytes while the intense reactivity was seen in round small cells morphologically resembling oligodendrocytes and in swollen large irregular shape cells morphologically resembling microglia.

The distribution of 8-OHdG staining was usually even across brain sections, however, it was noted that two DSCL cases displayed high immunoreactivity of DNA oxidation at the margins of the lesions creating a ring (Figure 3.5).

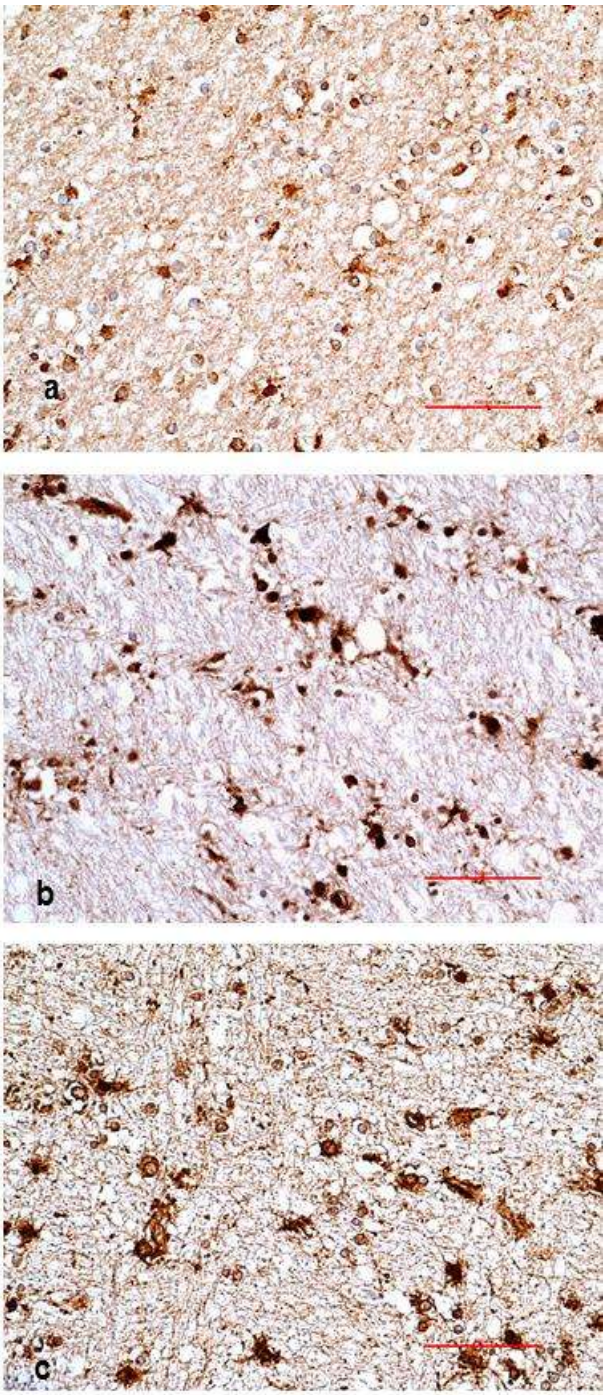

Figure 3.4: DNA oxidative damage is present in three groups of WM. (a) 8-OHdG immunostaining of a CNL brain showed intranuclear and perinuclear (cytoplasmic) reactivity. (b,c) 8-OHdG immunostaining of CL and DSCL brains showed intense reactivity associated with large cells resembling amoeboid microglia as well as star shaped cells resembling astrocytes. Scale bar=100µm

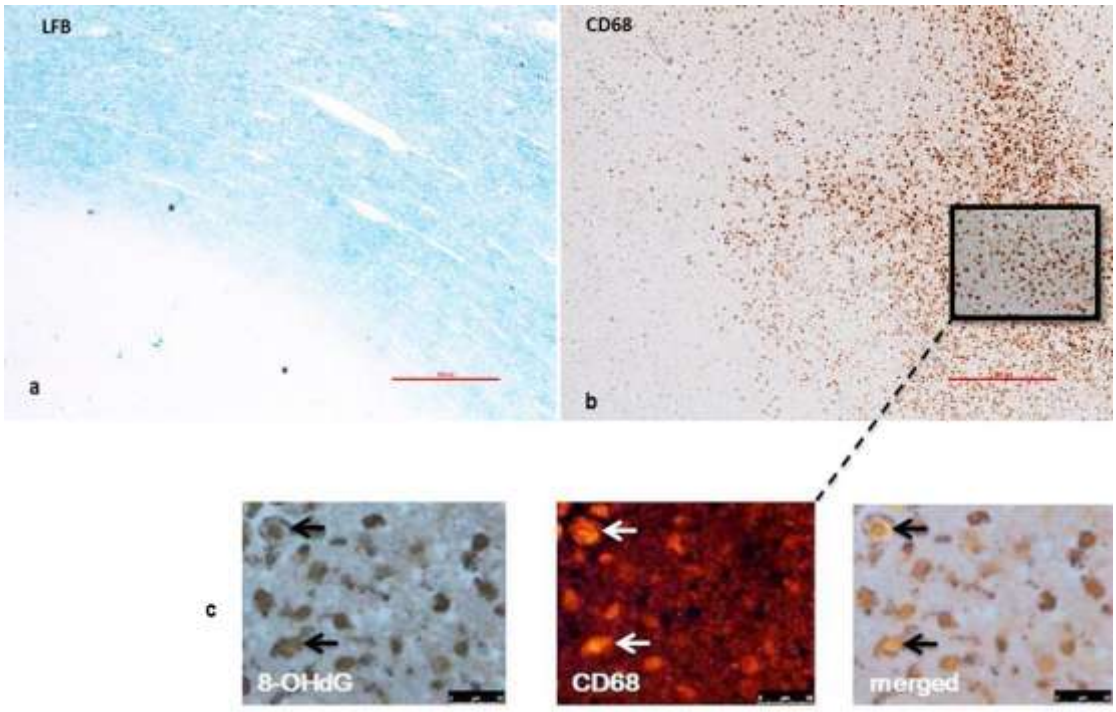

Figure 3.5: Oxidised microglia form the edge of an active lesion. Severe myelin attenuation demonstrated with LFB stain (a) is associated with extensive number of amoeboid microglia which forms an edge around the lesion (b) (could be named as macrophage reactive zone). (C) Co-locolisation of 8-OHdG with microglial marker (CD68) indicated an on-going DNA oxidation. A and b scale bar= 150µm. c scale bar=50µm

3.2.3 Detection of DNA oxidation in specific cell type population

8-OHdG reactivity was associated with cell types morphologically resembling microglia and oligodendrocytes. To determine the specific cell type, double labelling was performed using 8-OHdG and specific cell phenotype markers, including CD68 for microglia, OSP for oligodendrocytes, GFAP for astrocytes and collagen IV for endothelium of blood vessels nourishing the WM. Double labelling experiments were performed for qualitative investigation and was done on selected DSCL cases which revealed adequate tissue morphology. CNL and CL frozen sections were of inadequate quality and there for were not included in this part of the study.

In recent CFAS studies, it was shown that blood brain barrier dysfunction plays a significant role in WML pathology and may contribute to WML formation. For this reason, it was essential to investigate in this study the presence of oxidative stress in the endothelium of small vessels nourishing the deep WM which is an important factor seen in ischaemic WML and vascular dementia. Double labelling with 8-OHdG and Coll.IV, OSP, CD68 and GFAP revealed the presence of direct DNA damage in the endothelium, oligodendrocytes, microglia and astrocytes respectively in DSCL (Figure3.6 and Figure 3.7).

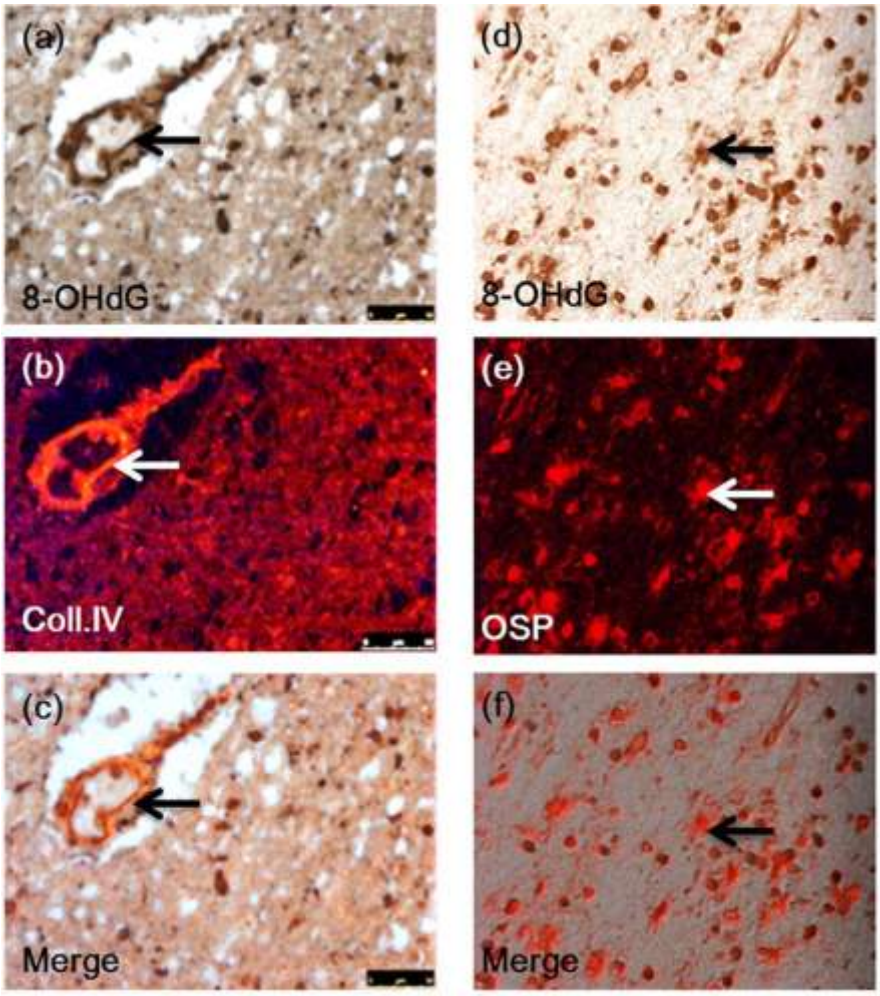

Figure 3.6: DNA oxidative damage is present in the endothelium as well as oligodendrocytes of WML. Double labelling with 8-OHdG and Coll. IV revealed the presence of oxidative damage in endothelium of a DSCL case (a,b,c) as well as in oligodendrocytes when double labelled with 8-OHdG and OSP (d,e,f). Scale bar=100µm

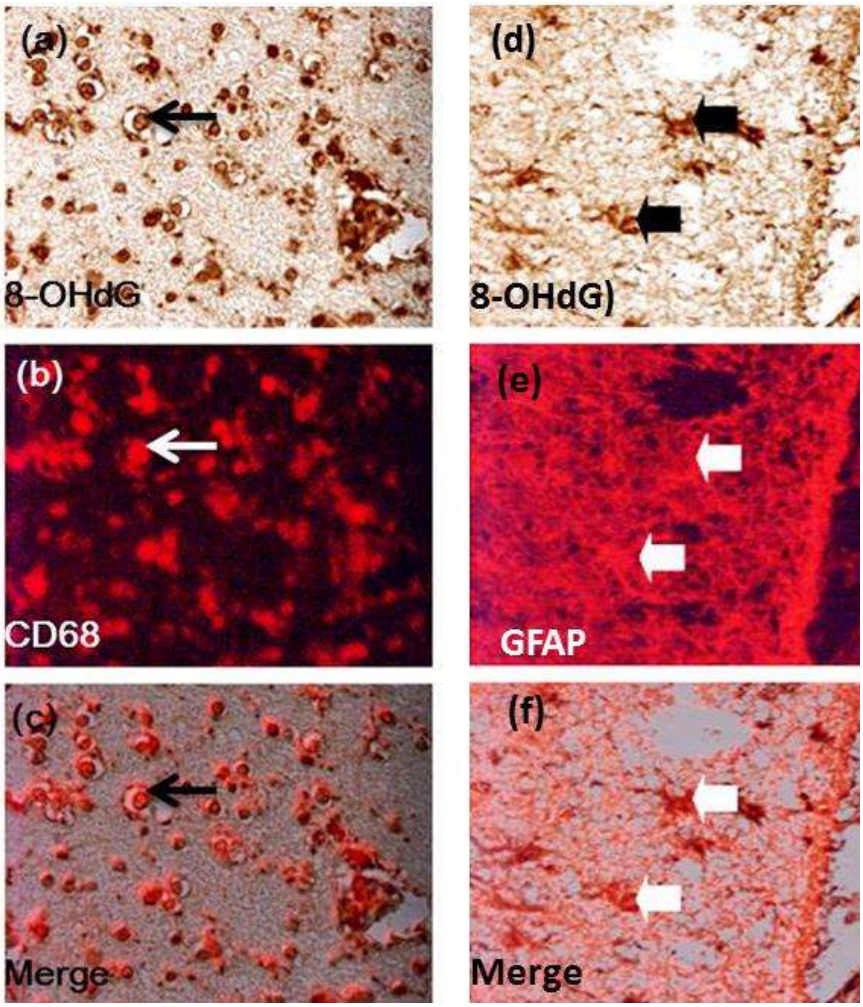

Figure 3.7: DNA oxidative damage is present in migroglia as well as astrocytes of WML. Double labelling with 8-0HdG and CD68 revealed the association of DNA damage with microglia (a,b,c) as well as astrocytes in WML using GFAP as a marker of astrocytes (d,e,f). Scale bar=100μm

3.2.4 Oxidative DNA damage is highly expressed in DSCL and CL WM

DNA oxidative damage was identified in all three groups of tissue (CNL, CL, DSCL). The protocol followed to quantify 8-OHdG within these groups was previously explained in details in materials and methods section. Briefly, within each region (CNL, CL and WML), 5 random fields were captured and images were transferred to a power point programme where a grid was overlaid on each image. The number of 8-OHdG positive nuclei and total number of nuclei were assessed in the five fields for each case, allowing determination of percentage positive nuclei. Only cells with positive nuclei, reflecting nuclear DNA oxidative damage, were assessed; cells with cytoplasmic only staining were not counted as positive.

Inter-observer variation was determined in 8-OHdG scoring between the two different observers. This variation showed a consistent bias related to the creation of two independent threshold in which S.M consistently scored the number of reactive nuclei in all three groups slightly lower than J.S scores. Nevertheless, the scores were very highly correlated (Correlation Coefficient=0.656**; $p<0.001$) indicating that the two observers ranked cases in a similar order (Figure 3.8). Means of the two observers' scores were used for the statistical comparisons between groups.

Quantification of 8-OHdG showed that DNA oxidative stress is not similar between the groups (Table 3.1). Statistically, there was a significant difference in the level of DNA oxidative damage between three groups (Kruskal-Wallis $p=0.01$) (Figure 3.9). Post-hoc analysis revealed a significant difference in the level of DNA oxidation between control and lesional control (Mann Whitney, $p=0.011<0.017$) and between control and DSCL ($p=0.007<0.017$). There was no significant difference in the level of oxidised DNA between lesional control and DSCL ($p=0.526>0.017$).

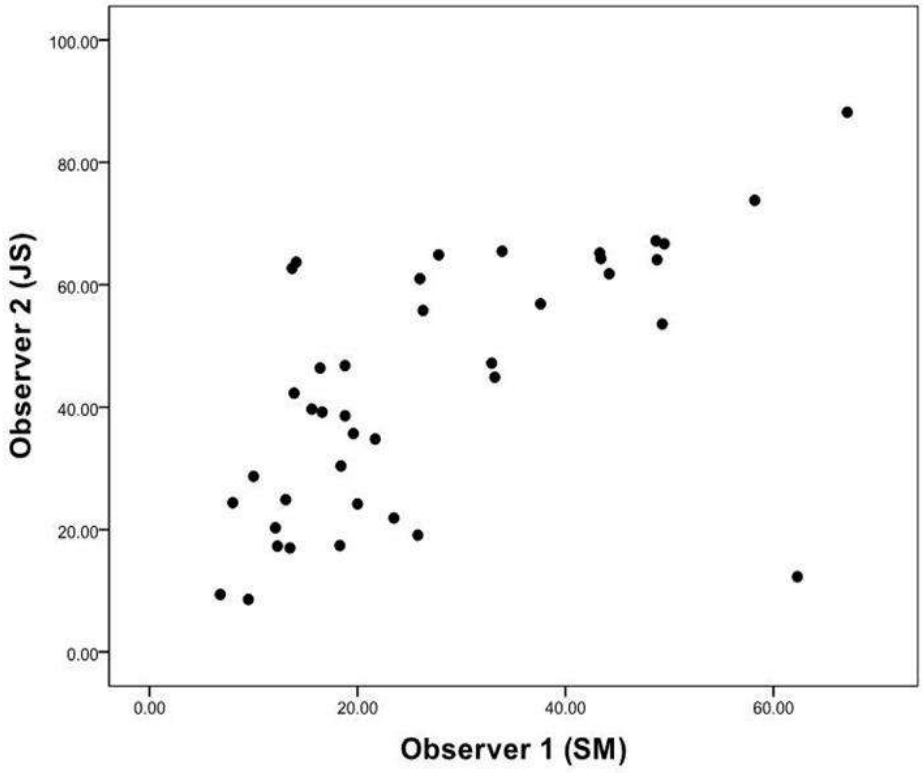

Figure 3.8: Distribution of the two observers' 8-OHdG scores. Although SM scores were consistently lower than JS in this scatter plot, they were highly correlated (Correlation Coefficient=0.656**)

Table 3.1: Description of the amount of oxidative stress among the cohort using quantification of 8-OHdG staining by calculating the percentage of positive nuclei present in the field

WM group	CNL	CL	DSCL
Median	19.35	41.05	37.75
Interquartile range	12.05	24.3	22.04

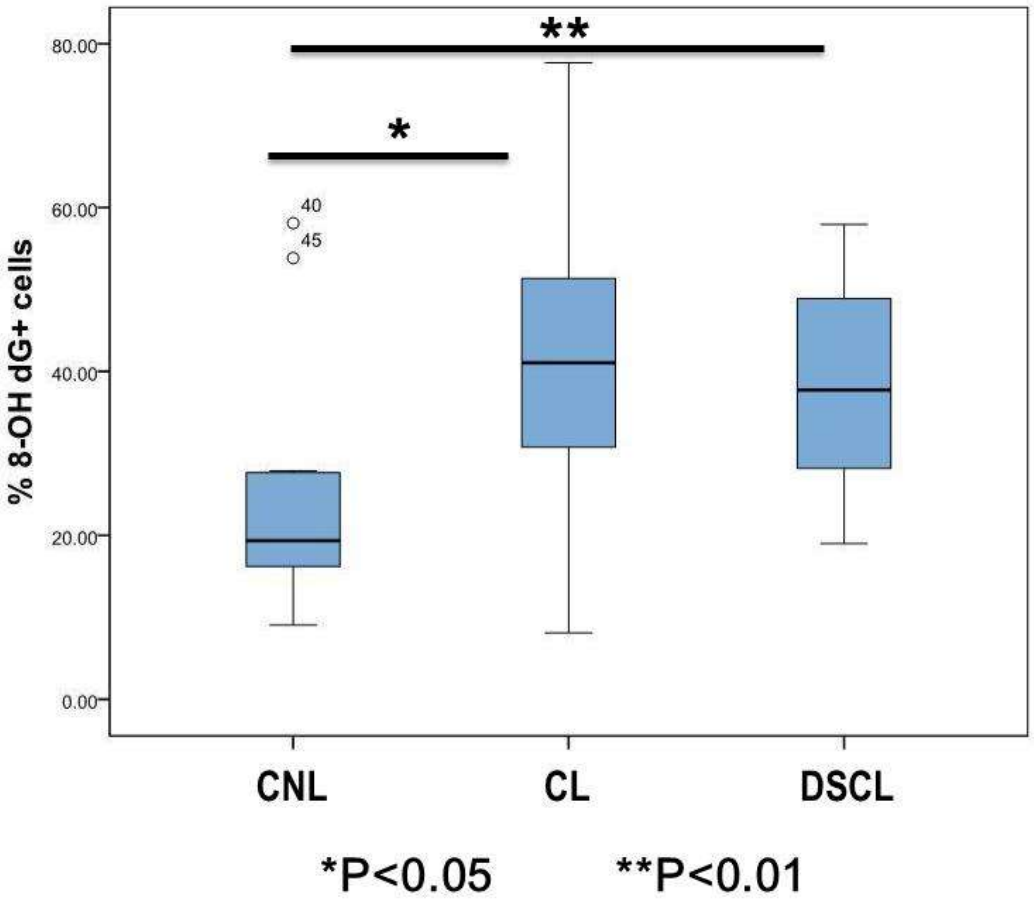

Figure 3.9: The level of oxidative DNA damage varies between groups. Box plot showing the level of DNA oxidation is significantly different between three groups **(**p=0.01**)**

3.2.5 Oxidative DNA damage repair response

In response to DNA modification in the presence of oxidative stress, DDR response enzymes are activated and can be used as an indicator for the cell response to DNA oxidation. Activation of this response in three groups of WM tissue was investigated by immunohistochemical localisation of tissue expression as well as total protein detection using Western blotting for DNA-PK and γ-H2AX.

3.2.5.1 Histological detection of DNA damage repair response

Despite several attempts at antigen retrieval using a variety of methods (including microwave, pressure cooker and enzyme digest retrieval techniques), the commercially available antibodies used to detect DNA damage response did not work consistently on CFAS FFPE cohort; therefore, frozen sections were used. DNA-PK and γ-H2AX reactivity was predominantly detected in the nucleus, although some cytoplasmic staining was also observed, in several types of cells morphologically resembling astrocytes, microglia and oligodendrocytes. However, in CL and DSCL tissue, the majority of DNA-PK and γ-H2AX reactive cells were small and round in shape likely representing oligodendrocytes (Figure 3.10).

The percentage of γH2Ax-positive nuclei was assessed and quantified (Table 3.2). The γH2Ax and 8OHdG counts showed a moderate correlation (Spearman=0.36) (p=0.07). The γH2Ax counts showed a similar effect with lesion type to the 8OHdG, although the effects were slightly attenuated (p=0.03) with CL being higher than CNL (p=0.03), though the other post-hoc adjusted comparisons were not significant (all p>0.05). (Figure 3.11)

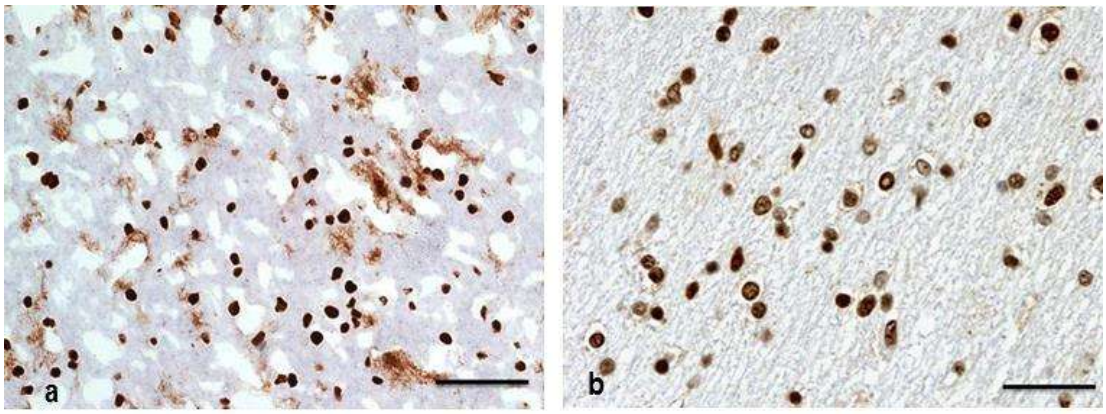

Figure 3.10: Detection of DDR activation in DSCL. DSCL frozen section showing evidence of DDR activity demonstrated by (a) γH2AX which stained the nucleus as well as the cytoplasm of various cell types; and (b) DNA-PK which showed nuclear and perinuclear staining of glial cells. Scale bar=50μm

Table 3.2: Quantification of γ-H2AX.

Marker		CNL	CL	WML
γH2Ax % positive nuclei	Mean (SD)	3.6 (6.8)	20.6 (22.6)	14.1 (17.5)
	Median (IQR)	0 (3.9)	14.7 (31.5)	3.2 (26.0)

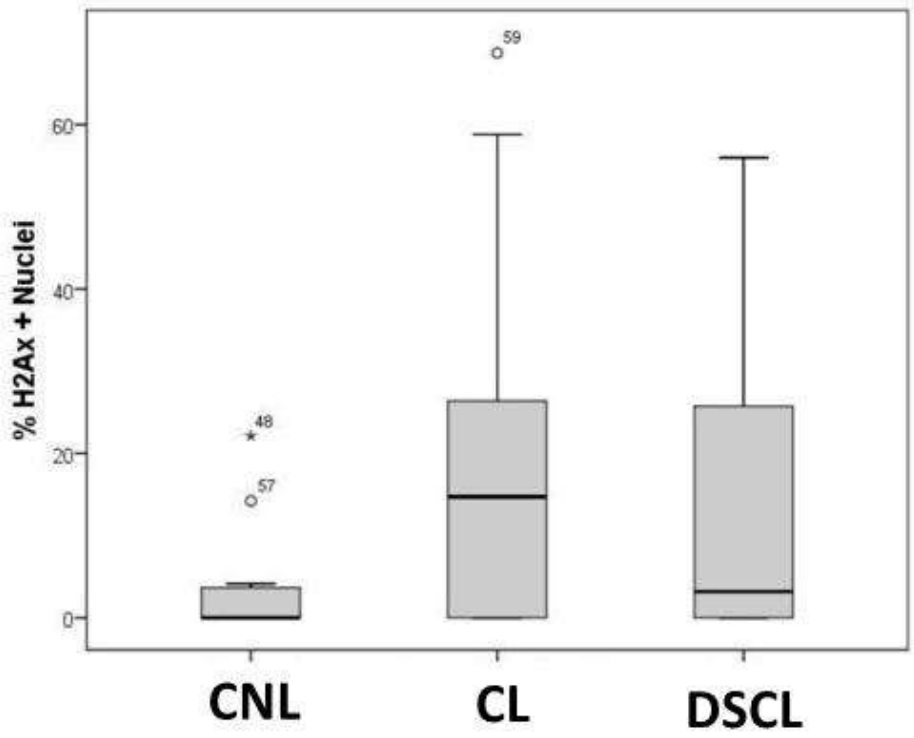

Figure 3.11: Quantification of γH2AX in three groups of WM. Box plot showing variation in γ-H2AX scores between CNL, CL and DSCL brains by which are not statistically significant, however, γ-H2AX expression in CL brains showed wide variation with some brains expressing high levels of DDR molecules

3.2.5.2 Detection of DNA damage response by total protein extraction

Protein oxidation is one of the products of oxidative stress that can be detected and quantified by the application of Western blotting. Whole tissue protein extracts from the three groups of WM (frozen cohort) was immunoblotted for DNA-PK and γ-H2AX.

3.2.5.2.1 Total γ-H2AX expression

The DNA damage response in three groups of WM was performed by Western blot analysis using antibodies directed against γ-H2AX where a band was detected at the correct protein size (17 kDa) (Figure 3.12). Different levels of the DNA damage response were detected and demonstrated the population variation in expression between individual samples among each group (Figure 3.11). Some of CNL cases revealed high level of DNA damage response while other DSCL cases revealed low levels of the same marker. This variation is shown to be consistent with pattern of γ-H2AX immunohistochemical staining where DNA damage response was concluded to be present but with case to case variation.

The quantification of DNA damage response on the protein level in three groups of WM using γ-H2AX did not reach clinical significance (Figure 3.13).

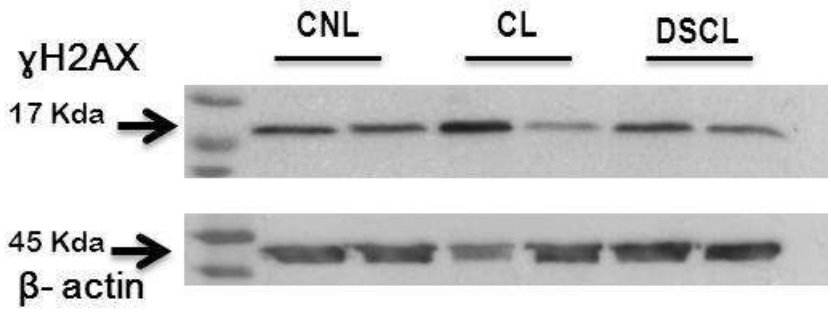

Figure 3.12: Western blot of γ-H2AX. Western blot of γ-H2AX showing bands at the expected protein size (17 kDa)

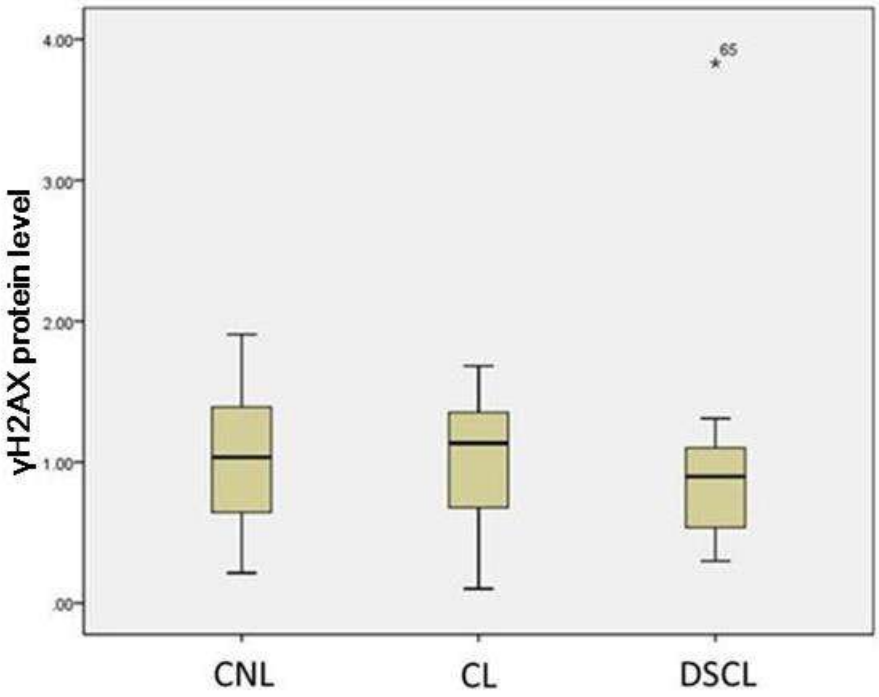

Figure 3.13: Quantification of γ-H2AX Western blot. Box plot showing the quantification of densitometry obtained from γ-H2AX Western blotting. The variation in DDR expression between three groups of WM did not reach statistical significance (p=0.3)

3.2.5.2.2 Detection of expression of catalytic subunit of DNA protein kinase

DNA-PK is another key marker of DDR where by its expression in WM and WML was investigated by Western blotting. However, due to multiple difficulties that were encountered during the course of this experiment, such as the big size of the protein, the determination of DNA-PK catalytic subunit was only qualitative were a band was detected at the correct protein size (480 kDa) (Figure 3.14).

3.2.5.2.3 Total MDA expression

MDA is a marker of lipid peroxidation which is also a key endpoint product of oxidation. A band was detected at the expected protein size (64 kDa) (Figure 3.15). Quantification of MDA by densitometry did not reach statistical significance. However, the box plot showed a trend that is similar to the 8-OHdG where by the widest variation in MDA marker was associated with CL brains (Figure 3.16).

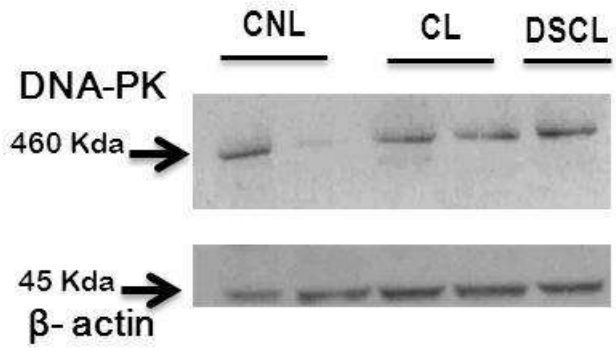

Figure 3.14: Detection of the expression of catalytic subunit of DNA protein kinase by Western blot. Western Blot of DNA-PK showing a band at the correct protein size (480 kDa)

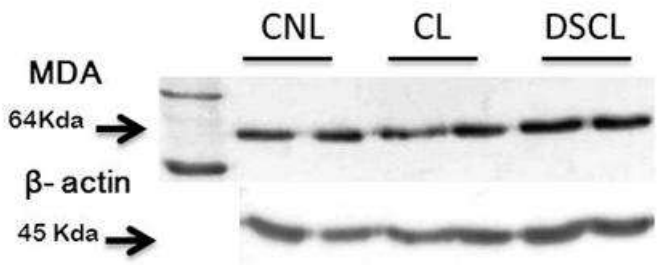

Figure 3.15: Expression of MDA by Western blot. MDA was detected at the correct protein size by Western blotting (64 kDa)

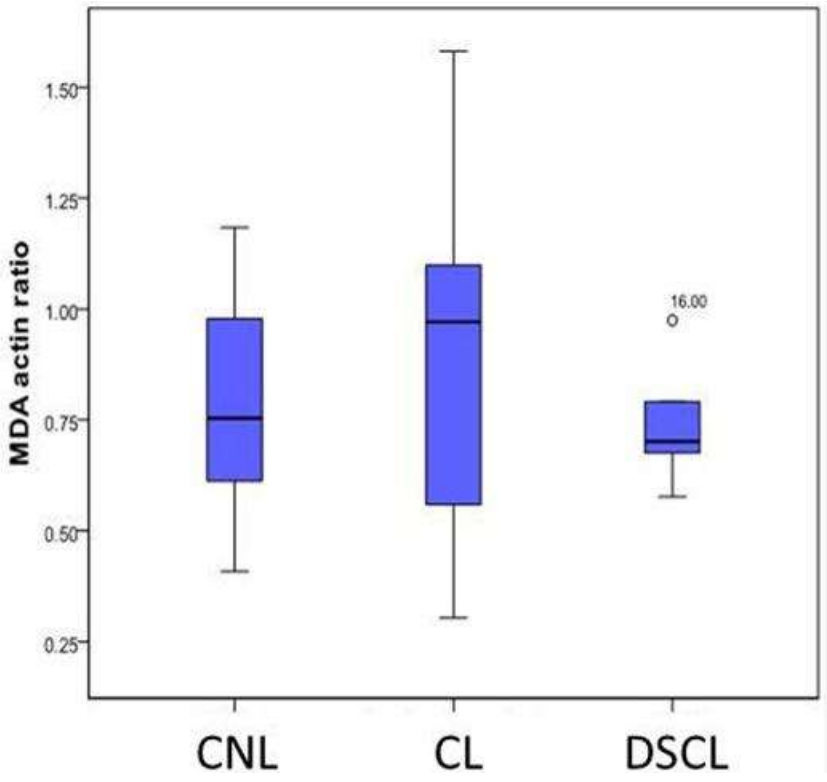

Figure 3.16: Quantification of MDA expression. Box plot showing the variation in MDA expression by Western blotting between three groups of WM (CNL, CL, DSCL). Although did not reach statistical significance, there was a similarity in the trend of MDA expression that mimicked the one of 8-OHdG by which the widest variation was associated with CL brains

3.3 Discussion

Evidence of an extensive oxidative DNA damage in WM and WML in the brains of the elderly in various cell types has been demonstrated in this part of the study. The current study also demonstrated that the increased level of DNA oxidation in lesional controls is very similar to the one quantified in DSCL which supporst the hypothesis that WML arise from a field effect in WM.

3.3.1 Oxidative DNA damage is a common pathology in aged WM

Recent research suggests that oxidative insult occurs on cellular DNA, proteins and lipids of AD human brains (Shackelford DA 2006; Simpson et al, 2010) as well as MS brains (Haider et al, 2011). The current study demonstrates that DNA oxidative damage is present at high levels in white matter lesions (DSCL), lesional controls as well as in control white matter.

DNA oxidative stress was seen in various cell types morphologically resembling oligodendrocytes, macrophages and astrocytes. Specifically in DSCL cases, consistent DNA oxidative damage was seen in enlarged amoeboid macrophages which may contain engulfed degraded myelin. However, in addition to nuclear reactivity, increased cytoplasmic and perinuclear 8-OHdG staining in the cohort suggest a role of RNA and /or mitochondrial DNA oxidation which further support the proposed role of ROS in glial cell oxidation and neurodegeneration (Nunomura et al, 2001).

Although the current study is looking at the pathology of WML in aged brains and their contribution to cognitive impairment, considerable similarities were observed between those WML of a suggested ischaemic origin and WML of an inflammatory origin seen in MS. Chronic active lesions in MS have a zone of preactivation that is packed with oxidised enlarged macrophages which contain remnants of early stage digested myelin (Haider et al, 2011). Moving towards the centre of the lesion, fewer macrophages were seen with later

stages of degraded myelin or absence (removed) of macrophages (Reviewed by Lassmann, 2011). Here, two of the DSCL cases showed similarities in the morphology of the lesions.. Dual staining showed that the area was packed with enlarged amoeboid oxidised microglia and towards the centre of the lesion, a decrease in the number of macrophages was noted. The centre of those two DSCL cases showed lack of cellular component. Further quantifying experiments will be carried out to further understand the nature of the zone of activity at the margins of lesions.

3.3.2 Oxidative DNA damage varies between groups

Quantifying DNA oxidation using 8-OHdG as a marker revealed a significant variation between the three groups: DSCL, lesional control and control WM. This suggests that DNA oxidative damage is present in the WM of aged human brain at different levels. However, while a significant increase in the level of DNA oxidation was seen in lesional controls and DSCL compared to controls, no significant increase between lesional controls and DSCL was detected. This indicates that the level of oxidative DNA damage in lesional controls is very similar to that seen in actual lesions which suggest that WML arise in field effect pathology of WM. The study by Simpson et al (2007) concluded that normal appearing WM have significantly increased number of activated microglia (MHC II reactivity) compared to controls. Furthermore, microarray analysis on normal appearing WM revealed alterations in 419 gene expressions associated with key functional pathways compared to control WM (Simpson et al, 2009). These two results along with this study provide strong evidence of active pathological processes on-going in WM outside the lesions. However, the pathogenesis is not yet fully understood as to whether it represents a pre-lesional change or a secondary response to active WML.

3.3.3 DNA oxidative damage may contribute to the pathology of WML

Several mechanisms have been proposed which might contribute to the pathology of WML associated with dementia and cognitive decline. Accumulating evidence of ischaemia,

blood brain barrier leakage and glial cell pathology strongly suggest a role in the pathology of WM. Evidence of hypoxia in WML and normal appearing WM (Simpson et al, 2010) reveals the presence of pathogenic free radicals and accumulating ROS in the WM of brain ageing. The findings of our study suggest a strong role of DNA oxidative damage which might be linked to accumulating ROS. Observed nuclear damage as well as cytoplasmic and mitochondrial oxidation reveals the wide cellular damage in WM tissue which might affect vital glial functions which if not repaired lead to senescence or premature apoptosis and degeneration (Zglinicki et al., 2005).

Activation of DDR has been reported in AD brains (Mullaart et al, 1990). A study conducted by Myung's group (2008) on AD brains demonstrated a variation in the level of ɣ H2AX in astrocytes, neurons and microglia reactivity with respect to Braak stage (Myung et al, 2008). In contrast, Simpson et al (2010) showed that DNA damage/repair is present in all Braak groups using CFAS brains.

Assessment of the DDR marker -ɣH2AX - in this part of the study did not show significant variation between the three groups of WM, which suggests that induction of the DDR might be independent from type of lesion. This could also be referred to type of sample quantified for DNA damage markers: quantification of 8-OHdG was performed manually by scoring only positive niclei which reflects the DNA oxidation, while WB was performed on a pool of whole tissue protein extraction which contained other cellular components that diluted the signal of nuclear DNA oxidation. Also, 8-OHdG was performed on FFPT which contained a bigger number of sample (n=15/group of WM), while the WB study was performed using frozen tissue with a smaller sample size (n=6/group).

ɣH2AX correlated with 8-OHdG scoring where both markers showed elevated level of expression associated with CL brains. Another key marker of DDR (DNA-PK) was also shown to be expressed in WM and WML by Western blotting, although its quantification was shown to be problematic. This could be related to several reasons, (i) the size of the

protein is very large (480 kDa) whereby it created some technical problems, (ii) the amount of protein yield from whole tissue extraction was very low and this could be referred to the quality of the tissue itself.

Lipid peroxidation is a key endpoint product of oxidative stress that was detected by MDA. Although the level of MDA expression did not significantly vary between group, the highest level detected was associated with CL brains which statistically created a trend that was similar to that one of 8-OHdG. This again supports the idea that there is a field effect of pathology that is wide spread into areas that are free of lesions. Expanding the number of examined cohort might improve the statistical power of tests and might actually yield significance.

In conclusion, extensive DNA damage was shown to be present in DSCL and CL brains in similar levels that were significantly higher when compared to CNL brains. This important observation suggests that although CL brains appear normal by MRI analysis, they are not actually normal and glial cell activation is present. The important question raised as a consequence of these findings is: Does extensive DDR activate cellular senescence and cell cycle check proteins in WML of the human ageing brain?

CHAPTER 4: INDUCTION OF SENESCENCE IN WM AND WML AS A DOWNSTREAM EFFECT OF PERSISTENT DNA DAMAGE RESPONSE IN THE HUMAN AGEING BRAIN

4.1 Introduction

DNA double strand breaks (DSB) are powerful inducers of a DNA damage response (DDR) characterised by the activation of ATM (ataxia telangiectasia mutated), a member of the phosphoinositide-3 kinase-like kinase (PIKK) family. This in turn causes phosphorylation of histone H2AX and activation of the cell cycle checkpoint protein p53 (Shiloh, 2003). DNA double strand breaks that fail to be repaired result in a persistent DDR, prolonged p53-dependent growth arrest and eventually irreversible senescence arrest or cell death (Beauséjour et al., 2003) (Refer to Figure 1.8 from chapter 1). Cellular senescence was first described by Hayflick and Moorhead over fifty years ago (Hayflick and Moorhead, 1961) as the ultimate loss of replicative cell capacity in somatic cell culture model. Since then, *in vitro* studies have suggested a number of important factors that trigger the senescence mechanism in which telomere uncapping is by far one of the most extensively investigated (Blackburn, 2000). It is known that short dysfunctional telomeres might induce growth arrest by activation of ATM pathway (Rouse and Jackson, 2002) and it was later suggested that uncapped telomeres might also trigger senescence by the formation of senescence associated DNA damage foci (SDfs) (Zglinicki et al., 2005) and could be used as an indicator for cellular senescence. Activation of the lysosomal hydrolase β-galactosidase is also widely used and accepted to be an important marker for cellular senescence (Cristofalo, 2005), along with other major changes in cellular morphology and in gene expression (Campisi, 1999, Narita et al., 2003, Jurk et al., 2012).

Until recently, senescent cells were thought to lack function. However, mounting evidence suggests that senescence is a dynamic, multi-step process that might drive cellular proliferation and immune system response (Rodier et al., 2009) and is thought to be initiated by the transition of the cell from a temporal to a stable cell-cycle arrest, which involves prolonged inhibition of Cdk–cyclin activity by p21, p16 or both (van Deursen, 2014).

Importantly, senescent cells develop a phenotype that goes far beyond their limited ability to proliferate and replicate in addition to a change in cellular structure and gene expression. Among the set of genes that are functionally altered in senescence are genes which encode proteins including proteases, cytokines and chemokines along with other growth factors that could alter tissue structure and function and initiate a proinflammatory microenvironment collectively known as a senescence associated secretory phenotype (SASP) (Kuilman and Peeper, 2009).

Emerging evidence suggests that the number of senescent cells *in vitro* expressing altered gene and protein expression increases with ageing (Franceschi et al., 2007, De Magalhães et al., 2009, van Deursen, 2014). Brain ageing is significantly associated with major structural and functional changes including the induction of an inflammatory response (Lucin and Wyss-Coray, 2009, Salminen et al., 2011). Astrocytes are the most numerous cellular type in the human brain where they play a significant role in maintaining brain homeostasis as well as an important role in response to tissue injury and in its repair (Chen and Swanson, 2003). Limited studies have looked at the cellular changes associated with human brain ageing and were performed *in vitro* using isolated primary human astrocytes. Salminen study (2011) was performed using astrocytes in cell culture model and had concluded that astrocytes are directly involved in brain ageing increased level of intermediate glial fibrillary acidic protein and vimentin filaments, (ii) increased expression of several cytokines and (iii) increased accumulation of proteotoxic aggregates. In addition, in vitro stress evokes a typical senescent phenotype in cultured astrocytes and, moreover, isolated astrocytes from aged brain display the proinflammatory phenotype. All of these observations indicate that astrocytes are capable of triggering the SASP and are a major component of it by altering brain microenvironment (Salminen et al., 2011).

To- date, only two studies have looked at cellular senescence as a downstream effect of persistent DNA damage *in vivo*. Jurk's group investigated cellular senescence and SASP using a mouse model (Jurk et al., 2012) which concluded that dysfunctional telomeres and/or

accumulated DNA damage can induce a DNA damage response leading to a phenotype in postmitotic neurons that resembles cell senescence in multiple features. Only one *in vivo* study has demonstrated cellular senescence in the ageing human brain which concluded that cortical neurons in AD individuals of low BRAAK stage, express the senescence marker β-galactosidase (Simpson et al., 2010b).

The aim of this part of the study was to investigate cellular senescence as a downstream effect of a persistent DNA damage response in WM and WML of the human ageing brain using β-galactosiadase as a marker of senescence. The presence of SASP was investigated by detecting changes in the gene expression profile that might alter cellular structure and function. Collectively, these events might feed into senescent state through activation of key cycle check proteins; therefore p53, p21 and p16 were investigated.

4.2 Results

4.2.1 Evidence of senescence in WM and WML

In order to determine whether senescent cells are a feature of brain ageing and WML, histochemical staining of WM and WML was performed to detect SA-β-gal expression, which is a characteristic enzyme produced by senescent cells. SA-β-gal was observed to various extents and in different staining patterns across all three groups of WM (CNL, CL, DSCL). .

In CNL brains, SA-β-gal reactivity in 5 out of 6 cases was uniform and very limited. Staining was observed in the pattern of condensed nuclear staining associated with small round cells morphologically resembling oligodendrocytes. However, one of the CNL cases revealed very high SA-β-gal granular reactivity in cellular cytoplasm as well as in the extracellular matrix allocated at the WM – cortex junction (Figure 4.1“a”).

In CL sections, SA-β-gal reactivity in deep WM was observed as condensed nuclear staining of small round cells morphologically resembling oligodendrocytes; while in the WM

adjacent to the deepest layer of the cortex, SA-β-gal reactivity was seen as granules within the cytoplasm of large cells with cellular processes, morphologically resembling astrocytes (Figure 4.1"c")

In DSCL, SA-β-gal reactivity was granular covering an area of the cytoplasm of large branched cells thought to be astrocytes. However, 4 out of 6 DSCL brains revealed more SA-β-gal staining in superficial WM near the deep layer of the cortex (Figure 4.1"e").

Semi-quantification of SA-β-gal reactivity was done manually by counting positive cells in five captured field of interest in each slide of each brain. Although the highest level of SA-β-gal reactivity was observed microscopically in the CL group, quantification of the number of SA-β-gal positive cells in three groups of WM did not reveal significant differences (Kruskal Wallis p=0.50).

Sections were also stained for p21, a cell cycle check protein, as another marker of senescence. p21 reactivity was observed only in 1 out of 6 CNL brains in an extracellular patchy pattern.

p21 immunoreactivity was detected in 3 out of 6 of the CL brains. Reactivity was occasionally seen in the nucleus but was mostly associated with the cytoplasm of elongated star- shaped cellular processes of cells morphologically resembling astrocytes. Very little p21 reactivity was observed in 2 out of 6 DSCL brains and was also associated with star shaped cells resembling astrocytes (Figure 4.2"a").

To detect the presence of a downstream effect of persistent DNA damage response that have activated apoptosis, the cohort was immunostained for activated caspase 3 which plays a central role in the execution-phase of cell apoptosis. Activated caspase 3 was detected in all groups of WM (CNL, CL, DSCL) with no significant differences in staining pattern. Immunoreactivity was associated with the nucleus and cytoplasm of large branching cells morphologically resembling astrocytes; with the nucleus and cytoplasm of enlarged

irregular shape cells morphologically resembling amoeboid microglia; and with small, round cells resembling oligodendrocytes (Figure 4.2"b"). Quantification of p21 and activated caspase 3 staining has shown to problematic due to the poor tissue morphology of the frozen sections. For this reason, the demonstrated data for those two markers was only descriptive.

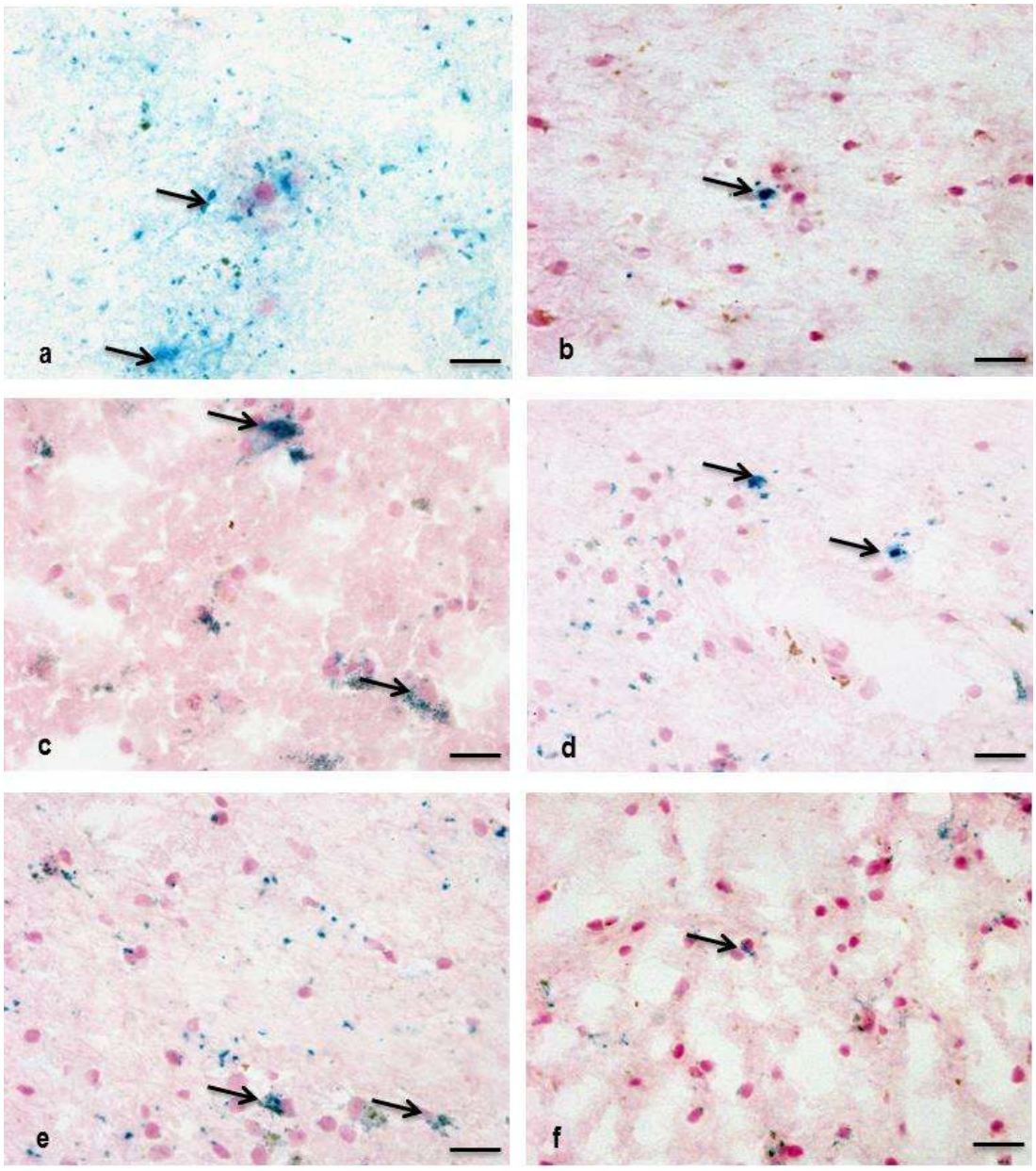

Figure 4.1: Expression of the senescence marker SA-β-gal. a-b, CNL sections: (a) CNL case associated with high SA-β-gal reactivity. (b) SA-β-gal associated with small round nucleus resembling oligodendrocytes. c-d, CL sections: (c) SA-β-gal associated with larger cells near the cortex-WM junction. (d) deep WM, reactivity associated with smaller round cells. e-f, DSCL sections: (e) WML near cortex showing SA-β-gal reactivity in larger cells. (f) SA-β-gal reactivity in deep MWL. Scale bar = 50μm

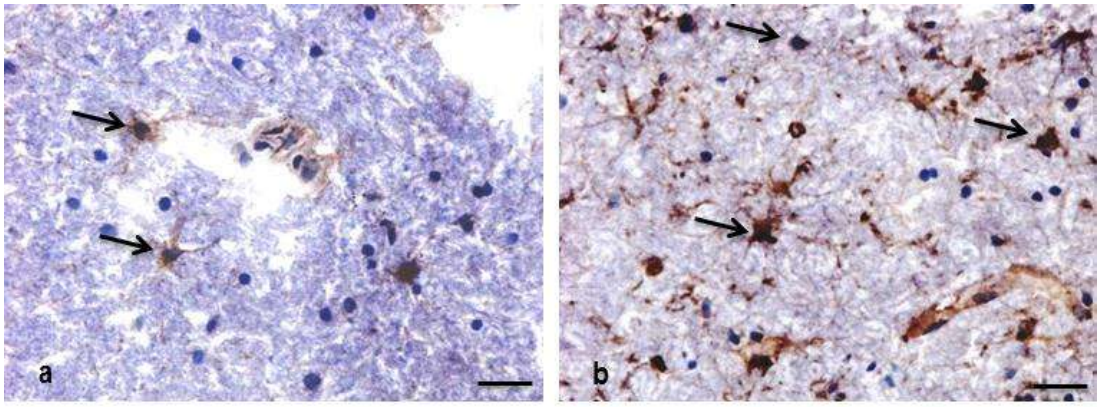

Figure 4.2: Expression of p21 and activated caspase 3. (a) p21 staining of CL section associated with the cytoplasm of star shaped cells (arrows) morphologically resembling astrocytes. (b) activated caspase 3 in CL section also associated with what is thought to be an astrocyte (arrow). Scale bar = 50µm

4.2.2 p16 expression

WM and WML sections were stained for p16 as an additional marker of cellular senescence. Although p16 immunoreactivity was mostly associated with CL and DSCL brains when compared to CNL, the pattern of staining was not consistent and case to case variation within a group was frequently seen. Throughout the three groups of WM (CNL, CL, DSCL), p16 reactivity was mainly detected in the superficial layer of WM immediately underneath layer VI of the cortex. However, very limited p16 reactivity was still observed in deep WM of 12 out of 15 DSCL and 14 out of 15 CL brains which were associated with round small cells resembling oligodendrocytes.

In CNL brains, 9 out of 15 cases showed low p16 reactivity (low intensity) compared to DSCL and CL brains, and was associated with the cytoplasm of cells resembling astrocytes and oligodendrocytes.

p16 staining of CL brains revealed intense reactivity in 11 out of 15 cases that was perinuclear and mostly seen in the cytoplasm of the star shaped cells resembling astrocytes. Numerous immunopositive nuclei were also observed but not as frequent as in DSCL sections. 4 out of 15 CL cases showed very minimal p16 reactivity.

In DSCL brains, p16 reactivity was associated with the nucleus as well as cytoplasm of large cells with long processes resembling astrocytes. However, one of the DSCL revealed p16 intense reactivity associated with large irregular shape cells that have vague nucleus, resembling "ghost" astrocytes. Some DSCL cases (6 out of 15) showed very low levels of immunoreactivity to p16, where it was primarily associated with the nuclei and cytoplasm of cells resembling astrocytes, with some punctate extracellular matrix staining also observed (Figure 4.3).

Quantification of p16 was performed by the autoanalyzer which was set up to calculate the proportion of positive cells present in each of the five captured fields of our

interest from each brain. Statistically there was no significant difference ($p=0.40$) in the level of p16 expression between the three groups of WM (Figure 4.4).

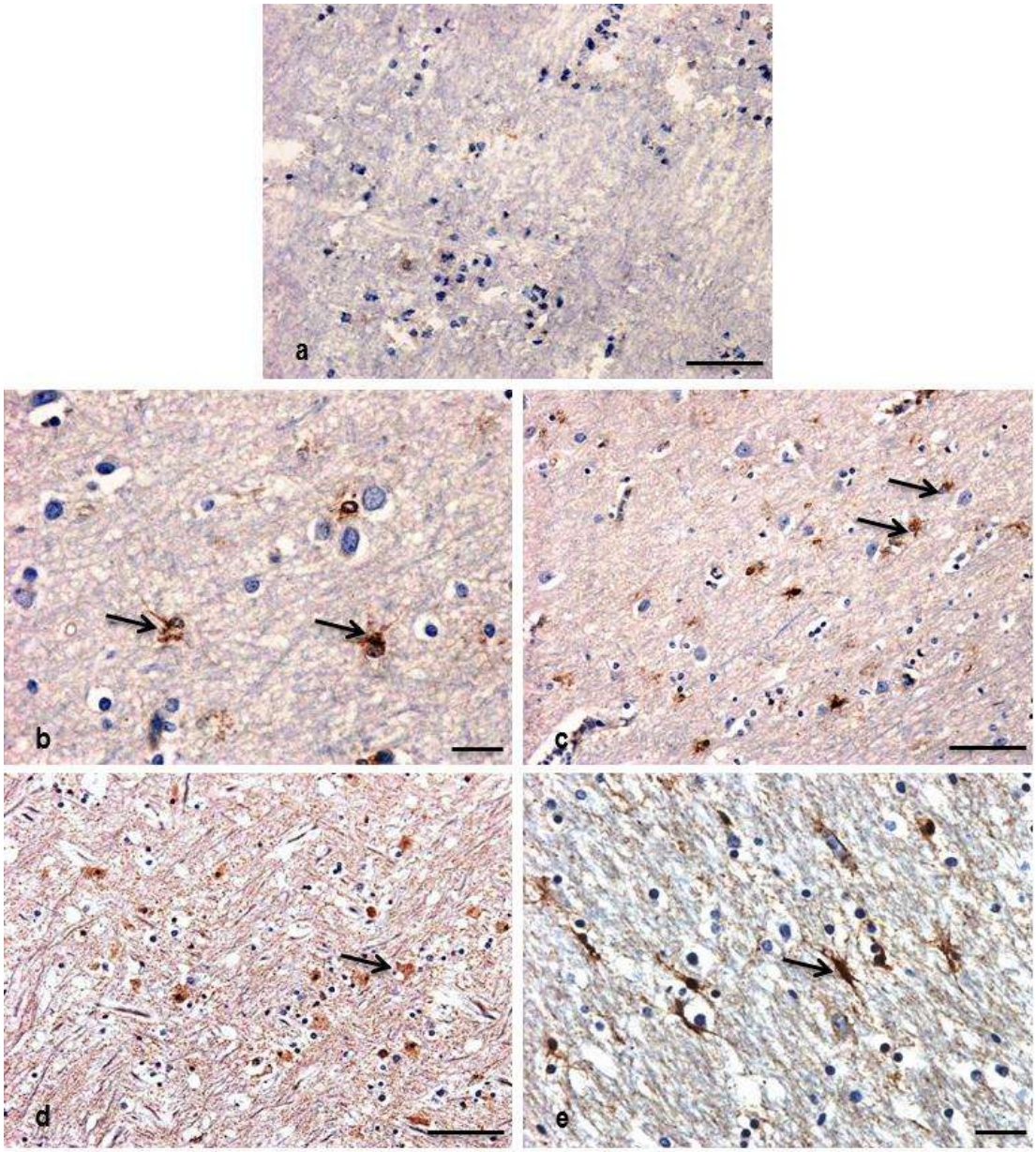

Figure 4.3: Activation of p16 cell cycle check protein as an indicator for cellular senescence. (a) CNL section showing low intensity of p16 reactivity. Scale bar = 100µm. b-c, p16 reactivity in CL sections at a high and low magnification respectively: (b) p16 is shown to be associated with star shaped cells morphologically resembling astrocytes (arrows), Scale bar = 50µm. (c) p16 positive cells lying adjacent to p16 negative cells. This could be owed to the activation of the SASP which stimulate senescent cells to commune their compromise to neighbouring cells which might lead to an immune response or low level of induction of inflammation. d-e, p16 reactivity in DSCL sections: (d) a DSCL brain showing reactivity of p16 in large irregular shaped cells that frequently lack nucleus (ghost cells) (arrows). Scale bar = 100µm. (e) p16 is associated with star shaped cells in another DSCL brain. Scale bar = 50µm

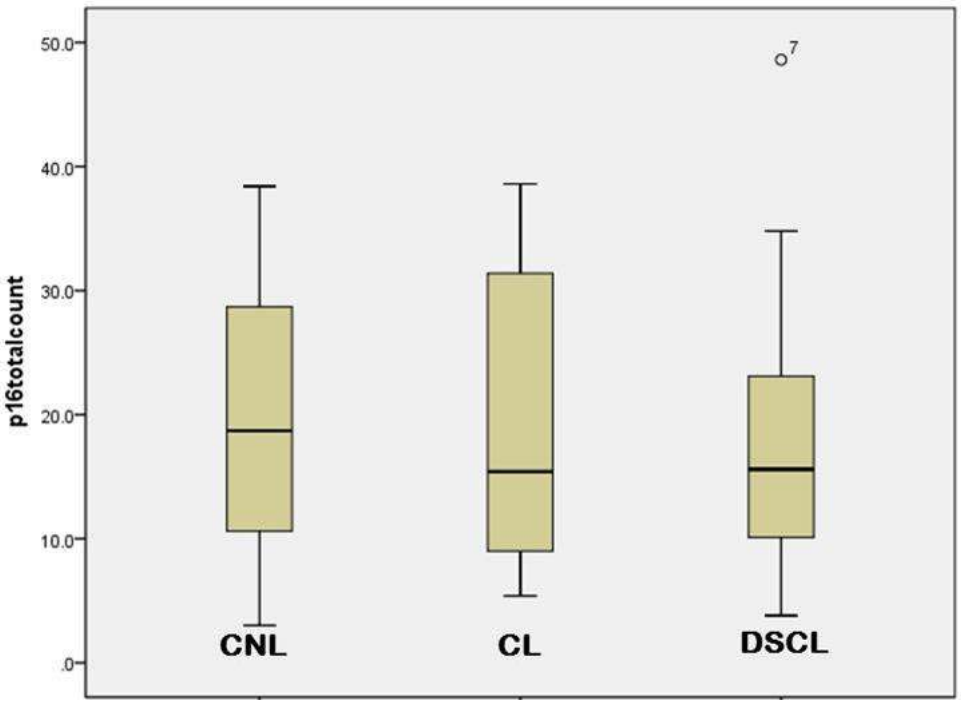

Figure 4.4: Quantification of p16 in three groups of WM (CNL, CL, DSCL). Quantification of p16 in three groups of WM did not reveal statistical difference by applying the Kruskal Wallis test (p=0.40)

4.2.3 Cellular senescence is associated with all glial subtypes

To determine the phenotype of the SA-β-gal$^+$ senescent cells, dual labelling experiments were performed for SA-β-gal with either the astrocyte marker GFAP, or the oligodendrocyte marker OSP or the microglial marker CD68.

Dual labelling was performed on 4 DSCL, 4 CL and 4 CNL frozen brains. However due to poor tissue morphology, the dual labelling in only one case from each group was assessed. GFAP $^+$ cells showed typical satellite morphology however, not all GFAP$^+$ astrocytes were SA-β-gal$^+$. Similarly, some, but not all, OSP$^+$ cells were SA-β-gal$^+$. In contrast, dual labelling SA-β-gal with the microglia marker CD68 revealed no co-localisation.

SA-β-gal was also dual labelled with p16 to study senescence pathway activation. However, due to poor frozen tissue morphology, co-localisation of p16 and SA-β-gal was only observed in 1 CL case in some cells with star shaped body morphologically resembling astrocytes. p16 reactivity was only seen in the cytoplasm of cells resembling astrocytes while SA-β-gal reactivity was distributed throughout the section in oval granular clusters. However, not all cells showed the co-localisation of both markers (Figure 4.5).

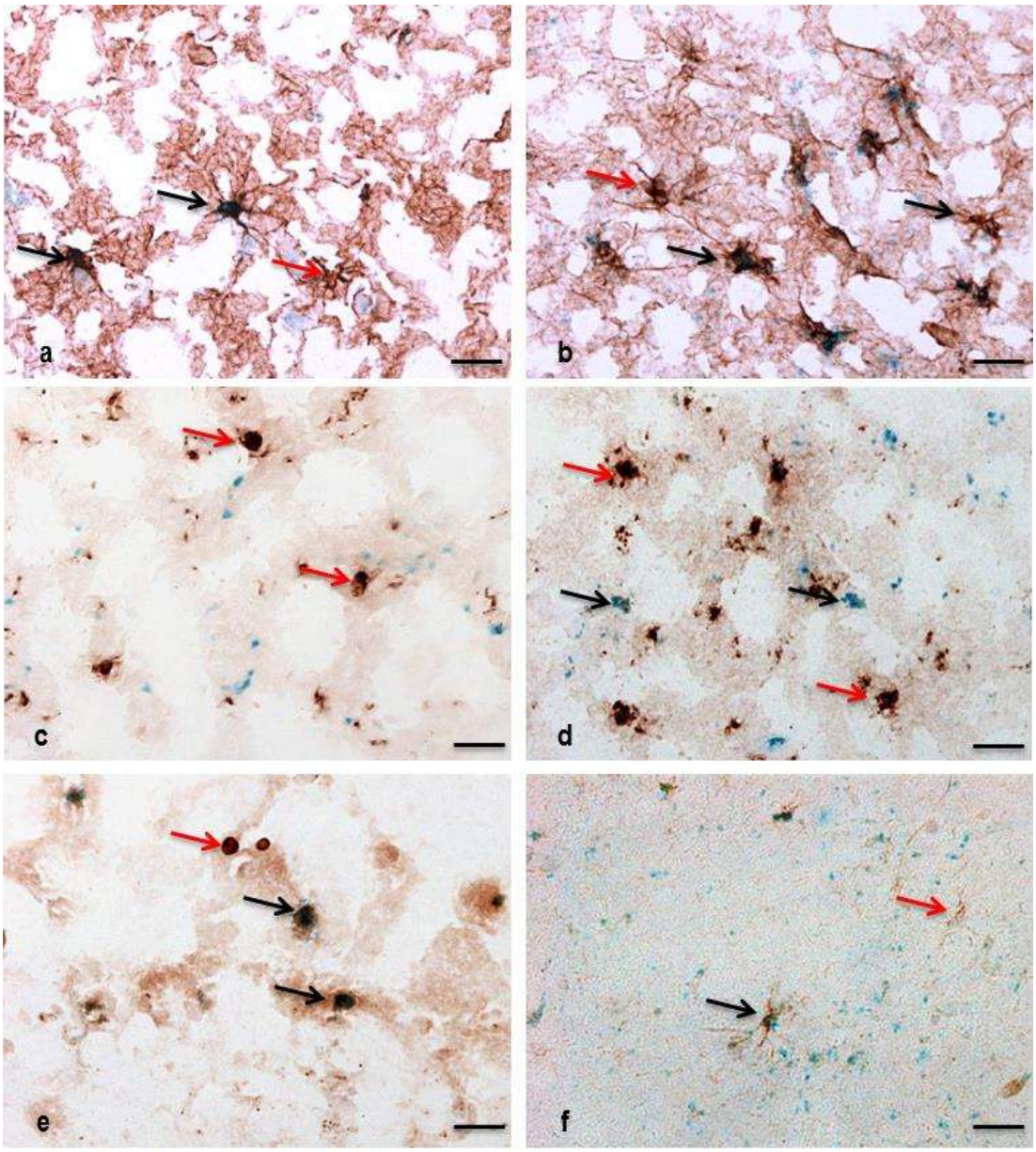

Figure 4.5: Senescence is associated with specific glial cell type. a-b: Double labelling of SA-β-gal and GFAP in a DSCL brain showing colocalisation in some astrocytes (black arrows) indicating an induction of senescence in an astrocyte. Red arrows indicate a non-senescent astrocyte. c-d: Double labelling of DSCL sections with SA-β-gal (black arrows) and CD68 (red arrows) does not show colocalisation. (e): Double labelling in DSCL with SA-β-gal and OSP showing colocalisation in some oligodentrocytes (black arrows) but not in others (red arrows). (f): Double labelling of SA-β-gal and p16 showing colocalisation in star shaped cell thought to be an astrocyte (Black arrow). The red arrow pointing to a $p16^{+}$ cell resembling an astrocyte that does not show evidence of senescence. The scale bar=50µm

4.2.4 Does p16 expression correlate with gliosis?

One of the hypotheses raised in this chapter based on the observation that astroglial cells are often associated with markers of cellular senescence, is that increased p16 expression is associated with gliosis in WM and WML. Therefore, serial sections were stained for GFAP, as a marker of astrocyte hypertrophy, and p16, as a marker of senescence.

GFAP immunoreactivity was observed in all three groups of WM (CNL, CL, DSCL). Astrocytes cytoplasm showed reactivity to GFAP associated with star shaped cellular processes.

GFAP reactivity showed a regular distribution of staining pattern in CNL and CL brains. Within DSCL, increased GFAP immunoreactivity was associated with swollen hypertrophic astrocytes revealing a densely gliotic pattern of staining. A distinct population of intensely $GFAP^+$ astrocytes were detected at the WM border with the cortex. It was also noted that $GFAP^+$ astrocytes frequently clustered around capillaries, and extended long processes to the blood vessels (Figure 4.6).

Quantitation of GFAP area immunoreactivity within the three groups of WM was performed on serial sections to those stained for p16 expression and did not differ between the three group ($p=0.47$) (Figure 4.7). However, It was noted that in 2 out of 15 of DSCL and 1 out of 15 of CNL brains, higher levels of GFAP immunoreactivity was associated with higher p16 expression (Figure 4.8).

Given the presence of p16 in the cytoplasm of astrocytes, we sought to determine whether p16 expression was associated with gliosis (irrespective of group). A non-significant trend (Pearson $r=0.36$, $p=0.052$) of increasing $p16^+$ cell count with GFAP area immunoreactivity was found (Figure 4.9).

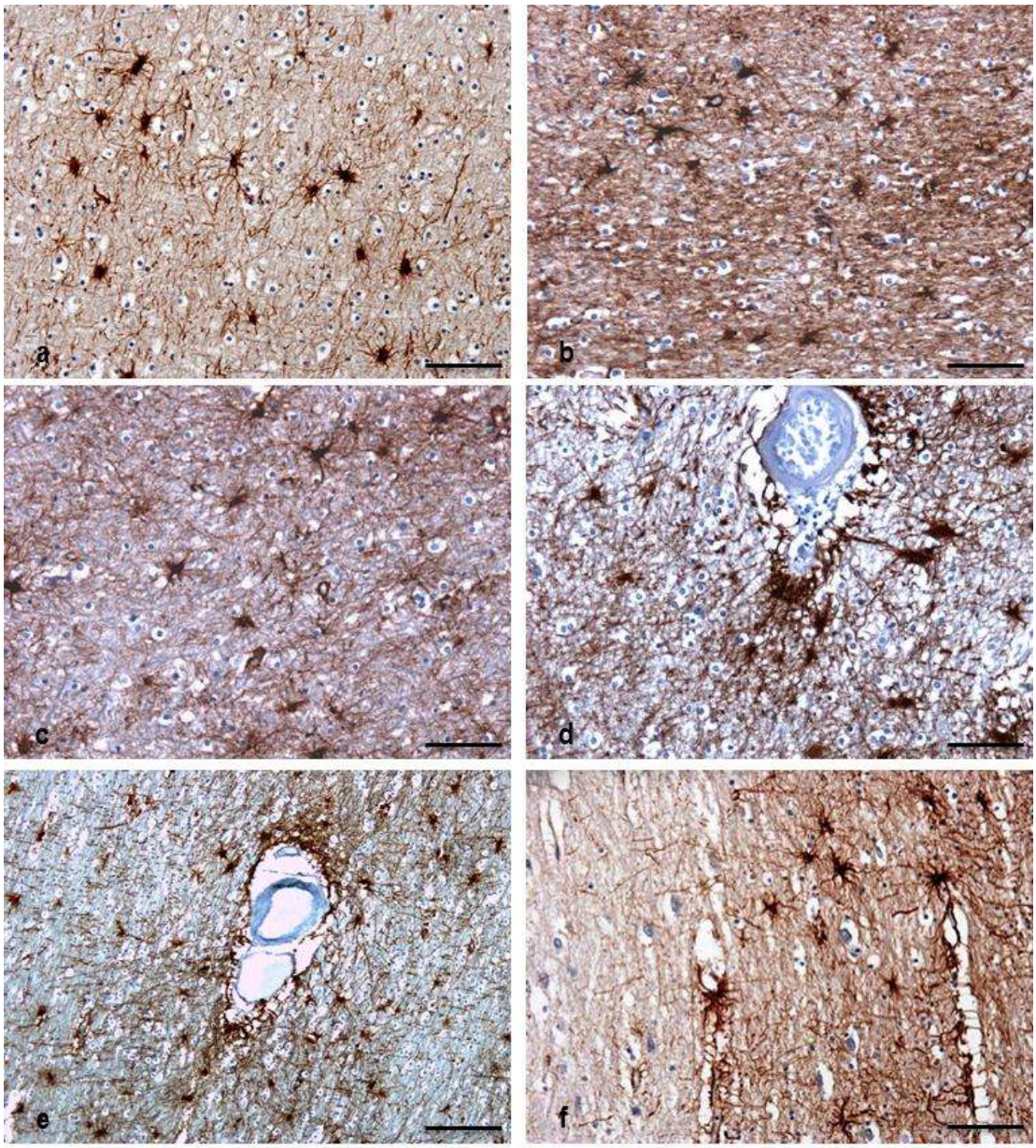

Figure 4.6: GFAP staining in three groups of WM (CNL, CL, DSCL). (a): GFAP staining in a CNL section showing typical star shaped astrocytes. (b, c): GFAP in CL sections showing high background specific staining reflecting the condensed astrocytic population. (d, e): GFAP in a DSCL brain showing a densely gliotic pattern of staining with clustering around nourishing capillaries. (f): GFAP staining in CL section showing proliferated astrocytes at the cortex-WM junction. Scale bar = 100µm

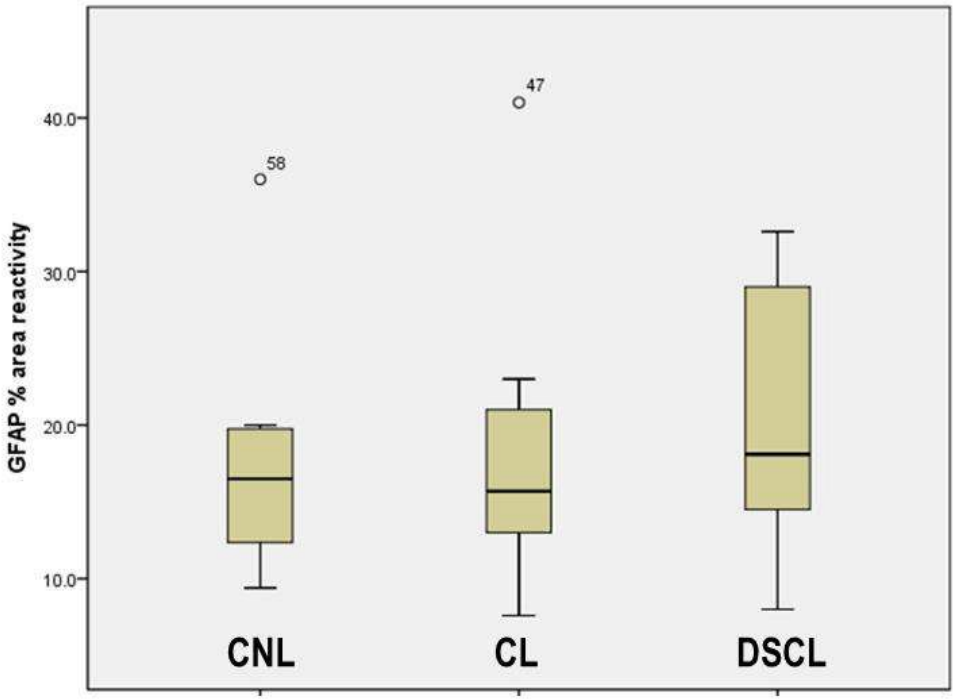

Figure 4.7: Quantification of GFAP in three groups of WM (CNL, CL, DSCL). Quantification of GFAP of WM did not reach significant difference by applying the Kruskal Wallis test (p=0.47)

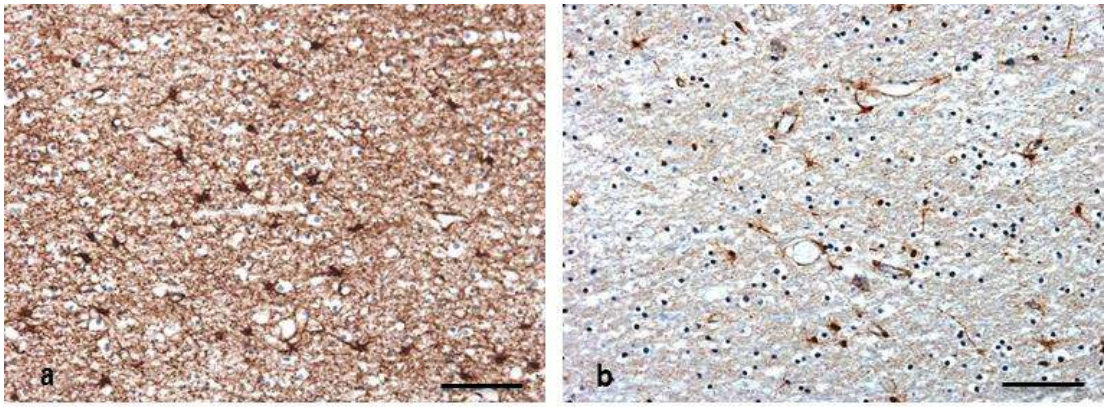

Figure 4.8: GFAP reactivity is associated with high p16 staining. (a): CL brain showing high gliotic GFAP reactivity, that was also associated with high p16 staining (b).

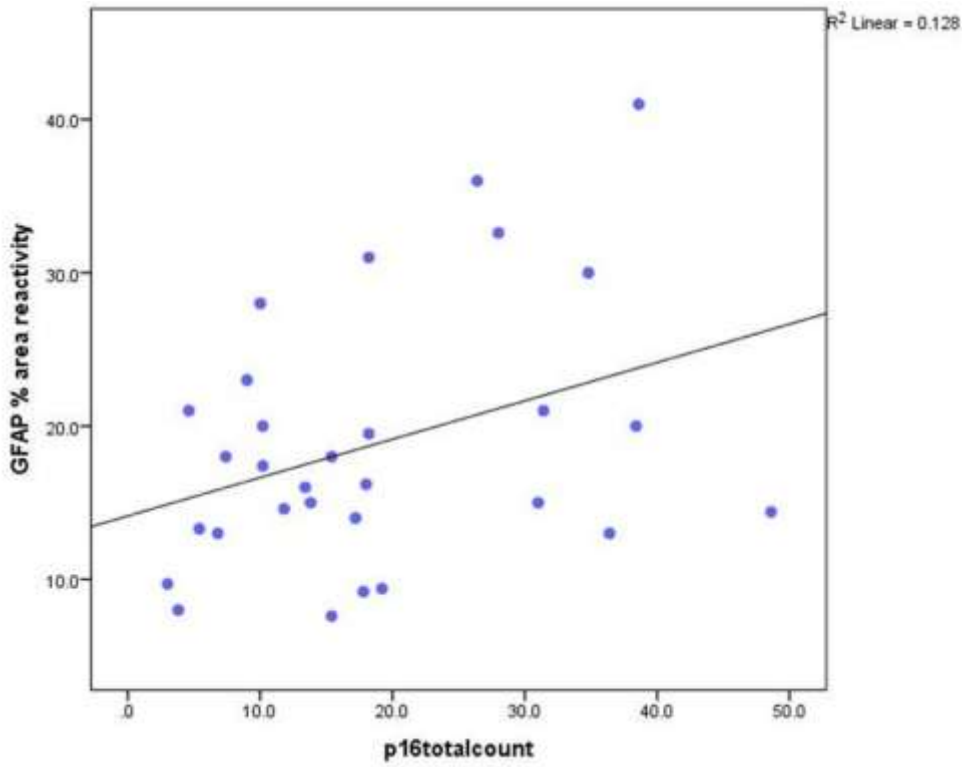

Figure 4.9: Scatterplot showing the association between p16 cell count and area immunoreactivity for GFAP. Using the Pearson's correlation coefficient, we were able to show, that although association between p16 cell count and area immunoreactivity for GFAP did not reach statistical significance (p=0.052), it was almost significant with a trend. This raises an interesting point where there might be an association between gliosis and induction of senescence or the opposite.

4.2.5 Investigation of DNA damage/ senescence gene expression in WM and WML using qPCR array

qPCR array experiment was performed to identify putative candidate molecules that might play a significant role in DDR/senescence activation in WM and WML. An initial screen was performed using randomly selected samples from CNL, CL and DSCL RNA extract on a commercially available 96 well RT-qPCR array plate. The plate was probed with 81 genes that are known to be implicated in DNA damage response and in senescence/cell cycle check. The result showed an alteration in a number of genes in between the three groups of WM, and for this, a selection of genes was made to customise 96 well qPCR array plate which contained only the genes of our interest, along with the housekeeping and quality control genes.

RNA from WM and WML was used to determine alterations in 18 selected gene expression using a customised qRT-PCR array plate that was designed after a wider screen was completed on 81 genes known to be implicated in DDR and senescence pathways. The expression of a panel of eighteen genes involved in DNA damage/ senescence pathways was compared between three groups of WM where findings further supported our previous pathological results which indicated that there is an elevated level of DNA oxidation and DDR in CL and DSCL brains when compared to CNL ones (Figure 4.10).

In particular, the expressions from the DDR genes were relatively increased in concentration in DSCL (*H2AFX*: 1.97; *ATM*: 1.68) when compared to CNL (Figures 4.11). Cell cycle checkpoint genes were also relatively expressed in a higher concentration in DSCL (*TP53:* 1.8; *CDKN1B* -encodes p27: 1.8) when compared to similar gene expression in CNL brains. The highest level of *TP53* expression was in the CL group (2.04) (Figure 4.12).

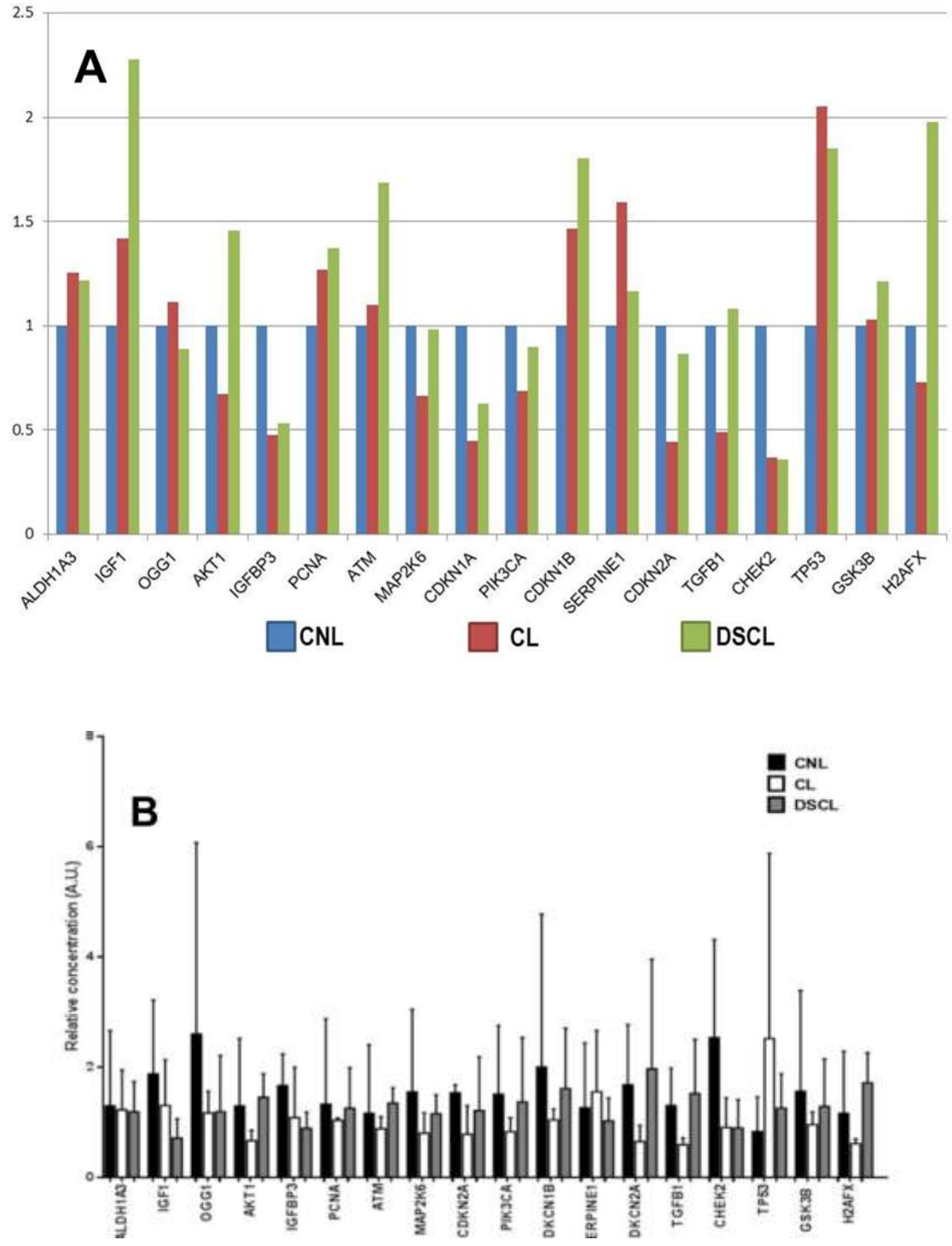

Figure 4.10: Variation in gene expression between three groups of WM (CNL, CL, DSCL) from RTqPCR array. (A) A comparative study in gene expression between 18 key genes that are involved in DDR and senescence/apoptotic pathways. Data shows an alteration in several genes such as H2AFX, ATM, TP53 and IGF-1. **(B)** Variation in gene expression between control non-lesional (CNL), control lesional (CL) and deep subcortical WML (here labelled DSCL) from RTqPCR array, Error bars represent standard deviations

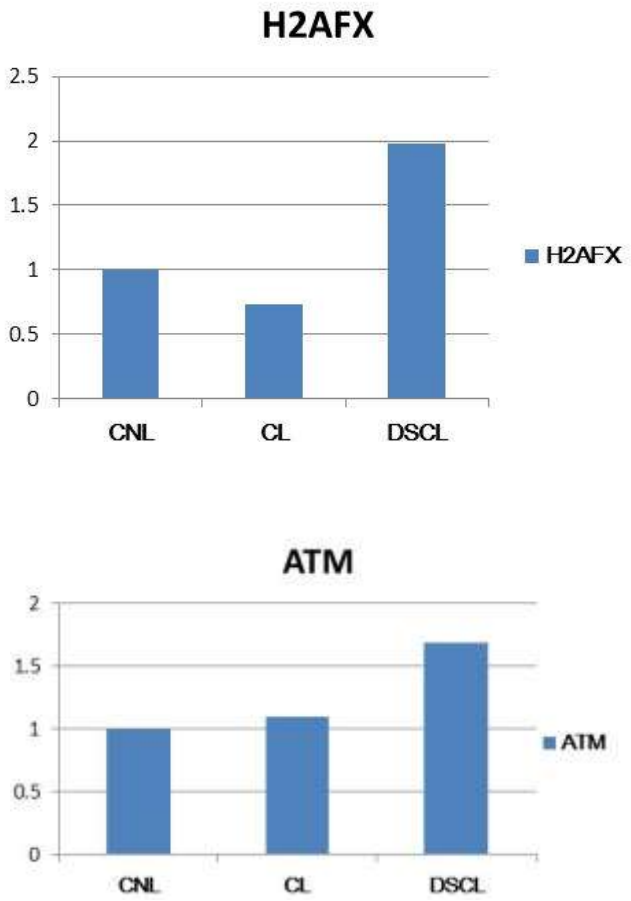

Figure 4.11: Variation in DDR gene expression between three groups of WM (CNL, CL, DSCL) from RTqPCR array. An elevated level of the two DDR gene expressions (H2AFX (Kruscal Wallis test p=0.09) and ATM (Kruskal Wallis test p=0.1)) in DSCL

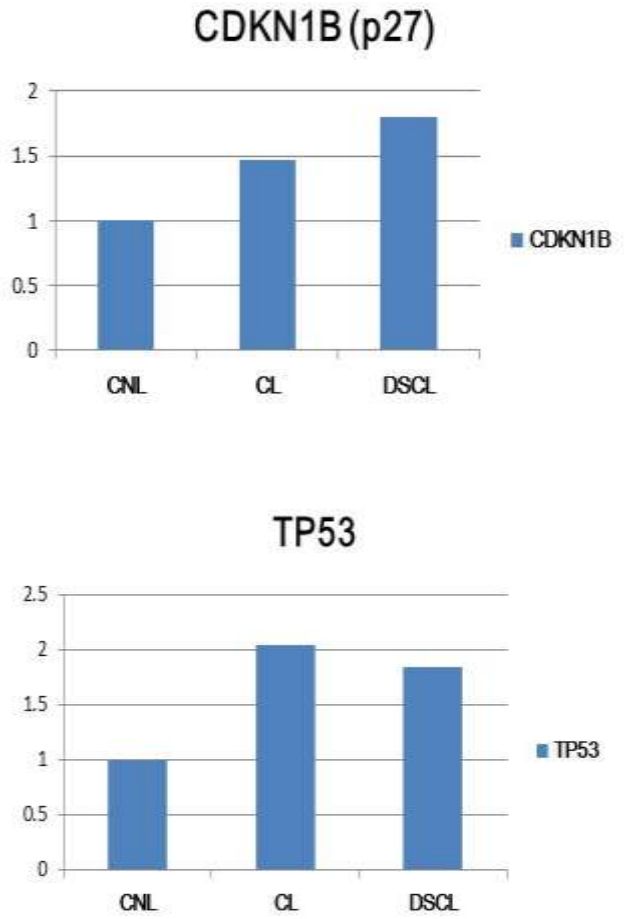

Figure 4.12: Variation in cell cycle check point gene expression between three groups of WM (CNL, CL, DSCL) from RTqPCR array. An elevated level of CDKN1B gene expression was associated with DSCL (Kruskal Wallis test p=0.12), while the highest level of TP53 was detected in the CL group of WM (Kruskal Wallis test p=0.09)

4.2.6 Investigation of p53 expression as an indicator for apoptotic pathway activation

As the previous qPCR data identified changes in p53 mRNA expression, and given the role of the protein in downstream effects of DNA damage, we immunostained for p53 protein. p53 reactivity was mainly observed in the nucleus and cytoplasm of large cells morphologically resembling astrocytes, in smaller ramified bipolar cells resembling microglia and in small round cells resembling oligodendrocytes. Moreover, CNL sections revealed intra-cellular process granular p53 reactivity that was not associated with DSCL or CL brains (Figure 4.13).

Expression of p53 showed significant variation between groups (Table4.1) (Kruskal Wallis, p=0.017) (Figure 4.14). p53 protein expression levels were lowest in the lesions which showed lower counts than the CL group (Mann Whitney p=0.004).

To determine $p53^{+}$ cellular phenotype, we dual labelled p53 with the microglial marker CD68 and with the astrocyte marker GFAP respectively. p53 was determined to be associated with microglia as well as with astrocytes in a DSCL brain (Figure 4.13).

Table 4.1: Quantification of p53 in three groups of WM

Marker		**CNL**	**CL**	**WML**
p53 % positive nuclei	Mean (SD)	15.4 (6.7)	20.9 (7.2)	12.2 (7.7)
	Median (IQR)	17.2 (14.7)	19.6 (13.9)	10.1 (12.7)

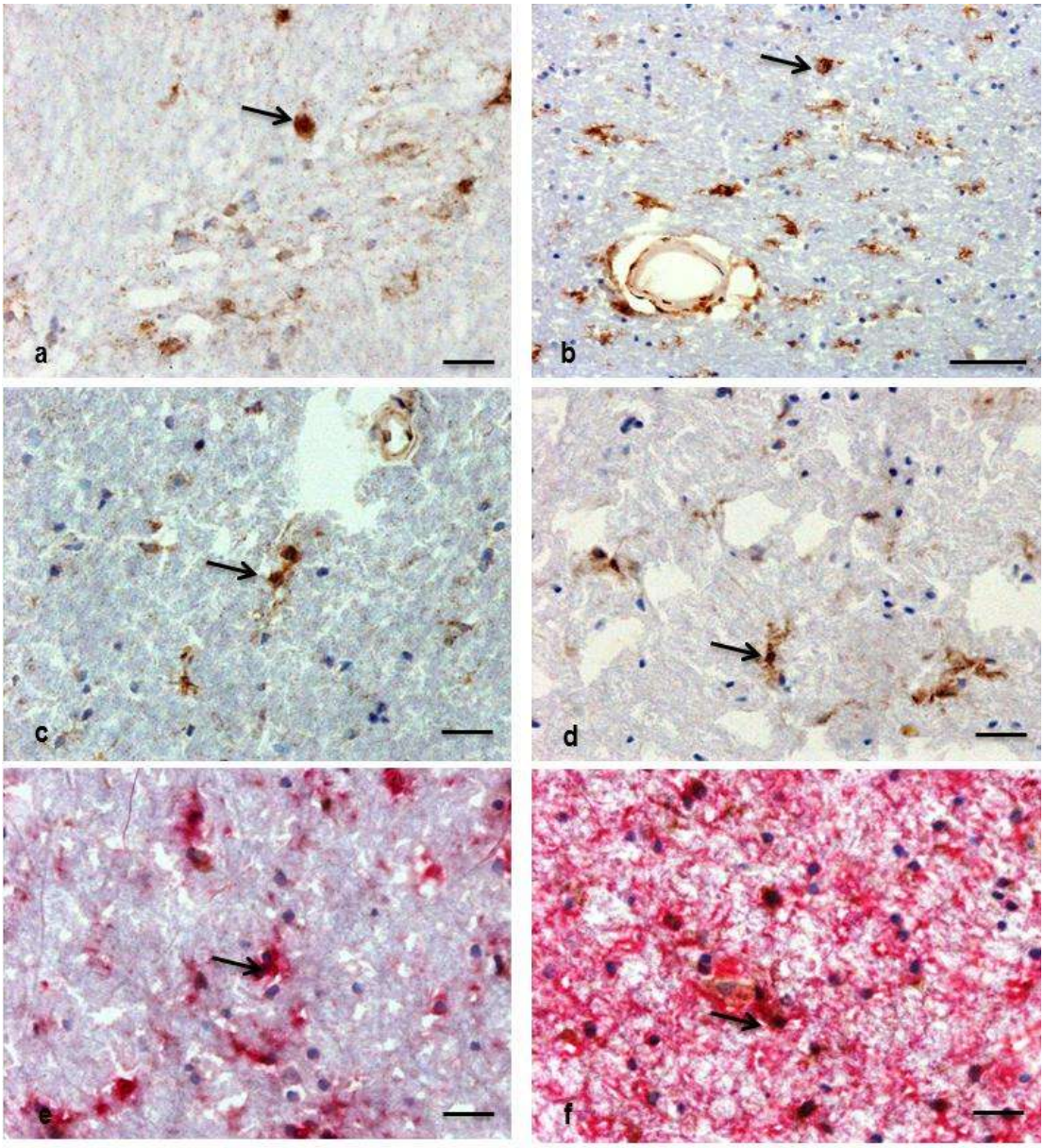

Figure 4.13: p53 staining in three groups of WM (CNL, CL, DSCL). (a): Cellular and extracellular granular p53 reactivity in CNL brain (arrow pointing to a p53 positive glial cell, resembling oligodendrocyte)**.** Scale bar = 50µm. b-c, p53 reactivity in CL brains is associated with multiple cell types morphologically resembling microglia and oligodendrocytes respectively (arrows). (b) low magnification showing p53 reactivity in glial cells as well as endothelial cells of a nourishing capillary. Scale bar = 100µm. (C) Higher magnification showing p53 reactivity in cell morphologically resembling microglia. Scale bar = 50µm. (d) p53 reactivity in a DSCL showing reactivity (arrow) in a cell morphologically resembling microglia. Scale bar = 50µm. e-f, Dual labelling of p53 with cell anatomical markers to determine type of glial cells associated with p53 activation. (e) Dual labelling of CD68 (red) and p53 (brown) showing some co-localisation in a DSCL brain (arrow). (f) Dual labelling of GFAP (red) and p53 (brown) in a DSCL brain showing colocalisation (arrow). Scale bar = 50µm

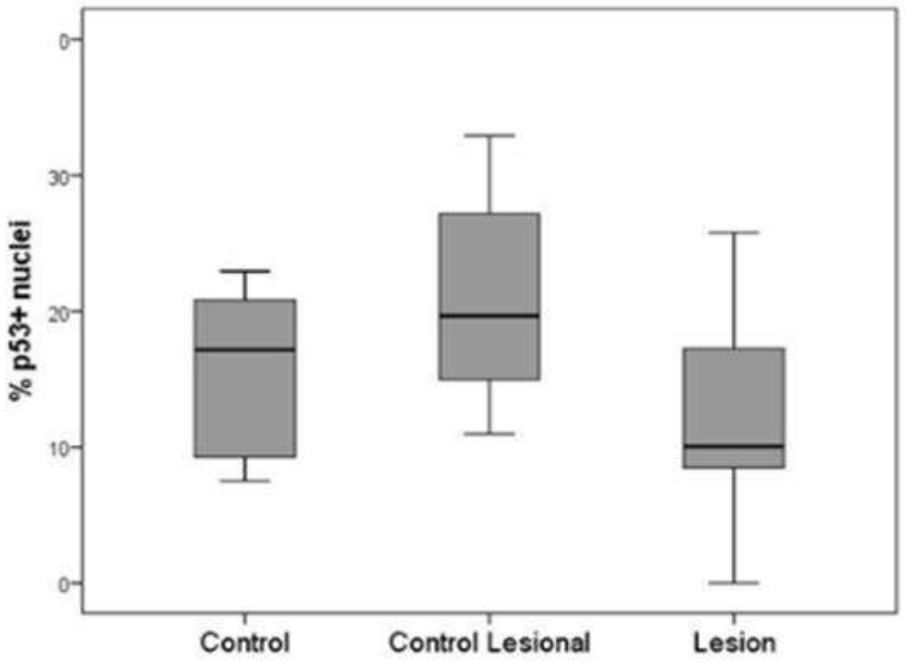

Figure 4.14: Quantification of p53 in three groups of WM (CNL, CL, DSCL). Boxplot showing variation in % of nuclei positive for p53 between the 3 groups, with higher values in the CL group

4.3 Discussion

In recent years, the concept and mechanism of cellular senescence has been studied extensively using cellular models where it is suggested to be a contributor to ageing and age related diseases (Herbig et al., 2006, Baker et al., 2008, Baker et al., 2011, Campisi, 2013). However, the current *in vivo* study is one of a few that have demonstrated the presence of cellular senescence in human aged brain and for the first time, studied cellular senescence as a consequence of persistent DNA damage to glial cells in WM and WML.

Long established research suggests that a significant amount of DNA damage and DDR is present in aged neurons, however, recent studies have realised the impact of several stressors such as oxidative stress on glial cells in WM and how it might contribute to myelin loss and cognitive decline (Simpson et al., 2009, Simpson et al., 2010d). Our recent findings support the role of oxidative stress in contributing to DNA damage in glial cells in CL and DSCL of the human ageing brain and as a downstream effect of persistent DDR, activation of senescence and apoptotic pathways.

Studying SA-β-gal activity as a marker of cellular senescence in glial cells did not reveal significant differences between the three groups of WM (CNL, CL, DSCL) but importantly, it reflected the variation that is likely to be seen in such a population based study that depends solely on the age of the participants and in this project on the presence/absence of WML.

SA-β-gal activity has been considered to be a marker of senescence in *in vitro* cell models and recent studies have demonstrated SA-β-gal activity in neurons in mouse brain (Jurk et al., 2012, van Deursen, 2014) and in human cortical astrocytes (Simpson et al., 2010b). The expression of SA-β-gal now identified in WM astrocytes and oligodendrocytes thus suggests induction of senescence mechanisms in glial cells. It is worth noting the difficulty quantifying SA-β-gal expression, as has also been reported by another group

(Lawless et al., 2010). In the current study there were no significant differences in the level of expression between the three groups of WM (CNL, CL, DSCL), therefore, senescence induction cannot specifically be associated with WML and may be related to other effectors such as age.

Several studies have demonstrated that brain ageing is associated with low levels of neuroinflammation (Godbout and Johnson, 2009, Lucin and Wyss-Coray, 2009, Lynch, 2009), and with an increase in the number of microglia as well as an increase in cytokine secretion (Salminen et al., 2011). In the current study, we demonstrated that although SA-β-gal activity was associated with astrocytes and oligodendrocytes, it was not associated with microglia. This could be linked to the SASP which sets a proinflammatory environment recruiting microglia to the site of damage. The senescent cells that accumulate in ageing WM may create a pro-inflammatory environment through the secretion of proinflammatory growth factors, proteases and chemokines (van Deursen, 2014), including transforming growth factor β1 (TGFβ1), insulin like growth factor (IGF) and IL-1α and IL-6 / IL-8 (Orjalo et al., 2009, Coppé et al., 2010).

TGFβ1 is a multifunctional cytokine that has profound effects on angiogenesis and plays a major role in maintenance of vessel wall integrity in the human CNS (Pepper, 1997). It has been reported that chronically increased astroglial secretion of TGFβ1 may promote an excessive secretion of basement membrane proteins associated with amyloid deposition in TGFβ1 mice that contribute to thickening of walls of capillaries. This was found to lead to microvascular degeneration in the cortex of an AD mouse model (Wyss-Coray et al., 2000, Salminen et al., 2011). TGFβ1 was one of the genes tested for altered expression in our customised qPCR plate; however, our data was inconsistent with Wyss-Coray's group result in which there was a decrease in the level of TGFβ1 expression in CL brain when compared to CNL and DSCL (Wyss-Coray et al., 2000). This may reflect the different complexity between WM and the cortex where pathology in those two major brain compartments is

hugely variable. The field effect of WML on areas free of lesions (i.e. CL) might be an important trigger that stimulates glial cells to change their gene expression, including TGFβ1. However, whether this change is a defence mechanism or whether it is a compromise from glial cells that will probably lead to WML formation is unknown.

IGF-1 is a cytokine that has long been known for its role in the periphery as a metabolic hormone. However, only recently the importance of IGF-1 in the CNS has been recognised where it plays a key role in brain development and function (Castilla-Cortázar et al., 2014). IGF-1 is critical for nerve protection against pathological insults that are associated with neurodegeneration by being responsible for activation of anti-apoptotic cascades, and by induction of myelination both *in vivo* (Mozell and McMorris, 1991) and *in vitro* (McMorris et al., 1986). There is a growing body of evidence suggesting the association of altered IGF-1 levels in the brain with neurodegenerative diseases such as AD, Parkinson's disease (PD) and Huntington disease (HD) (Rollero et al., 1998, Humbert et al., 2002, Picillo et al., 2013) with the variation of IGF-1 secreted level between neurons and astrocytes. This was first reported by Moloney et al, (2010) where they concluded that IGF-1 secretion was decreased in neurons but increased in astrocytes in AD patients (Moloney et al., 2010). Our data showed a consistency with this study where we demonstrated an increase in the level of IGF-1 gene expression in DSCL brains. This makes the study of IGF-1 of critical importance in the onset and progression of ageing and age related diseases.

A persistent DDR is a major stimulus that induces cellular senescence mainly by engaging either or both of the p53/p21 and p16 master transcriptional regulators (Beauséjour et al., 2003). p53 regulates the transcription of a large number of genes that include cell cycle arrest, apoptosis, DNA repair, cell growth and proliferation (Sengupta and Harris, 2005, Hasty and Christy, 2013). Thus p53 activity is critical to maintain genomic integrity, cell growth and proliferation during times of stress. The p53 qPCR and immunohistochemistry data in the current study showed a significant increase in the level of p53 reactivity in CL brains, where a field effect of WM damage is present. However, it is

unclear whether this stress induced response was initiated to minimise further damage and prevent further loss of cell function and myelin attenuation, or whether it contributes to WML formation. Several studies have addressed this important question from a similar prospective and studied the potential positive and negative sides of the SASP where one important suggested function is to ensure that damaged cells communicate their compromised state to neighbouring healthy ones and prepare the tissue for repair. Another function of the SASP is to trigger the immune system to identify and remove such a damaged cell (Campisi, 2013). On the other side, studies have also demonstrated the involvement of the SASP in age related pathology by driving tissue degeneration ultimately by activation of proteins, such as p16 that is expressed by most senescent cells where its function is to enforce the senescence growth arrest (Campisi et al., 2011). In the current study, astrocytes were predominantly associated with a SASP in both CL and DSCL brains, and considering the important role that astrocytes play, it is suggested that there is "a gain of function" in this cell population that might have created the largest component of the SASP. However, we have demonstrated that not all astrocytes express p16 which suggest that although there were senescent astrocytes detected, not all of them were part of the SASP.

Cellular senescence is established and regulated by at least two major pathways: the p53/p21 and p16/pRB pathways (Campisi, 2013), and although both pathways lead to a similar cellular phenotype, the stimulus is different. The p53/p21 pathway is initiated by genomic or epigenetic damage that creates direct DNA damage (Rodier et al., 2009, Rodier et al., 2011), while the p16 pathway is activated after a prolonged exposure of the cell to DNA damage that created a prolonged DDR. This chronic DDR is the one that would trigger p16 activation (Takahashi et al., 2006, Freund et al., 2011). We have shown that there is a similarity in the level of GFAP and p16 expression in DSCL which suggests that gliosis is associated with a senescence phenotype that is not induced by direct DNA damage but rather by persistent DDR resulting in an irreversible growth arrest that is associated with a well-

established lesion. This sets the possibility that induction of senescence in astrocytes in WM may involve mechanisms other than direct DNA oxidation.

In summary, our results show that senescence is a feature of WM in the human ageing brain in oligodendrocytes and astrocytes. Detection of p53 activation by qPCR and by immunohistochemistry indicates induction of apoptosis/senescence as a result of direct DNA damage that was previously demonstrated to be significantly increased in CL and DSCL when compared to CNL brains. p16 is another indicator of cellular senescence and we found its activation to be associated with gliosis. However, this was not statistically significant but rather raises an interesting question about the different pathways and causes that triggers senescence as a downstream effect of persistent DNA damage. Senescence in ageing WM was also found to be closely associated with the SASP which is characterised by alteration of glial gene expression and glial cell proliferation. Expression of several key genes involved in DDR and apoptotic/senescence pathways was found to be affected in CL and DSCL brains. Also, the recruitment of microglia to the sight of damage which are negative for SA-β-gal is another indicator for the SASP induction by neighbouring senescent cells that secret proteases and cytokines to activate the immune response.

This *in vitro* study is one of the very few that looked at the presence and activation of cellular senescence in the aged human brain and it is the first one to investigate senescence in WM and WML. However, studying such pathology at its end stage on post-mortem human brain is challenging. Several attempts of antibodies used in the immunohistochemistry study were not successful due to the difficulty in antigen retrieval, and double labelling study was almost impossible to quantify due to the poor tissue morphology. Case to case variation within a group of WM was often seen and this reflects the difficulty expected when dealing with human tissue from a population based study. Nevertheless, the outcome of this part of the study compliments the previous observation which showed that there is a significant increase of DNA oxidation in CL and DACL brains using the 8-OHdG as a marker of direct DNA damage. This comes consistent with the

available literature: persistent DNA damage activates senescence/apoptosis in glial cells in aged WM through multiple pathways and is also associated with a SASP. Several interesting research ideas can be investigated in the future, such as the effect of SASP on astrocytes and how this will alter its function in WML and the surrounding WM.

CHAPTER 5: THE USE OF LIQUID CHROMATOGRAPHY/MASS SPECTROMETRY IN DEVELOPING AN ANALYTICAL METHOD TO DETECT GUANOSINE DNA BASE OXIDATION AS A MARKER OF DNA DAMAGE

5.1 Introduction

During oxidative phosphorylation, almost 2% of total oxygen consumed by cell to perform numerous endogenous processes form reactive oxygen species (ROS) (Markesbery, 1997). The state where the internal produced ROS exceeds those being detoxified is known as oxidative stress. Increasing evidence suggests that oxidative stress is a major contributor to ageing as well as neurodegenerative diseases. ROS, especially hydroxyl radicals, can attack protein, lipid, mtDNA as well as nDNA (Cooke et al., 2003) and cause change in protein expression, lipid peroxidation, DNA double strand breaks and base modification (Lovell et al., 1999). The most commonly analysed marker to assess the extent of oxidative stress and its end point damage to DNA is the 8-hydroxy-2-deoxy-guanosine (8-OHdG) (Herbert et al., 1996, Gabbita et al., 1998, Dizdaroglu et al., 2002).

Although 8-OHdG is a direct biomarker for oxidative DNA damage that can be detected in human tissue by immunohistochemistry, quantification techniques could be subjective and debatable. 8-OHdG scoring completed in the first part of this study was performed by two different observers (S.M and J.S) to check for consistency, and although the scores were highly correlated, S.M threshold was consistently lower than J.S. This show the subjectivity within histological studies that implies personal observation and judgment as a main factor. For this reason, quantification of immunohitochemical markers by manual scoring is not a gold standard protocol.

For this reason, cellular 8-oxodG has been extensively analysed *in vitro* (cell cultures) and *in vivo* (rat liver, human CNS) using high performance liquid chromatography coupled to an electrochemical detector (HPLC-ECD), mass spectrometry (HPLC-MS), or liquid chromatography interfaced with electrospray ionization mass spectrometry (LC ESI MS) (Matter et al., 2006, Wang et al., 2006, Boysen et al., 2010). This gold star technique is a powerful tool that does not rely on amplification thus DNA post-transcriptional modification is preserved and could be directly assessed.

Studies have shown previously that oxidised DNA is increased in AD (Gabbita et al., 1998, Wang et al., 2005) and in mild cognitive impairment (Wang et al., 2005). In this study, we aimed at detecting and quantifying 8-OHdG as a direct marker of DNA oxidation in three groups of WM using tandem mass detection (HPLC-MS/MS). This will compliment and validate our previous immunohistochemistry findings of this marker where we will be able to detect and quantify accurately the number of modified guanosine base in the presence of persistent DNA damage.

The main aim of this part of the study was to develop and optimise a method to detect and quantify base modification in DNA extracted from human autopsy tissue. Setting up the machine was not a straight forward technique and was very time consuming. A developed technique for the use of liquid chromatography/tandem mass spectrometry (LC/MS/MS) selected reaction monitoring (SRM) method that utilises online column-switching valve technology to detect the biomarker of oxidative stress. To allow for the accurate quantitation of guanosine base, corresponding [$^{15}N_5$]-labelled stable isotope internal standard was added to samples prior DNA hydrolysis.

The European Standards Committee for Oxidative DNA Damage (ESCODD) has highlighted the possibility of artificial formation of 8-oxodG during the process of DNA extraction and hydrolysis. This could be due to the high affinity of guanine base to oxidation in the presence of such harsh experimental conditions which could lead to false positive results. Previously, protocols have been revised to include antioxidants, metal chelators, or free radical minimising agents during sample preparation for the prevention of false oxidation (ESCODD, 2003). Boysen et al., (2010) group has been working for several years to establish a reliable and reproducible protocol that is used with ultra-high pressure liquid chromatography–heat assisted electro spray ionization–tandem mass spectrometry (UPLC–HESI–MS/MS) to detect 8-OHdG with the prevention of artificial oxidation formation (Boysen et al., 2010). Their technique utilises Tetramethylpiperidine 1-oxyl (TEMPO), and for the success that their study made, we have chosen to also use the TEMPO in our

protocols to prevent formation of artificial DNA damage. TEMPO was added to all samples prior to DNA extraction.

In a typical scenario, DNA would be extracted from tissue then DNA will be digested in the presence of [$^{15}N_5$]-labelled stable isotope. Samples will then be injected into HPLC where DNA bases will get separated and passed on to MS.

Experiments started by calibration using commercially available standards then control extracted DNA (from fish) and finally our human brain samples were introduced. The main objective of this work is to validate the previous findings of the significant elevation of DNA oxidative damage in CL and DSCL brains using a developed protocol that utilises MS as a gold star technique to detect and quantify the amount of guanine base modification as a product of oxidation.

3.2 Results

3.2.1 DNA isolation

DNA was isolated from three groups of WM (CNL, CL, DSCL) as described previously. To avoid the formation of artificial DNA oxidation, DNA hydrolysis was performed in the presence of TEMPO, which is a chemical that has been used in previous studies where by it significantly decrease the amount of oxidation that could be introduced to samples while processing them. The concentration of isolated DNA was then measured using the nano-drop, which varied from as little as 20ng/µl to 200ng/µl.

3.2.2 Enzyme hydrolysis

In the presence of 150Pmol 0f [$^{15}N_5$]-labelled stable isotope, the adjusted concentration of genomic DNA was digested by DNA-degradase enzyme containing Alkaline Phosphatase to generate the corresponding nucleosides ((sugar + the DNA base (without the phosphate group). To check that DNA was digested adequately, a simple gel electrophoresis was done for the digested sample vs a non-digested DNA extract (Figure 5.1). The results confirm the isolated genomic DNA was hydrolysed.

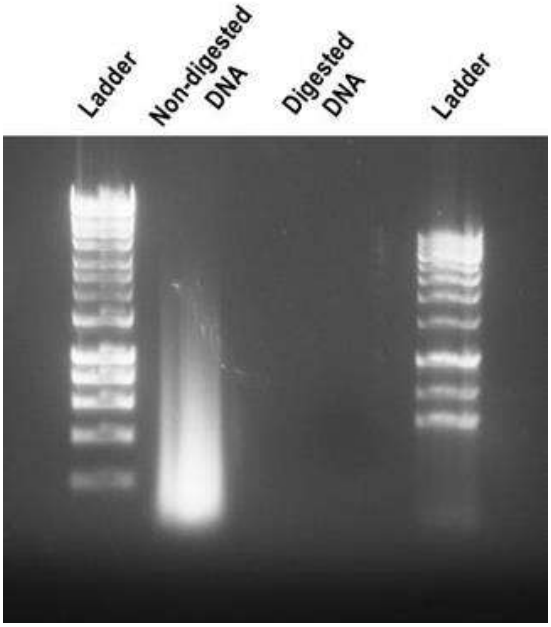

Figure 5.1: DNA hydrolysis. Gel electrophoresis showing the adequate hydrolysis of DNA isolated from DSCL brain using DNA degradase enzyme vs an undigested isolated DNA from the same DSCL brain in the absence of the degradase enzyme

3.2.3 HPLC analysis of the enzymatic hydrolysis of DNA

The main aim of the MS work was to establish a reliable technique to measure and compare the endogenous level of 8-OHdG present in DNA from the three groups of WM (CNL, CL, DSCL). However, to allow an accurate quantification of the adduct, a corresponding internal [$^{15}N_5$]-labelled stable isotope was added to samples prior to running them on the HPLC. This enabled the construction of calibration lines by preparing a series of standards each containing varying amounts of [$^{15}N_5$]-labelled stable isotope added to 10ug of genomic DNA and the concentration of the solutions will be calculated using the extinction coefficient by determining the UV absorbance at 260nm (Singh et al., 2009).

As part of our setup, we started our experiment with running a couple of blanks followed by injecting different concentrations of the four DNA nucleoside standards separately (Deoxyguanosine, Deoxyadenosine, Deoxycytidine and Deoxythymidine) into the HPLC until an effective signal was detected. A peak was detected for each standard using the UV detector (Figure 3.4) and a note was recorded for each standard retention time (i.e. the time spent for each sample to travel through the columns after the detection of the peak and until it gets dispensed from the machine). After that, the experiment was repeated and fractions containing standards were collected carefully according to their retention times in separate tubes.

To characterise the enzymatic hydrolysis of DNA, HPLC analysis was performed to separate the nucleosides in conjunction with UV analysis (260nm) using the C30 hypercarb column. Nucleoside standard were used to optimise the gradients and enable verification based on their retention times. The HPLC analysis of Deoxycytidine is shown in figure 5.2. One of the challenges of using HPLC to analyse or purifiy 8-OHdG is the co-elution with the abundant nucleoside dG (Boysen et al., 2010). Therefore the proposed HPLC needs to separate the 8-OHdG from dG. A comparison of the HPLC analysis of [$^{15}N_5$]- 8-OHdG

compared to dG is shown in figure 5.3. The fraction was also collected after noting the retention time did not overlap with the dG.

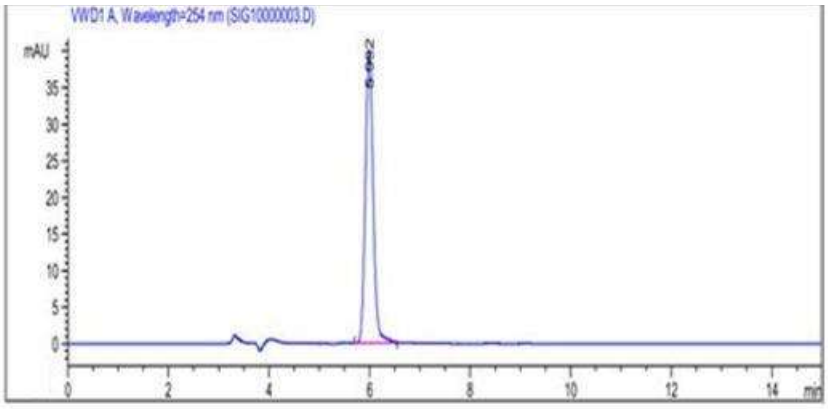

Figure 5.2: HPLC detection of Deoxycytidine. By injecting 100µM of DC a peak was detected using the UV light (260nm)

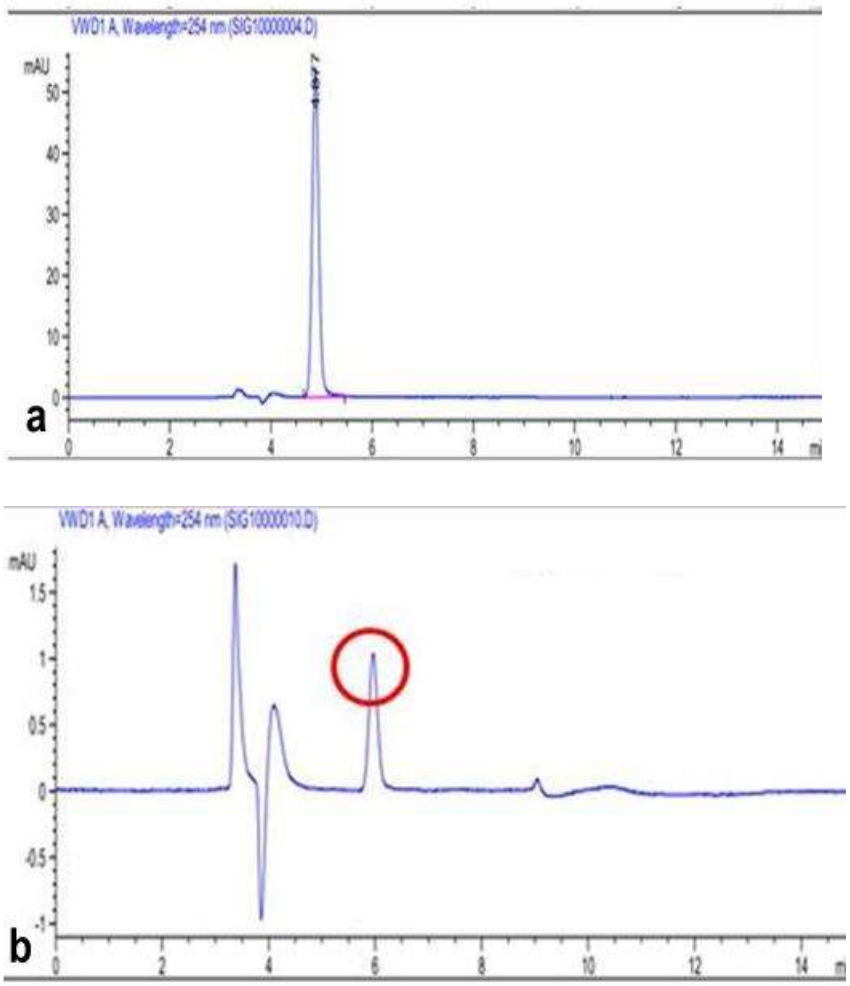

Figure 5.3: A comparision between Deoxyguanosine and the [15N5]- 8-OHdG HPLC analysis. (a) an adequate peak was detected by injecting 100µM of DG at a retention time that was separated from the [15N5]- 8-OHdG pesk (b). Both were detected by UV (260nm) detector

Following optimisation of the HPLC for the analysis of the four nucleoside standards, the hydrolysed DNA isolated from a control DNA sample was injected (genomic DNA from fish). Multiple concentrations were assessed (10µg/µl, 50µg/µl and 100µg/µl). The adequate concentration was 50µg/µl where we were able to see the four separate DNA bases' peaks (Deoxyguanosine, Deoxyadenosine, Deoxycytidine and Deoxythymidine) (Figure 5.4). Fractions were also then collected according to the correct retention times. To further verify the nucleosides the fractions were collected with the aim to directly infuse into the mass spectrometer to further verify the nucleosides. Unfortunately following fractionation, the MS was unable to detect the corresponding masses of the nucleosides, due to the low concentration of the samples collected which were below the detection senstivity of the instrument.

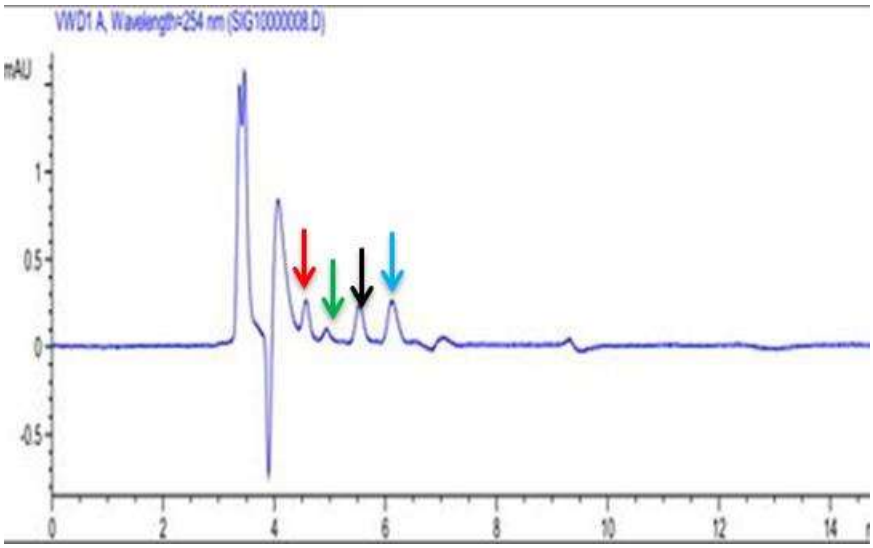

Figure 5.4: HPLC analysis of control DNA sample. Detection of four DNA nucleosides peaks separated by HPLC and detected by UV detector (260nm): Deoxyadenosine (red arrow), Deoxyguanosine (green arrow), Deoxycytidine (black arrow), Deoxythymidine (blue arrow) at different retention times

3.2.7 LC MS analysis of nucleosides using a Hypercarb porous graphite column

Since the previous protocol proved unsucsessful, we developed an alternative approach using liquid chromatography directly interfaced to the mass spectrometer. This system Combines the physical separation capabilities of HPLC with the mass analysis capabilities of mass spectrometry (MS) where sample is injected under high pressure (mobile phase) through a column that is packed with a stationary phase hyper-carb column C30 (stationary phase) which is a reversed phase liquid chromatography that is designed to provide high quality separation of hydrophobic structurally related products. To ensure a better sensitivity of analytes detection, I set the sample to flow in a lower flow rate (0.15ml/min) which should improve the sensitivity of detection. I started by injecting 150pmol of [$^{15}N_5$]- 8-OHdG. The mass spectra revealed an unexpected mass (323 m/z rather than 289 m/z expected for the M+H+ species). To confirm this observation, a different standard was prepared (5hydroxymethylC) and injected into the LC MS using the same column which also showed that oxidation had occurred. From this outcome we concluded that the Hyper-carb C30 column has the potential to oxidise chemical compounds and it had clearly oxidised the [$^{15}N_5$]-labelled stable isotope and changed its spectrum window (Figure 5.5).

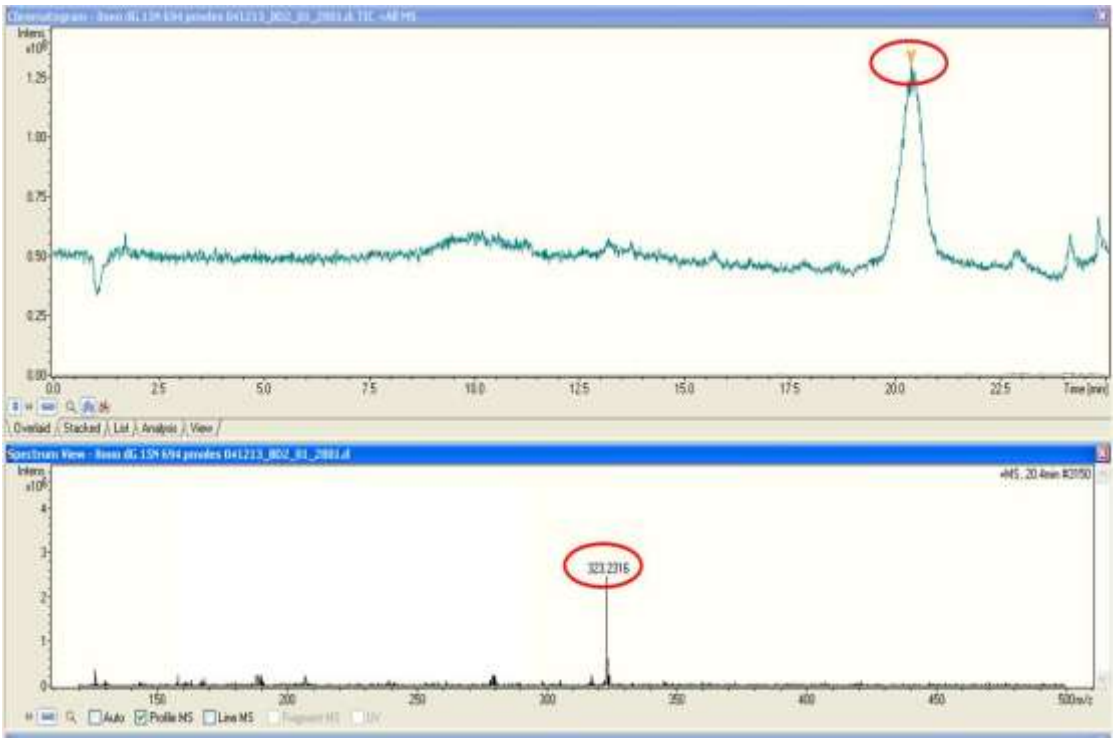

Figure 5.5: Detection of [$^{15}N_5$]- 8-OHdG using the C30 columnon the LC MS. Injection of 150pmol of [$^{15}N_5$]- 8-OHdG using the hypercarb C30 column revealed an unexpected mass (323 m/z) which indicates an evidence of artificial oxidation

3.2.8 LC MS analysis of nucleosides in conjunction with C18 reverse phase chromatography

Since the hyper-carb C30 caused oxidation to the [$^{15}N_5$]-labelled stable isotope, we used another stationary phase column (C18). Similar to C30, the C18 is also a reversed phase liquid chromatography. The difference between the two columns is in the length of the carbon chain attached to the silica surface. Accordingly, C18 colum has packing material compoused of silica particles attached to C18 Carbon units, while the C30 column will have packing materilas coated with C30 hydrophobic units.

3.2.9 Analysis of the enzymatic hydorlysis of DNA using LC MS

Followong enzymatic digestion of the control DNA sample using DNA Degradase the resulting nucleosides were analysed using LC MS on the C18 stationary phase column. Four nucleosides were detected with their corresponding masses. Deoxyguanosine was detected at 268 m/z (Figure 5.6), Deoxyadenosine was detected at 252 m/z (Figure 5.7), Deoxycytidine at 228 m/z (Figure 5.8) and Deoxythymidine at 243m/z (Figure 5.9). The [$^{15}N_5$]-8OHdG was then injected into the LC MS using the C18 column this time and a peak was detected at the correct mass (289 m/z) (Figure 5.10).

In order to confirm that the [$^{15}N_5$]-labelled stable isotope mass spectra was different from the four nucleosides standards, we overlapped the peaks and it clearly showed the retention time of the [$^{15}N_5$]-labelled stable isotope did not overlap with either dC, dG, dA or dG (Figure 5.11).

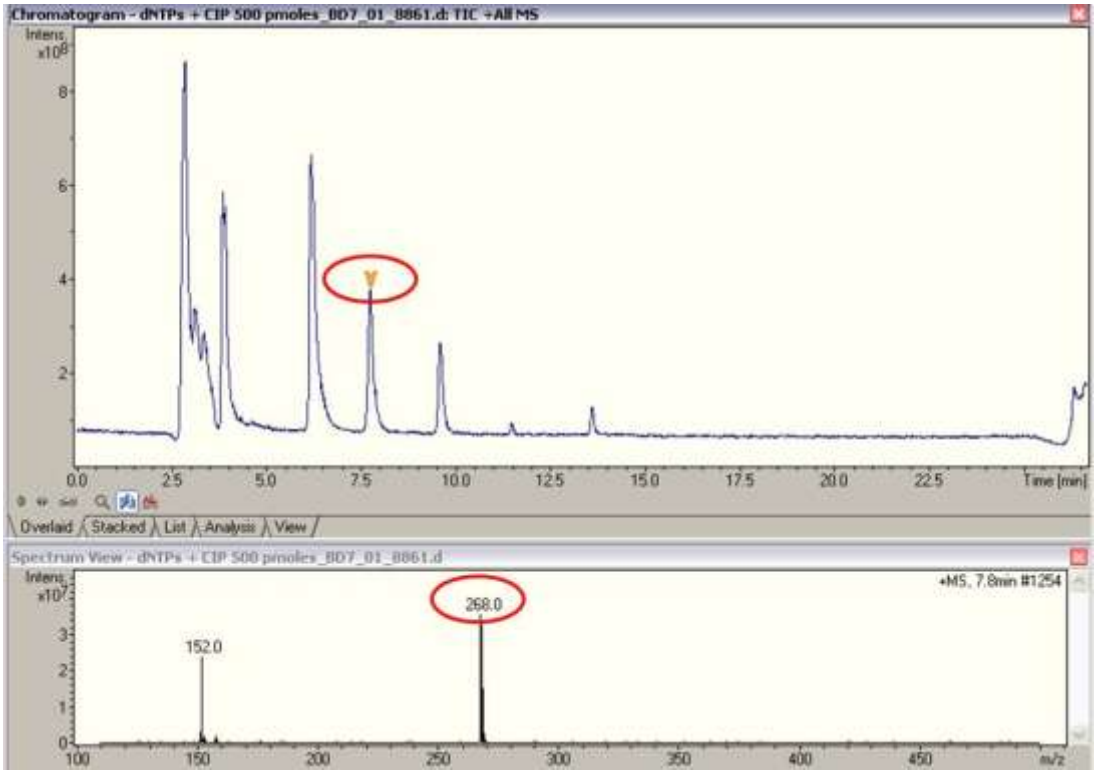

Figure 5.6: Detection of Deoxyguanosine from digested control DNA sample on the LC MS. Deoxyguanosine was detected at its correct mass (268 m/z) using the C18 column

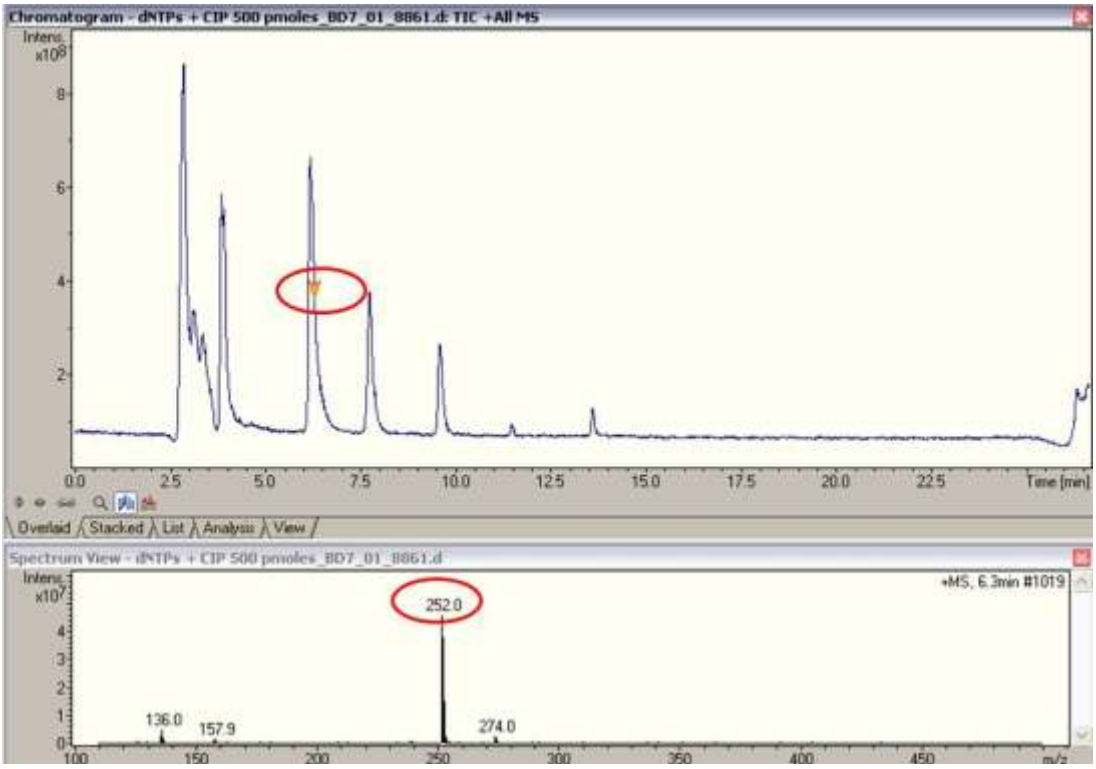

Figure 5.7: Detection of Deoxyadenosine from digested control DNA sample on the LC MS. Deoxyadenosine was detected at its correct mass (252 m/z) using the C18 column

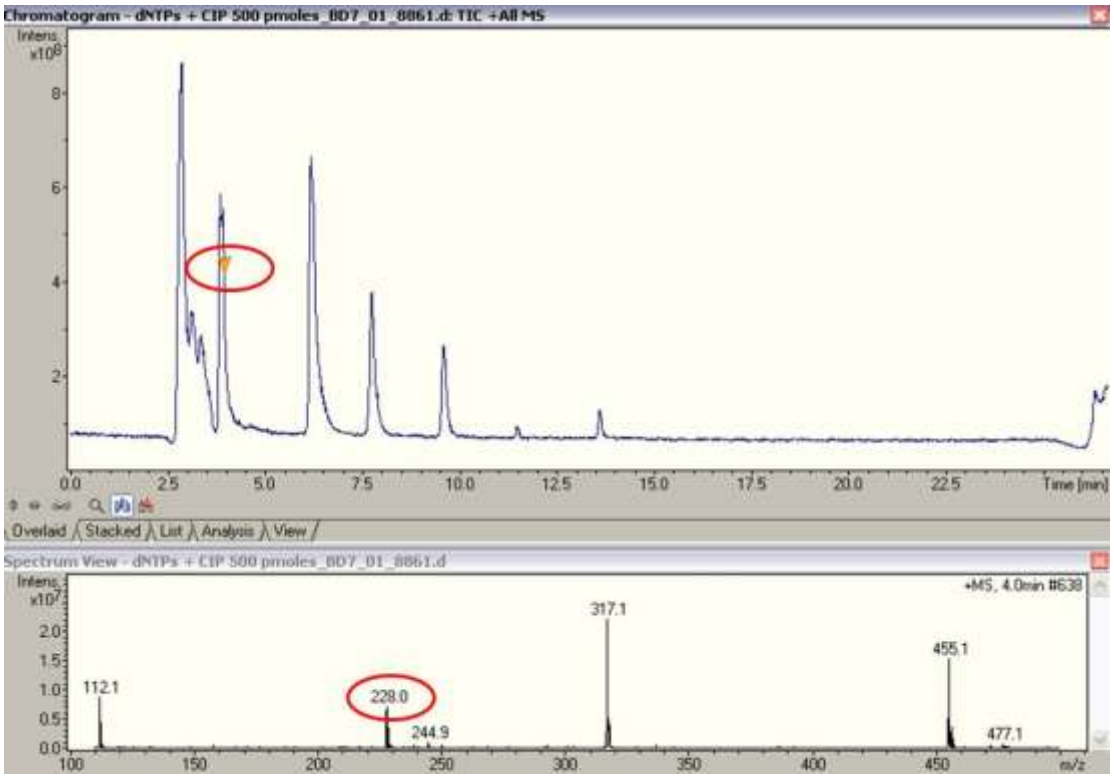

Figure 5.8: Detection of Deoxycytidine from digested control DNA sample on the LC MS. Deoxycytidine was detected at its correct mass (228 m/z) using the C18 column

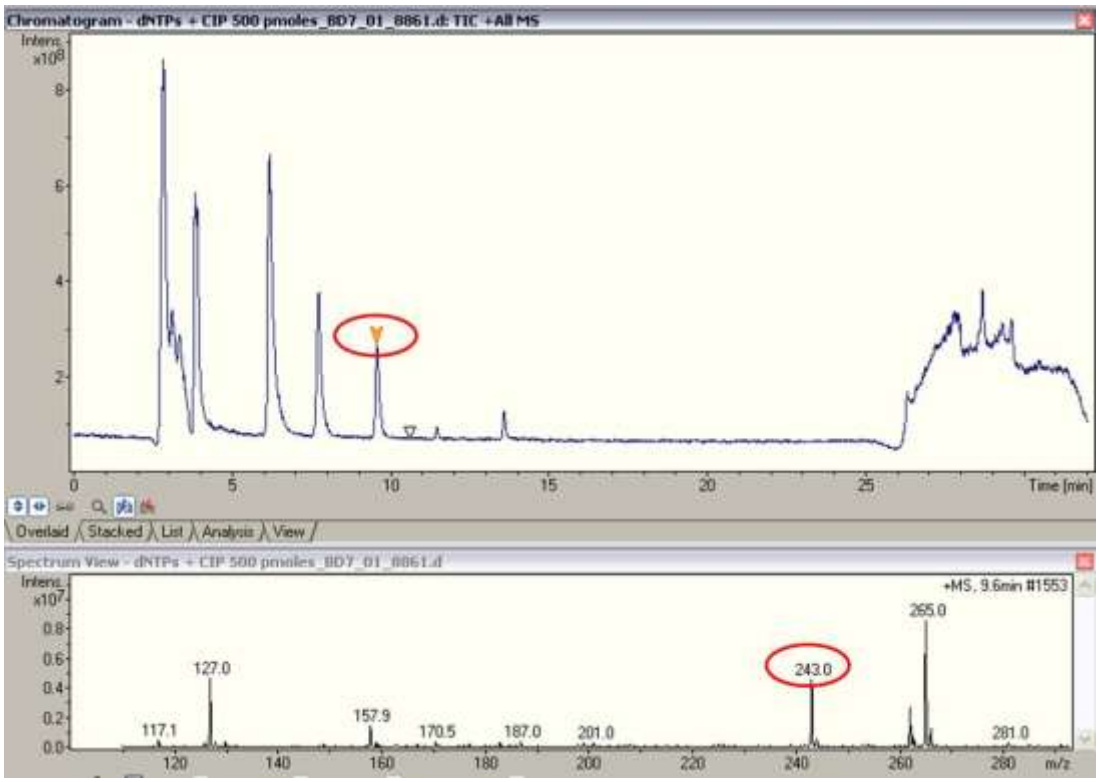

Figure 5.9: Detection of Deoxythymidine from digested control DNA sample on the LC MS. Deoxythymidine was detected at its correct mass (243 m/z) using the C18 column

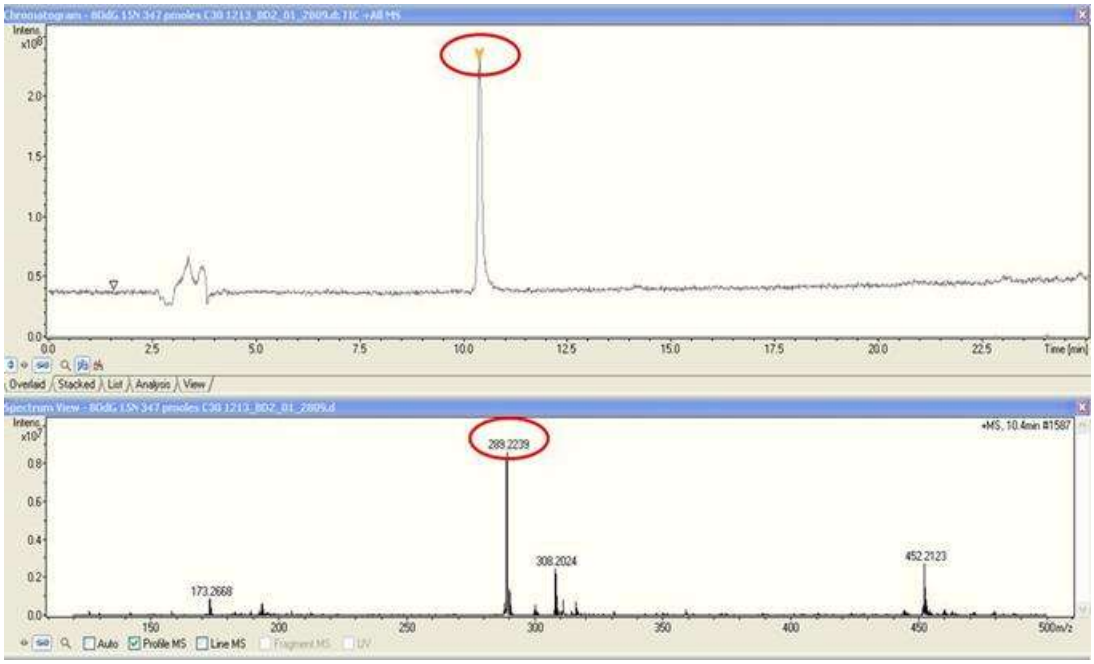

Figure 5.10: Detection of [$^{15}N_5$]-8OHdG on the LC MS using the C18 column. The [$^{15}N_5$]-8OHdG was detected at its correct mass (289 m/z) using the C18 column

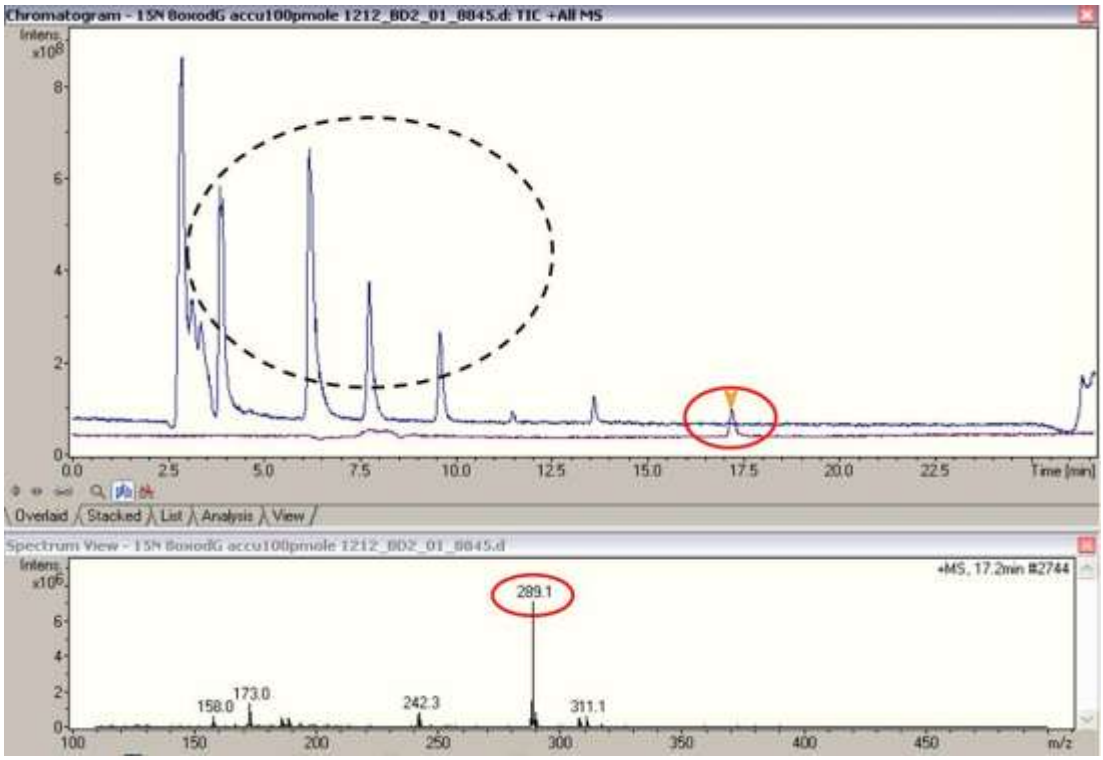

Figure 5.11: Aanalysis of control DNA sample on the LC MS did not overlap with [$^{15}N_5$]-8OHdG. An overlay of the control DNA sample profile with the [$^{15}N_5$]-8OHdG clearly showed the four DNA nucleosides did not overlap with [$^{15}N_5$]-8OHdG using the C18 column

3.2.11 LC MS analysis of nucleosides generated from DNA isolated from ageing brain

After the establishment of a system that was able to separate and detect nucleosides standards as well as the [$^{15}N_5$]-labelled stable isotope, we e injected our previously treated DNA isolated from a DSCL spiked with [$^{15}N_5$]-8OHdG. Four nucleosides were successfully separated and detected at their correct mass (dG 268 m/z) (Figure 5.12), dA was detected at 252 m/z (Figure 5.13), dC at 228 m/z (Figure 5.14) and dT at 243 m/z (Figure 5.15) on the LC MS. However, the peaks were of low abundance. Higher concentration (15µg) of DNA digest was prepared (extracted from 15 brain sections of 25µm thickness each) and the experiment was repeated with no significant change in the abundance of the nucleosides detected. Furthermore the presence of unknown analytes were detected that were much more abundant than the expected nucleosides.

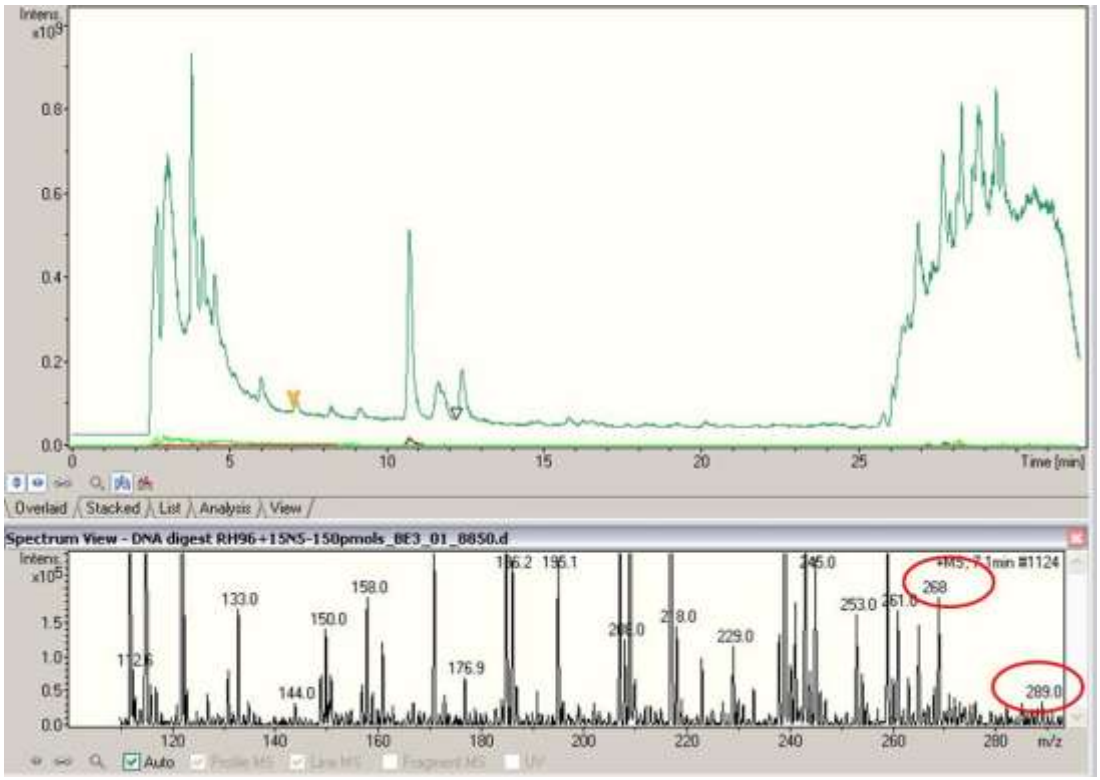

Figure 5.12: Injection of hydrolysed DNA from DSCL: Detection of dG and [$^{15}N_5$]-8OHdG. Analysis of DSCL hydrolysed DNA using the LC MS revealed a small peak of dG that was detected at the correct mass (268 m/z) and did not overlap with the [$^{15}N_5$]-8OHdG peak (289 m/z) using the C18 column

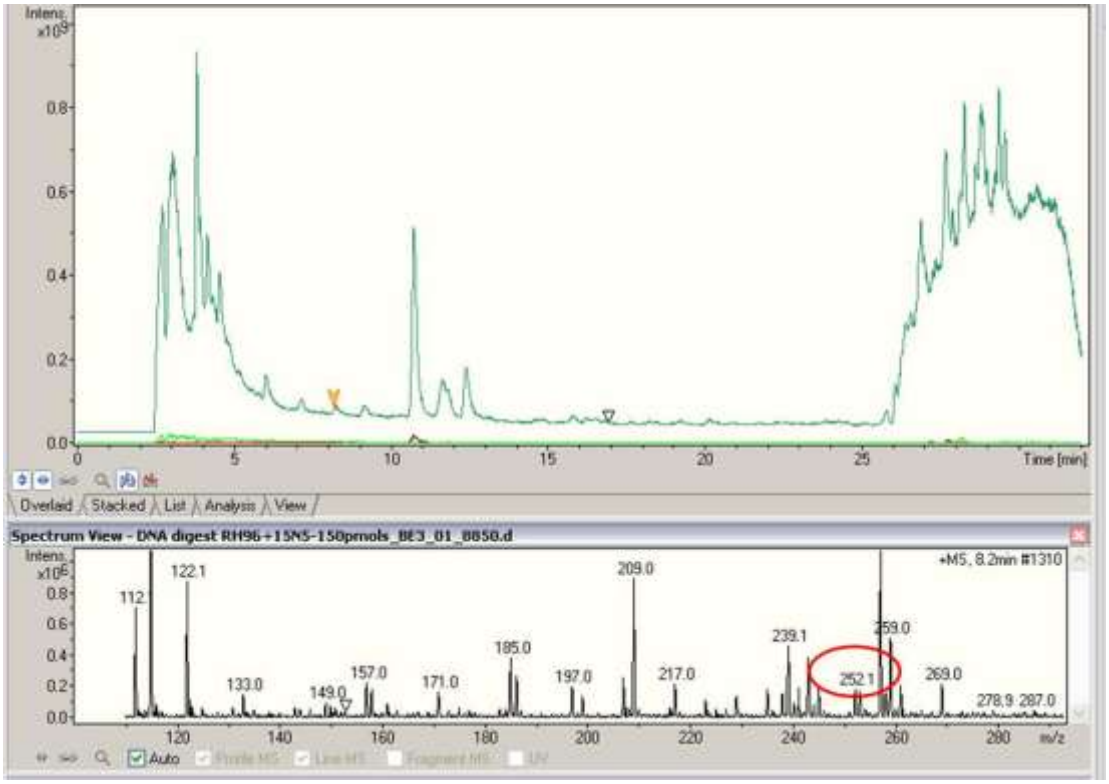

Figure 5.13: Injection of hydrlysed DNA from DSCL: Detection of dA. Analysis of DSCL hydrolysed DNA using the LC MS revealed a very small peak of dA that was detected at the correct mass (252 m/z) using the C18 column

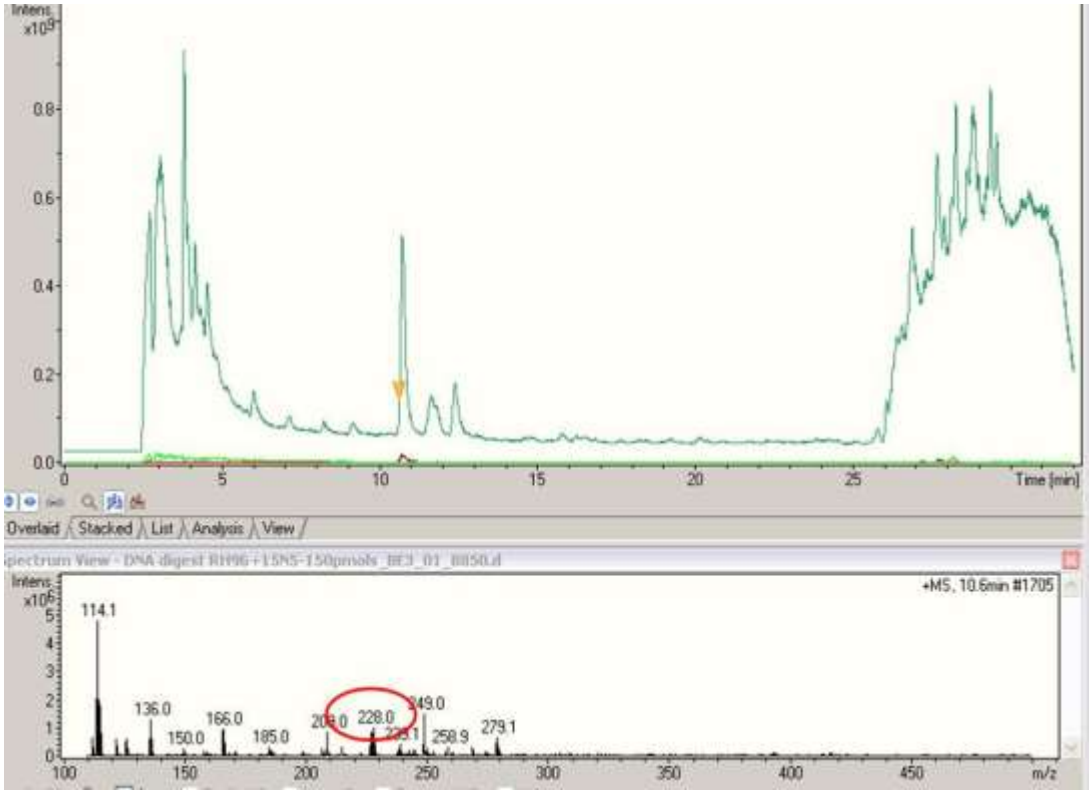

Figure 5.14: Injection of hydrlysed DNA from DSCL: Detection of dC. Analysis of DSCL hydrolysed DNA using the LC MS revealed a very small peak of dC that was detected at the correct mass (228 m/z) using the C18 column

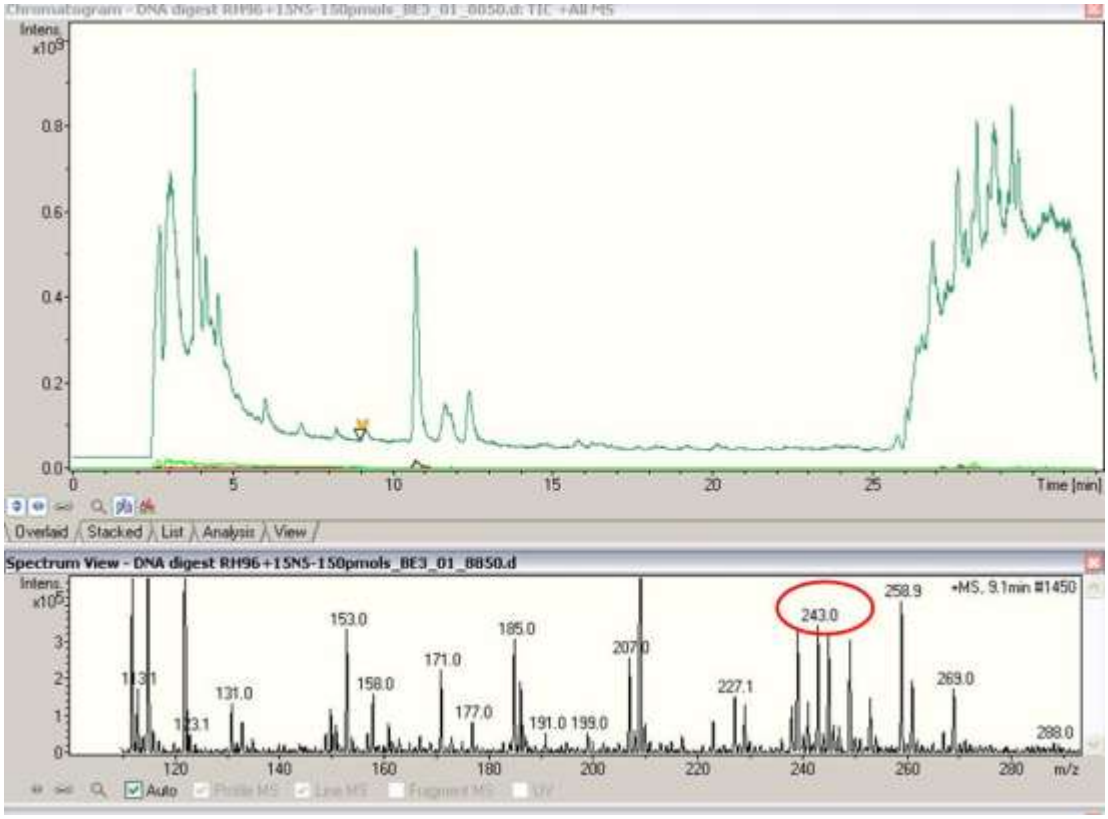

Figure 5.15: Injection of hydrlysed DNA from DSCL: Detection of dT. Analysis of DSCL hydrolysed DNA using the LC MS revealed a small peak of dT that was detected at the correct mass (243 m/z) using the C18 column

5.3 Discussion

Oxidative damage to neurons has been previousely reported to play a significant role in neurodegenerative disease such as AD (Epstein and Martin, 1999, Markesbery and Carney, 1999, Lovell et al., 2001). This increased level of cellular damage includes elevated level of DNA base oxidation, protein oxidation and lipid peroxidation (Lovell et al., 1995, Gabbita et al., 1998, Butterfield and Boyd-Kimball, 2004). Beacasue of the critical role of DNA in cellular function, oxidative DNA damage may be one of the most important factors that contribute to neurodegeneration (Wang et al., 2005).

In this study, it has been reported that the level of oxidative nDNA damage is significantly increased in WML and the surrounding WM in the brain of the elderly using 8-OHdG as a predominant marker of direct DNA oxidation by application of immunohistochemistry techniques. To validate this important observation, HPLC/ MS has been chosen as a gold star technique to compliment the previous findings where a developed method to detect 8-OHdG by MS was accomplished taking into account the critical need to prevent oxidation of the sample – both during extraction using TEMPO, and by the use of C18 column and not the C30 hypercarb column.

The use of highly sensitive and specific mass spectrometry-based methods to detect DNA damage was intended to detect and quantify Guanosine base modification which reflects DNA oxidation since Guanine is the DNA base that is most vurneable to be oxidised in the presence of cellular insult to produce 8-Hydroxy-2'deoxy-Guanosine. The study structure included the three groups of WM (CNL, CL, DSCL) where DNA was isolated to be analysed. However, since the main objective was to quantify the level of DNA oxidation, it was cruicial to eliminate the induction of any artificial oxidative damage that could be created in the process of sample preparation where it has been previousely reported that the addition of TEMPO to samples significantly decreased the level of artifitial damage (Boysen

et al., 2010). For this reason, additions of this chemical compound during DNA isolation took place with all samples and controls.

Taking into account previous studies which successfully used HPLC/MS as a tool to detect 8-OHdG as a marker of oxidation in different types of biological tissue, such as rat liver, an analytical methodology has been developed in this project to analyse nucleoside modification. Setting up the system was not straight forward, requiring extensive calibration for the sample as well as the machine. HPLC was adjusted several times for its parameters such as column pressure and temperature. It has been reported previousely that those parameters in addition to the pH of the column are very critical in the separation and analysis of samples by HPLC (Boysen et al., 2010). The developed methodology was optimised and modified several times for instance by increasing extracted DNA concentration or by changing the column used in order to determine the best conditions that produce good sensitivity and precision. For example, it was noted by decreasing the flow of sample in the HPLC column will produce a better sensitivity of sample retention times. However, after the collection of separate fractions as a product of HPLC analysis, the MS was not able to detect them. This might be due to the fact that fraction collection requires calculation of the time the peak was detected on the monitor in the presence of UV detector added to it the estimated time the samples traveled from the UV sight to the dispensing column. Although this was carefully performed, an extra amount of the gradient (buffer) might have probably got mixed with the sample an produced a diluted concentration that was way too low for the MS to detect. This was overcomed by changing the technique to be run on LC that is connected directly to the MS (LC/MS).

The use of LC/MS has shown to separate and detect the four nucleocide bases at their correct mass. However, when the [$^{15}N_5$]-8OHdG stable isotope was injected, it was shown that it was detected at a different mass which reflects a possible artificial oxidation that has been introduced to the stable isotope by the hyperCarb C30 stationary phase column. This observation has not been reported before in the literature. In order to overcome

this, the column has been changed to the C18 stationary phase which proved to give more accurate result and the analysis of [$^{15}N_5$]-8OHdG on the LC/MS was detected at its correct mass.

After a prof of the established setting of the the LC/MS principle has been shown, the induction of the isolated DNA sample from a DSCL brain has been performed. Although four peaks of DNA nucleosides were dtetcted at their correct masses, the intensity of the peaks was very low and associated with allot of noise that it was very difficult to isolate our peaks of interest from the high background of contamination. This could be to the fact of dealing with the quality of post-mortem tissue that has previously shown to be inadequate when dealing with such a technique that is highly sensitive. It was also noted during DNA isolation experiments that the amount of total genomic DNA retrieved from the three groups of WM brain sections was very little and it only reached the lower scale of isolated DNA concentration that was previously reported to be used in literature. Again this could also be owed to the possible poor quality of the human tissue we are using in the LC/MS analysis.

In conclusion, a new approach to DNA damage detection and quantification has been developed. The LC/MS is a high quality technique that is reliable and widely used in analysis of different bio-molecules. However, due to this machine's high sensitivity, establishing a new system that can be applied in the current project to validate previous findings using the 8-OHdG as a marker of DNA oxidation, was very time consuming and required further calibration that did not meet my time line. In the future, the established technique can be reconcidered for DNA analysis of better quality samples and with higher amount of genomic DNA. Making use of the developed technique will create significant literature that would add allot to our understanding of DNA damage and its contribution to WML formation and neurodegeneration.

CHAPTER 6: GENERAL DISCUSSION

To date, the number of true population based studies that exist are very limited which makes this a distinctive opportunity to investigate the early events associated with glial pathology in WM and WML of the human ageing brain. Also, the study has investigated post-mortem human brain tissue blindly, depending only on categorisation of WM using MRI scans and not depending on age, sex or mental status of volunteers. , which makes it different from classical well-defined case/control type of studies where clinical observation and diagnosis accuracy are unstable factors. The study has defined a number of important observations and issues that will be discussed in this chapter.

6.1 Summary of results

Oxidative stress affects macrocellular components including DNA, lipids and proteins where these end products have been linked to several pathologies including neurodegenerative diseases. The first part of the current study showed oxidative DNA damage and an extensive DNA damage response in glial cells in the ageing brain, especially within DSCL. In addition the study also demonstrated oxidative DNA damage and the activation of this DDR not only in the well-defined areas of WM attenuation (DSCL), but also in areas that are free of lesions (CL) and appeared normal on MRI scans. This study offered an insight into glial cell pathology in the ageing brain and demonstrated that the DSCL arise in a field of glial pathology.

DNA damage (8-OHdG) was a feature of the three groups of WM (CNL, CL, DSCL) in the ageing brain. Interestingly, the level of oxidative DNA damage in the CL brains is very similar to the level detected in DSCL. This indicates that, although CL brains appear normal by MRI analysis, their profile is more similar to DSCL than to control WM free of WML. In fact, CL WM contains a high level of DNA damage associated with glial cells which could probably activate several key down-stream effect pathways including senescence. This raises the question whether this early pathological event of glial cell

activation is a forerunner in lesion formation, or whether it is a protective mechanism to prevent lesion formation.

Presence of cellular senescence was defined by detecting SA-β-gal activity, in all three groups of WM and was associated with oligodendrocytes and astrocytes but not microglia in all groups. Also, activation of cell cycle check proteins (p53, p21 and p16) was significantly increased in CL brains, confirming that WML arise in a field effect of glial pathology. Studies have reported p53 activation in the presence of senescence which if it persists, activates p21 (Campisi, 2013). Activation of this pathway induces senescent cells to alter their gene expression profile resulting in the production and secretion of a range of pro-inflammatory cytokines, proteases and chemokines collectively known as a SASP, which in turn could affect neighbouring cells and set a proinflammatory microenvironment. The SASP is well defined in cell culture models but to date, very few studies have looked at the SASP *in vivo* (Simpson et al., 2010b, Jurk et al., 2012, Garwood et al., 2014). The current study looked at expression changes in key genes implicated in senescence pathways and showed that there is an alteration of genes expression indicating the presence of a SASP.

Markers of senescence were predominantly associated with astrocytes which play a key role in a number of important functions of the human brain such as maintaining the homeostasis of the microenvironment. Therefore, impaired astrocytes function may impact WM pathology and might contribute to a formation of a lesion.

The current study also developed a method that quantifies the amount of modified DNA base associated with extensive DNA damage, with the aim of validating the immunohistochemical detection of 8-OHdG using mass-spectrometry. Previous studies have detected guanosine base modification in rats using MS as this base is highly vulnerable to oxidation (Boysen et al., 2010). In this chapter, setting up a system that was able to detect the four DNA bases as well as the 8-OHdG [$^{15}N_5$] stable isotope was accomplished taking into account important issues such as using the TEMPO and a suitable C18 column to

prevent any artificial oxidation that might be introduced during the course of experiment. However, quantifying guanosine in WM and WML has shown to be problematic and very time consuming where this will be further discussed in the limitations and the future directions at the end of this chapter.

6.2 WML and oxidative stress: implications for novel therapeutic approaches

Basic research into the proposed impact of oxidative stress in the ageing brain has identified several approaches for the possible therapeutic treatment of age-related pathologies. Oxidative stress plays a crucial role in ageing and age related disease(s) whereby oxidative stress is implicated in vascular dementia, stroke and ischaemic pathologies (Floyd and Hensley, 2002). Several key therapeutic approaches to minimise the effect of oxidative stress on cognition in the elderly are available, and can mainly be categorised into two groups: antioxidants and anti-inflammatory drugs (Behl, 1999, Floyd and Hensley, 2002).

Antioxidant therapy has been used as a therapeutic treatment in a number of neurodegenerative disorders including AD, PD and ischaemia (Hall and Braughler, 1989, Ames et al., 1993, Halliwell, 2006). A number of antioxidants have been tested *in vitro* on models of neuronal cell death, and include Vitamin E, melatonin hormone and mifepristone. The studies concluded that the use of such anti-oxidants had a small effect on neuronal survival in the presence of an insult such as oxidative stress (Braughler et al., 1989, Moosmann et al., 1997, Behl, 1999). Studies investigating the effect of Vitamin E in AD patients have shown interesting results (Sano et al., 1997, Hamilton et al., 2001). Given the time frame Sano's study was performed within (two years), there was a delayed small effect on cognitive performance. The results of the trial gave major hope that a longer treatment might yield a better effect (Grundman, 2000, MGEKN et al., 2008).

Accumulating evidence strongly suggests a role for inflammatory mechanisms (though not frank inflammation) in neurodegenerative diseases such as AD and WML (Lleo

et al., 2007, Simpson et al., 2007b). Therefore, therapy targeted against the inflammatory mechanism associated with astrocytes and microglia has been considered as an approach for treatment (Lleo et al., 2007). The effect of non-steroidal anti-infammatory drugs (NSAIDs) was shown to be beneficial on slowing the progression of AD (Breitner, 1996, Lleo et al., 2007). The main activity of NSAIDs is the inhibition of COX (an enzyme responsible of inflammation and pain) which will disrupt prostaglandin synthesis that will in turn block ROS formation (Breitner, 1996, Behl, 1999).

The current study is nested within a large population based study which randomly selects individuals based solely on their age, thereby truly reflecting the burden of dementia in the general population of the UK. Such a uniquely population based approach is ideal to be applied on collaborative studies of clinical controlled therapeutic trials of the effect of NSAIDs for instance, to define whether NSAIDs can actually prevent or treat the symptoms of AD and dementia from a broader prospective. Also, most of the available clinical therapies for cognitive impairment target the well-defined pathologies such as misfolded proteins in AD brains using Abeta (A β) immunisation, but as our knowledge about the early effect of pathologies associated with several diseases of the CNS continues to increase, the need for a therapeutic approach that predicts and rescues this impairment also increases. The current study demonstrates that oxidative damage creates a field effect on glia in the ageing brain. Furthermore, oxidative DNA damage and an associated DDR are common in CL WM indicating that WML may arise in an ongoing field effect of pathology. If targeted early enough, the WM may be rescued and further damage caused by increased ROS production prevented, thereby reducing the DDR and preventing induction of senescence or altered cellular functions.

6.3 Future work

LC/MS work

The current study successfully optimised DNA extraction and detection of nuclear bases using LC/MS method, however, measurement of guanosine base modification in WM and WML from CFAS tissue was not successfully fulfilled due to the inadequate quality of post mortem tissue.

Had time allowed, this method would have complemented and validated the immunohistochemical part of the study which quantitated 8-OHdG oxidative damage in three groups of WM. Future studies to complete the optimisation of the LC/MS protocol should be completed using larger volumes of high quality DNA extracted from CFAS brains. The system has been optimised and proven to detect the four DNA bases, and offers a good opportunity to accomplish the quantification of oxidatively modified guanosine in the future.

Investigation of the role of astrocytes in SASP mediation

The current study clearly demonstrated the involvement of astrocytes in senescence, as determined by detection of both activated SA-β-gal and p16. Histological observation and dual labelling studies of senescence markers showed that astrocytes were predominantly affected. To date, only a few papers in the current literature implicate astrocytes in SASP mediation (Salminen et al., 2011) which suggest a change of astrocytic function and gene expression in the presence of senescence in ageing pathology. The current study showed an altered gene expression of pooled cDNA that was isolated from whole tissue. Future studies to isolate individual cell populations from post mortem material derived from DSCL, CL and CNL brains using laser capture microdisection (LCM) could be applied to examine the gene expression profile of astrocytes against microglia and against oligodendrocytes. This approach will determine key pathways that might be affected in glial cell signalling in the presence of an insult such as oxidative stress. Therapeutic targets are developed from such

approaches where this could make a good potential in the field of neurodegeneration. A recent paper suggests that senescence pathways might be modulated and so be an intervention target (Dalle Pezze et al., 2014).

6.4 Limitations of the study

General limitations

Working with post mortem human brain tissue has a number of advantages and disadvantages as well. A key advantage when studying human degenerative diseases is that preserved human brain give a clear reflection of the ongoing pathology. Since most degenerative diseases are believed to be multifactorial that are probably an outcome of multiple cellular compensations in an altered microenvironment, the human retrieved CNS is the best model to demonstrate the wide picture of events. Animal models are also of great use whereby they are economically better, easier to replace and maintain; however, a major drawback especially when studying human brain pathology including WM, is the small size of the animals' brain (rodents are mostly used to study human CNS diseases) which does not reflect the actual state of human pathology. In particular, they do not have large areas of white matter, and there are not good models of white matter ischaemic lesions in rodents. Cellular models have been used extensively in the field of neurodegenerative diseases, but a major disadvantage of this model of study is that it usually focuses on a single cell type to be cultured and phenotyped. Cellular models lack the actual interaction that is ongoing in the human brain which involves multiple cell types with multiple functions and different signalling pathways.

One of the major limitations of working with post mortem human brain tissue is that it is considered as the endpoint of pathology. Dealing with such a broad spectrum of factors that might collectively contribute to the pathology seen in CFAS wide population based study; case to case variation was common using different biomarkers during the course of research. This reflects the diversity in the elderly population in the UK and on the scientific

level, makes it more challenging to define significant differences between tested groups of a given pathology. Such an issue might be overcome by expanding the cohort to yield a stronger statistical power. Another major obstacle is the quality of the preserved human CNS tissue. This important factor creates variability in several parameters such as post mortem delay and pH of the retrieved tissue. Since CFAS is a multicentre population based study, inconsistency in fixation policies and procedures for those parameters are likely to be seen.

Antigen detection

There are a number of issues regarding the limitations of immunohistochemical studies. Although the antibodies used in this study which were commercially available are well characterised antibodies and have been proven to be very specific, several issues have been encountered during the course of work. A major one was the difficulty in retrieving the antigen. This is owed to the prolonged fixation of CFAS brain tissue in formalin (over 10 years) which formed cross links that act as a shield masking the epitopes and making it very difficult to retrieve the antigen binding sites. This issue was overcome by the usage of harsh antigen retrieval methods such pressure cooker treatment. However, some antibodies failed to bind to the specific binding sites on tissue sections. As an alternative, frozen sections were used, which indeed did not have the antigen retrieval issue, but is of poor cellular morphology comparing to the well-preserved cellular morphology seen in FFPE sections.

Setting up of LC/MS

The setting up and optimisation of the LC/MS was challenging in such a sensitive system. Given the fact that extracted DNA from post-mortem material was of relatively poor quality, it made it even harder to detect the peaks of our interest on the MS. The masses were associated with background noise of surrounding molecules. Also, the issue with the C30 column which introduced artificial oxidation was not expected and took a while to be successfully resolved. If time had of permitted, longer optimisation of the sample and the machine, and better quality of DNA extracted may all have yielded better quality MS results.

BIBLIOGRAPHY

(1998) Cognitive function and dementia in six areas of England and Wales: the distribution of MMSE and prevalence of GMS organicity level in the MRC CFA Study. The Medical Research Council Cognitive Function and Ageing Study (MRC CFAS). Psychol Med 28:319-335.

(2001) Pathological correlates of late-onset dementia in a multicentre, community-based population in England and Wales. Neuropathology Group of the Medical Research Council Cognitive Function and Ageing Study (MRC CFAS). Lancet 357:169-175.

Acosta JC, Banito A, Wuestefeld T, Georgilis A, Janich P, Morton JP, Athineos D, Kang T-W, Lasitschka F, Andrulis M (2013) A complex secretory program orchestrated by the inflammasome controls paracrine senescence. Nature cell biology 15:978-990.

Al-Mashhadi S, Simpson J, Heath P, Dickman M, Forster G, Matthews F, Brayne C, Ince P, Wharton S (2014) Oxidative Glial Cell Damage Associated with White Matter Lesions in the Ageing Human Brain. Brain Pathology.

Ames BN, Shigenaga MK, Hagen TM (1993) Oxidants, antioxidants, and the degenerative diseases of aging. Proceedings of the National Academy of Sciences 90:7915-7922.

Andersen JK (2004) Oxidative stress in neurodegeneration: cause or consequence?

Baker DJ, Perez-Terzic C, Jin F, Pitel KS, Niederländer NJ, Jeganathan K, Yamada S, Reyes S, Rowe L, Hiddinga HJ (2008) Opposing roles for p16Ink4a and p19Arf in senescence and ageing caused by BubR1 insufficiency. Nature cell biology 10:825-836.

Baker DJ, Weaver RL, van Deursen JM (2013) p21 both attenuates and drives senescence and aging in BubR1 progeroid mice. Cell reports 3:1164-1174.

Baker DJ, Wijshake T, Tchkonia T, LeBrasseur NK, Childs BG, van de Sluis B, Kirkland JL, van Deursen JM (2011) Clearance of p16Ink4a-positive senescent cells delays ageing-associated disorders. Nature 479:232-236.

Bandettini PA (2009) What's new in neuroimaging methods? Ann N Y Acad Sci 1156:260-293.

Beauséjour CM, Krtolica A, Galimi F, Narita M, Lowe SW, Yaswen P, Campisi J (2003) Reversal of human cellular senescence: roles of the p53 and p16 pathways. The EMBO journal 22:4212-4222.

Beckman KB, Ames BN (1998) The free radical theory of aging matures. Physiological reviews 78:547-581.

Behl C (1999) Alzheimer's disease and oxidative stress: implications for novel therapeutic approaches. Progress in neurobiology 57:301-323.

Benz G, Hölzel D, Schmoeckel C (1991) Inflammatory cellular infiltrates in melanocytic nevi. The American journal of dermatopathology 13:538-542.

Bergles DE, Roberts JD, Somogyi P, Jahr CE (2000) Glutamatergic synapses on oligodendrocyte precursor cells in the hippocampus. Nature 405:187-191.

Bitto A, Sell C, Crowe E, Lorenzini A, Malaguti M, Hrelia S, Torres C (2010) Stress-induced senescence in human and rodent astrocytes. Experimental cell research 316:2961-2968.

Blackburn EH (2000) Telomere states and cell fates. Nature 408:53-56.

Blessed G, Black SE, Butler T, Kay DW (1991) The diagnosis of dementia in the elderly. A comparison of CAMCOG (the cognitive section of CAMDEX), the AGECAT program, DSM-III, the Mini-Mental State Examination and some short rating scales. Br J Psychiatry 159:193-198.

Blumberg J (2004) Use of biomarkers of oxidative stress in research studies. The Journal of nutrition 134:3188S-3189S.

Bodnar AG, Ouellette M, Frolkis M, Holt SE, Chiu C-P, Morin GB, Harley CB, Shay JW, Lichtsteiner S, Wright WE (1998) Extension of life-span by introduction of telomerase into normal human cells. Science 279:349-352.

Boiteux S, Gellon L, Guibourt N (2002) Repair of 8-oxoguanine in< i> Saccharomyces cerevisiae</i>: interplay of DNA repair and replication mechanisms< sup> 2, 3</sup>. Free Radical Biology and Medicine 32:1244-1253.

Bokov A, Chaudhuri A, Richardson A (2004) The role of oxidative damage and stress in aging. Mechanisms of ageing and development 125:811-826.

Boysen G, Collins LB, Liao S, Luke AM, Pachkowski BF, Watters JL, Swenberg JA (2010) Analysis of 8-oxo-7, 8-dihydro-2′-deoxyguanosine by ultra high pressure liquid chromatography–heat assisted electrospray ionization–tandem mass spectrometry. Journal of Chromatography B 878:375-380.

Bradley-Whitman MA, Timmons MD, Beckett TL, Murphy MP, Lynn BC, Lovell MA (2014) Nucleic acid oxidation: an early feature of Alzheimer's disease. Journal of neurochemistry 128:294-304.

Braughler J, Hall E, Jacobsen E, McCall J, Means E (1989) The 21-aminosteroids: Potent inhibitors of lipid peroxidation for the treatment of central nervous system trauma and ischemia. Drugs Future 14:143-152.

Breitner M, MPH, John CS (1996) The role of anti-inflammatory drugs in the prevention and treatment of Alzheimer's disease. Annual review of medicine 47:401-411.

Bronge L, Bogdanovic N, Wahlund LO (2002) Postmortem MRI and histopathology of white matter changes in Alzheimer brains. A quantitative, comparative study. Dement Geriatr Cogn Disord 13:205-212.

Burrows CJ, Muller JG (1998) Oxidative nucleobase modifications leading to strand scission. Chemical reviews 98:1109-1152.

Butterfield DA, Boyd-Kimball D (2004) Amyloid β-Peptide (1-42) Contributes to the Oxidative Stress and Neurodegeneration Found in Alzheimer Disease Brain. Brain Pathology 14:426-432.

Caldecott KW (2008) Single-strand break repair and genetic disease. Nature Reviews Genetics 9:619-631.

Campisi J (1999) Cancer, aging and cellular senescence. In vivo (Athens, Greece) 14:183-188.

Campisi J (2005) Senescent cells, tumor suppression, and organismal aging: good citizens, bad neighbors. Cell 120:513-522.

Campisi J (2013) Aging, cellular senescence, and cancer. Annual review of physiology 75:685-705.

Campisi J, Andersen JK, Kapahi P, Melov S (2011) Cellular senescence: a link between cancer and age-related degenerative disease? In: Seminars in cancer biology, vol. 21, pp 354-359: Elsevier.

Campuzano O, Castillo-Ruiz M, Acarin L, Castellano B, Gonzalez B (2009) Increased levels of proinflammatory cytokines in the aged rat brain attenuate injury-induced cytokine response after excitotoxic damage. Journal of neuroscience research 87:2484-2497.

Candeias LP, Steenken S (2000) Reaction of HO. with Guanine Derivatives in Aqueous Solution: Formation of Two Different Redox-Active OH-Adduct Radicals and Their Unimolecular Transformation Reactions. Properties of G (-H). Chemistry-A European Journal 6:475-484.

Castilla-Cortázar I, Guerra L, Puche J, Muñoz U, Barhoum R, Escudero E, Lavandera J (2014) An experimental model of partial insulin-like growth factor-1 deficiency in mice. Journal of physiology and biochemistry 70:129-139.

Chen Y, Swanson RA (2003) Astrocytes and brain injury. Journal of Cerebral Blood Flow & Metabolism 23:137-149.

Cheryl A. Hawkes, Nimeshi Jayakody, David A. Johnston, Ingo Bechmann and Roxana O. Carare (2014) Failure of Perivascular Drainage of β-amyloid in Cerebral Amyloid Angiopathy. Brain pathology 24: 396-403.

Cho S-G, Choi E-J (2002) Apoptotic signaling pathways: caspases and stress-activated protein kinases. Journal of biochemistry and molecular biology 35:24-27.

Ciccia A, Elledge SJ (2010) The DNA damage response: making it safe to play with knives. Molecular cell 40:179-204.

Cooke MS, Evans MD, Burd RM, Patel K, Barnard A, Lunec J, Hutchinson PE (2001) Induction and excretion of ultraviolet-induced 8-oxo-2'-deoxyguanosine and thymine dimers in vivo: implications for PUVA. J Invest Dermatol 116:281-285.

Cooke MS, Evans MD, Dizdaroglu M, Lunec J (2003) Oxidative DNA damage: mechanisms, mutation, and disease. The FASEB Journal 17:1195-1214.

Copeland JR, Dewey ME, Wood N, Searle R, Davidson IA, McWilliam C (1987) Range of mental illness among the elderly in the community. Prevalence in Liverpool using the GMS-AGECAT package. Br J Psychiatry 150:815-823.

Coppé J-P, Desprez P-Y, Krtolica A, Campisi J (2010) The senescence-associated secretory phenotype: the dark side of tumor suppression. Annual Review of Pathological Mechanical Disease 5:99-118.

Coppé J-P, Patil CK, Rodier F, Sun Y, Muñoz DP, Goldstein J, Nelson PS, Desprez P-Y, Campisi J (2008) Senescence-associated secretory phenotypes reveal cell-nonautonomous functions of oncogenic RAS and the p53 tumor suppressor. PLoS biology 6:e301.

Copple IM, Goldring CE, Kitteringham NR, Park BK (2008) The Nrf2–Keap1 defence pathway: role in protection against drug-induced toxicity. Toxicology 246:24-33.

Cristofalo V (2005) SA β Gal staining: biomarker or delusion. Experimental gerontology 40:836-838.

Curtis MA, Faull RL, Glass M (2006) A novel population of progenitor cells expressing cannabinoid receptors in the subependymal layer of the adult normal and Huntington's disease human brain. J Chem Neuroanat 31:210-215.

Dalle Pezze P, Nelson G, Otten EG, Korolchuk VI, Kirkwood TB, von Zglinicki T, Shanley DP (2014) Dynamic Modelling of Pathways to Cellular Senescence Reveals Strategies for Targeted Interventions. PLoS computational biology 10:e1003728.

Davydov V, Hansen LA, Shackelford DA (2003) Is DNA repair compromised in Alzheimer's disease? Neurobiol Aging 24:953-968.

De Magalhães JP, Curado J, Church GM (2009) Meta-analysis of age-related gene expression profiles identifies common signatures of aging. Bioinformatics 25:875-881.

de Nadal E, Ammerer G, Posas F (2011) Controlling gene expression in response to stress. Nature Reviews Genetics 12:833-845.

de Vries HE, Witte M, Hondius D, Rozemuller AJ, Drukarch B, Hoozemans J, van Horssen J (2008) Nrf2-induced antioxidant protection: a promising target to counteract ROS-mediated damage in neurodegenerative disease? Free Radical Biology and Medicine 45:1375-1383.

Denchi EL, Attwooll C, Pasini D, Helin K (2005) Deregulated E2F activity induces hyperplasia and senescence-like features in the mouse pituitary gland. Molecular and cellular biology 25:2660-2672.

Ding Q, Dimayuga E, Markesbery WR, Keller JN (2004) Proteasome inhibition increases DNA and RNA oxidation in astrocyte and neuron cultures. Journal of neurochemistry 91:1211-1218.

Dizdaroglu M, Jaruga P, Birincioglu M, Rodriguez H (2002) Free radical-induced damage to DNA: mechanisms and measurement< sup> 1, 2</sup>. Free Radical Biology and Medicine 32:1102-1115.

Epstein FH, Martin JB (1999) Molecular basis of the neurodegenerative disorders. New England Journal of Medicine 340:1970-1980.

ESCODD (2003) Measurement of DNA oxidation in human cells by chromatographic and enzymic methods. Free radical biology & medicine 34:1089-1099.

Esposito F, Russo L, Chirico G, Ammendola R, Russo T, Cimino F (2001) Regulation of p21 waf1/cip1 expression by intracellular redox conditions. IUBMB life 52:67-70.

Farkas E, Donka G, de Vos RA, Mihaly A, Bari F, Luiten PG (2004) Experimental cerebral hypoperfusion induces white matter injury and microglial activation in the rat brain. Acta Neuropathol 108:57-64.

Farrall AJ, Wardlaw JM (2009) Blood-brain barrier: ageing and microvascular disease--systematic review and meta-analysis. Neurobiol Aging 30:337-352.

Fernando MS, Ince PG (2004) Vascular pathologies and cognition in a population-based cohort of elderly people. J Neurol Sci 226:13-17.

Fernando MS, O'Brien JT, Perry RH, English P, Forster G, McMeekin W, Slade JY, Golkhar A, Matthews FE, Barber R, Kalaria RN, Ince PG (2004) Comparison of the pathology of cerebral white matter with post-mortem magnetic resonance imaging (MRI) in the elderly brain. Neuropathol Appl Neurobiol 30:385-395.

Fernando MS, Simpson JE, Matthews F, Brayne C, Lewis CE, Barber R, Kalaria RN, Forster G, Esteves F, Wharton SB, Shaw PJ, O'Brien JT, Ince PG (2006) White matter lesions in an unselected cohort of the elderly: molecular pathology suggests origin from chronic hypoperfusion injury. Stroke 37:1391-1398.

Fiala ES, Conaway CC, Mathis JE (1989) Oxidative DNA and RNA damage in the livers of Sprague-Dawley rats treated with the hepatocarcinogen 2-nitropropane. Cancer Research 49:5518-5522.

Fillenbaum GG, van Belle G, Morris JC, Mohs RC, Mirra SS, Davis PC, Tariot PN, Silverman JM, Clark CM, Welsh-Bohmer KA (2008) Consortium to Establish a Registry for Alzheimer's Disease (CERAD): The first twenty years. Alzheimer's & Dementia 4:96-109.

Filley CM (2010) White matter: organization and functional relevance. Neuropsychol Rev 20:158-173.

Finkel T (2001) Reactive oxygen species and signal transduction. IUBMB life 52:3-6.

Finkel T, Holbrook NJ (2000) Oxidants, oxidative stress and the biology of ageing. Nature 408:239-247.

Floyd RA, Hensley K (2002) Oxidative stress in brain aging: implications for therapeutics of neurodegenerative diseases. Neurobiology of aging 23:795-807.

Franceschi C, Capri M, Monti D, Giunta S, Olivieri F, Sevini F, Panourgia MP, Invidia L, Celani L, Scurti M (2007) Inflammaging and anti-inflammaging: a systemic perspective on aging and longevity emerged from studies in humans. Mechanisms of ageing and development 128:92-105.

Freund A, Patil CK, Campisi J (2011) p38MAPK is a novel DNA damage response-independent regulator of the senescence-associated secretory phenotype. The EMBO journal 30:1536-1548.

Gabbita SP, Lovell MA, Markesbery WR (1998) Increased nuclear DNA oxidation in the brain in Alzheimer's disease. Journal of neurochemistry 71:2034-2040.

Garwood CJ, Simpson JE, Al Mashhadi S, Axe C, Wilson S, Heath PR, Shaw PJ, Matthews FE, Brayne C, Ince PG (2014) DNA damage response and senescence in endothelial cells of human cerebral cortex and relation to Alzheimer's neuropathology progression: a population-based study in the MRC-CFAS cohort. Neuropathology and applied neurobiology.

Geschwind N (1965) Disconnexion syndromes in animals and man. II. Brain 88:585-644.

Godbout JP, Johnson RW (2009) Age and neuroinflammation: a lifetime of psychoneuroimmune consequences. Immunology and allergy clinics of North America 29:321-337.

Griswold CM, Matthews AL, Bewley KE, Mahaffey JW (1993) Molecular characterization and rescue of acatalasemic mutants of Drosophila melanogaster. Genetics 134:781-788.

Grundman M (2000) Vitamin E and Alzheimer disease: the basis for additional clinical trials. The American journal of clinical nutrition 71:630s-636s.

Haigis MC, Yankner BA (2010) The aging stress response. Molecular cell 40:333-344.

Hall ED, Braughler JM (1989) Central nervous system trauma and stroke: II. Physiological and pharmacological evidence for involvement of oxygen radicals and lipid peroxidation. Free Radical Biology and Medicine 6:303-313.

Halliwell B (2006) Oxidative stress and neurodegeneration: where are we now? Journal of neurochemistry 97:1634-1658.

Hamilton ML, Van Remmen H, Drake JA, Yang H, Guo ZM, Kewitt K, Walter CA, Richardson A (2001) Does oxidative damage to DNA increase with age? Proceedings of the National Academy of Sciences 98:10469-10474.

Harman D (1955) Aging: a theory based on free radical and radiation chemistry: University of California Radiation Laboratory Berkeley, CA.

Harper JW, Elledge SJ (2007) The DNA damage response: ten years after. Molecular cell 28:739-745.

Harris SL, Levine AJ (2005) The p53 pathway: positive and negative feedback loops. Oncogene 24:2899-2908.

Hasty P, Christy BA (2013) p53 as an intervention target for cancer and aging. Pathobiology of aging & age related diseases 3.

Hayflick L, Moorhead PS (1961) The serial cultivation of human diploid cell strains. Experimental cell research 25:585-621.

Herbert KE, Evans MD, Finnegan MT, Farooq S, Mistry N, Podmore ID, Farmer P, Lunec J (1996) A novel HPLC procedure for the analysis of 8-oxoguanine in DNA. Free Radical Biology and Medicine 20:467-473.

Herbig U, Ferreira M, Condel L, Carey D, Sedivy JM (2006) Cellular senescence in aging primates. Science 311:1257-1257.

Ho CY, Li HY (2010) DNA damage during mitosis invokes a JNK-mediated stress response that leads to cell death. Journal of cellular biochemistry 110:725-731.

Hoeijmakers JH (2009) DNA damage, aging, and cancer. New England Journal of Medicine 361:1475-1485.

Horner PJ, Power AE, Kempermann G, Kuhn HG, Palmer TD, Winkler J, Thal LJ, Gage FH (2000) Proliferation and differentiation of progenitor cells throughout the intact adult rat spinal cord. J Neurosci 20:2218-2228.

Humbert S, Bryson EA, Cordelières FP, Connors NC, Datta SR, Finkbeiner S, Greenberg ME, Saudou F (2002) The IGF-1/Akt pathway is neuroprotective in Huntington's disease and involves Huntingtin phosphorylation by Akt. Developmental cell 2:831-837.

Inaba M, White L, Bell C, Chen R, Petrovitch H, Launer L, Abbott RD, Ross GW, Masaki K (2011) White Matter Lesions on Brain Magnetic Resonance Imaging Scan and 5-Year Cognitive Decline: The Honolulu-Asia Aging Study. J Am Geriatr Soc.

Inoue M, Sato EF, Nishikawa M, Park A-M, Kira Y, Imada I, Utsumi K (2003) Mitochondrial generation of reactive oxygen species and its role in aerobic life. Current medicinal chemistry 10:2495-2505.

Itoh K, Wakabayashi N, Katoh Y, Ishii T, O'Connor T, Yamamoto M (2003) Keap1 regulates both cytoplasmic-nuclear shuttling and degradation of Nrf2 in response to electrophiles. Genes to Cells 8:379-391.

Jackson SP, Bartek J (2009) The DNA-damage response in human biology and disease. Nature 461:1071-1078.

Jaiswal AK (2004) Nrf2 signaling in coordinated activation of antioxidant gene expression. Free Radical Biology and Medicine 36:1199-1207.

Jeyapalan JC, Ferreira M, Sedivy JM, Herbig U (2007) Accumulation of senescent cells in mitotic tissue of aging primates. Mechanisms of ageing and development 128:36-44.

Johnson SC, Rabinovitch PS, Kaeberlein M (2013) mTOR is a key modulator of ageing and age-related disease. Nature 493:338-345.

Jurk D, Wang C, Miwa S, Maddick M, Korolchuk V, Tsolou A, Gonos ES, Thrasivoulou C, Jill Saffrey M, Cameron K (2012) Postmitotic neurons develop a p21-dependent senescence-like phenotype driven by a DNA damage response. Aging cell 11:996-1004.

Kaplon J, Zheng L, Meissl K, Chaneton B, Selivanov VA, Mackay G, van der Burg SH, Verdegaal EM, Cascante M, Shlomi T (2013) A key role for mitochondrial

gatekeeper pyruvate dehydrogenase in oncogene-induced senescence. Nature 498:109-112.

Keller JN, Schmitt FA, Scheff SW, Ding Q, Chen Q, Butterfield DA, Markesbery WR (2005) Evidence of increased oxidative damage in subjects with mild cognitive impairment. Neurology 64:1152-1156.

Keyse SM, Emslie EA (1992) Oxidative stress and heat shock induce a human gene encoding a protein-tyrosine phosphatase.

Kregel KC, Zhang HJ (2007) An integrated view of oxidative stress in aging: basic mechanisms, functional effects, and pathological considerations. American Journal of Physiology-Regulatory, Integrative and Comparative Physiology 292:R18-R36.

Kuilman T, Peeper DS (2009) Senescence-messaging secretome: SMS-ing cellular stress. Nature Reviews Cancer 9:81-94.

Lawless C, Wang C, Jurk D, Merz A, Zglinicki Tv, Passos JF (2010) Quantitative assessment of markers for cell senescence. Experimental gerontology 45:772-778.

Leaper SA, Murray AD, Lemmon HA, Staff RT, Deary IJ, Crawford JR, Whalley LJ (2001) Neuropsychologic correlates of brain white matter lesions depicted on MR images: 1921 Aberdeen Birth Cohort. Radiology 221:51-55.

Lenaz G, Cavazzoni M, Genova ML, D'Aurelio M, Pich MM, Pallotti F, Formiggini G, Marchetti M, Castelli GP, Bovina C (1998) Oxidative stress, antioxidant defences and aging. Biofactors 8:195-204.

Lindahl T, Barnes D (2000) Repair of endogenous DNA damage. In: Cold Spring Harbor symposia on quantitative biology, vol. 65, pp 127-134: Cold Spring Harbor Laboratory Press.

Lleo A, Galea E, Sastre M (2007) Molecular targets of non-steroidal anti-inflammatory drugs in neurodegenerative diseases. Cellular and molecular life sciences 64:1403-1418.

Lo YY, Wong JM, Cruz TF (1996) Reactive oxygen species mediate cytokine activation of c-Jun NH2-terminal kinases. Journal of Biological Chemistry 271:15703-15707.

López-Otín C, Blasco MA, Partridge L, Serrano M, Kroemer G (2013) The hallmarks of aging. Cell 153:1194-1217.

Lovell MA, Ehmann WD, Butler SM, Markesbery WR (1995) Elevated thiobarbituric acid-reactive substances and antioxidant enzyme activity in the brain in Alzheimer's disease. Neurology 45:1594-1601.

Lovell MA, Gabbita SP, Markesbery WR (1999) Increased DNA oxidation and decreased levels of repair products in Alzheimer's disease ventricular CSF. Journal of neurochemistry 72:771-776.

Lovell MA, Markesbery WR (2007) Oxidative DNA damage in mild cognitive impairment and late-stage Alzheimer's disease. Nucleic Acids Res 35:7497-7504.

Lovell MA, Xie C, Markesbery WR (2000) Acrolein, a product of lipid peroxidation, inhibits glucose and glutamate uptake in primary neuronal cultures. Free Radical Biology and Medicine 29:714-720.

Lovell MA, Xie C, Markesbery WR (2001) Acrolein is increased in Alzheimer’s disease brain and is toxic to primary hippocampal cultures. Neurobiology of aging 22:187-194.

Lucin KM, Wyss-Coray T (2009) Immune activation in brain aging and neurodegeneration: too much or too little? Neuron 64:110-122.

Lynch MA (2009) Age-related neuroinflammatory changes negatively impact on neuronal function. Frontiers in aging neuroscience 1.

Markesbery WR (1997) Oxidative stress hypothesis in Alzheimer's disease. Free Radical Biology and Medicine 23:134-147.

Markesbery WR, Carney JM (1999) Oxidative alterations in Alzheimer's disease. Brain Pathology 9:133-146.

Martindale JL, Holbrook NJ (2002) Cellular response to oxidative stress: Signaling for suicide and survival*. Journal of cellular physiology 192:1-15.

Matsuzawa A, Ichijo H (2005) Stress-responsive protein kinases in redox-regulated apoptosis signaling. Antioxidants & redox signaling 7:472-481.

Matter B, Malejka-Giganti D, Csallany AS, Tretyakova N (2006) Quantitative analysis of the oxidative DNA lesion, 2, 2-diamino-4-(2-deoxy-β-D-erythro-pentofuranosyl) amino]-5 (2H)-oxazolone (oxazolone), in vitro and in vivo by isotope dilution-capillary HPLC-ESI-MS/MS. Nucleic acids research 34:5449-5460.

Matthews FE, Brayne C, Lowe J, McKeith I, Wharton SB, Ince P (2009) Epidemiological pathology of dementia: attributable-risks at death in the Medical Research Council Cognitive Function and Ageing Study. PLoS Med 6:e1000180.

McMorris FA, Smith TM, DeSalvo S, Furlanetto RW (1986) Insulin-like growth factor I/somatomedin C: a potent inducer of oligodendrocyte development. Proceedings of the National Academy of Sciences 83:822-826.

Meek K, Dang V, Lees-Miller SP (2008) DNA-PK: the means to justify the ends? Advances in immunology 99:33-58.

MGEKN I, Quinn R, Tabet N (2008) Vitamin E for Alzheimer's disease and mild cognitive impairment. Cochrane Database Syst Rev 3.

Miwa S, Beckman KB, Muller FL (2008) Oxidative stress in aging: Springer.

Moloney AM, Griffin RJ, Timmons S, O'Connor R, Ravid R, O'Neill C (2010) Defects in IGF-1 receptor, insulin receptor and IRS-1/2 in Alzheimer's disease indicate possible resistance to IGF-1 and insulin signalling. Neurobiology of aging 31:224-243.

Moosmann B, Uhr M, Behl C (1997) Neuroprotective potential of aromatic alcohols against oxidative cell death. FEBS letters 413:467-472.

Mori S, Oishi K, Faria AV (2009) White matter atlases based on diffusion tensor imaging. Curr Opin Neurol 22:362-369.

Mozell R, McMorris F (1991) Insulin-like growth factor I stimulates oligodendrocyte development and myelination in rat brain aggregate cultures. Journal of neuroscience research 30:382-390.

Nakabeppu Y, Tsuchimoto D, Ichinoe A, Ohno M, Ide Y, Hirano S, Yoshimura D, Tominaga Y, Furuichi M, Sakumi K (2004) Biological significance of the defense mechanisms against oxidative damage in nucleic acids caused by reactive oxygen species: from mitochondria to nuclei. Annals of the New York Academy of Sciences 1011:101-111.

Narita M, Nuñez S, Heard E, Narita M, Lin AW, Hearn SA, Spector DL, Hannon GJ, Lowe SW (2003) Rb-mediated heterochromatin formation and silencing of E2F target genes during cellular senescence. Cell 113:703-716.

Navarro A, Boveris A (2004) Rat brain and liver mitochondria develop oxidative stress and lose enzymatic activities on aging. American Journal of Physiology-Regulatory, Integrative and Comparative Physiology 287:R1244-R1249.

Navarro A, Del Pino MJS, Gómez C, Peralta JL, Boveris A (2002) Behavioral dysfunction, brain oxidative stress, and impaired mitochondrial electron transfer in aging mice. American Journal of Physiology-Regulatory, Integrative and Comparative Physiology 282:R985-R992.

Naylor R, Baker D, van Deursen J (2012) Senescent cells: a novel therapeutic target for aging and age-related diseases. Clinical Pharmacology & Therapeutics 93:105-116.

Nelson G, Wordsworth J, Wang C, Jurk D, Lawless C, Martin-Ruiz C, von Zglinicki T (2012) A senescent cell bystander effect: senescence-induced senescence. Aging cell 11:345-349.

Nguyen T, Nioi P, Pickett CB (2009) The Nrf2-antioxidant response element signaling pathway and its activation by oxidative stress. Journal of Biological Chemistry 284:13291-13295.

Nishimura S (2002) Involvement of mammalian OGG1 (MMH) in excision of the 8-hydroxyguanine residue in DNA< sup> 1, 2</sup>. Free Radical Biology and Medicine 32:813-821.

Nunomura A, Honda K, Takeda A, Hirai K, Zhu X, Smith MA, Perry G (2006) Oxidative damage to RNA in neurodegenerative diseases. BioMed Research International 2006.

Nunomura A, Perry G, Aliev G, Hirai K, Takeda A, Balraj EK, Jones PK, Ghanbari H, Wataya T, Shimohama S (2001) Oxidative damage is the earliest event in Alzheimer disease. Journal of Neuropathology & Experimental Neurology 60:759-767.

Orjalo AV, Bhaumik D, Gengler BK, Scott GK, Campisi J (2009) Cell surface-bound IL-1α is an upstream regulator of the senescence-associated IL-6/IL-8 cytokine network. Proceedings of the National Academy of Sciences 106:17031-17036.

Parkes TL, Elia AJ, Dickinson D, Hilliker AJ, Phillips JP, Boulianne GL (1998) Extension of Drosophila lifespan by overexpression of human SOD1 in motorneurons. Nature genetics 19:171-174.

Passos JF, Nelson G, Wang C, Richter T, Simillion C, Proctor CJ, Miwa S, Olijslagers S, Hallinan J, Wipat A (2010) Feedback between p21 and reactive oxygen production is necessary for cell senescence. Molecular systems biology 6.

Pepper MS (1997) Transforming growth factor-beta: vasculogenesis, angiogenesis, and vessel wall integrity. Cytokine & growth factor reviews 8:21-43.

Perry R, Oakley A (1993) Newcastle brain map. Neuropsychiatric Disorders 1:1-10.

Picillo M, Erro R, Santangelo G, Pivonello R, Longo K, Pivonello C, Vitale C, Amboni M, Moccia M, Colao A (2013) Insulin-like growth factor-1 and progression of motor symptoms in early, drug-naïve Parkinson's disease. Journal of neurology 260:1724-1730.

Pombo CM, Bonventre JV, Molnar A, Kyriakis J, Force T (1996) Activation of a human Ste20-like kinase by oxidant stress defines a novel stress response pathway. The EMBO journal 15:4537.

Poon HF, Calabrese V, Scapagnini G, Butterfield DA (2004) Free radicals and brain aging. Clinics in geriatric medicine 20:329-359.

Popescu BO, Toescu EC, Popescu LM, Bajenaru O, Muresanu DF, Schultzberg M, Bogdanovic N (2009) Blood-brain barrier alterations in ageing and dementia. J Neurol Sci 283:99-106.

Praticò D (2008) Evidence of oxidative stress in Alzheimer's disease brain and antioxidant therapy. Annals of the New York Academy of Sciences 1147:70-78.

Purvis JE, Karhohs KW, Mock C, Batchelor E, Loewer A, Lahav G (2012) p53 dynamics control cell fate. Science 336:1440-1444.

Qiao M, Malisza KL, Del Bigio MR, Tuor UI (2001) Correlation of cerebral hypoxic-ischemic T2 changes with tissue alterations in water content and protein extravasation. Stroke 32:958-963.

Radak Z, Boldogh I (2010) 8-Oxo-7, 8-dihydroguanine: links to gene expression, aging, and defense against oxidative stress. Free Radical Biology and Medicine 49:587-596.

Radak Z, Zhao Z, Goto S, Koltai E (2011) Age-associated neurodegeneration and oxidative damage to lipids, proteins and DNA. Molecular aspects of medicine 32:305-315.

Reddy SP (2008) The antioxidant response element and oxidative stress modifiers in airway diseases. Current molecular medicine 8:376.

Rodier F, Coppé J-P, Patil CK, Hoeijmakers WA, Muñoz DP, Raza SR, Freund A, Campeau E, Davalos AR, Campisi J (2009) Persistent DNA damage signalling triggers senescence-associated inflammatory cytokine secretion. Nature cell biology 11:973-979.

Rodier F, Muñoz DP, Teachenor R, Chu V, Le O, Bhaumik D, Coppé J-P, Campeau E, Beauséjour CM, Kim S-H (2011) DNA-SCARS: distinct nuclear structures that

sustain damage-induced senescence growth arrest and inflammatory cytokine secretion. Journal of cell science 124:68-81.

Rogakou EP, Pilch DR, Orr AH, Ivanova VS, Bonner WM (1998) DNA double-stranded breaks induce histone H2AX phosphorylation on serine 139. Journal of biological chemistry 273:5858-5868.

Rollero A, Murialdo G, Fonzi S, Garrone S, Gianelli MV, Gazzerro E, Barreca A, Polleri A (1998) Relationship between cognitive function, growth hormone and insulin-like growth factor I plasma levels in aged subjects. Neuropsychobiology 38:73-79.

Roman GC, Erkinjuntti T, Wallin A, Pantoni L, Chui HC (2002) Subcortical ischaemic vascular dementia. Lancet Neurol 1:426-436.

Rouse J, Jackson SP (2002) Interfaces between the detection, signaling, and repair of DNA damage. Science 297:547-551.

Salminen A, Ojala J, Kaarniranta K, Haapasalo A, Hiltunen M, Soininen H (2011) Astrocytes in the aging brain express characteristics of senescence-associated secretory phenotype. European Journal of Neuroscience 34:3-11.

Sano M, Ernesto C, Thomas RG, Klauber MR, Schafer K, Grundman M, Woodbury P, Growdon J, Cotman CW, Pfeiffer E (1997) A controlled trial of selegiline, alpha-tocopherol, or both as treatment for Alzheimer's disease. New England Journal of Medicine 336:1216-1222.

Scheltens P, Barkhof F, Leys D, Pruvo JP, Nauta JJ, Vermersch P, Steinling M, Valk J (1993) A semiquantative rating scale for the assessment of signal hyperintensities on magnetic resonance imaging. J Neurol Sci 114:7-12.

Schmittgen TD, Livak KJ (2008) Analyzing real-time PCR data by the comparative CT method. Nature protocols 3:1101-1108.

Sengupta S, Harris CC (2005) p53: traffic cop at the crossroads of DNA repair and recombination. Nature Reviews Molecular Cell Biology 6:44-55.

Serrano M, Lin AW, McCurrach ME, Beach D, Lowe SW (1997) Oncogenic< i> ras</i> Provokes Premature Cell Senescence Associated with Accumulation of p53 and p16< sup> INK4a</sup>. Cell 88:593-602.

Shafit-Zagardo B, Kress Y, Zhao ML, Lee SC (1999) A novel microtubule-associated protein-2 expressed in oligodendrocytes in multiple sclerosis lesions. J Neurochem 73:2531-2537.

Shan X, Chang Y, Lin C-lG (2007) Messenger RNA oxidation is an early event preceding cell death and causes reduced protein expression. The FASEB Journal 21:2753-2764.

Shibutani S, Takeshita M, Grollman AP (1991) Insertion of specific bases during DNA synthesis past the oxidation-damaged base 8-oxodG.

Shiloh Y (2003) ATM and related protein kinases: safeguarding genome integrity. Nature Reviews Cancer 3:155-168.

Siegel JJ, Amon A (2012) New insights into the troubles of aneuploidy. Annual review of cell and developmental biology 28:189.

Simpson J, Ince P, Haynes L, Theaker R, Gelsthorpe C, Baxter L, Forster G, Lace G, Shaw P, Matthews F (2010a) Population variation in oxidative stress and astrocyte DNA damage in relation to Alzheimer-type pathology in the ageing brain. Neuropathology and applied neurobiology 36:25-40.

Simpson JE, Fernando MS, Clark L, Ince PG, Matthews F, Forster G, O'Brien JT, Barber R, Kalaria RN, Brayne C, Shaw PJ, Lewis CE, Wharton SB (2007a) White matter lesions in an unselected cohort of the elderly: astrocytic, microglial and oligodendrocyte precursor cell responses. Neuropathol Appl Neurobiol 33:410-419.

Simpson JE, Hosny O, Wharton SB, Heath PR, Holden H, Fernando MS, Matthews F, Forster G, O'Brien JT, Barber R, Kalaria RN, Brayne C, Shaw PJ, Lewis CE, Ince PG (2009) Microarray RNA expression analysis of cerebral white matter lesions reveals changes in multiple functional pathways. Stroke 40:369-375.

Simpson JE, Ince PG, Haynes LJ, Theaker R, Gelsthorpe C, Baxter L, Forster G, Lace GL, Shaw PJ, Matthews FE, Savva GM, Brayne C, Wharton SB (2010b) Population variation in oxidative stress and astrocyte DNA damage in relation to Alzheimer-type pathology in the ageing brain. Neuropathol Appl Neurobiol 36:25-40.

Simpson JE, Ince PG, Higham CE, Gelsthorpe CH, Fernando MS, Matthews F, Forster G, O'Brien JT, Barber R, Kalaria RN, Brayne C, Shaw PJ, Stoeber K, Williams GH, Lewis CE, Wharton SB (2007b) Microglial activation in white matter lesions and nonlesional white matter of ageing brains. Neuropathol Appl Neurobiol 33:670-683.

Simpson JE, Ince PG, Lace G, Forster G, Shaw PJ, Matthews F, Savva G, Brayne C, Wharton SB (2010c) Astrocyte phenotype in relation to Alzheimer-type pathology in the ageing brain. Neurobiol Aging 31:578-590.

Simpson JE, Wharton SB, Cooper J, Gelsthorpe C, Baxter L, Forster G, Shaw PJ, Savva G, Matthews FE, Brayne C, Ince PG (2010d) Alterations of the blood-brain barrier in cerebral white matter lesions in the ageing brain. Neurosci Lett 486:246-251.

Singh R, Teichert F, Verschoyle RD, Kaur B, Vives M, Sharma RA, Steward WP, Gescher AJ, Farmer PB (2009) Simultaneous determination of 8-oxo-2′-deoxyguanosine and 8-oxo-2′-deoxyadenosine in DNA using online column-switching liquid chromatography/tandem mass spectrometry. Rapid Communications in Mass Spectrometry 23:151-160.

Sohal RS, Weindruch R (1996) Oxidative stress, caloric restriction, and aging. Science 273:59-63.

Soubeyrand S, Schild-Poulter C, Hache RJ (2004) Structured DNA promotes phosphorylation of p53 by DNA-dependent protein kinase at serine 9 and threonine 18. European Journal of Biochemistry 271:3776-3784.

Starr JM, Farrall AJ, Armitage P, McGurn B, Wardlaw J (2009) Blood-brain barrier permeability in Alzheimer's disease: a case-control MRI study. Psychiatry Res 171:232-241.

Stiff T, O'Driscoll M, Rief N, Iwabuchi K, Löbrich M, Jeggo PA (2004) ATM and DNA-PK function redundantly to phosphorylate H2AX after exposure to ionizing radiation. Cancer research 64:2390-2396.

Stucki M, Jackson SP (2006) γH2AX and MDC1: anchoring the DNA-damage-response machinery to broken chromosomes. DNA repair 5:534-543.

Sun Y, Oberley LW (1996) Redox regulation of transcriptional activators. Free Radical Biology and Medicine 21:335-348.

Takahashi A, Ohtani N, Yamakoshi K, Iida S-i, Tahara H, Nakayama K, Nakayama KI, Ide T, Saya H, Hara E (2006) Mitogenic signalling and the p16INK4a–Rb pathway cooperate to enforce irreversible cellular senescence. Nature cell biology 8:1291-1297.

Tang DG, Tokumoto YM, Raff MC (2000) Long-term culture of purified postnatal oligodendrocyte precursor cells. Evidence for an intrinsic maturation program that plays out over months. J Cell Biol 148:971-984.

Tchkonia T, Zhu Y, van Deursen J, Campisi J, Kirkland JL (2013) Cellular senescence and the senescent secretory phenotype: therapeutic opportunities. The Journal of clinical investigation 123:966-972.

Trachootham D, Lu W, Ogasawara MA, Valle NR-D, Huang P (2008) Redox regulation of cell survival. Antioxidants & redox signaling 10:1343-1374.

Turken A, Whitfield-Gabrieli S, Bammer R, Baldo JV, Dronkers NF, Gabrieli JD (2008) Cognitive processing speed and the structure of white matter pathways: convergent evidence from normal variation and lesion studies. Neuroimage 42:1032-1044.

Uttara B, Singh AV, Zamboni P, Mahajan R (2009) Oxidative stress and neurodegenerative diseases: a review of upstream and downstream antioxidant therapeutic options. Current neuropharmacology 7:65.

van Deursen JM (2014) The role of senescent cells in ageing. Nature 509:439-446.

Von Zglinicki T (2002) Oxidative stress shortens telomeres. Trends in biochemical sciences 27:339-344.

Waghmare SP, Dickman MJ (2011) Characterization and quantification of RNA post-transcriptional modifications using stable isotope labeling of RNA in conjunction with mass spectrometry analysis. Analytical chemistry 83:4894-4901.

Wang J, Markesbery WR, Lovell MA (2006) Increased oxidative damage in nuclear and mitochondrial DNA in mild cognitive impairment. Journal of neurochemistry 96:825-832.

Wang J, Xiong S, Xie C, Markesbery W, Lovell M (2005) Increased oxidative damage in nuclear and mitochondrial DNA in Alzheimer's disease. Journal of neurochemistry 93:953-962.

Wang S, Leonard SS, Ye J, Gao N, Wang L, Shi X (2004) Role of reactive oxygen species and Cr (VI) in Ras-mediated signal transduction. Molecular and cellular biochemistry 255:119-127.

West SC (2003) Molecular views of recombination proteins and their control. Nature reviews Molecular cell biology 4:435-445.

Wharton SB, Brayne C, Savva GM, Matthews FE, Forster G, Simpson J, Lace G, Ince PG (2011) Epidemiological Neuropathology: The MRC Cognitive Function and Aging Study Experience. J Alzheimers Dis 25:359-372.

White L, Small BJ, Petrovitch H, Ross GW, Masaki K, Abbott RD, Hardman J, Davis D, Nelson J, Markesbery W (2005) Recent clinical-pathologic research on the causes of dementia in late life: update from the Honolulu-Asia Aging Study. J Geriatr Psychiatry Neurol 18:224-227.

Wickens AP (2001) Ageing and the free radical theory. Respiration physiology 128:379-391.

Wojtera M, Sikorska B, Sobow T, Liberski PP (2005) Microglial cells in neurodegenerative disorders. Folia Neuropathol 43:311-321.

Wyss-Coray T, Lin C, Sanan DA, Mucke L, Masliah E (2000) Chronic overproduction of transforming growth factor-β1 by astrocytes promotes Alzheimer's disease-like microvascular degeneration in transgenic mice. The American journal of pathology 156:139-150.

Zaccai J, Ince P, Brayne C (2006) Population-based neuropathological studies of dementia: design, methods and areas of investigation--a systematic review. BMC Neurol 6:2.

Zglinicki Tv, Saretzki G, Ladhoff J, Fagagna F, Jackson S (2005) Human cell senescence as a DNA damage response. Mechanisms of ageing and development 126:111-117.

Zhang HJ, Drake VJ, Xu L, Hu J, Domann FE, Oberley LW, Kregel KC (2002) Redox regulation of adenovirus-induced AP-1 activation by overexpression of manganese-containing superoxide dismutase. Journal of virology 76:355-363.

APPENDICES

Image 1: Ethical approval form fo the current CFAS study

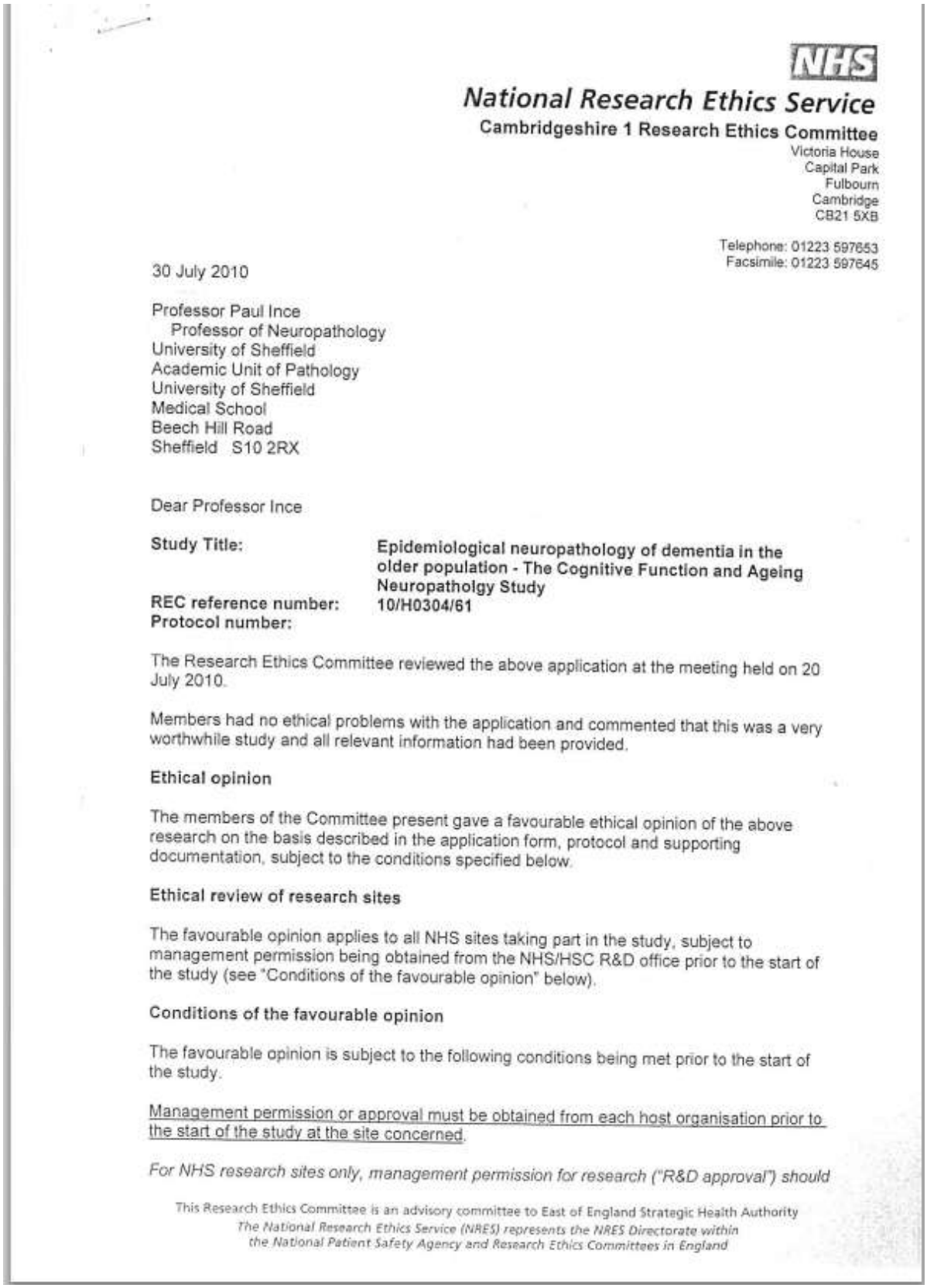

NHS

National Research Ethics Service

Cambridgeshire 1 Research Ethics Committee

Victoria House
Capital Park
Fulbourn
Cambridge
CB21 5XB

Telephone: 01223 597653
Facsimile: 01223 597645

30 July 2010

Professor Paul Ince
Professor of Neuropathology
University of Sheffield
Academic Unit of Pathology
University of Sheffield
Medical School
Beech Hill Road
Sheffield S10 2RX

Dear Professor Ince

Study Title: **Epidemiological neuropathology of dementia in the older population - The Cognitive Function and Ageing Neuropatholgy Study**

REC reference number: **10/H0304/61**

Protocol number:

The Research Ethics Committee reviewed the above application at the meeting held on 20 July 2010.

Members had no ethical problems with the application and commented that this was a very worthwhile study and all relevant information had been provided.

Ethical opinion

The members of the Committee present gave a favourable ethical opinion of the above research on the basis described in the application form, protocol and supporting documentation, subject to the conditions specified below.

Ethical review of research sites

The favourable opinion applies to all NHS sites taking part in the study, subject to management permission being obtained from the NHS/HSC R&D office prior to the start of the study (see "Conditions of the favourable opinion" below).

Conditions of the favourable opinion

The favourable opinion is subject to the following conditions being met prior to the start of the study.

Management permission or approval must be obtained from each host organisation prior to the start of the study at the site concerned.

For NHS research sites only, management permission for research ("R&D approval") should

This Research Ethics Committee is an advisory committee to East of England Strategic Health Authority
The National Research Ethics Service (NRES) represents the NRES Directorate within the National Patient Safety Agency and Research Ethics Committees in England

Permission for papers re-print

JOHN WILEY AND SONS LICENSE TERMS AND CONDITIONS

Nov 24, 2014

This is a License Agreement between Sufana Al Mashhadi ("You") and John Wiley and Sons ("John Wiley and Sons") provided by Copyright Clearance Center ("CCC"). The license consists of your order details, the terms and conditions provided by John Wiley and Sons, and the payment terms and conditions.

All payments must be made in full to CCC. For payment instructions, please see information listed at the bottom of this form.

License Number	3513821095239
License date	Nov 21, 2014
Licensed content publisher	John Wiley and Sons
Licensed content publication	Neuropathology and Applied Neurobiology
Licensed content title	DNA damage response and senescence in endothelial cells of human cerebral cortex and relation to Alzheimer\'s neuropathology progression: a population-based study in the Medical Research Council Cognitive Function and Ageing Study (MRC-CFAS) cohort
Licensed copyright line	© 2014 British Neuropathological Society
Licensed content author	Claire J. Garwood,Julie E. Simpson,Sufana Al Mashhadi,Claire Axe,Suzanna Wilson,Pamela R. Heath,Pamela J. Shaw,Fiona E. Matthews,Carol Brayne,Paul G. Ince,Stephen B. Wharton
Licensed content date	Nov 17, 2014
Start page	802
End page	814
Type of use	Dissertation/Thesis
Requestor type	Author of this Wiley article
Format	Print and electronic
Portion	Full article
Will you be translating?	No
Title of your thesis / dissertation	Oxidative stress and DNA damage in white matter lesions of the human ageing brain
Expected completion date	Nov 2014
Expected size (number of pages)	230
Total	0.00 GBP

RE-PRINTS OF PUBLICATIONS

Oxidative Glial Cell Damage Associated with White Matter Lesions in the Aging Human Brain

Sufana Al-Mashhadi[1,2]; Julie E. Simpson[1]; Paul R. Heath[1]; Mark Dickman[3]; Gillian Forster[1]; Fiona E. Matthews[4]; Carol Brayne[5]; Paul G. Ince[1]*; Stephen B. Wharton[1]*; on behalf of Medical Research Council Cognitive Function and Ageing Study

[1] Sheffield Institute for Translational Neuroscience, [3] Department of Chemical and Biological Engineering, University of Sheffield, Sheffield, [4] Medical Research Council Biostatistics Unit, and [5] Institute of Public Health, University of Cambridge, Cambridge, UK, [2] King Fahad Medical City, Riyadh, Saudi Arabia.

Keywords
dementia, DNA damage, ischemic white matter, white matter disease, white matter lesions.

Corresponding author:
Paul Ince, MD, Sheffield Institute for Translational Neuroscience, University of Sheffield, 385A Glossop Road, Sheffield, S10 2HQ, UK (E-mail: *p.g.ince@sheffield.ac.uk*)

Received 20 August 2014
Accepted 7 October 2014
Published Online Article Accepted 14 October 2014

* Joint senior authors.

doi:10.1111/bpa.12216

Abstract

White matter lesions (WML) are common in brain aging and are associated with dementia. We aimed to investigate whether oxidative DNA damage and occur in WML and in apparently normal white matter in cases with lesions. Tissue from WML and control white matter from brains with lesions (controls lesional) and without lesions (controls non-lesional) were obtained, using post-mortem magnetic resonance imaging-guided sampling, from the Medical Research Council Cognitive Function and Ageing Study. Oxidative damage was assessed by immunohistochemistry to 8-hydroxy-2′-deoxoguanosine (8-OHdG) and Western blotting for malondialdehyde. DNA response was assessed by phosphorylated histone H2AX (*γH2AX*), p53, senescence markers and by quantitative Reverse transcription polymerase chain reaction (RT-PCR) panel for candidate DNA damage-associated genes. 8-OHdG was expressed in glia and endothelium, with increased expression in both WML and controls lesional compared with controls non-lesional ($P < 0.001$). γH2Ax showed a similar, although attenuated difference among groups ($P = 0.03$). Expression of senescence-associated β-galactosidase and p16 suggested induction of senescence mechanisms in glia. Oxidative DNA damage and a DNA damage response are features of WML pathogenesis and suggest candidate mechanisms for glial dysfunction. Their expression in apparently normal white matter in cases with WML suggests that white matter dysfunction is not restricted to lesions. The role of this field-effect lesion pathogenesis and cognitive impairment are areas to be defined.

INTRODUCTION

White matter lesions (WML), which can be identified in life as areas of increased signal on T2-weighted magnetic resonance imaging (MRI) scans, are a common feature of the aging brain (7, 23). They are associated with dementia, depression, impaired motor function and Alzheimer's disease, and may be risk factors for progression of mild cognitive impairment to dementia and to stroke (2, 3, 5, 8, 9, 17, 18, 30, 41, 43). The Medical Research Council Cognitive Function and Ageing Study (CFAS) is a longitudinal study of dementia and frailty in the population with a brain donation cohort, permitting assessment of neuropathologic correlates (26, 28, 45). In CFAS, WML have been found to be an independent predictor of cognitive impairment (12).

With a role in cognitive impairment, the pathogenesis of WML, and associated dysfunction in surrounding white matter are important questions. The association of vascular risk factors and vascular pathology with WML suggests that they are a manifestation of small vessel disease (25, 29, 31). Pathologically, WML consist of areas of white matter loss, or myelin attenuation, associated with astrogliosis, microgliosis and apoptosis of oligodendrocytes and astrocytes (1, 21, 34, 37). While they have been considered to represent infarction or incomplete infarction (10, 11), and there is histopathologic evidence for a role for hypoperfusion (14), their pathology and pathogenesis is likely to be more complex (45) and still remains poorly defined.

Studies of the pathology and pathogenesis of WML are hampered by the difficulty in recognizing these lesions in the autopsy brain. The CFAS approach has been to use post-mortem MRI of brain slices to guide sampling of WML (13). This allows sampling of lesions, and of control white matter from cases with deep subcortical lesions (controls lesional, CL), which appears normal on routine histologic examination, and from cases without lesions (controls non-lesional, CNL). These studies have defined the glial pathology of WML and shown up-regulation of microglial activity (37, 39). Expression of hypoxia-related molecules in WML supports a role for ischemia (14), but there is also evidence of blood–brain barrier leakage (38), suggesting that blood–brain barrier dysfunction may play a role in their pathogenesis. Periventricular WML appear to show some pathologic differences from WML in deep subcortical white matter; furthermore, lesions in these two locations may have different clinical effects (20). The current study focuses on deep subcortical WML (hereafter referred to simply as WML). Our previous work also demonstrated that

apparently normal white matter from cases with lesions shows microglial activation and altered transcriptional profile, similar to those of the lesions (35, 37). This "field effect" suggests that WML (in a deep subcortical location) are associated with more widespread white matter abnormality.

Hypoxia/ischemia and inflammatory mechanisms, which have been demonstrated in this cohort, are associated with oxidative stress, which may impair cellular function. In this study we therefore hypothesized that oxidative DNA damage is a feature of WML pathology and pathogenesis that might impair glial cell function. We have therefore examined markers of oxidative damage and of a DNA damage response in WML and in the two control groups, with (CL) and without (CNL) lesions elsewhere in the white matter.

METHODS

Cohort and tissues

Formalin-fixed paraffin-embedded (FFPE) and frozen samples of white matter were obtained from the MRC–CFAS, with Research Ethics Committee approval. Briefly, the study [previously reviewed in (45)] is based around six UK centers, with recruitment from family practitioner registries based on age at entry (>65 years). For this study, FFPE samples were obtained from the Newcastle cohort and frozen samples from the Cambridge cohort. Using a similar case control structure to our previous white matter studies (37–39), the cohort consisted of: (i) samples of deep subcortical WML (DSCL); (ii) control white matter from cases with lesions elsewhere (CL); and (iii) controls from cases without WMLs (CNL). Tissue sampling from formalin-fixed coronal cerebral slices to create FFPE blocks was guided by post-mortem MRI scans to identify WML, as previously described (13). Immunohistochemistry was carried out on sections from 43 FFPE blocks derived from 40 individuals, 18 men, 22 women (WML 15 cases, mean age 86 range 74–89; CL 13 cases mean age 84.6 range 74–91; CNL 15 cases mean age 82.5 range 65–101). For frozen tissue samples, MRI scans of the formalin-fixed contralateral brain hemispheres were used as a guide to map WML, as they tend to be distributed roughly symmetrically between the two brain hemispheres. Luxol fast blue stain for myelin loss and immunohistochemisty to the microglial marker CD68 were then performed on the frozen samples to confirm the lesion/non-lesional status of the sampled blocks, as lesions show myelin loss and activated, amoeboid microglia. Twenty individuals (eight men, 12 women) provided 27 frozen blocks for analysis, comprising 11 WML (mean age 88.7 range 74–102), eight CNL (mean age 88 range 74–95) and eight CL (mean age 86.8 range 75–95).

Immunohistochemistry

FFPE blocks were sectioned at 6 μm and frozen tissue sectioned at 8 μm before fixation in ice-cold acetone at 4°C for 10 minutes. Immunohistochemistry was performed using a standard ABC method (Vector Laboratories, Peterborough, UK) and the signal visualized using 3,3′-diaminobenzidine. A summary of the primary antibodies and their conditions, including antigen retrieval, is shown in Table 1. Negative controls consisted of sections incubated with isotype controls or with omission of the primary antibody.

Double-staining experiments to localize 8-hydroxy-2′-deoxoguanosine (8-OHdG) to specific cell types were performed on FFPE sections. Staining for 8-OHdG was performed using the same conditions as for single staining and the signal visualized using the diaminobenzidine chromogen. Sections were then placed in Tris-buffered saline (TBS) buffer, incubated with 1.5% relevant normal sera for 1 h at room temperature (RT) before they were incubated with avidin-biotin blocking kit (Vector Laboratories), according to the manufacturer's instructions. Sections were incubated with the second primary antibody for cell type [GFAP, CD68, oligodendrocyte-specific protein (OSP), collagen IV] at 4°C overnight. Sections were washed thoroughly with TBS buffer and incubated with the relevant biotinylated secondary antibody for 1 h at RT, followed by streptavidin-Tetramethylrhodamine isothiocyanate (TRITC) (1:100 in TBS) for an hour at (RT) in the dark. Sections were rinsed in TBS, air dried in the dark and mounted with Vectamount containing 4′,6-diamidino-2-phenylindole (DAPI) (Vector Laboratories). Sections were stored in the dark at 4°C and visualized in bright field to view oxidative damage (8-OHdG) and a fluorescent field to co-localize the damage with specific cellular phenotypes. Image capture was performed using CellᴧR (Olympus Biosystems, Watford, UK) and Leica DMI4000B, UK. Co-localization of staining was analyzed using Corel Paint Shop Pro X (Corel, Maidenhead, UK).

Quantification of 8-OHdG and γH2Ax immunohistochemistry

Within each region (CNL, CL and WML), five random fields were captured using a Nikon Eclipse 80i microscope (Nikon UK, Kingston upon Thames). Images were transferred to a PowerPoint program where a grid was overlaid on each image (Figure 1A). The number of 8-OHdG positive nuclei and total number of nuclei were assessed in the five fields for each case, allowing determination of percentage positive nuclei. For 8-OHdG, only cells with positive nuclei, reflecting nuclear DNA oxidative damage, were assessed; cells with cytoplasmic only staining were not counted as positive.

Histochemistry for senescence-associated β-galactosidase (SA-β-gal)

Prior to use, components of the SA-β-gal histochemical staining kit (Sigma-Aldrich, Gillingham, UK) were thawed on ice and the X-gal solution heated to 37°C for 1 h to activate. The frozen sections were warmed to RT for 5 minutes, fixed in ready-made fixation solution for 6 minutes at RT followed by three rinses in 1× PBS. Freshly prepared staining mixture was then added, the sections were covered with parafilm and incubated overnight at 37°C. Sections were rinsed in TBS, counter-stained with nuclear fast red for 30 s followed by a rinse in deionized water before they were dehydrated, cleared and mounted in DPX. SA-β-gal activity was microscopically detected by the presence of a blue, insoluble precipitate within the cell. SA-β-gal was assessed semi-quantitatively in images captured at low magnification (×20 objective). The following scoring criteria were used: no positive cells (0); less than two positive cells per field (+); two to five positive cells (++); more than six isolated positive cells (+++).

To determine if SA-β-gal activity was associated with astrocytes, microglia and/or oligodendrocytes, GFAP-, CD68- and

Table 1. Antibodies: sources and conditions.

Antibody	Species	Dilution and conditions	Antigen retrieval	Supplier
Primary antibodies for immunohistochemistry				
8-OHdG	Mouse monoclonal	1/400 1 h RT	Pressure cooker access revelation (x10, pH 6.5)	Abcam, Cambridge UK
γH$_2$AX	Rabbit monoclonal	1/1000 1 h RT	Pressure cooker EDTA pH8	R&D Systems, Abingdon UK
DNA-PK	Mouse monoclonal	1/400 1 h RT	Pressure cooker EDTA pH8	Merck Biosciences Ltd, Nottingham UK
GFAP	Rabbit polyclonal	1/1000 1 h RT	Pressure cooker TSC pH6	DakoCytomation, Ely UK
OSP	Rabbit polyclonal	1/250 1 h RT	Pressure cooker TSC pH6	Abcam, Cambridge UK
CD68	Mouse monoclonal	1/100 1 h RT	10 min in microwave TSC pH6.3	Dako UK Ltd, Ely
Collagen IV	Mouse monoclonal	1/500 O/N at 4°C	10 min in microwave TSC pH6.3	Sigma-Aldrich, Gillingham UK
P16	Mouse monoclonal	1/100 1 h RT	Pressure cooker EDTA pH8	Bio-Genex, Fremont CA, USA
P53	Mouse monoclonal	1/50 O/N at 4°C	Pressure cooker EDTA pH8	Santa Cruz Biotechnology Inc., Heidelberg, Germany
P21	Mouse monoclonal	1/50 O/N at 4°C	Pressure cooker TSC pH6	Abcam, Cambridge UK
Primary antibodies for Western blotting				
γH$_2$AX	Rabbit monoclonal	1/1000	NA	R&D systems, Abingdon UK
DNA-PK	Mouse monoclonal	1/1000	NA	Abcam, Cambridge UK
MDA	Rabbit polyclonal	1/1000	NA	Cell Biolabs, Cambridge UK
β-actin	Mouse monoclonal	1/1000	NA	Abcam, Cambridge UK
Secondary antibodies				
Goat anti-mouse HRP	Mouse polyclonal	1/5000	NA	DakoCytomation, Ely UK
Goat anti-rabbit HRP	Rabbit polyclonal	1/5000	NA	DakoCytomation, Ely UK

8-OHdG = 8-hydroxy-2'-deoxoguanosine; γH2Ax = Phosphorylated histone H2Ax; DNA-PK = DNA protein kinase; EDTA = Ethylenediaminetetraacetic acid; GFAP = Glial Fibrillary Acidic Protein; HRP = horseradish peroxidise; NA = not applicable; OSP = oligodendrocytes; RT = room temperature; TSC = Tris-saline-citrate buffer.

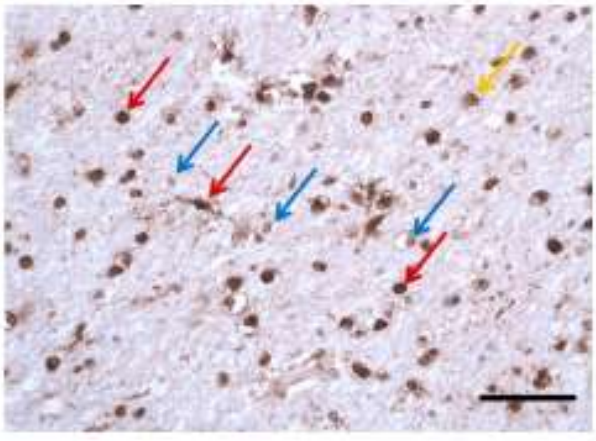

Figure 1. Immunohistochemistry to 8-hydroxy-2'-deoxoguanosine showing strongly labeled nuclei (red arrows), unlabelled nuclei (blue arrows) and nuclei with faint reactivity (yellow arrow). Scale bar 50 μm.

OSP-stained sections (using a standard ABC method as earlier) were double–labeled, respectively, with SA-β-gal. To determine the associations of SA-β-gal activity with cell cycle checkpoint protein p16, immunolabeled frozen sections (using ABC kit) were double-labeled with SA-β-gal.

Western blotting

Frozen white matter samples (approximately 0.5 g of tissue) from WML, CL and CNL were homogenized and sonicated for 30 s in buffer. Samples were then microfuged at 14 000 rpm for 30 minutes at 4°C. The supernatant was collected and stored at −80°C until required, while the pellet, which contained insoluble protein, was discarded. Bradford assay (reagents from Thermo Scientific, Loughborough, UK) was performed to determine protein concentration. Prior to blotting, protein samples were diluted in an appropriate volume of homogenate buffer to ensure equal protein concentrations (approximately 50 μg) for loading. Proteins were separated by sodium dodecylsulphate-polyacrylamide gel electrophoresis [15% for γH2AX, 8% for MDA and 6% for DNA protein kinase (DNA-PKcs)] and transferred to a polyvinyl difluoride immobilin transfer membrane (Millipore, Dundee, UK). Membranes were incubated overnight with rabbit anti-γH2AX (1:1000;

R&D Systems, UK), rabbit anti-MDA primary antibody (1:1000; Cell Biolabs, Cambridge, UK) or mouse anti-DNA-PKcs (1:500; Calbiochem, UK), followed by the appropriate horseradish peroxidise (HRP)-linked secondary antibody (1:1000; DakoCytomation, Ely, UK). To confirm equal protein loading, the membrane was reprobed for β-actin (1:5000; AbCam, Cambridge, UK). Proteins were detected using an enhanced chemiluminescence kit (Amersham, UK) for chemiluminescence based-immunodetection of HRP. Membranes were developed and scanned using the G:box (Syngene, Cambridge, UK). Images were captured using the Intelli Chemi setting in the GeneSnap software (Syngene). Densitometric analysis was carried out in GeneTools (Syngene). Developed bands were manually framed in equally sized rectangular boxes that were manually designed to fit the largest band. Background was corrected by the software automatically. Raw data of the pixel intensity and the intensity of the bands in proportion to a defined control were calculated and the intensity of developed bands of interest normalized to the loading control.

Reverse transcription quantitative polymerase chain reaction (RT-qPCR) array

RNA extraction was performed from 50 µg of frozen tissue from each of 10 samples from the frozen cohort (three CNL, three CL, four WML). RNA was extracted using the Direct-zol RNA MiniPrep kit (Zymo Research, Irvine, CA, USA). RNA quality was checked on the Agilent 2100 Bioanalyser (Agilent, Palo Alto, CA, USA) using an RNA 6000 Nano kit. RNA concentration was measured on the Nanodrop Spectrophotometer (ND1000, Labtech International, Uckfield, UK). RNA integrity number (RIN) numbers were 2.5, 3.1 and 4.2 for CNL cases, 2.9, 2.8 and 2.7 for CL and 2.4, 3, 3 and 1.1 for WML. 96 well RT-qPCR arrays were obtained from Qiagen (Manchester, UK), custom designed for assessment of gene expression related to senescence and DNA damage (see Supplementary Figure S1). The selection of genes was made from those available on the commercial senescence and oxidative stress-based array based on our prior knowledge and a literature search for likely candidates. RT-qPCR was performed according to the manufacturer's instructions. Three housekeeping genes, comprising β-actin, glyceraldehyde phosphate dehydrogenase and β-2 microglobulin, were included in the arrays to enable normalization of the data. The average Ct and standard deviation (SD) for the three genes was determined for each group [average (SD) for: CNL 25.71 (1.54); CL 22.49 (0.47); WML 25.45 (1.56)] and the average used for normalization within each group. Further normalization to the CNL group (to a value of 1) was used to determine fold changes for each gene in the CL and WML groups. The plate was also designed with a genomic DNA control, which detects non-transcribed genomic DNA contamination with a high level of sensitivity. A reverse-transcription control tested the efficiency of the reverse-transcription reaction and a positive PCR control (PPC) tested the polymerase chain reaction.

Statistic analysis

Statistic analyses for the immunohistochemical data were carried out in Stata v12 (StataCorp LP, College Station TS, USA). Multiple readings by different readers were investigated using intra-class correlation coefficient (ICC) for consistency. Quantitative comparisons among groups were compared using analysis of variance, taking into account non-independent structure of the data and paired sampling of measures. *Post hoc* group differences were calculated using the Tukey–Kramer pairwise, after adjustment for multiple levels. All results were additionally checked using non-parametric techniques and multilevel models. Associations were assessed using Spearman's correlation coefficient.

RESULTS

Oxidative stress

Oxidative damage to nuclear DNA was assessed by immunohistochemistry to 8-OHdG, with positivity ranging from faintly to strongly positive (Figure 1). In many cells, reactivity was also observed in the cytoplasm, presumably reflecting oxidative damage to RNA and/or mitochondrial DNA; cytoplasmic reactivity was not assessed further in this study. Double-labeling immunohistochemistry demonstrated reactivity in astrocytes, oligodendrocyte, microglia and endothelial cells, although 8-OHdG-labelled astrocytes were uncommon (Figure 2).

Variability in the intensity of nuclear staining inevitably resulted in some subjectivity in the assessment of positive cells. All cases were therefore quantified by two observers (SM and JS; Supporting Information Figure S2). There was a systematic difference between the level quantified by the two observers; however, they were consistent in scale (ICC = 0.75, 95% confidence interval 0.53–0.87, $P < 0.001$). Both measures were therefore used and adjusted for in the analysis, although the results are similar with the mean value. There was a significant difference in the percentage of 8-OHdG-positive nuclei amogn the three groups (Table 2, Figure 3A, $P < 0.001$), with differences seen between CNL and CL and between CL and WML (both $P < 0.05$), but not seen between CL and WML ($P > 0.20$).

Western blotting for malondialdehyde (MDA) revealed a band at the expected size of 64 kDa (Figure 3D). There was no statistic difference seen in the MDA levels among any of the groups ($P = 0.65$ (Table 2, Figure 3B).

DNA damage response

The DNA damage response marker γH2Ax and the catalytic subunit of DNA-PKcs showed widespread nuclear expression in white

Table 2. Quantification of markers.

Marker		CNL	CL	WML
8-OHdG % positive nuclei	Mean (SD)	24.7 (14.8)	41.8 (17.6)	38.5 (12.4)
	Median (IQR)	19.4 (12.1)	41.1 (24.3)	37.8 (22.1)
MDA	Mean (SD)	0.8 (0.28)	0.91 (0.44)	0.74 (0.15)
	Median (IQR)	0.75 (0.53)	0.97 (0.72)	0.70 (0.25)
γH2Ax % positive nuclei	Mean (SD)	3.6 (6.8)	20.6 (22.6)	14.1 (17.5)
	Median (IQR)	0 (3.9)	14.7 (31.5)	3.2 (26.0)
p53 % positive nuclei	Mean (SD)	15.4 (6.7)	20.9 (7.2)	12.2 (7.7)
	Median (IQR)	17.2 (14.7)	19.6 (13.9)	10.1 (12.7)

8-OHdG = 8-hydroxy-2′-deoxoguanosine; CNL = controls non-lesional; IQR = interquartile range; MDA = malondialdehyde; SD = standard deviation; WML = white matter lesions.

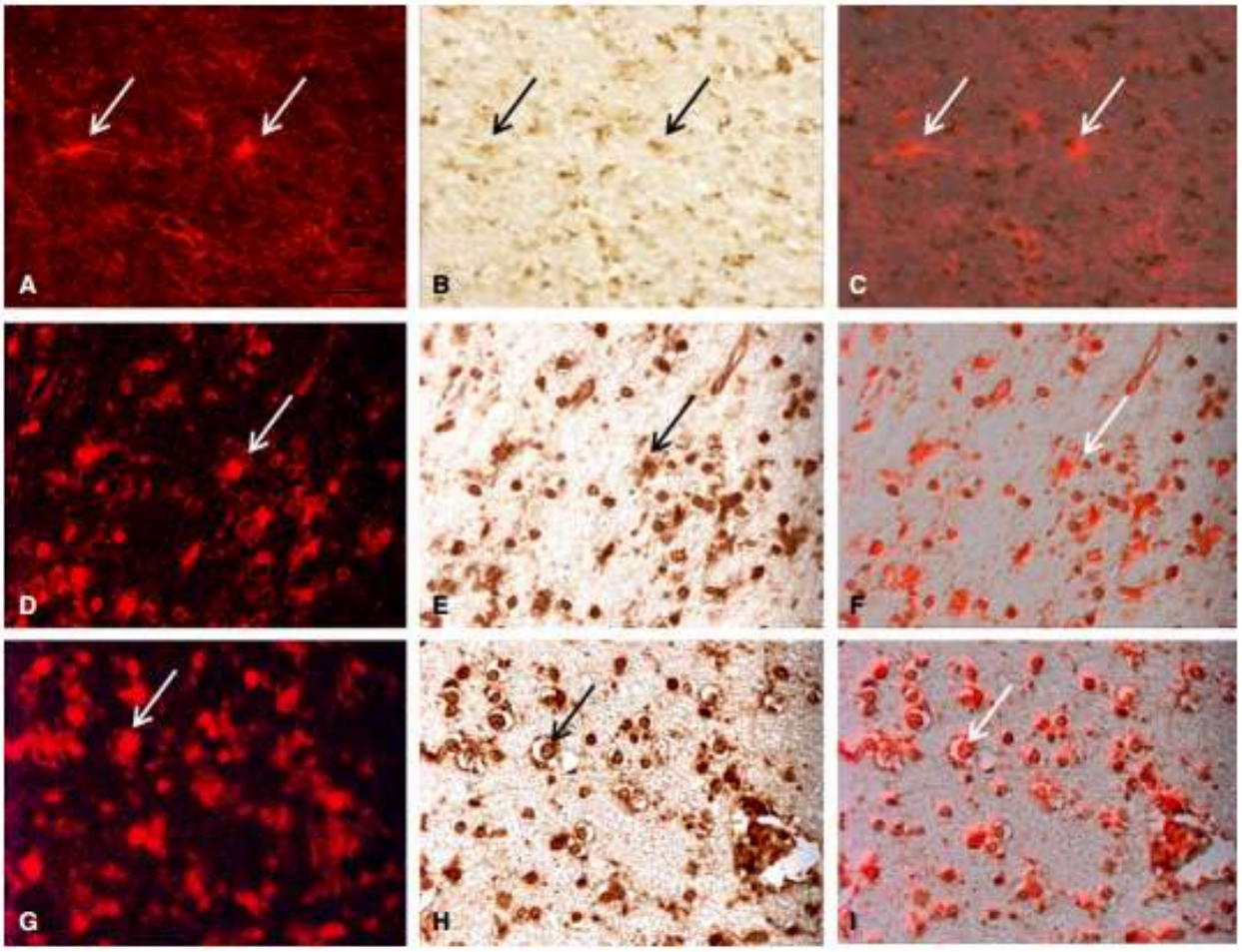

Figure 2. Double-labeling studies for cell specific markers (red fluorescent label). **A.** GFAP; **D.** oligodendrocyte-specific protein; **G.** CD68. 8-hydroxy-2′-deoxyguanosine detected with 3,3′-diaminobenzidine (DAB) label visualized under light microscopy (**B, E, H**). Merged images shown in **C, F** and **I.** Arrows identify example double-labeled cells. Scale bar 50 μm.

matter, with bands on Western blotting of 17 kDa and 480 kDa, respectively (Figure 4). The percentage of γH2Ax-positive nuclei was assessed and quantified (Table 2). The γH2Ax and 8-OHdG counts showed a moderate correlation (Spearman = 0.36). The γH2Ax counts showed a similar effect with lesion type to the 8-OHdG, although the effects were slightly attenuated ($P = 0.03$) with CL being higher than CNL ($P = 0.03$), although the other *post hoc* adjusted comparisons were not significant (all $P > 0.05$). (Figure 3C). To determine whether nuclear oxidative DNA damage may have a detrimental effect on white matter cells, we examined the expression of markers for senescence. SA-β-gal activity was demonstrated histochemically in white matter, suggesting induction of senescence mechanisms (Figure 5A), but was not group-specific. Double-labeling studies demonstrated that SA-β-gal activity was present in astrocytes (GFAP+) and oligodendrocytes (OSP+), but was not observed in CD68-positive microglia (Figure 5B–D).

To further assess the possibility of senescence induction, we examined expression of the cell cycle checkpoint protein p16. This was expressed in astroglial cells, where it co-localized with SA-β-gal activity (Figure 5E). Quantification of SA-β-gal and p16 did not reveal differences between groups. Given the presence of p16 in the cytoplasm of astrocytes, we sought to determine whether p16 expression was associated with gliosis (irrespective of group). A weak relationship between p16 + cell count with GFAP area immunoreactivity was found (rho = 0.29, $P = 0.11$ Figure 6), but not in the p16 area immunoreactivity (rho = 0.17, $P = 0.40$).

We compared the expressions of several mRNA species using a customized qRT-PCR panel (Supporting Information Figure S1) to seek further evidence for a pattern increased expression of genes related to DNA damage/senescence in CL and WML and to identify additional candidate senescence or DNA damage proteins (Figure 7A). For ease of comparison we compared changes in each gene in WML and CL, respectively, to CNL. In particular, expressions of *H2AX*, *TP53*, and *CDKN1B* (encodes p27) were increased by >1.5-fold in WML compared with CNL, while expression of the *TP53* gene was also increased by >twofold in CL cases. Based on this RNA expression pattern, and the pivotal role of p53 in apoptosis and senescence, we selected p53 for further quantification. We therefore immunostained for p53 protein (Figure 7B) and

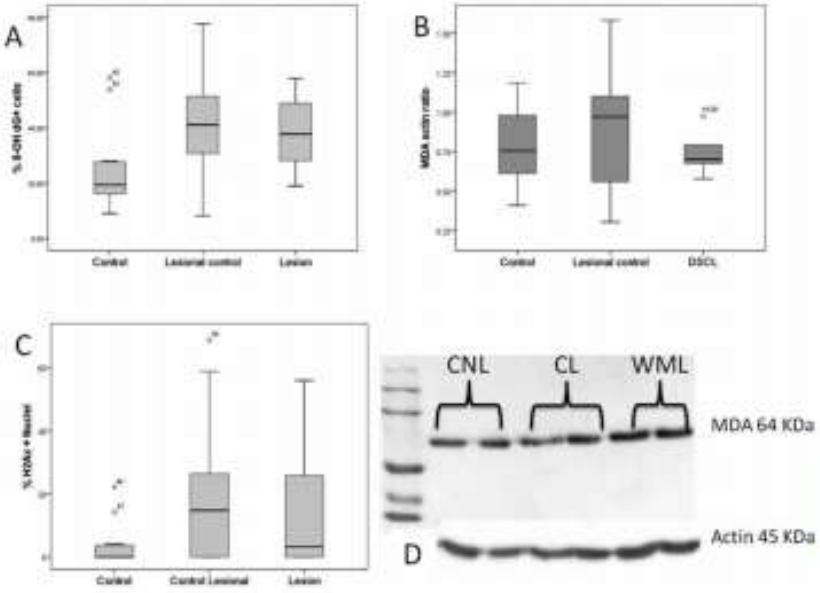

Figure 3. Box plots showing variation in 8-hydroxy-2'-deoxoguanosine counts **(A)**, malondialdehyde (MDA) protein by western blot **(B)** and γH2Ax counts among the three groups. **D.** Example Western blot for MDA showing expected size band at 64 kDa.

quantified expression. Expression of p53 showed significant variation among groups ($P = 0.01$. Figure 7C). As for the RNA, the highest levels of p53 expression were in the CL group, and the expression pattern was similar to those of the other oxidative damage markers (see Figure 3). However, for p53 protein expression, levels were lowest in the lesions that showed lower counts than the CL group and the control group ($P = 0.001$, CL and $P = 0.08$ CNL).

DISCUSSION

The expression of markers of oxidative damage and of DNA damage response in WML and in CL suggests that oxidative stress plays a role in the pathogenesis of WML. The highest levels of expression were observed in apparently normal white matter from cases with lesions (CL), indicating that oxidative damage in white matter in cases with WML is extensive. Oxidative cell damage has previously been shown in white matter in multiple sclerosis, using immunohistochemistry to 8-OHdG and lipid peroxidation markers, and associated with evidence of cellular injury (15). In that situation, injury correlated with inflammation. Our study now shows that similar cellular mechanisms may cause glial damage in the context of age-related "ischemic" white matter pathology. Although not primarily inflammatory, as in multiple sclerosis, inflammation is a feature of WML and surrounding apparently normal white matter, where microglial activation is increased (37)

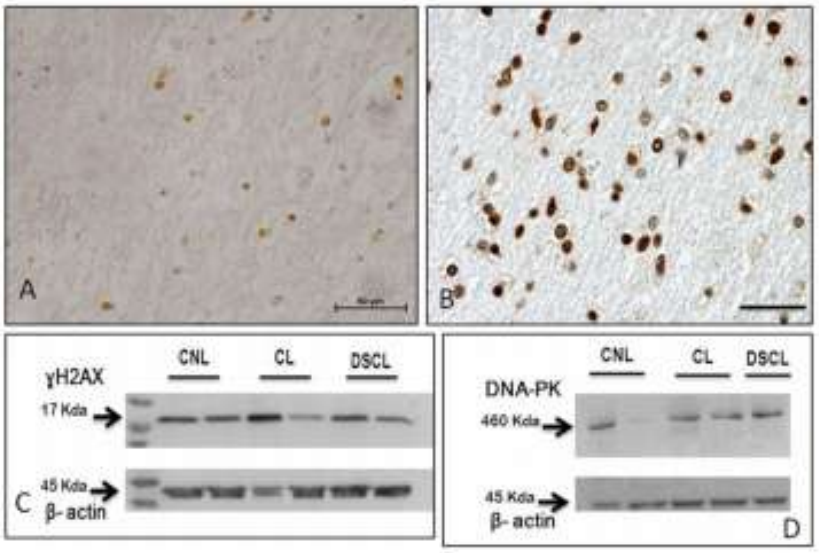

Figure 4. Immunohistochemistry showing nuclear expression of γH2Ax **(A)** and DNA protein kinase **(B)**. Scale bars 50 μm. **C** and **D.** Western blots detecting bands of the expected sizes.

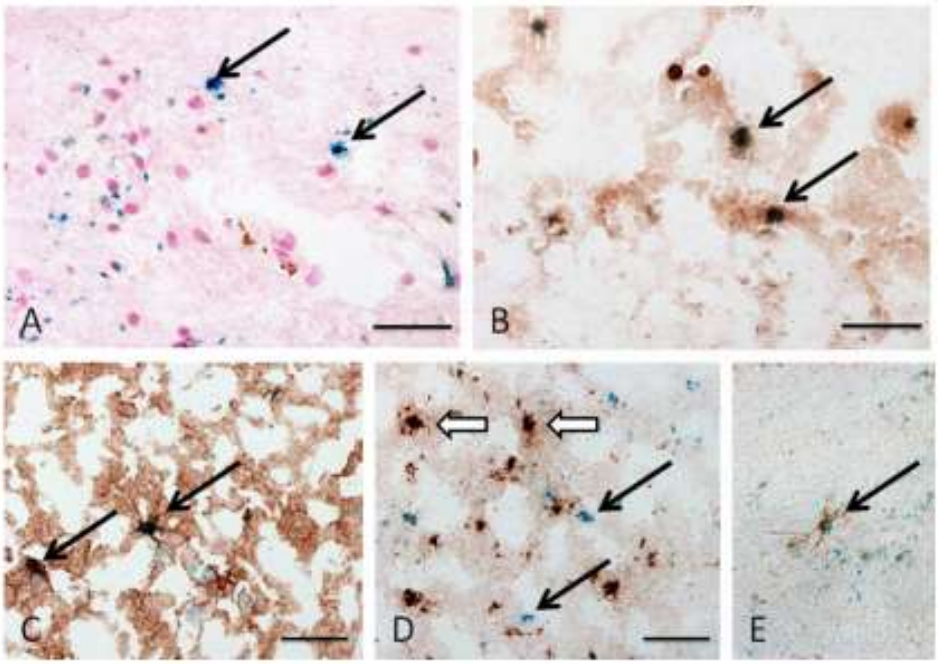

Figure 5. Expression of senescence markers. **A.** β-gal expression in cells (arrows). **B.** β-gal (blue) colocalized with oligodendrocyte-specific protein (brown) indicating expression in oligodendrocytes (arrows). **C.** Colocalization of β-gal with the astrocyte marker GFAP (arrows). **D.** β-gal and CD68 double-staining. β-gal reactivity (arrows) does not colocalize with CD68 (open arrows). **E.** Colocalization of β-gal with p16 (arrow).

and blood–brain barrier changes may have proinflammatory effects (32). So, inflammatory processes, in addition to effects of chronic ischemia and aging effects are possible contributors to oxidative DNA damage in ischemic white matter pathology.

The principal marker selected for this study was 8-OHdG, an oxidative modification to a base that has been widely used as a marker of oxidative DNA damage, including in studies of aging and Alzheimer's disease, because of its relative sensitivity resulting from its low oxidation potential (27, 40). Antibodies to this marker also label oxidative damage to RNA and mitochondrial DNA, but in this study, as we were interested in the nuclear DNA damage response, we have focused on nuclear expression. A limitation of our quantification is that we counted immunopositive cells, but once a detection threshold is reached, this does not take account of the extent of DNA base modification within a particular cell, and so may underestimate the real variability. The pattern of highest levels of damage in lesional control tissue was also supported by assessment of MDA, a marker of lipid peroxidation, and γH2Ax, a histone that is phosphorylated in response to DNA double strand breaks, markers that we have previously used in studies in CFAS (36). Expression of MDA and γH2Ax did not reach significance, presumably related to the extent of intrinsic inter-case variation in human autopsy material and limited sample size. However, they showed the same pattern of variation among groups as the 8-OHdG, while the good correlation between 8-OHdG and γH2Ax is consistent with the induction of a DNA damage response in cells with the oxidative nucleic acid modification.

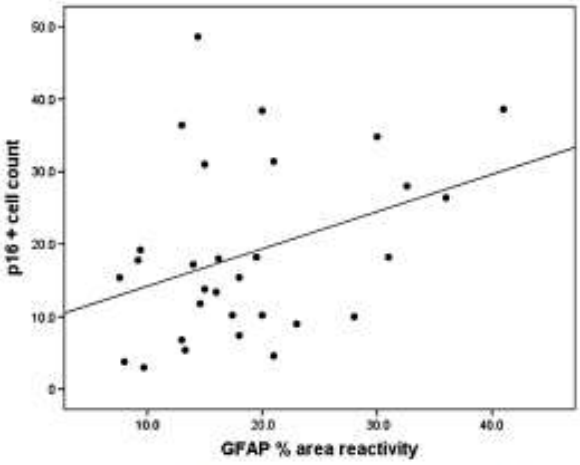

Figure 6. Scatterplot showing the association between p16 cell count and area immunoreactivity for GFAP.

Higher levels of oxidative/DNA damage were seen in lesional controls than in the WML themselves. This may suggest that pathogenic mechanisms are more active in surrounding apparently normal white matter than in the established lesions. We have previously shown microglial activation in lesional control white matter (37), while gene microarray studies show similar pathway alterations in lesional control white matter and WML (35). We therefore suggested a "field-effect," whereby WML are association

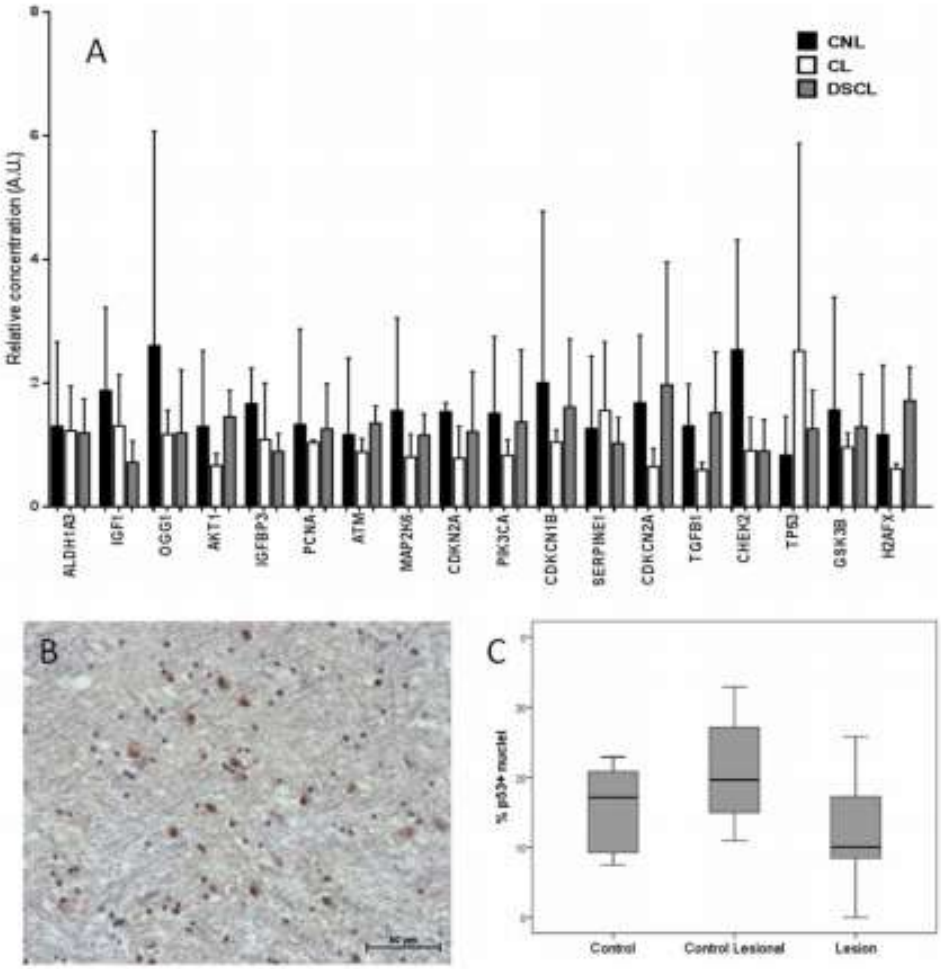

Figure 7. A. Variation in gene expression between control non-lesional, control lesional (CL) and deep subcortical (here labeled DSCL) from RTqPCR array, Error bars represent standard deviations **B.** Expression of p53 (scale bar 50 μm). **C.** Boxplot showing variation in percentage of nuclei positive for p53 among the three groups, with higher values in the CL group.

with more widespread white matter dysfunction. The present results suggest that oxidative stress and DNA damage may contribute to this environment, causing glial cell dysfunction in this non-lesional white matter. The relationship of this to lesion pathogenesis, particularly whether these changes provide an environment in which MRI-recognizable lesions develop or whether it is secondary to the lesions, and its contribution to cognitive dysfunction remain to be determined.

Double-labeling studies demonstrated DNA damage in glia and endothelial cells. Expression in individual cell types is an important question, but our double-labeling was not sufficiently clear to allow reliable quantitation in these preparation. We therefore did not attempt to quantify the cell types separately. 8-OHdG expression was uncommon in GFAP-positive astrocytes, paralleling findings in multiple sclerosis where most 8-OHdG cells were oligodendrocytes (15).

DNA damage can cause cell dysfunction or loss via apoptosis, and a persistent DNA damage response can induce senescence (44). The expression array study further supported increased expression of genes associated with DNA damage, particularly p53, which can mediate apoptosis, cell cycle processes and senescence following DNA damage (16).

SA-β-gal activity has been considered to be a marker of senescence in tissues. Senescence as a process was defined initially as a cell culture phenotype involving cessation of replication (replicative senescence), but it is becoming recognized in human tissue and senescent cells have recently been identified in neurons in brain (19, 42) and in cortical astrocytes (36). The expression of SA-β-gal now identified in white matter astrocytes and oligodendrocytes thus suggests induction of senescence mechanisms in glial cells. This was supported in astrocytes by the expression of the cell cycle checkpoint protein p16, which is involved in

some senescence induction pathways (42), and which appeared to co-localize with SA-β-gal in these cells. Astrocytes have been suggested to show features of senescence and a senescence-associated secretory phenotype in association with GFAP up-regulation in brain aging (33). The co-expression of p16 and SA-β-gal in our study, and the suggestion of an association between p16 and gliosis, raises the question of whether p16 is involved in induction of gliosis and senescence in these cells. It should be noted, although, that cells that double-stained for 8-OHdG and GFAP were uncommon, so it is possible that induction of senescence in astrocytes in white matter may involve mechanisms other than 8-OHdG-associated DNA damage.

Quantification of SA-β-gal expression was difficult in these tissues, as has been previously noted in tissue sections (24), and we did not demonstrate clear differences among our groups. Therefore, at this stage, we cannot be certain of its relation to lesions, as compared with other potential drivers, such as age. However, senescent cells are not only dysfunctional, but may also contribute to tissue damage through the senescence-associated secretory phenotype, which can have various effects within the tissue including pro-inflammatory effects (6, 22). It therefore has potentially important implications for age-related WMLs through a variety of possible mechanisms, including loss of glial support for myelin and axons, and for the induction of pro-inflammatory environment and microglia.

Human autopsy-based studies necessarily have a number of limitations, related to inherent inter-individual variability and peri/post-mortem factors. In addition the cohort size was relatively small. This may have masked differences between the groups for some of the markers. While a strength of the CFAS cohort is its population base, it should also be noted that the cases here were pre-selected to represent WML, CL and CNL, so this study is not population representative, but is in essence a case control study nested within the CFAS population neuropathology cohort. We also do not yet have detailed data on axonal pathology in white matter, so that we are not able in this study to take account of interactions with axonal damage that might be arising secondary to cortical pathology, such as Alzheimer's, which can produce white matter damage (4).

In conclusion, oxidative DNA damage and a DNA damage response are features of the pathogenesis of WML and more so of the apparently normal white matter in cases with lesions, contributing to the concept that WML are associated with a field-effect of white matter abnormality. Activation of downstream processes, such as senescence, are candidate mechanisms for altered glial function in white matter. Age-related WML pathogenesis therefore involves active cellular processes, especially in surrounding white matter, which need to be understood as they may be molecular targets for improving white matter function and repair, and for preventing new lesions.

ACKNOWLEDGEMENTS

This study and SAl-M were supported by a scholarship from the King Fahad Medical City, Saudi Arabia. JES is funded by the Medical Research Council (MR/J004308/1). CFAS is supported by the Department of Health and the Medical Research Council (grants MRC/G9901400 and MRC U.1052.00.0013); the UK NIHR Biomedical Research Centre for Ageing and Age-Related Disease Award to the Newcastle upon Tyne Hospitals Foundation Trust; the Cambridge Brain Bank is supported by the NIHR Cambridge Biomedical Research Centre; The Cambridgeshire and Peterborough NIHR CLAHRC; Nottingham University Hospitals NHS Trust; University of Sheffield and the Sheffield Teaching Hospitals NHS Foundation Trust; The Thomas Willis Oxford Brain Collection, supported by the Oxford Biomedical Research Centre; The Walton Centre NHS Foundation Trust, Liverpool. We would like to acknowledge the essential contribution of the liaison officers, the general practitioners, their staff, and nursing and residential home staff. We are grateful to our respondents and their families for their generous gift to medical research, which has made this study possible. SBW also receives support from ARUK and BBSRC.

REFERENCES

1. Akiguchi I, Tomimoto H, Suenaga T, Wakita H, Budka H (1997) Alterations in glia and axons in the brains of Binswangers disease patients. *Stroke* **28**:1423–1429.
2. Barber R, Scheltens P, Gholkar A, Ballard C, McKeith I, Ince P *et al* (1999) White matter lesions on magnetic resonance imaging in dementia with Lewy bodies, Alzheimer's disease, vascular dementia, and normal aging. *J Neurol Neurosurg Psychiatry* **67**:66–72.
3. Breteler M, Van Swieten J, Bots M, Grobbee D, Claus J, Van Den Hout J *et al* (1994) Cerebral white matter lesions, vascular risk factors, and cognitive function in a population-based study: the Rotterdam Study. *Neurology* **44**:1246–1252.
4. Chalmers K, Wilcock G, Love S (2005) Contributors to white matter damage in the frontal lobe in Alzheimer's disease. *Neuropathol Appl Neurobiol* **31**:623–631.
5. Clerici F, Caracciolo B, Cova I, Fusari I, Maggiore L, Galimberti D *et al* (2012) Does vascular burden contribute to the progression of mild cognitive impairment to dementia? *Dement Geriatr Cogn Disord* **34**:235–243.
6. Coppe J-P, Desprez P-Y, Krtolica A, Campisi J (2012) The senescence-associated secretory phenotype: the dark side of tumor suppression. *Ann Rev Pathol* **5**:99–118.
7. De Leeuw F-E, De Groot J, Achten E, Oudkerk M, Ramos L, Heijboer R *et al* (2001) Prevalence of cerebral white matter lesions in elderly people: a population based magnetic resonance imaging study. The Rotterdam Scan Study. *J Neurol Neurosurg Psychiatry* **70**:9–14.
8. Debette S, Markus H (2010) The clinical importance of white matter hyperintensities on brain magnetic resonance imaging: systematic review and meta-analysis. *Br Med J* **341**:c3666.
9. Devine M, Fonseca J, Walker Z (2013) Do cerebral white matter lesions influence the rate of progression from mild cognitive impairment to dementia? *Int Psychogeriatr* **25**:120–127.
10. Englund E, Brun A (1990) White matter changes in dementia of Alzheimer's type: the difference in vulnerability between cell compartments. *Histopathology* **16**:433–439.
11. Englund E, Brun A, Alling C (1988) White matter changes in dementia of Alzheimer's type. *Brain* **111**:1425–1439.
12. Fernando M, Ince P (2004) Vascular pathologies and cognition in a population-based cohort of elderly people. *J Neurol Sci* **226**:13–17.
13. Fernando M, O'Brien J, Perry R, English P, Forster G, McMeekin W *et al* (2004) Comparison of the pathology of cerebral white matter with post-mortem magnetic resonance imaging (MRI) in the elderly brain. *Neuropathol Appl Neurobiol* **30**:385–395.
14. Fernando M, Simpson J, Matthews F, Brayne C, Lewis C, Barber R *et al* (2006) White matter lesions in an unselected cohort of the elderly: molecular pathology suggests origin from chronic hypoperfusion injury. *Stroke* **37**:1391–1398.

15. Haider L, Fischer M, Frischer J, Bauer J, Hoftberger R, Botond G *et al* (2011) Oxidative damage in multiple sclerosis lesions. *Brain* **134**:1914–1924.
16. Hasty P, Christy B (2013) p53 as an intervention target for cancer and aging. *Pathobiol Aging Age Relat Dis* **3**:22702.
17. Ikram M, Luijendijk H, Vernooij M, Hofman A, Niessen W, van der Lugt A *et al* (2010) Vascular brain disease and depression in the elderly. *Epidemiology* **21**:78–81.
18. Inaba M, White L, Bell C, Chen R, Petrovich H, Launer L *et al* (2011) White matter lesions on brain magnetic resonance imaging scan and 5-year cognitive decline: the Honolulu–Asia Aging Study. *J Am Geriatr Soc* **59**:1484–1489.
19. Jurk D, Wang C, Miwa S, Maddick M, Korolchuk V, Tsolou A *et al* (2012) Postmitotic neurons develop a p21-dependent senescence-like phenotype driven by a DNA damage response. *Ageing Cell* **11**:996–1004.
20. Kee H, Lee J, Na D, Kim S, Cheong H, Moon S *et al* (2011) Different associations of periventricular and deep white matter lesions with cognition, neuropsychiatricy symptoms, and daily activities in dementia. *J Geriatr Psychiatry Neurol* **24**:84–90.
21. Kobayashi K, Hayashi M, Nakano H, Fukutani Y, Sasaki K, Shimazaki M *et al* (2002) Apoptosis of astrocytes with enhanced lysosomal activity and oligodendrocytes in white matter lesions in Alzheimer's disease. *Neuropathol Appl Neurobiol* **28**:238–251.
22. Kuilman T, Peeper D (2009) Senescence-messaging secretome: SMS-ing cellular stress. *Nat Rev Cancer* **9**:81–94.
23. Launer L, Berger K, Breteler M, Dufouil C, Fuhrer R, Giampaoli S *et al* (2006) Regional variability in the prevalence of cerebral white matter lesions: an MRI study in 9 European countries (CASCADE). *Neuroepidemiology* **26**:23–29.
24. Lawless C, Wang C, Jurk D, Merz A, Von Zglinicki T, Passos J (2010) Quantitative assessment of markers for cell senescence. *Exp Gerontol* **45**:772–778.
25. Lee S, Kim J, Chung S, Kim B, Ahn K, Lee K (2011) White matter hyperintensities (WMH) are associated with intracranial atherosclerosis rather than extracranial atherosclerosis. *Arch Gerontol Geriatr* **53**:e129–e132.
26. Matthews F, Brayne C, Lowe J, McKeith I, Wharton S, Ince P (2009) Epidemiological pathology of dementia: attributable-risks at death in the MRC Cognitive Function and Ageing Study. *PLoS Med* **6**:e1000180.
27. Moller P, Lohr M, Folkmann J, Mikkelsen L, Loft S (2010) Aging and oxidatively damaged nuclear DNA in animal organs. *Free Radic Biol Med* **48**:1275–1285.
28. MRC–CFAS (2001) Pathological correlates of late-onset dementia in a multicentre, community-based population in England and Wales. *Lancet* **357**:169–175.
29. Ovbiagele B, Saver J (2006) Cerebral white matter hyperintensities on MRI: current concepts and therapeutic implications. *Cerebrovasc Dis* **22**:83–90.
30. Prins N, van Dijk E, den Heijer T, Vermeer S, Jolles J, Koudstaal P *et al* (2005) Cerebral small-vessel disease and decline in information processing speed, executive function and memory. *Brain* **128**:2034–2041.
31. Raiha I, Tarvonen S, Kurki T, Rajala T, Sourander L (1993) Relationship between vascular factors and white matter low attenuation of the brain. *Acta Neurol Scand* **87**:286–289.
32. Rosenberg G (2009) Inflammation and white matter damage in vascular cognitive impairment. *Stroke* **40**(Suppl. 1):S20–S23.
33. Salminen A, Ojala J, Kaarniranta K, Haapasalo A, Hiltunen M, Soininen H (2011) Astrocytes in the aging brain express characteristics of senescence-associated secretory phenotype. *Eur J Neurosci* **34**:3–11.
34. Scheltens P, Barkhof F, Leys D, Wolters E, Ravid R, Kamphorst W (1995) Histopathologic correlates of white matter changes on MRI in Alzheimer's disease and normal aging. *Neurology* **45**:883–888.
35. Simpson J, El-Sayad O, Wharton S, Heath P, Holden H, Fernando M *et al* (2009) Microarray RNA expression analysis of cerebral white matter lesions reveals changes in multiple functional pathways. *Stroke* **40**:369–375.
36. Simpson J, Ince P, Haynes L, Theaker R, Gelsthorpe C, Baxter L *et al* On behalf of the MRC Cognitive Function and Ageing Neuropathology Study Group (2010) Population variation in oxidative stress and astrocyte DNA damage in relation to Alzheimer-type pathology in the ageing brain. *Neuropathol Appl Neurobiol* **36**:25–40.
37. Simpson J, Ince P, Higham C, Gelsthorpe C, Fernando M, Matthews F *et al* On behalf of the MRC Cognitive Function and Ageing Neuropathology Study Group (2007) Microglial activation in white matter lesions and nonlesional white matter of ageing brains. *Neuropathol Appl Neurobiol* **33**:670–683.
38. Simpson J, Wharton S, Cooper J, Gelsthorpe C, Baxter L, Forster G *et al* (2010) Alterations of the blood–brain barrier in cerebral white matter lesions in the ageing brain. *Neurosci Lett* **486**:246–251.
39. Simpson JE, Fernando M, Clark L, Ince P, Matthews F, Forster G *et al* (2007) White matter lesions in an unselected cohort of the elderly: astrocytic, microglial and oligodendrocyte precursor cell responses. *Neuropathol Appl Neurobiol* **33**:410–419.
40. Sonnen J, Breitner J, Lovell M, Markesbery W, Quinn J, Montine T (2008) Free radical-mediated damage to brain in Alzheimer's disease and its transgenic mouse models. *Free Radic Biol Med* **45**:219–230.
41. Srikanth V, Beare R, Blizzard L, Phan T, Stapleton J, Chen J *et al* (2009) Cerebral white matter lesions, gait, and the risk of incident falls. A prospective population-based study. *Stroke* **40**:175–180.
42. van Deursen J (2014) The role of senescent cells in ageing. *Nature* **509**:439–446.
43. Viana-Baptista M, Bugalho P, Jordao C, Ribeiro O, Esperanca-Pina J, Ferro J (2011) Motor dysfunction correlates with frontal white matter ischemic changes in patients with leukoaraiosis. *J Aging Res* **2011**:950341.
44. Von Zglinicki T, Saretzki G, Ladhoff J, d'Adda di Fagagna F, Jackson S (2005) Human cell senescence as a DNA damage response. *Mech Ageing Dev* **126**:111–117.
45. Wharton S, Brayne C, Savva G, Matthews F, Forster G, Simpson J *et al* (2011) Epidemiological neuropathology: the MRC Cognitive Function and Ageing Study experience. *J Alzheimers Dis* **25**:359–372.

SUPPORTING INFORMATION

Additional Supporting Information may be found in the online version of this article at the publisher's web-site:

Figure S1. Genes included in the customized RT-qPCR array.
Figure S2. Counting of 8-OHdG-positive cells. **A.** Grid overlay to facilitate counting. **B.** Bland–Altmann plot showing variation in counts between two observers; the red line represents the mean difference in counts between observers while blue lines are the limits of agreement (mean difference ± 2 SD of mean difference). **C.** Correlation between two observers showing very good agreement for ranking of cases according to 8-OHdG counts.

Neuropathology and Applied Neurobiology (2014), **40**, 802–814 doi: 10.1111/nan.12156

DNA damage response and senescence in endothelial cells of human cerebral cortex and relation to Alzheimer's neuropathology progression: a population-based study in the Medical Research Council Cognitive Function and Ageing Study (MRC-CFAS) cohort

C. J. Garwood*, J. E. Simpson*, S. Al Mashhadi*†, C. Axe*, S. Wilson*, P. R. Heath*, P. J. Shaw*, F. E. Matthews‡, C. Brayne§, P. G. Ince* and S. B. Wharton*, on behalf of the MRC Cognitive Function and Ageing Study

**Sheffield Institute for Translational Neuroscience, University of Sheffield, Sheffield, ‡MRC Biostatistics Unit and §Institute of Public Health, University of Cambridge, Cambridge, UK, and †King Fahad Medical City, Riyadh, Saudi Arabia*

C. J. Garwood, J. E. Simpson, S. Al Mashhadi, C. Axe, S. Wilson, P. R. Heath, P. J. Shaw, F. E. Matthews, C. Brayne, P. G. Ince and S. B. Wharton, on behalf of the MRC Cognitive Function and Ageing Study (2014) *Neuropathology and Applied Neurobiology* 40, 802–814

DNA damage response and senescence in endothelial cells of human cerebral cortex and relation to Alzheimer's neuropathology progression: a population-based study in the Medical Research Council Cognitive Function and Ageing Study (MRC-CFAS) cohort

Aims: Abnormalities of the brain microvasculature in Alzheimer's disease have led to the vascular hypothesis of the disease, which predicts that vascular changes precede neuronal dysfunction and degeneration. To determine the spectrum of endothelial injury in the elderly and its relation to Alzheimer-type neuropathology we investigated DNA damage in a population-based sample derived from the Medical Research Council Cognitive Function and Ageing Study. **Methods:** We examined endothelial damage in frontal and temporal cortex ($n = 97$) using immunohistochemistry for γH2AX and DNA–protein kinase (DNA-PKcs). To determine the effects of endothelial DNA damage at the earliest stages of Alzheimer's pathology we further focused our analysis on cases classified as Braak 0–II and examined endothelial senescence using histochemistry for β-galactosidase and the expression of genes related to DNA damage and senescence using quantitative polymerase chain reaction (qPCR). **Results:** We demonstrated large variation in endothelial DNA damage which was not associated with Alzheimer's neuropathology. Endothelial DNA-PKcs correlated with neuronal and glial DNA-PKcs counts. Focusing our further analysis on Braak 0–II cases, qPCR analysis demonstrated a trend to increased TP53 ($P = 0.064$) in cases with high compared with low endothelial DNA damage which was supported by immunohistochemical analysis of p53. Endothelial β-galactosidase expression was associated with increased neuronal ($P = 0.033$) and glial ($P = 0.038$), but not endothelial DNA-PKcs expression. **Conclusions:** Damage to brain endothelial cells occurs early in relation to, or independently of, Alzheimer pathology, and parallels that in neurones and glia. Endothelial DNA damage and senescence are a brain ageing process that may contribute to dysfunction of the neurovascular unit in some elderly individuals.

Keywords: ageing, Alzheimer's disease, DNA damage, endothelial cells, senescence

Correspondence: Stephen B. Wharton, Sheffield Institute for Translational Neuroscience, 385a Glossop Road, Sheffield S10 2HQ, UK. Tel: +44 (0)114 222 2235; Fax: +44 (0)114 222 2272; E-mail: s.wharton@sheffield.ac.uk

Introduction

The brain endothelium regulates influx and efflux of substances into the brain and is the site of the blood–brain barrier (BBB) [1]. As a component of the neurovascular unit (NVU), normal endothelial function is key to maintaining homeostasis within the central nervous system (CNS) and, in conjunction with astrocytes, couples neuronal metabolic requirements to activity. Case–control studies comparing Alzheimer's disease (AD) with normal aged controls have shown that microvascular pathology is a feature of AD [2]. Abnormalities include a reduction in microvascular density and the presence of string vessels, which are capillaries where the basement membrane is retained but where the endothelial cells have been lost, resulting in a collapsed capillary segment [3]. These changes, which imply endothelial cell injury and loss, may be important in AD pathogenesis by producing ischaemia, leading to a misery perfusion state, where neurones survive but have reduced metabolic function. While these findings imply endothelial dysfunction in established AD, it is unclear how they relate to the progression of the disease, to other changes in the ageing brain, and whether they may contribute to adverse brain ageing independently of AD.

Blood–brain barrier leakage is a feature of brain ageing and occurs early in AD [4]. In the population-based Medical Research Council Cognitive Function and Ageing Study (MRC-CFAS) neuropathology cohort, histopathological evidence of BBB leakage demonstrated a relationship to the burden of AD pathology, increasing with AD progression [5]. Astrocytes play a key role in the NVU and are involved in maintaining the BBB and regulating endothelial function. We have shown that astrocyte pathology develops early in relation to AD progression [6] and recently, using microarray analysis of the transcriptome, we have shown down-regulation of astrocyte signalling with AD progression [7]. This astrocyte pathology provides additional evidence for NVU dysfunction. This is supported by experimental data in Aβ transgenic mice that develop Aβ deposition and amyloid angiopathy. Impaired astrocyte endothelial interactions and compromised microvascular function are early features in this model [8]. The presence of NVU dysfunction in some aged individuals without AD suggests that it may contribute to AD development or may be an independent contributor to cognitive impairment, rather than being a secondary effect of established AD. This raises the possibility that interventions targeted at endothelial function and the NVU may be of value as an additional approach to dementia.

We have used autopsy brains donated to MRC-CFAS for this work. As a population-representative study [9,10], this allows study of the spectrum of endothelial pathology in brain ageing and its relationship to the stage of AD pathology and other pathological markers in an unbiased way, thus providing complementary insights to those derived from studies with a case control design.

We hypothesized that endothelial injury from oxidative and other stressors results in endothelial dysfunction as an early event in AD progression. We determined: (i) the population variation in endothelial injury in cerebral cortex; (ii) the relationship to measures of AD pathology; and (iii) the relationship to markers of neuronal and astrocyte oxidative injury.

Methods

Human CNS tissue

Formalin-fixed paraffin embedded tissue from two neocortical brain areas, the lateral temporal cortex (Brodmann areas 21/22) and the frontal neocortex (Brodmann areas 8/9) ($n = 97$) was obtained from the MRC-CFAS tissue bank, in accordance with Multi-Centre Research Ethics Committee approval (REC ref 12/EM/0118). This study has previously been described in detail [11,12] (http://www.cfas.ac.uk). All cases used in this study were derived from a single CFAS centre (Cambridge) thereby maintaining the unbiased, population basis of the study. The average age of death was 85.6 years [standard deviation (SD) 7.5 years; range 70–103 years], *post mortem* delay (PMD) was 23.9 h (SD 20.7 h; range 2–108 h) and tissue pH 6.47 (SD 0.40; range 4.9–7.3). Because of the population basis of the cohort there are no predefined clinicopathological diagnostic groups and findings have been assessed in relation to neuropathological lesions and not in relation to classical diagnostic categories. However, for information, 8 cases would have satisfied CERAD criteria for AD, 14 cases had probable AD and 20 cases possible AD (the remaining cases were not classified as having AD). Braak and Braak neurofibrillary tangle staging of the cohort using the AT8 antibody to phospho-tau has previously been examined as part of the core study. As part of the MRC-CFAS study individuals are regularly interviewed and undergo geriatric mental state-

Table 1. Antibody source and specificity

Antibody	*Isotype*	*Dilution (time, temperature)*	*Antigen retrieval method*	*Supplier*
γH2AX	Rabbit IgG	1:1000 (1 h, RT)	PC, EDTA pH 8.0	R&D systems
DNA-PKcs	Mouse IgG	1:400 (1 h, RT)	PC, EDTA pH 6.0	Calbiochem
DNA-PKcs	Mouse IgG	1:400 (o/n,4°C)	PC, EDTA pH 6.0	Abcam
p53	Mouse IgG	1:200 (1 h, RT)	MW, TSC pH 6.0	Santa Cruz

o/n, overnight; RT, room temperature; PC, pressure cooker; MW, microwave.

automated geriatric examination for computer-assisted taxonomy (GMS-AGECAT) and mini-mental state examination (MMSE) [12,13] and dementia status at death is determined by assessing all information available for each individual. Within this cohort, 29 individuals had dementia, 62 had no dementia and 10 had an unknown dementia status at death.

Immunohistochemistry

Immunohistochemistry was carried out on formalin-fixed paraffin embedded tissue using a standard ABC method with diaminobenzidine (DAB) (Vector Laboratories, Peterborough, UK) as substrate and isotype-specific antibody controls confirming the specificity of staining. Sections were counterstained with Periodic acid Schiff (PAS) to highlight the basement membrane of cerebral vessels thereby enabling the endothelial cells within them to be easily identified. Primary antibodies and their conditions are outlined in Table 1. Two commercially available monoclonal antibodies for the DNA-PK catalytic subunit (DNA-PKcs) were used over the course of this study, as one of the antibodies was discontinued. An antibody from Abcam was used on the frontal cortex and an antibody from Calbiochem on the temporal cortex, no bias between the values obtained with the two antibodies was demonstrated.

Quantification of immunoreactivity

γH2AX-, DNA-PKcs- and p53-positive endothelial cell nuclei were quantified on a bright-field microscope with images captured using a 20× objective (Olympus Cell-R, Olympus Biosystems, UK). For each case, multiple contiguous fields were assessed from Layer II through to the WM border and the number of positively stained endothelial cells together with the total number of endothelial cells were counted. Sections were scored independently by two observers, blind to any patient information. Following statistical analysis of the DNA-PKcs staining, cases were categorized as having either high or low DNA-PK staining and the five cases with the highest DNA-PKcs expression and the 5 cases with the lowest were taken forward for further analysis, including quantitative polymerase chain reaction (qPCR) for changes in specific DNA damage- and senescence-associated genes and immunohistochemistry. Cases were only selected if they were classified as Braak stage 0–II (transentorhinal tau pathology) as these cases represent early AD cases.

Laser capture microdissection of vessels and analysis by RT-PCR

Cases with the highest or lowest DNA-PKcs staining together with little to no tau pathology (Braak I–II) were further analysed by qPCR. The mean (SD) age for the low DNA-PKcs group was 80.6 (7.5) years ($n = 5$) and for the high DNA-PKcs group was 83.6 (7.6) years ($n = 5$); mean PMD (range) was 23.5 (12–48) h and 7.5 (4–46) h for the low and high DNA-PKcs groups respectively. None of these cases had a final CERAD diagnosis of definite, probable or possible AD and dementia status is not known in one case.

To isolate vessels laser capture microdissection was performed on Toluidine Blue stained frozen sections. Briefly, sections were fixed in ice-cold acetone for 3 min, stained with Toluidine blue for 30 s, rinsed in water and dehydrated in a graded series of alcohol before clearing in xylene. Sections were then left to air dry in an air flow hood for a minimum of 60 min prior to laser capture microdissection. Vessels were isolated using a PixCell II laser-capture microdissection system (Arcturus® AB Applied Biosystems, Mountain View, CA, USA) and total RNA extracted using the Pico Pure RNA isolation kit according to the manufacturer's instructions (AB Applied

Biosystems). Extracted RNA was analysed for quantity (Nanodrop 1000 spectrophotometer) and quality (2100 Bioanalyser, RNA 6000 Pico LabChip, Agilent, Palo Alto, CA, USA) prior to amplification using the Affymetrix 3' IVT express kit (Affymetrix, CA, USA). 0.9–1.5 μg of RNA was then taken forward for analysis using customized RT²*Profiler* PCR array plate (Qiagen, Hilden, Germany) which simultaneously assayed 18 genes which were specifically selected based on their involvement in either senescence and/or DNA damage pathways (*ALDH1A3, IGF1, OGG1, AKT1, IGFBP3, PCNA, ATM, MAP2K6, CDKN1A, PIK3CA, CDKN1B, SERPINE1, CDKN2A, TGFB1, CHEK2, TP53, GSK3B, H2AX*) and gene changes statistically analysed using a Mann–Whiney test (GraphPad Prism).

Senescence staining

Histochemistry for senescence-associated β-galactosidase (SA-β-galactosidase) was performed on all frozen sections of frontal cortex (contralateral hemisphere) which were classified as having early Alzheimer pathology (Braak stage 0–II cases, $n = 24$). For information the average age of death of these cases was 82 years (range 70–102 years), PMD was 20.44 h (SD 16.5 h, range 3–76 h) and average brain pH 6.53 (SD 0.304, range 6.0–7.3) Expression of SA-β-galactosidase activity was assessed using the Senescence Cells Staining Kit (Sigma, Dorset, UK). Sections were examined on a Nikon eclipse 80i microscope. The entire cortex represented in the frozen section was examined with the ×10 objective and putative β-galactosidase positive microvascular profiles examined at ×40 objective for confirmation. Microvascular reactivity in capillaries and other microvessels was scored semiquantitatively in the region of most intense staining as: 0 – no microvascular reactivity; 1 – isolated positive vessels (up to 5/section); 2 – multiple positive vessels; 3 – frequent multiple positive vessels (>1 vessel per × 10 objective field). Only one case demonstrated category 3 reactivity, so this was combined with the category 2 group for analysis.

Statistical analysis was performed using IBM SPSS Statistics version 20. Differences in DNA-PKcs-positive cells between β-galactosidase score groups was determined by Kruskal–Wallis and the trend across groups, to increase with β-galactosidase score, was assessed by Jonkheere-Terpstra. Correlation between p53 and DNA-PKcs endothelial immunoreactivity was measured using Spearman's Rank Correlation Coefficient, significance was accepted at $P < 0.05$.

Results

Expression of endothelial DNA damage response markers

Immunostaining for γH2AX revealed a predominantly nuclei-specific signal that was present in a proportion of all cell types (Figure 1A,B). γH2AX-positive endothelial cells were identified by their typical elongated shape within the PAS-stained basement membrane (Figure 1A). Similarly, DNA-PKcs staining was mostly confined to the nuclei of cells and DNA-PKcs-positive endothelial cells were evident (Figure 1C). There was wide variation in the staining pattern across the cohort for both γH2AX and DNA-PKcs (Table 2). In addition to endothelial DNA-PKcs and γH2AX immunoreactivity, a proportion of the nuclei of neurones and small cells (glia and small neurones) stained positive for both of these markers (Figure 1B,C).

In order to determine whether the DNA-PKcs antibodies yielded similar results, the Calbiochem antibody was also used on 17 frontal cases. There was no bias between the values obtained in the two cases (Abcam mean 58.66, SD 23.1; Calbiochem mean 67.2, SD 25.56; paired *t*-test $t = -1.85$, 16df, $P = 0.083$). The mean difference between the scores was 8.54 with limits of agreement (given by mean difference $\pm 2 \times SD_{diff}$) 29.52–46.6% [comparison of two observers – SW and JS frontal cortex (10 cases) – excellent correlation (Spearman rank, $r_s = 0.906$, $P < 0.001$)]. DNA-PKcs in temporal cortex shows a good correlation with DNA-PKcs in frontal cortex (Spearman rank $r_s = 0.44$, $P < 0.001$), but DNA-PKcs does not correlate with γH2AX. Values for DNA-PKcs were higher in frontal cortex, but as a different antibody was used, it was not possible to determine the significance of this.

We next examined the relationship between DNA-PKcs and γH2AX immunocounts in endothelial cells in temporal cortex with their respective counts in neurones and cells with small nuclei (including glial cells), as previously defined [14]. DNA-PKcs in endothelial cells correlated with that in neurones (Figure 2A; $r_s = 0.69$, $P < 0.001$) and glia (Figure 2B; $r_s = 0.68$, $P < 0.001$) and also with γH2Ax in neurones ($r_s = 0.35$, $P = 0.001$) and glia ($r_s = 0.0.33$, $P = 0.001$). However, there was no correlation between γH2AX in endothelial cells and either DNA-PKcs or γH2AX in neurones or glia. Due to the inconsistently in γH2AX staining in endothelium and the variability observed the analysis for this marker was not

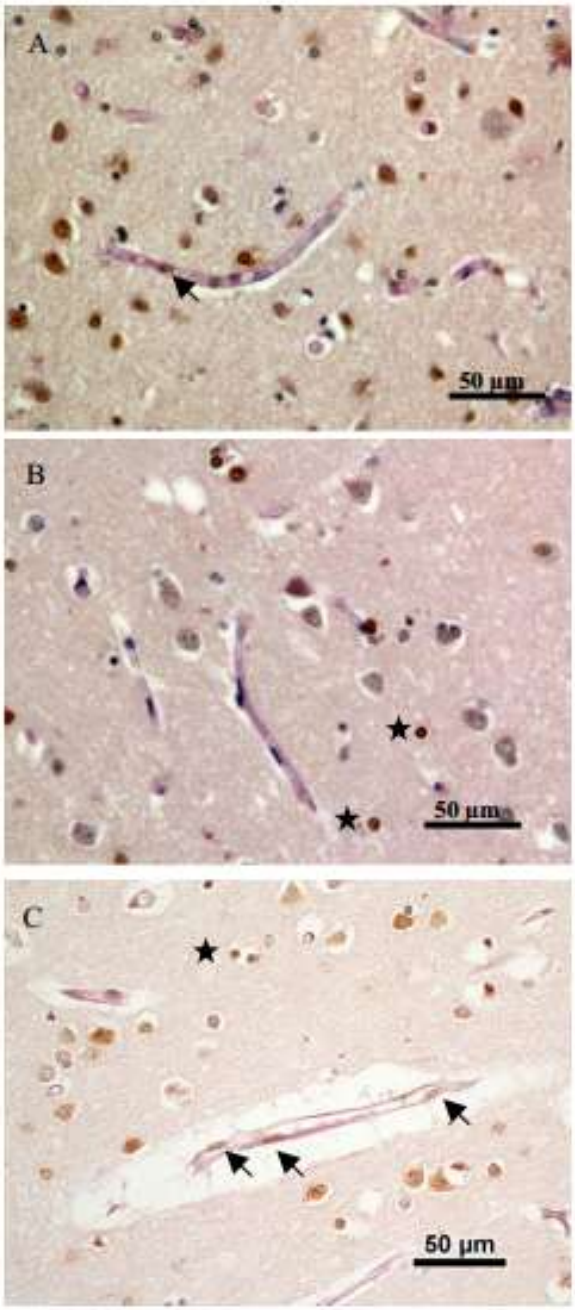

Figure 1. Immunoreactivity for DNA-damage markers. (A) γH2AX immunoreactivity in the temporal cortex (arrowhead indicates positive endothelial cell) and (B) γH2AX-negative endothelium in the temporal cortex. (C) DNA-PKcs immunoreactivity in the frontal cortex of the ageing brain, arrowheads indicate DNA-PKcs positive endothelial cells. Endothelial cell nuclei are identified by their typical elongated shape within the PAS-stained basement membrane. The nuclei of pyramidal cells together with small nuclei (glia) were also positive for DNA-PKcs and γH2AX (B, C, positive small nuclei indicated by stars).

extended into the frontal cortex and further analysis was carried out using DNA-PKcs as a marker of DNA damage as this correlated well with previous measures of DNA damage in the brain parenchyma as measured by γH2AX and DNA-PKcs.

Relationship endothelial DNA damage to Alzheimer's neuropathology and dementia

We compared DNA-PKcs and γH2AX to measures of local AD neuropathology in temporal cortex. For comparisons with CERAD type scores of diffuse and neuritic plaques and neurofibrillary tangles, the moderate-severe score groups were combined. DNA-PKcs and γH2AX were then compared between groups with scores of no pathology, mild, moderate to severe for each of the respective neuropathological lesions. Endothelial DNA-PKcs expression was not related to neuritic plaques (Kruskal–Wallis $P = 0.66$), diffuse plaques ($P = 0.50$) or neurofibrillary tangles ($P = 0.11$) and there were no correlations with area immunoreactivity for phospho-tau (AT8) (Spearman's rank, $r_s = -0.11$, $P = 0.30$) or Aβ ($r_s = 0.12$, $P = 0.26$). Similarly, there were no relationships between endothelial cell γH2AX expression and the presence of neuritic amyloid plaques (Kruskal–Wallis, $P = 0.338$) and neurofibrillary tangle burden ($P = 0.242$). The association of DNA-PKcs endothelial expression with local vascular pathology was also examined. Microinfarcts were recorded as being absent or present and there were no differences in DNA-PKcs according to microinfacts (Mann–Whitney; $P = 0.71$) and no correlation with microvascular density ($r_s = 0.056$, $P = 0.592$).

To analyse the relationship of endothelial DNA-PKcs with global measures of pathology the average of the frontal and temporal DNA-PKcs endothelial counts was used, and variation in endothelial DNA-PKcs was determined between Braak and Braak neurofibrillary tangle groups (entorhinal, stages I–II; limbic, stages III–IV; isocortical, stages V–VI). There were no differences in DNA-PKcs between Braak and Braak groups (Figure 3A, Kruskal–Wallis, $P = 0.18$) and analysing frontal and temporal DNA-PKcs separately gave the same result. Similarly γH2Ax in temporal cortex endothelium shows no relationship to neurofibrillary tangle stage (Figure 3B, $P = 0.579$).

We sought to determine the relationship between endothelial DNA damage and dementia status. Counts of

Table 2. Population variation in the expression of the DNA damage-related molecules γH2AX and DNA-PKcs as detected by immunohistochemistry

Marker	*γH2AX*	*DNA-PKcs*	
Cortex region	*Temporal*	*Temporal*	*Frontal*
Mean (SD)	19.01 (10.30)	35.85 (28.44)	66.38 (21.16)
Median (IQR)	17.14 (11.11–24.66)	33.33 (10.0–59.38)	71.25 (54.41–83.93)
FC	2.2	1.8	1.5

SD, standard deviation; IQR, interquartile range; FC, fold change from 25th to 75th percentile.

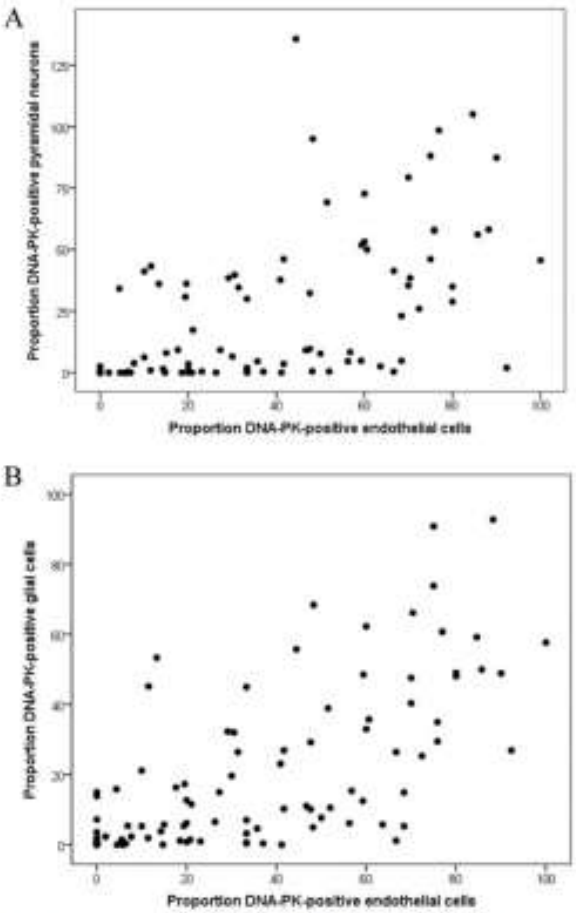

Figure 2. Relationship between endothelial DNA-PKcs and parenchymal DNA-PKcs. Expression of DNA-PKcs in endothelium correlates with DNA-PKcs-positive pyramidal neurones (A) and with DNA-PKcs-positive glia (B).

DNA-PKcs-positive or γH2AX-positive endothelial cells showed no association with dementia status (Figure 3C).

There was no correlation of either γH2AX or DNA-PKcs with *post mortem* delay (γH2AX: $r_s = -0.061$, $P = 0.58$; DNA-PKcs: $r_s = 0.016$, $P = 0.89$. Tissue pH, which is a good measure of tissue integrity, did not correlate with γH2AX but there were correlations between pH and DNA-PKcs in temporal cortex, such that a more acidic pH is associated with lower DNA-PKcs measures ($r_s = 0.45$, $P < 0.001$), and frontal cortex ($r_s = 0.31$, $P = 0.005$).

Effects of endothelial DNA-PKcs at early stages of Alzheimer's neuropathology

As endothelial damage appears to be an early feature of neurodegeneration, we focused further analysis on cases with little Alzheimer's neuropathology (Braak and Braak stages I–II) only. We sought to determine whether an endothelial DNA damage response, reflected by DNA-PKcs positive endothelial cells, was associated with changes in other DNA damage- and senescence-associated genes that might impair endothelial function. Cases were categorized into high DNA-PKcs ($n = 5$) or low DNA-PKcs ($n = 5$). DNA-PKcs was used as the primary readout of the DNA damage response as we have found this to give the more consistent pattern of staining on both frozen and FFPE tissue (compared with γH2AX).

A multiplex qPCR analysis for a panel of genes associated with DNA damage and/or senescence was performed using RT²*Profiler* PCR array plates on RNA extracted from endothelial cells isolated by laser capture microdissection of capillaries. There was a trend towards increased *TP53*, which encodes p53 and is involved in cell cycle regulation, the initiation of apoptosis and DNA repair, as the endothelial DNA damage response increased (Figure 4; Mann–Whitney test, $P = 0.064$). There were no significant differences between high and low DNA-PKcs cases for any of the other genes analysed (Supplementary Figure S1) which might be due to the small number of cases used together with the inherent variability seen when using human tissue.

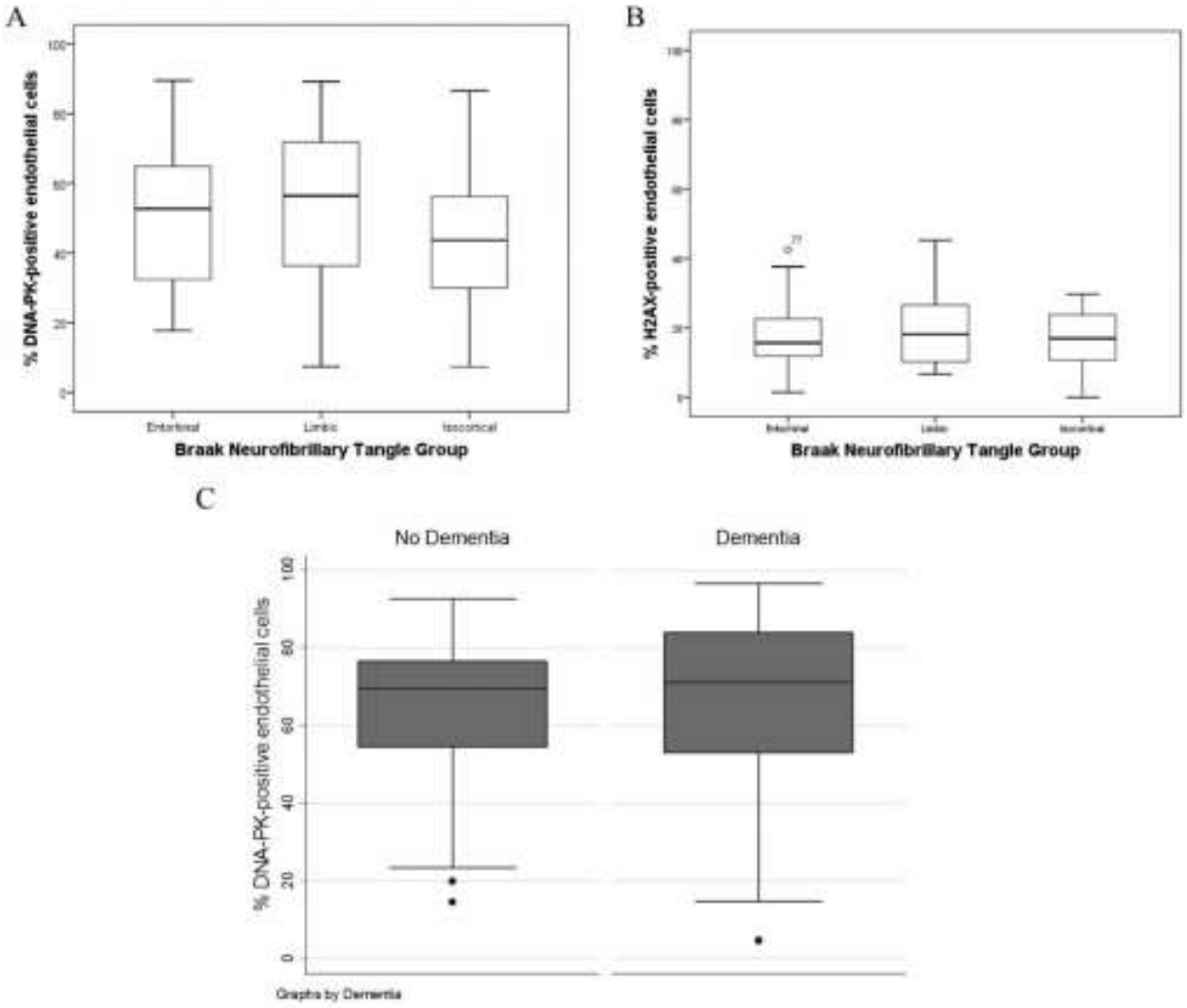

Figure 3. Relationship of endothelial DNA-PKcs to Braak staging and dementia status. Expression of (A) DNA-PKcs or (B) γH2AX in endothelium shows no association with Braak staging or with (C) dementia status.

Relationship to markers of endothelial apoptosis

To further investigate the findings of the qPCR analysis we sought to determine using immunohistochemistry whether an endothelial DNA-damage response was associated with increased p53 immunoreactivity. p53-positive endothelial cells could be clearly identified within vessels (Figure 5A,B) and immunocounts revealed a trend towards increased p53 immunoreactivity as the endothelial DNA damage response increased (Figure 5C; $r_s = 0.443$, $P = 0.0510$), supporting the findings of the qPCR analysis.

Relationship to endothelial senescence

To determine whether an endothelial DNA damage response was associated with induction of endothelial/microvascular senescence, SA-β-galactosidase activity was assessed in microvascular structures of frontal cortex using histochemical staining on all Braak 0–II cases ($n = 24$). Microvascular reactivity for SA-β-galactosidase was seen in 13 (54%) of cases; 6 with an expression score of 1 and 7 with a score of 2–3. Expression was segmentally present along capillary structures and focally in larger microvessels (Figure 6A–C). We did not attempt to

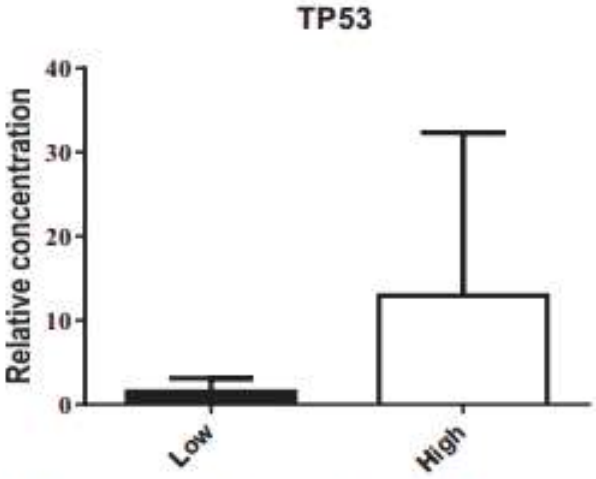

Figure 4. qPCR analysis comparing high and low DNA damage in individuals with a low burden of pathology (Braak I–II). Values represent mean ± SEM; $n = 5$, Mann–Whitney test; $P = 0.0635$.

define either arterioles or venules and while expression by capillary sized vessels implies endothelial expression, the lack of resolution of the technique means we did not determine whether there is also smooth muscle or pericytic expression in the larger microvessels. Although there was a trend to increased DNA-PKcs positive endothelial cells with higher β-galactosidase score (Figure 6D), this was not significant. There was also an association with increasing DNA-PKcs positive pyramidal neurones and for small nuclei in frozen tissue that reached statistical significance (Figure 6E; Jonkheere-Terpstra, $P = 0.033$ and 0.038 respectively).

Discussion

There is growing evidence that vascular dysfunction is important in the development of AD, with brain imaging studies from both humans and mice showing evidence of vascular dysfunction prior to neurodegeneration and cognitive decline in AD [15]. In addition, epidemiological studies have reported that stroke, cardiac disease and atherosclerosis are risk factors for developing AD [16,17]. These findings have given rise to the vascular hypothesis of neurodegeneration which posits that cerebral hypoperfusion precedes the development of pathology and leads to a 'crisis among neurones and glia'. This hypothesis would predict: (i) vascular changes early in relation to neurodegeneration and (ii) population variation, especially prior to neurodegeneration, as endothelial processes in some individuals would predispose them to poorer cognitive outcomes [3,18]. In this study we sought to determine the population variation in endothelial dysfunction and investigate whether this was associated with the development of Alzheimer-type pathology in a well-defined ageing cohort.

Using DNA-PKcs and γH2AX as measures of the DNA damage response we found large variation in DNA damage in the population. We also found that endothelial DNA damage as measured by DNA-PKcs is comparable to that present in brain parenchymal compartment (as measured by both γH2AX and DNA-PKcs) and that it is not associated with burden of Alzheimer-type pathology, suggesting that this is occurring early in relation to Alzheimer-type pathology or is independent of AD pathology. This supports previous findings from our research group which demonstrated similar variation in astrocytic DNA damage in the same cohort with no significant relationship of astrocytic or neuronal DNA damage to neurofibrillary tangles [19]. The implication of endothelial cells in this process would support the vascular hypothesis of dementia that early changes in the neurovasculature contribute to the development of AD. Microinfarcts which are common in patients with vascular or mixed dementia [20] and are a known risk factor for AD showed no association with DNA damage in our cohort.

Here we used both DNA-PKcs and γH2AX as markers of DNA damage. DNA-PKcs is a nuclear serine/threonine kinase which is activated upon association with DNA and is a crucial component of the DNA double-strand break (DSB) response [21]. The histone H2AX is phosphorylated at serine 139 in response to DSBs, with the resulting phosphoprotein termed γH2AX; DNA-PK is one of the kinases involved in phosphorylating H2AX.

DNA-PKcs was the more reliable marker of DNA damage as immunostaining in the frontal cortex correlated with that in the temporal cortex and we have previously found that the proportion of DNA-PKcs positive neurones in FFPE frontal cortex significantly correlates with the detection of DNA-PKcs by Western blotting (Simpson *et al.*, unpub. obs.). We measured changes in the catalytic subunit of DNA-PK which is reduced following focal infarcts [22] and in response to inactivation of the p53 inducible gene resulting in a deficient DNA damage response [23]. One reason why γH2AX might be a less reliable marker for DNA damage than DNA-PKcs is due to the difficulties faced in detecting phosphoproteins; phosphatases can dephosphorylate residues during tissue preparation

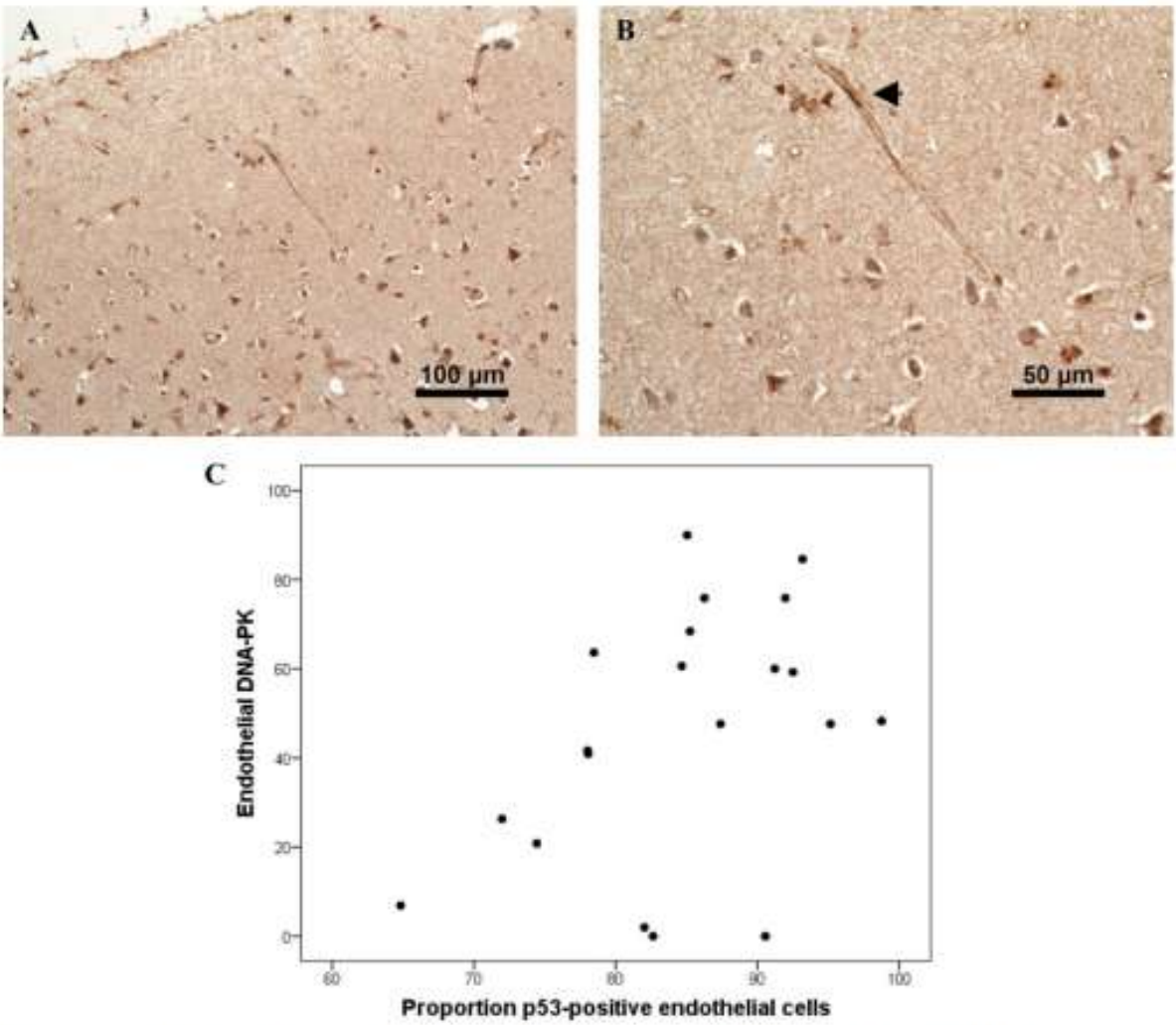

Figure 5. p53 immunoreactivity in cases with high vs. low DNA damage and limited tangle pathology (Braak 0–II). (A) p53 immunoreactivity can be seen throughout the brain parenchyma, (B) depicts a p53-positive endothelial cell within the basement membrane in the frontal cortex (arrowhead). (C) Association of endothelial DNA-PKcs with p53 immunoreactivity; this association showed a trend to significance (Spearman's: $P = 0.051$).

(that is, during fixation) and the low stoichiometry of phosphorylation means that of the total protein pool relatively little is likely to be phosphorylated in response to a given stimulus. There was an effect of tissue pH on DNA-PKcs, although this is the opposite to what would be expected if a poor pre-agonal state (associated with low tissue pH) was accounting for the variation in DNA-PKcs. This is consistent with observations in our previous study [14] and may suggest sensitivity of the immunohistochemical process for DNA-PKcs is affected by tissue pH.

A range of factors relevant to brain ageing, such as oxidative stress, Aβ-deposition and inflammation could injure endothelium. Reactive oxygen species may cause permanent or transient damage to nucleic acids within the cells, leading to such events as DNA strand breakage and degradation of DNA [24]. Endothelial damage manifested by oxidative stress is known to result in endothelial dysfunction which includes impaired endothelial-mediated vasorelaxation and a reduced ability of blood vessels to dilate (hypoperfusion) thus impairing

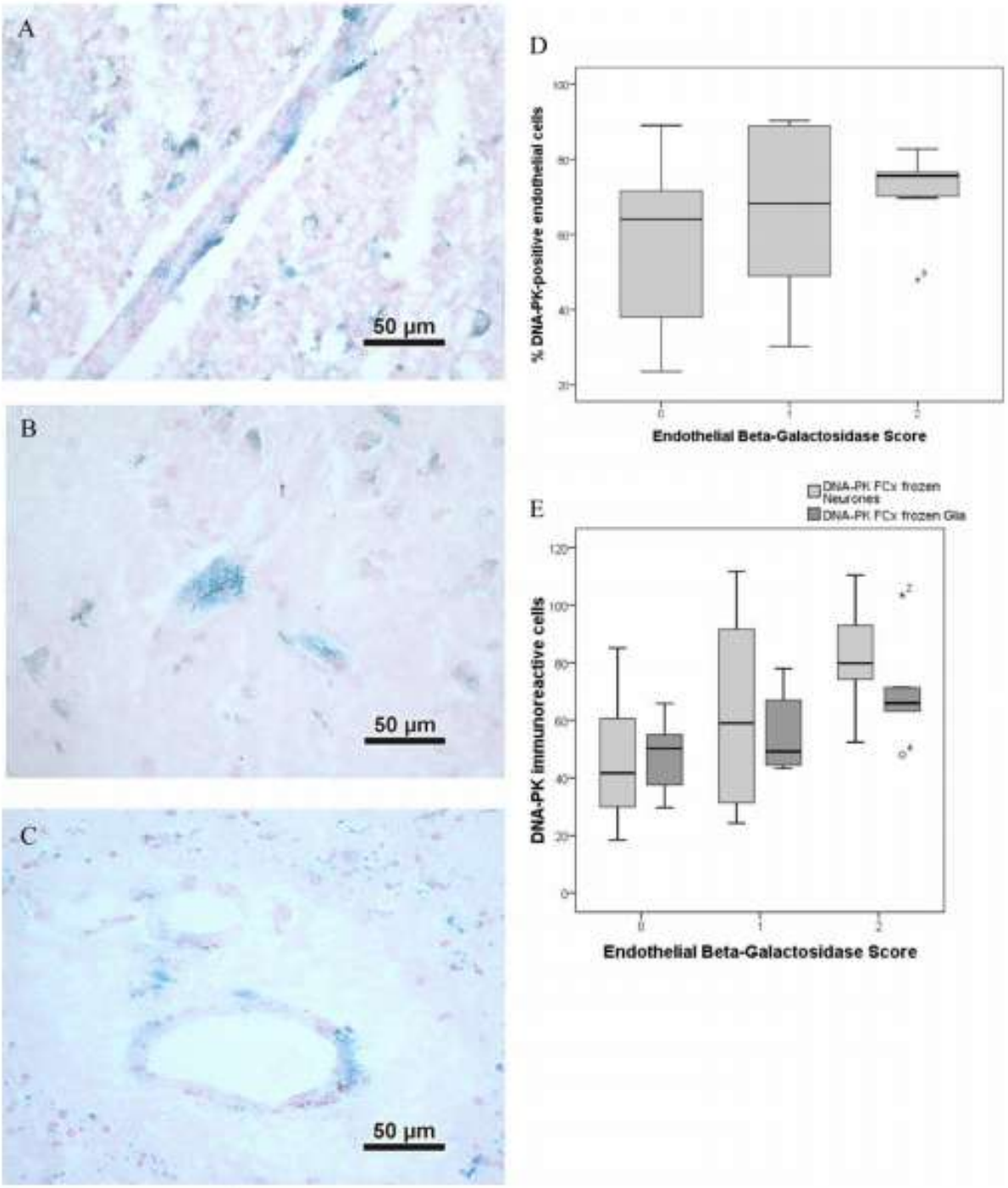

Figure 6. Vascular activity of β-galactosidase demonstrated by histochemistry in frontal cortex. (A) Focal reactivity along a vessel, (B) focal reactivity of branching vessel, and (C) segmental activity of part of the circumference of a small vessel. There is a trend to increased β-galactosidase activity with increased DNA damage ($P = 0.050$) (D); there is also a significant increase in β-galactosidase activity as the overall burden of DNA damage increase (neurones, glia and endothelium) ($P = 0.038$) (E).

angiogenic responses and causing unbalanced endothelial apoptosis [25].

Brain endothelial cells differ from other endothelial cells in that although they are lined by a fused basement membrane, formed by an endothelial basement membrane and an astrocytic basement membrane, there is no large extracellular space between the brain microcapillaries and the neural compartment [26], this close apposition means that endothelial cells are exposed to changes in the brain microenvironment. The brain itself is highly sensitive to oxidative stress due to its high oxygen metabolic rate, high levels of iron and large numbers of unsaturated fatty acids [27]. Therefore, although endothelium is at the interface between brain and systemic circulation, the correlation with parenchymal cell damage suggests endothelium may share the brain's oxidative stress environment. Furthermore, endothelial cells might be predisposed to damage from reactive oxygen species due to the high numbers of mitochondria they possess [28].

Persistent DNA damage in brain endothelium may have a number of consequences including the induction of apoptosis. p53, a protein involved in the induction of apoptosis and cell cycle arrest, showed a trend to increase at both the RNA and protein level, suggesting that there is increased apoptosis in endothelium in response to DNA damage. In addition we investigated whether a DNA damage response is linked with senescence induction in endothelial cells. Although senescence is typically used as a term to describe cultured cells which reach the end of their proliferative potential (Hayflick phenomenon) there is emerging evidence that cells in the CNS, including post-mitotic cells, exhibit markers of senescence [29,30]. Using β-galactosidase activity as a marker of senescence we found that as endothelial DNA damage increases it appears that endothelial cells also show evidence of senescence. Cellular senescence is accompanied by increases in the production and secretion of a number of cytokines, chemokines and proteases, this specific secretory profile is termed the senescence-associated secretory phenotype (SASP) [31]. Acquisition of SASP by endothelial cells could further disrupt the delicate brain microenvironment.

The effect of persistent DNA-damage response in endothelial cells is likely to be manifold; endothelial apoptosis resulting in string vessels and reduction of blood flow to the brain; disruption of the BBB leading to further dysfunction due to the unregulated passage of molecules into the parenchyma; generalized NVU dysfunction which will impact both astrocytes and neurones; and potentially senescence induction leading to reduced function and a pro-inflammatory environment.

In conclusion we show that DNA damage to brain endothelial cells in a population-derived sample occurs early in relation to (or independent of) Alzheimer pathology and is likely to be associated with ageing. This could result in suboptimal perfusion of the cerebral tissue as well as a failure of perivascular clearance of interstitial fluid and Aβ [32,33]. Damage to these cells mirrors that in the parenchyma indicating that these cells, which form part of the NVU, share the same oxidative environment or that the intricate network within the NVU results in a bystander effect in response to damage. This suggests further detailed studies of endothelial molecular pathology in brain ageing is warranted and this is currently underway in our research group. In addition, as this study does not show the cognitive or pathological trajectory of those individuals with high levels of DNA-dependent protein kinase, studies utilizing animal models or longitudinal imaging studies could further answer these questions.

Acknowledgements

This study and C.J.G. were supported by a grant from Alzheimer's Research UK (PG2010-5). J.E.S. is funded by the MRC (MR/J004308/1). The CFAS study is supported by the Department of Health and the Medical Research Council (grants MRC/G9901400 and MRC U.1052.00.0013); the UKNIHR Biomedical Research Centre for Ageing and Age-related Disease Award to the Newcastle upon Tyne Hospitals Foundation Trust; the Cambridge Brain Bank is supported by the NIHR Cambridge Biomedical Research Centre; The Cambridgeshire and Peterborough NIHR CLAHRC; Nottingham University Hospitals NHS Trust; University of Sheffield and the Sheffield Teaching Hospitals NHS Foundation Trust; The Thomas Willis Oxford Brain Collection, supported by the Oxford Biomedical Research Centre; The Walton Centre NHS Foundation Trust, Liverpool. We would like to acknowledge the essential contribution of the liaison officers, the general practitioners, their staff, and nursing and residential home staff. We are grateful to our respondents and their families for their generous gift to medical research, which has made this study possible.

Author contributions

S.B.W. and J.E.S. jointly conceived of, and supervised, the study. C.A. and S.W. performed immunohistochemistry,

C.J.G. and J.E.S. performed laser capture microdissection and S.A.M. and P.R.H. performed qPCR analysis. F.E.M. and C.B. carried out statistical analysis of the CFAS cohort. P.J.S. and P.G.I. provided advice and guidance. C.J.G. wrote the paper with input from S.B.W. and J.E.S.

Conflicts of interest

There are no conflicts of interest to disclose.

References

1 Zlokovic B. The blood-brain barrier in health and chronic neurodegenerative disorders. *Neuron* 2008; 57: 178–201
2 Brown W, Thore C. Cerebral microvascular pathology in ageing and neurodegeneration. *Neuropathol Appl Neurobiol* 2011; 37: 56–74
3 Zlokovic BV. Neurovascular pathways to neurodegeneration in Alzheimer's disease and other disorders. *Nat Rev Neurosci* 2011; 12: 723–38. PubMed PMID: 22048062, Epub 4 November 2011
4 Farrall A, Wardlaw J. Blood-brain barrier: ageing and microvascular disease – systematic review and meta-analysis. *Neurobiol Aging* 2009; 30: 337–52
5 Viggars A, Wharton S, Simpson J, Matthews F, Brayne C, Savva G, Garwood C, Drew D, Shaw PJ, Ince PG. Alterations in the blood brain barrier in ageing cerebral cortex in relationship to Alzheimer-type pathology: a study in the MRC-CFAS population neuropathology cohort. *Neurosci Lett* 2011; 505: 25–30
6 Simpson J, Ince P, Lace G, Forster G, Shaw P, Matthews F, Savva G, Brayne C, Wharton SB, on behalf of the MRC Cognitive Function and Ageing Neuropathology Study Group. Astrocyte phenotype in relation to Alzheimer-type pathology in the ageing brain. *Neurobiol Aging* 2010; 31: 578–90
7 Simpson J, Ince P, Shaw P, Heath P, Raman R, Garwood C, Gelsthorpe C, Baxter L, Forster G, Matthews FE, Brayne C, Wharton SB, on behalf of the MRC Cognitive Function and Ageing Neuropathology Study Group. Microarray analysis of the astrocyte transcriptome in the ageing brain: relationship to Alzheimer's pathology and APOE genotype. *Neurobiol Aging* 2011; 32: 1795–807
8 Merlini M, Meyer E, Ulmann-Schuler A, Nitsch R. Vascular β-amyloid and early astrocyte alterations impair cerebrovascular function and cerebral metabolism in transgenic arcAb mice. *Acta Neuropathol* 2011; 122: 293–311
9 Wharton SB, Brayne C, Savva GM, Matthews FE, Forster G, Simpson J, Lace G, Ince PG. Epidemiological neuropathology: the MRC Cognitive Function and Aging Study experience. *J Alzheimers Dis* 2011; 25: 359–72. PubMed PMID: 21422529, Epub 23 March 2011
10 Stephan BCM, Wharton SB, Simpson J, Matthews FE, Ince P, Brayne C. The epidemiological neuropathology of dementia and the implications for drug development. *Neurodegener Dis Manag* 2012; 2: 471–82
11 Cognitive function and dementia in six areas of England and Wales: the distribution of MMSE and prevalence of GMS organicity level in the MRC CFA Study. The Medical Research Council Cognitive Function and Ageing Study (MRC CFAS). *Psychol Med* 1998; 28: 319–35. PubMed PMID: 9572090, Epub 8 May 1998
12 Pathological correlates of late-onset dementia in a multicentre, community-based population in England and Wales. Neuropathology Group of the Medical Research Council Cognitive Function and Ageing Study (MRC CFAS). *Lancet* 2001; 357: 169–75. PubMed PMID: 11213093, Epub 24 February 2001
13 Savva GM, Wharton SB, Ince PG, Forster G, Matthews FE, Brayne C. Age, neuropathology, and dementia. *N Engl J Med* 2009; 360: 2302–9. PubMed PMID: 19474427, Epub 29 May 2009
14 Simpson J, Ince P, Haynes L, Theaker R, Gelsthorpe C, Baxter L, Forster G, Lace GL, Shaw PJ, Matthews FE, Savva GM, Brayne C, Wharton SB, on behalf of the MRC Cognitive Function and Ageing Neuropathology Study Group. Population variation in oxidative stress and astrocyte DNA damage in relation to Alzheimer-type pathology in the ageing brain. *Neuropathol Appl Neurobiol* 2010; 36: 25–40
15 Bell RD, Zlokovic BV. Neurovascular mechanisms and blood-brain barrier disorder in Alzheimer's disease. *Acta Neuropathol* 2009; 118: 103–13. Pubmed Central PMCID: PMC2853006, PubMed PMID: 19319544, Epub 26 March 2009
16 Breteler MM. Vascular involvement in cognitive decline and dementia. Epidemiologic evidence from the Rotterdam Study and the Rotterdam Scan Study. *Ann N Y Acad Sci* 2000; 903: 457–65. PubMed PMID: 10818538, Epub 20 May 2000
17 de la Torre JC. Is Alzheimer's disease a neurodegenerative or a vascular disorder? Data, dogma, and dialectics. *Lancet Neurol* 2004; 3: 184–90. PubMed PMID: 14980533, Epub 26 February 2004
18 de la Torre JC, Mussivand T. Can disturbed brain microcirculation cause Alzheimer's disease? *Neurol Res* 1993; 15: 146–53. PubMed PMID: 8103579, Epub 1 June 1993
19 Simpson JE, Ince PG, Haynes LJ, Theaker R, Gelsthorpe C, Baxter L, Forster G, Lace GL, Shaw PJ, Matthews FE, Savva GM, Brayne C, Wharton SB. Population variation in oxidative stress and astrocyte DNA damage in relation to Alzheimer-type pathology in the ageing brain. *Neuropathol Appl Neurobiol* 2010; 36: 25–40. PubMed PMID: 19422529, Epub 9 May 2009
20 Faraco G, Iadecola C. Hypertension: a harbinger of stroke and dementia. *Hypertension* 2013; 62: 810–17. PubMed PMID: 23980072, Epub 28 August 2013

21 Smith GC, Jackson SP. The DNA-dependent protein kinase. *Genes Dev* 1999; 13: 916–34. PubMed PMID: 10215620, Epub 24 April 1999
22 Love S, Barber R, Wilcock GK. Neuronal death in brain infarcts in man. *Neuropathol Appl Neurobiol* 2000; 26: 55–66. PubMed PMID: 10736067, Epub 29 March 2000
23 Li B, Shang ZF, Yin JJ, Xu QZ, Liu XD, Wang Y, Zhang SM, Guan H, Zhou PK. PIG3 functions in DNA damage response through regulating DNA-PKcs homeostasis. *Int J Biol Sci* 2013; 9: 425–34. Pubmed Central PMCID: PMC3654439, PubMed PMID: 23678292, Epub 17 May 2013
24 Hemnani T, Parihar MS. Reactive oxygen species and oxidative DNA damage. *Indian J Physiol Pharmacol* 1998; 42: 440–52. PubMed PMID: 10874342, Epub 30 June 2000
25 Rizzo M, Leaver H. Brain endothelial cell death: modes, signaling pathways, and relevance to neural development, homeostasis, and disease. *Mol Neurobiol* 2010; 42: 52–63
26 Wolburg H, Noell S, Wolburg-Buchholz K, Mack A, Fallier-Becker P. Agrin, aquaporin-4, and astrocyte polarity as an important feature of the blood-brain barrier. *Neuroscientist* 2009; 15: 180–93. PubMed PMID: 19307424, Epub 25 March 2009
27 Chong ZZ, Li F, Maiese K. Oxidative stress in the brain: novel cellular targets that govern survival during neurodegenerative disease. *Prog Neurobiol* 2005; 75: 207–46. PubMed PMID: 15882775, Epub 11 May 2005
28 Coomber BL, Stewart PA. Morphometric analysis of CNS microvascular endothelium. *Microvasc Res* 1985; 30: 99–115. PubMed PMID: 4021842, Epub 1 July 1985
29 Jurk D, Wang C, Miwa S, Maddick M, Korolchuk V, Tsolou A, Gonos ES, Thrasivoulou C, Saffrey MJ, Cameron K, von Zglinicki T. Postmitotic neurons develop a p21-dependent senescence-like phenotype driven by a DNA damage response. *Aging Cell* 2012; 11: 996–1004. Pubmed Central PMCID: PMC3533793, PubMed PMID: 22882466, Epub 14 August 2012
30 Bhat R, Crowe EP, Bitto A, Moh M, Katsetos CD, Garcia FU, Johnson FB, Trojanowski JQ, Sell C, Torres C. Astrocyte senescence as a component of Alzheimer's disease. *PLoS ONE* 2012; 7: e45069. Pubmed Central PMCID: PMC3440417, PubMed PMID: 22984612, Epub 18 September 2012
31 Freund A, Orjalo AV, Desprez PY, Campisi J. Inflammatory networks during cellular senescence: causes and consequences. *Trends Mol Med* 2010; 16: 238–46. Pubmed Central PMCID: PMC2879478, PubMed PMID: 20444648, Epub 7 May 2010
32 Kalaria RN. The blood-brain barrier and cerebrovascular pathology in Alzheimer's disease. *Ann N Y Acad Sci* 1999; 893: 113–25. PubMed PMID: 10672233, Epub 15 February 2000
33 Hawkes CA, Gatherer M, Sharp MM, Dorr A, Yuen HM, Kalaria R, Weller RO, Carare RO. Regional differences in the morphological and functional effects of aging on cerebral basement membranes and perivascular drainage of amyloid-beta from the mouse brain. *Aging Cell* 2013; 12: 224–36. PubMed PMID: 23413811, Epub 19 February 2013

Supporting information

Additional Supporting Information may be found in the online version of this article at the publisher's web-site:

Figure S1. qPCR analysis comparing high and low DNA damage in individuals with a low burden of pathology (Braak I–II). Values represent mean ± SEM; n = 5.

Received 17 March 2014
Accepted after revision 27 April 2014
Published online Article Accepted on 27 May 2014